Meera Ramesh

A multi scale approach to the study of lime-cement mortars in masonry

UMinho | 2021

Meera Ramesh

A multi scale approach to the study of lime-cement mortars in masonry

Universidade do Minho
Escola de Engenharia

March 2021

Universidade do Minho
Escola de Engenharia

Meera Ramesh

A multi scale approach to the study of lime-cement mortars in masonry

Doctoral Thesis
Civil Engineering

Work conducted under supervision of
Professor Doutor Miguel Ângelo Dias Azenha
and
Professor Doutor Paulo José Brandão Barbosa Lourenço

March 2021

Acknowledgments

This journey has been extremely gratifying and deeply joyful, and I am grateful to many wonderful people who have helped me through it.

I would like to start by acknowledging Professor Miguel Azenha. In the last four years, he has helped shape not only this work but my approach to research in general. Not once did he shoot down any idea, regardless of how crazy it seemed, and allowed me to discover my dead ends, while gently pushing the research back on track when I got carried away. He has been honest and kind in equal measures and has insisted on paying attention to details. I am equally grateful to Professor Paulo Lourenco, who was one of the first people I sought advice from about pursuing a Ph.D. He has always taken out the time to guide the project and given invaluable technical feedback. By example, he has taught me to network and collaborate and to never lose the bird's eye view of a project. With both of them, I hope to maintain the mentor-mentee relationship for the rest of my professional career, since it is one of the most valuable things I have obtained from this Ph.D.

I would like to acknowledge FCT Portugal for my scholarship and the mortar task force of the European Lime Association, for funding a part of this Ph.D. I would especially like to thank Dr. Peter, Mr. Givens, and Dr. Rompaey, who have guided this research through important technical discussions and crucial feedback.

This Ph.D. would have been impossible without the lab technicians in the University of Minho – Marco, Mr. Matos, Mr. Martins, Carlos, Mr. Goncalves, Cesar, and Luciano. I'm ever so grateful to each of them, they've all been generous with their time, gracious and kind, and a lot of fun to work with.

I would like to thank my friends in Guimaraes, who are now family - Xinyu, Antonio, Telma, Rafael, Pilar, Leslie, Alberto, Elesban, Giorgos, Ioana, and Nicoleta. Things have a way of fading into the fabric of time, and I am certain I will not be able to carry every part of this journey with me. So what I hope remains, are the relationships I have developed here, all the wonderful people I became friends with, and those that I met in passing. They have all made this journey more fun and meaningful.

Finally, I would like to thank some of the most important people in my life. My parents, Meenakshi and Ramesh, who have given me wings to fly and roots to come back to, who encourage me to travel and to learn new things, to take risks, fall, and start over. They are my foundation. My sister, Padmini, who is half my heart and encourages me to be more passionate and caring. And to Soham, who has patiently walked this journey with me, adding humor to dull days, and comfort to the difficult ones. I feel extremely privileged and thankful for all the love that these people bring into my life.

STATEMENT OF INTEGRITY

I hereby declare having conducted my thesis with integrity. I confirm that I have not used plagiarism or any form of falsification of results in the process of the thesis elaboration.

I further declare that I have fully acknowledged the Code of Ethical Conduct of the University of Minho.

A multi scale approach to the study of lime-cement mortars in masonry

Abstract

In masonry constructions, the choice of mortar composition is usually guided by requirements of the final application, which could range from new constructions to conservation projects. Often, lime and cement are combined, to overcome their shortcomings and consequently serve as a suitable binder in masonry mortars. Depending on their proportion in the mixture, it may be possible to obtain the desired range of characteristics in different mechanical properties like strength, stiffness, shrinkage, porosity, and so on. And even though the practice of combining lime and cement in masonry mortars has been around for many years, its benefits have not yet been addressed in a systematic, quantitative manner. Often, seemingly significant differences in the mechanical behavior of mortars do not reflect proportionally in changes in mechanical properties at the masonry level. Thus, the aim of this experimental research is focused on investigating the quantitative benefits of substituting cement with lime in masonry mortars, at the mortar as well as masonry level.

Performance indicators have been determined from a structured experimental campaign of mechanical behavior of blended mortars, characterizing several properties for multiple lime-cement mix proportions: workability, compressive and flexural strength, stiffness, drying shrinkage, and open porosity, among others. The factor of aging has also been accounted for, with selected tests being performed up to 365 days, to account for the carbonation of lime in the mortars. Based on the breadth of experimental results that were obtained, patterns were analyzed through regression analyses, to estimate mechanical properties of mix proportions that were not physically tested in the laboratory. From the results obtained, the most suitable proportions were identified and consequently subjected to further experimentation at the masonry level. The response of brick masonry constructed with two different lime-cement mortars was compared with that of cement mortar in masonry, specifically focusing on differences in strength, stiffness, and ductility. In parallel, the influence of lime-cement mortars on the flexural strength of masonry, parallel, and perpendicular to the bed joints was also assessed. The final stage of this research involved quasi-static cyclic loading, to study the in-plane shear response of masonry wall panels, supplemented by experimental information on the shear bond strength of masonry, all focused on assessing the influence of lime-cement mortars compared to a cement mortar.

Key words: Cyclic loads; E-modulus; Lime-cement mortars; Mechanical behavior; Unreinforced brick masonry;

Abordagem multi-escala ao estudo de argamassas mistas de cal e cimento em alvenaria

Resumo

Nas construções em alvenaria, a escolha da composição da argamassa costuma ser orientada pelos requisitos da aplicação final, seja na construção nova ou reabilitação. É frequente o recurso à combinação de cal e cimento para superar respetivas deficiências individuais obtendo-se um ligante adequado em argamassas de alvenaria. Dependendo das proporções de cal e cimento na mistura, pode ser possível obter uma faixa desejada de características em diferentes propriedades. No entanto, apesar da prática de combinar cal e cimento em argamassas de alvenaria já existir há muitos anos, os seus benefícios ainda não foram analisados de forma sistemática e quantitativa. As diferenças significativas no comportamento mecânico das argamassas não refletem necessariamente alterações proporcionais nas propriedades mecânicas no nível da alvenaria. Assim, o objetivo desta investigação experimental centra-se na investigação quantitativa dos benefícios decorrentes da substituição parcial do cimento por cal em argamassas de alvenaria, tanto ao nível da argamassa como ao nível do comportamento da alvenaria.

Os indicadores de desempenho foram determinados a partir de uma campanha experimental focada no comportamento mecânico de argamassas mistas de cal e cimento, caracterizando diversas propriedades para múltiplas proporções de mistura cal-cimento: trabalhabilidade, resistência à compressão e flexão, módulo de elasticidade, retração de secagem e porosidade aberta, entre outras. O envelhecimento também foi contabilizado, através de realização de ensaios até aos 365 dias de idade. Com base na amplitude dos resultados experimentais obtidos, foram efetuadas análises de regressão para estimar as propriedades mecânicas das proporções da mistura que não foram testadas fisicamente em laboratório. Foram identificadas as proporções cal-cimento mais adequadas e, consequentemente, escolhidas para o programa experimental à escala da alvenaria. A resposta de provetes de alvenaria construídos com duas argamassas mistas contendo razões cal-cimento diferentes foi comparada com a da alvenaria executada com argamassa de cimento. Paralelamente, foi avaliada a influência das argamassas mistas de cimento-cal na resistência à flexão de provetes de alvenaria. Finalmente, foi estudada a resposta ao corte no plano de painéis de parede de alvenaria com carregamento cíclico quase estático, com enfoque na avaliação da influência das argamassas de cimento-cal comparativamente à argamassa de cimento.

Palavras-chave: Alvenaria de tijolo não armada Argamassas; Argamassas mistas de cal e cimento; Carregamento cíclico; Comportamento mecânico; Módulo de Elasticidade;

Contents

List of symbols

a	Predefined crack length
l	Length of specimen
h	Height of specimen
b	Width of specimen
d	Depth of specimen
⌀	Diameter
t	Thickness of specimen
E	Elastic modulus
γ	Surface energy
G	Shear modulus
σ	Normal or vertical compressive stress
ε	Strain
τ	Shear stress
G_f	Fracture energy
W	Work done
W_m	Measured work
W_{um}	Unmeasured work
f_k	Characteristic compressive strength of masonry
f	Mean compressive strength of masonry
E_m	Elastic modulus of masonry
f_b	Compressive strength of brick
f_u	Compressive strength of unit
f_m	Compressive strength of mortar
α	Exponent related to compressive strength of unit
β	Exponent related to compressive strength of mortar
K	Coefficient relating compressive strength of masonry with unit and mortar
ε_m	Strain in masonry at peak load
ε_y	Strain in masonry at 70% of peak load
E_0	Initial tangent modulus of elasticity of masonry
K_m	Secant stiffness at peak load

K_y	Secant stiffness at 70% peak load
K_e	Initial secant stiffness
f_c	Compressive strength
f_f	Flexural strength
f_t	Tensile strength
f_{jt}	Tensile strength of mortar bed joint
ϕ	Angle of internal friction
T	Time
ρ	Bulk density
g	Gravity due to acceleration
ψ	Angle of dilatancy
d_u	Ultimate displacement
d_e	Idealized elastic displacement
d_y	Yield displacement
d_0	Displacement corresponding to 10% of load, post peak
μ	Ductility factor
μ_e	Ductility associated with pre-peak behavior
μ_p	Ductility associated with post-peak behavior
τ_{max}	Maximum shear stress
V_d	Shear resistance
h_o	Effective height
l_1	Distance between inner bearings of loading arms
l_2	Distance between supports
l_s	Length of span
l_c	Length under compression
υ	Poisson's ratio
υ_i	Poisson's ratio – initial
υ_f	Poisson's ratio – final
l_{ch}	Characteristic length
j	Ratio of lateral to vertical stresses
κ	Vertical stress distribution at compressed toe (Equation 16)
α_v	Shear ratio (Effective height/Width)

τ_c	Shear strength associated with the cracked section
τ_w	Shear strength associated with the whole section
f_{vo}	Initial shear strength
f_{vko}	Characteristic initial shear strength
f_{xk1}	Characteristic flexural strength, parallel to bed joints
f_{xk2}	Characteristic flexural strength, perpendicular to bed joints
c	Cohesion
f_{vk}	Shear bond strength
γ_m	Partial safety factor
f_{tb}	Tensile strength of brick
A_{env}	Area under the envelope
H_{dmax}	Horizontal force corresponding to maximum displacement
d_{max}	Maximum displacement
H_{cr}	Lateral force at which the first significant crack occurs
H_{max}	Maximum lateral force
d_{cr}	Displacement at which the first significant crack occurs
d_{Hmax}	Displacement corresponding to maximum lateral force
H_u	Ultimate lateral resistance
$Drift_{cr}$	Drift at cracking
$Drift_{Hmax}$	Drift at maximum horizontal capacity
$Drift_{max}$	Drift at maximum displacement
E_N	Normalized cumulative energy
$E_{dissipated}$	Energy dissipated in each cycle
n	Load cycle
H_f	Lateral flexural capacity
r	Ratio of height to length of wall
H_s	Maximum shear capacity
γ	Safety factor
$f_{f,beam}$	Flexural strength corresponding to beam
$f_{f,joint}$	Flexural strength corresponding to joint
$stdev_{f,joint}$	Standard deviation corresponding to flexural strength of a joint
$stdev_{f,beam}$	Standard deviation corresponding to flexural strength of a beam

j	Vertical stress distribution at compressed toe

List of abbreviations

EN	European Standards (Norms)
BS	British Standards
ASTM	American Society for Testing and Materials
MIP	Mercury Intrusion Porosimetry
SEM	Scanning Electron Microscopy
EMM-ARM	Elasticity Modulus Measurement through Ambient Response Method
IUPAC	International Union of Pure and Applied Chemistry
TGA	Thermogravimetric Analysis
UPV	Ultrasound Pulse Velocity
LOI	Loss on ignition
PSD	Particle size distribution
RH	Relative humidity
IRA	Initial rate of absorption
y	Binder to aggregate, % by volume
x	Lime content in binder (% by volume)
BET	Brunauer–Emmett–Teller
w/b	Water to binder
CEM	Cement conforming to EN 197-1
IO	Immediate Occupancy
LS	Life Safety
CP	Collapse Prevention
LVDT	Linear Variable Differential Transformer
UMinho	University of Minho
MTF	Mortar task force
EULA	European Lime Association
CoV	Coefficient of variation
TSTM	Temperature Stress Testing Machine
BTJASPE	BéTon au Jeune Age, Suivi de la Prise et du module d'Elasticité

List of chemical compounds and phases

SO_3	Sulfur trioxide
MgO	Magnesium oxide
Al_2O_3	Aluminum oxide
Fe_2O_3	Ferric oxide
K_2O	Potassium oxide
SiO_2	Silicon dioxide
CaO	Calcium oxide
C_2S	Dicalcium silicate (Belite)
C_3S	Tricalcium silicate (Alite)
TiO_2	Titanium dioxide
C_3A	Tricalcium Aluminate
C_4AF	Tetracalcium alumino ferrite
AFt	Calcium trisulfoaluminate hydrate (Ettringite)
AFm	Calcium monosulfoaluminate
C-S-H	Calcium silicate hydrate
CH	Portlandite
$Ca(OH)_2$	Calcium hydroxide
Ca	Calcium
Si	Silicon
$CaCO_3$	Calcium carbonate
CO_2	Carbon dioxide
C-A-H	Calcium Aluminate Hydrate
Al	Aluminum
O	Oxygen

List of figures

List of tables

To my sister, Padmini, who is kind, thoughtful, and fearless. For you, a thousand times over.

1. Introduction

1.1 Problem statement

Air lime mortars and Portland cement mortars commonly used in heritage and modern constructions respectively offer different benefits and limitations in terms of their aesthetics and mechanical properties to masonry. Air lime has been in use for many centuries, with the earliest record of constructions employing lime dating back to around 4000 BC in ancient Egypt [1]. Air lime has demonstrated durability by being a part of monuments from ancient Rome and the Mohenjo-Daro civilization, located in modern-day India and Pakistan, as well as in ancient Chinese and Syrian civilizations [2-4]. Portland cement, on the other hand, was discovered relatively recently in 1824 by Joseph Aspdin and its discovery took the construction industry by storm [5]. To date, it remains one of the cheapest and most widespread construction materials available around the world [6]. Portland cement mortar offers a very good range of compressive strength and sets rapidly in the presence of water, making it a commercially lucrative option to be used as a binder in mortars [7]. But recent studies in the field of mortar-masonry unit interaction suggest that for effective use in construction, masonry mortar systems need further work in developing specific characteristics like workability, the capability to accommodate movement in masonry, and moisture vapor permeability [8]. Though several admixtures and plasticizers have been adopted to achieve these goals, lime remains a popular option [7, 9, 10].

While it is known that mortar does not contribute to the compressive strength of masonry significantly, it does influence its stiffness and deformation capacity [11]. More specifically, the use of greater quantities of lime in the binder has been associated with lower stiffness, and greater ductility of masonry [12, 13]. Further, studies have also shown that when two mortars have comparable strength, the one with more lime leads to better flexural tensile bond strength in masonry [14]. And even though the practice of combining lime and cement in masonry mortars has been around for many years [2, 15], its benefits have not yet been addressed in important aspects of the mechanical behavior of masonry such as its response to in-plane combined vertical and horizontal cyclic loading. The aim of the research is therefore focused on investigating the quantitative effects of adding hydrated lime to cement mortars, to obtain improved structural performance of unreinforced masonry, through a systematized experimental campaign.

1.2 Objectives of research

The ultimate goal of any construction is to ensure that masonry exhibits satisfactory structural performance as a composite entity. Since the mortar-unit interface often acts as the weak link between masonry units, it is essential to know the mechanical behavior of mortar and the extent to which its properties influence the mechanical behavior of masonry. This doctoral research aims to understand the impact of combining lime and cement in the binder of a mortar, from the point of view of mechanical behavior of mortar as well as masonry. The specific goals have been divided into parts and presented below:

1.2.1 Mortar level

At the mortar level, the goal was to investigate and quantify the mechanical behavior of different lime-cement mortars. Specific properties that were targeted have been listed below:

1. Quantification of change in the strength of lime-cement mortars as a function of the lime-cement ratio in the binder, time, and binder-aggregate ratio (B/Ag) (up to 365 days of age).
2. Correlation of compressive strength with other properties such as flexural strength, and with ultrasound pulse velocity (UPV), and bulk density.
3. Characterization of E-modulus of lime-cement mortars in early ages (0-7 days) as well as later ages (up to 90 days).
4. Investigation of mechanical characteristics such as drying shrinkage, open porosity, fracture energy, and Poisson's ratio of mortars, focusing on the effect of the lime-cement ratio in their binder (up to 90 days of age).

1.2.2 Masonry level

At the masonry level, the goal was to compare the structural performance of unreinforced brick masonry focusing on the impact of the mortar (cement vs lime-cement). The following aspects were focused on:

1. The behavior of masonry under vertical compression; Strength, stiffness, and deformation capacity as a function of the type of mortar used.
2. The role of the mortar in the out-of-plane behavior of masonry; Flexural strength of masonry in directions parallel and perpendicular to the bed joint.

3. The shear bond strength in masonry, subjected to different normal pre-compression levels as a function of the type of mortar used.
4. The response of masonry shear wall panels subject to in-plane quasi-static combined vertical and lateral loading as a function of the type of mortar used, and corresponding changes in energy dissipation, stiffness degradation, and drift capacity.

1.3 Scope of research

Age of study and nature of properties

In terms of time, at the mortar level, specimens were tested for strength and density up to 365 days of age. Based on the data available from literature, it was found that the evolution of most mechanical properties stabilizes by 90 days of age. After this period, changes in properties, if any, were found to be minor and therefore masonry specimens were cured for 90 to 150 days of age before they were tested for different mechanical properties. Long-term properties have not been studied in this research.

Furthermore, this research is focused on quasi-static monotonic tests except for E-modulus and in-plane cyclic loading tests. The response of lime-cement mortared masonry to dynamic loads has not been addressed in this thesis.

The scale of study and size of specimens

Out of the different possible scales of study, the ones chosen in this research include mortar level, brick-mortar bond level, the level of masonry wallets, and the level of masonry wall panels. The full-scale behavior of walls was not studied here in this thesis. Similarly, studies at the paste level have not been explored.

- At the mortar level, the size of specimens has mostly been focused on prisms (40×40×160 mm^3) or cylinders (60 mm ∅, 120 mm height).
- At the level of brick-mortar interaction, triplet specimens were 215 mm long and high, and 102 mm wide.
- At the level of masonry wallets, the specimens were all single leaf (102 mm thick) and 440 mm wide; Depending on the property being investigated, the length of the specimens varied from 450 mm to 890 mm.
- At the level of masonry wall panels, the specimens were all single leaf (102 mm thick) and 900 mm in width and length.

Type of unit used to construct masonry

It is acknowledged that the structural performance of masonry depends on the unit used for construction, the type of mortar, and their consequent interaction. However, since the focus of this research is on the mortar, only one type of unit has been selected for studying the mechanical behavior of masonry, i.e., solid frogged clay bricks with a high suction rate. This way, differences in the behavior of masonry could be attributed to the mortar, since all other parameters including type of unit, construction protocols, and the testing methods were the same.

Standards used as guidelines for tests

It is also recognized, that requirements of the structural performance of masonry vary based on the geographical region in which it is constructed. For this research, the standards used were European, with the EN 1015 series [16] used for the mortar specimens, EN 1052 series [17] adopted for the masonry specimens, and Eurocode 6 [18] for the design recommendations.

1.4 Methodology of research

1.4.1 Research question

The global question in this research was to investigate the effect of partial replacement of cement with lime in mortars on the structural performance of unreinforced brick masonry. Improved structural performance of masonry, would depend on the specific property being considered and could mean higher material strength, greater deformation capacity, improved bond strength, and so on.

1.4.2 Variables used

The variables used in any research can typically be categorized into three types namely dependent, independent, and moderating. Independent variables are those that are being studied and cause changes in the outcome. Dependent variables are the outcomes that are being studied and are of interest to the research. Moderating variables influence the intensity or strength of the relationship between dependent and independent variables. Since this research is split into different scales of study (mortar and masonry), the variables for each of them have been described below (Figure 1, Figure 2):

- **Mortar level study**

1. Independent variables – The lime-cement ratio in the binder or the amount of lime in the binder (10%, 25%, 33.3%, 50%, 66.7%, 75%, and 90%), and amount of binder in the mix or the B/Ag ratio (1:3, 1:4, 1:5, and 1:6), and time in terms of the number of days at which the mix was tested.

2. Dependent variables – All mechanical and physical properties that were studied at the mortar level, such as mechanical strength and stiffness, drying shrinkage, open porosity, and so on.
3. Moderating variable – The amount of water used in each of the mixes or w/b ratio, which was decided based on a target flow table value.

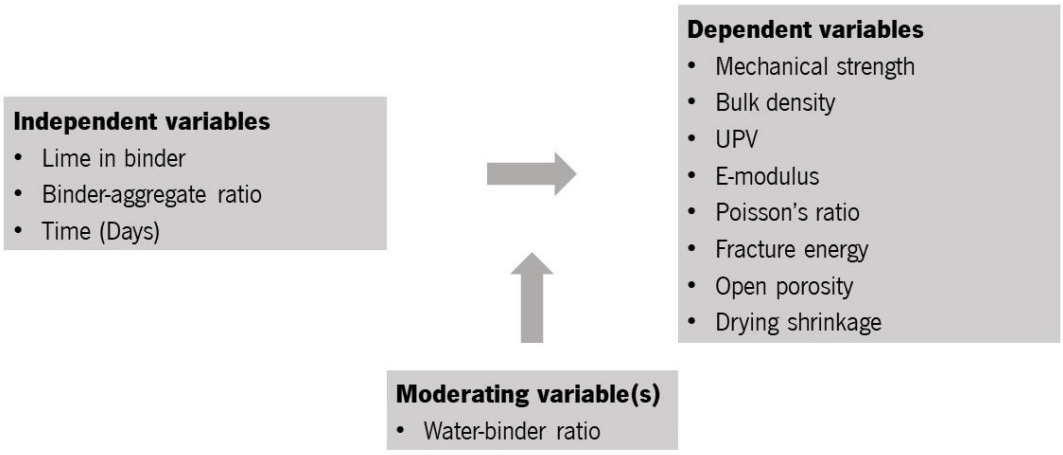

Figure 1: Dependent, independent, and moderating variables for mortar level research

➢ **Masonry level study**

1. Independent variable – The type of mortar used to construct masonry.
2. Dependent variables – All mechanical properties studied such as compressive strength, flexural strength, shear bond strength, and so on.
3. Moderating variable – The type of unit used for masonry construction, in this research, was high suction solid frogged clay brick.

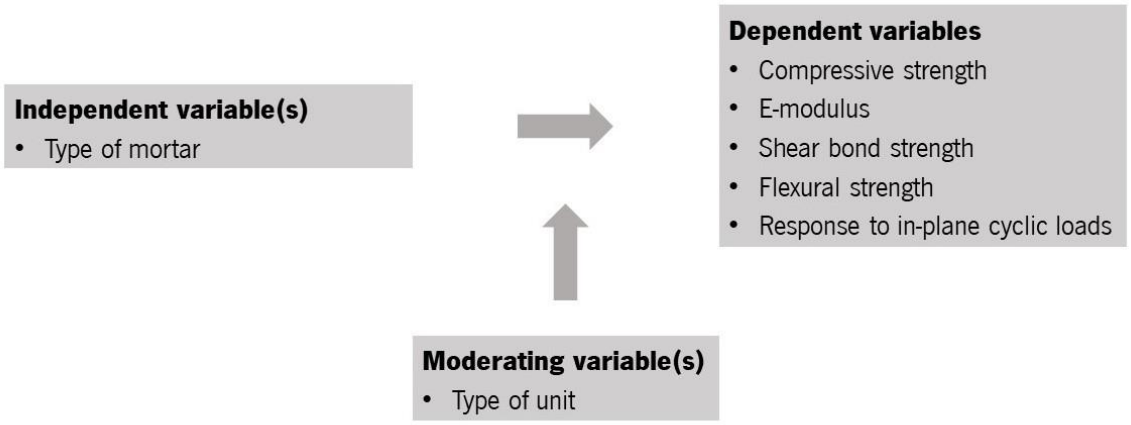

Figure 2: Dependent, independent, and moderating variables for masonry level research

1.5 Outline of research

The outline of the thesis has been highlighted below, with a summary of the contents of each of the chapters:

Chapter 2 – Lime-cement mortars and their role in masonry

This chapter is a state of the art report, which aims at providing the reader with context for the experiments performed in this research and the discussion on results obtained that ensue in the subsequent chapters.

The first section covers a description of the two relevant binders - Portland cement and air lime, a summary of their chemistry and hardening mechanisms. The second section is a summary of lime-cement mortars. Different mechanical properties such as strength, stiffness, deformability, and porosity have been covered, and wherever available, the influence of the presence of lime on these properties has been discussed. And finally, the third section of this chapter is about the role of mortar in masonry focusing on the mechanical behavior of masonry as a function of lime content in the binder of the mortar.

Chapter 3 – Materials and methods

The discussion in this chapter covers the choice of materials used as binders and aggregates in the mortars, the unit selected for masonry construction, and curing conditions for mortar and masonry specimens. It also outlines the design of the mortar mixes, based on the workability (target flow table value) selected. The protocols used to cast and cure mortars, and to construct masonry have also been discussed in detail. Finally, this chapter presents a summary of the different experiments performed and the size and number of specimens used for each of the tests.

Chapter 4 – Mechanical properties of lime-cement mortars

This chapter discusses the results obtained from experiments performed on mortars. The water binder ratio of different mortars as a function of the lime content in the binder and the B/Ag ratio of the mortar has been presented. Subsequently, the results of mechanical strength, ultrasound pulse velocity, and density of 15 lime-cement mortars, have been analyzed. Experimental results have been supplemented with quantification of different factors such as lime-cement ratios, B/Ag ratios, and curing ages, and their impact on the strength of lime-cement mortars. Relations between compressive strength, flexural strength, ultrasound pulse velocity, and density, have also been explored.

Thereafter other mechanical properties have been discussed including stiffness at very early ages (0 to 7 days), and up to 90 days, fracture energy, Poisson's ratio, drying shrinkage, and open porosity. The focus

here was to explore the impact of the quantity of lime on those mechanical properties that are not studied frequently in literature, as well as to characterize a few commonly used lime-cement mixes, so that a range of expectable values could be presented, for future references.

Chapter 5 – Influence of lime-cement mortars on the mechanical behavior of masonry

This chapter begins with a characterization of two lime-cement mixes chosen from the study in the previous chapter, and introduces a reference cement mortar, for the sake of comparison. The mortars are characterized for strength and stiffness, in curing conditions similar to that of the masonry specimens. Furthermore, the mechanical characterization of the chosen clay brick has also been presented.

The bulk of the chapter focuses on tests performed on masonry specimens according to European standards. The tests include compression, E-modulus, flexural strength in parallel and perpendicular directions, and finally, the behavior of masonry wall panels when subjected to in-plane cyclic loads. The main goal of this chapter is to understand if lime in the mortar affects the different mechanical properties of masonry. Experimental results have been analyzed and discussed in the said context and have also been compared with the requirements of Eurocode 6.

Chapter 6 – Conclusions and recommendations for future work

This chapter highlights the main contributions of this research by summarizing the findings at the mortar level as well as masonry level. Based on the conclusions of the present work, recommendations have also been presented for further systematic research in this field of study.

2. Lime-cement mortars and their role in masonry

2.1 Introduction

The chapter begins with an introduction to the two binders used – lime and cement, along with a summary of their hardening mechanisms, individual and combined, to provide context for the kinetics of the reactions, rate of development of mechanical properties, and optimum curing conditions.

Subsequently, masonry mortars have been introduced and accompanied by an overview of the current state of knowledge on lime-cement blended mortars. Following this, a discussion has been provided on important properties at the mortar level; workability, compressive and flexural strength, ultrasound pulse velocity (UPV), E-modulus, Poisson's ratio, fracture energy, drying shrinkage, and open porosity.

The second aspect of this chapter addresses the role of mortars in masonry, with a special emphasis on the behavior of lime-cement mortars. Four important parameters, that are usually used to characterize masonry have been discussed; compressive strength, E-modulus, flexural strength, and shear bond strength. The final section discusses the response of masonry wall panels subject to combined vertical and in-plane cyclic shear loads.

2.2 Binders

2.2.1 Cement and hydration

Portland cement is a hydraulic binding material formed by grinding clay and limestone together and calcining the mixture at a temperature of 1450˚C [19]. The mixture obtained after calcination is called clinker which often has a few lumps or nodules and in the final step is ground/crushed into a powder (fineness ≤ 75 μm) along with calcium sulfate to form cement (Figure 3) [5, 20]. The calcium sulfate, in the form of gypsum or otherwise, helps in controlling the hardening of cement after hydration and its rate of setting [2].

The European standard EN 197-1 [21] defines cement as a hydraulic binder that is finely ground, and inorganic, which when mixed with water hardens and gains strength through a series of hydraulic reactions. EN 197-1 [21] recognizes twenty-seven distinct types of cement and groups them into five main types based on their compositions, namely CEM I - Portland, CEM II – Portland composite, CEM III - Blastfurnace, CEM IV - Pozzolanic, and CEM V - Composite. Additionally, different types of cement may also fall into strength classes based on the compressive strength attained by mortars formed by them

(cement, water, and standard sand) at 28 days. The classes are 32.5, 42.5, and 52.5 MPa and each of them has a type N (ordinary) and R (high) early strength (at 2 and 7 days). Such categorization also accounts for performance requirements of initial setting time and soundness (expansion).

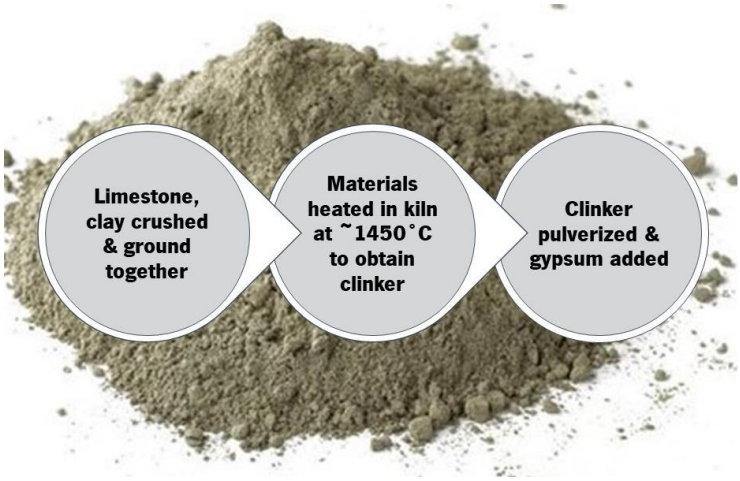

Figure 3: Depiction of the process of cement production

In terms of chemical composition, the clinker usually has the elements – silicon, aluminum, calcium, and iron in the form of their oxides (SiO_2, Al_2O_3, CaO, Fe_2O_3), though the proportions may vary depending on the source of the raw materials employed and based on the properties desired in the end product [20, 22]. In order of importance, the main phases of cement clinker are C_3S (Alite), C_2S (Belite), C_3A (Aluminate), and C_4AF (Ferrite) [23]. The quantity of alite present in the clinker varies between 50% to 80% by weight and contributes to early strength gain by resulting in the formation of an almost amorphous phase of calcium silicate hydrate (C-S-H gel), which has a ratio of calcium to silica (Ca/Si) of approximately 1.45 to 1.75 and Portlandite or calcium hydroxide, also represented as CH [24]. Three common crystal structures of alite are known to be possible, depending on the temperature and impurities present; triclinic (with three polymorphs T1, T2, T3), monoclinic (with three polymorphs M1, M2, M3), and rhombohedral (R) (620-980˚C, 980-1070˚C and >1070˚C respectively), which accounts for a total of seven possibilities [25, 26]. As the clinker cools down, two of the monoclinic polymorphs have been observed to prevail, M1 and M3, depending on the presence of sulfate or magnesium impurities respectively [27-29].

C_2S or Belite is formed in lower quantities than alite, constituting 15-30% by weight of clinker, and has a relatively more regular crystal structure than alite, with 5 known polymorphs [30]. It is less reactive than alite, and becomes a significant phase only approximately 10 days after hydration [31]. While cement clinkers may have more than one polymorph of belite, the most common type is β-belite which is less hydraulic compared to the other belite polymorphs and is known to have monoclinic structure at room

temperature [30, 32]. Belite also contributes to the formation of C-S-H gel but at a slower rate and hence contributes to the gain of strength at a later stage [20]. The other two phases of cement clinker are tricalcium aluminate (C_3A) and tetracalcium aminopherase (C_4AF), present in quantities of 5-10% or 5-15% of the clinker, respectively (Figure 4). The former tends to react with water rapidly, leading to undesirable early setting of cement (flash set), which is often offset by adding gypsum to the clinker; the latter is not reported to cause such issues [20].

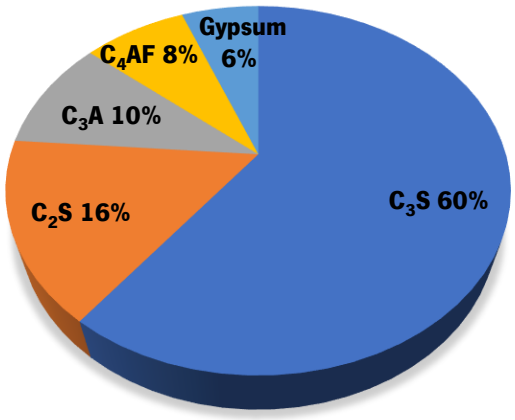

Figure 4: Typical composition of Portland cement (CEM I) [33]

The hydration of cement, which results in its hardening, is a complex reaction, the kinetics of which depend on a multitude of factors such as its fineness and specific surface area, and its phase compositions [2]. Broadly speaking, the mechanism of cement hydration occurs through a process of dissolution and precipitation [34]. In the first step of dissolution, calcium sulfate, as well as phases of tri-calcium silicates, break down into ions, forming an aqueous solution [2]. For the next step to occur in hydration, it is essential that the resulting products of hydration must be less soluble than the anhydrous phases. Since C-S-H gel is less soluble than alite regardless of the concentration of CH in the solution, alite always hydrates into C-S-H [34]. Typically belite does not hydrate at the same time as when alite is undergoing hydration, because the concentration of the solution tends to be higher than the solubility of belite [34]. In this second phase of precipitation, i.e., recombination of the ions into a solid phase that is energetically more favorable, alite dissolves to form C-S-H around cement particles, C_3A dissolves to form an aluminate gel which reacts with sulfates to form ettringite and all the initial reaction collectively cause a large amount of heat release [2]. The first exothermic stage of the hydration reaction usually lasts only for a few minutes and is followed by the dormant period. The most commonly accepted theory for this induction period is that further reaction is inhibited because of the formation of metastable C-S-H on the surface of alite [2]. The next stage is the accelerated hydration of alite leading to the formation of C-S-H

gel and Portlandite. This stage is almost exclusively guided by the nucleation and growth of C-S-H [35]. It has been proposed that small nuclei of C-S-H form on alite particle and thereafter, the growth of these nuclei control the hydration kinetics, at a rate proportional to the free area of the nuclei [36]. This period could last between 3 to 24 hours, with 30% of the cement typically expected to have reacted, and is subsequently followed by a stage called deceleration which corresponds to slowing down of relations, and slower gain of strength in cement, with time [37]. In this period, hydration continues but its process becomes diffusion controlled, and the hydration of belite becomes significant but the overall rate of reaction and evolution of heat are reported to reduce [2, 37].

Finally, the main products of Portland cement hydration rare C-S-H, reportedly occupying 50-60% of the volume of solid phase, and CH is reported to make up 20-25% of the volume [2]. Two other phases that occur during the hydration process are AFm and Aft, and are also known as monosulfoaluminate and ettringite [38]. Ettringite is formed from the reaction between gypsum and tricalcium aluminate or calcium ferrite phases and helps in avoiding the formation of hydrogarnet, which leads to flash setting of cement [39]. Ettringite is also attributed to expansion cracks in certain cases [39]. If all the gypsum added, reacts before aluminate, ettringite converts to a more stable phase of monosulfoaluminate with lesser sulfate. This instability occurs due to a sudden drop in the concentration of sulfate ions in the pores. Otherwise, ettringite reacts with aluminate to form monosulfoaluminate through a different chemical reaction [39, 40].

2.2.2 Air lime and carbonation

Calcium carbonate ($CaCO_3$) commonly referred to as limestone, is quarried from the earth in its raw form (marble, chalk, and shell) and treated to produce Calcium Oxide (CaO) quicklime (Figure 5). This treatment, known as calcination takes place in a kiln at around 900˚C and releases carbon dioxide as a result of the endothermic reaction that occurs [41]. Since this form of lime is highly reactive and unstable to handle, typically water is added to it, and the resulting hydrated air lime is then used to prepare mortars. The technology used to produce air lime can influence the properties of the mortars it acts as a binder for, in both the fresh as well as hardened states [2]. If water is added to quicklime to hydrate it in a controlled manner and stoichiometric ratios it gets converted into a powder. This process of hydration (dry process), causing a rapid expansion in volume, results in the formation of calcium hydroxide or $Ca(OH)_2$ called hydrated lime [42]. Depending on the grade of lime, the available lime content could vary from 70% to 90% [43]. Air lime could also be dolomitic, which involves the presence of mainly oxides and

hydroxides of calcium-magnesium, ranging from 5% to 30% by volume [43]. Usually, lime that is used in the industry is obtained through the dry process of hydration [10].

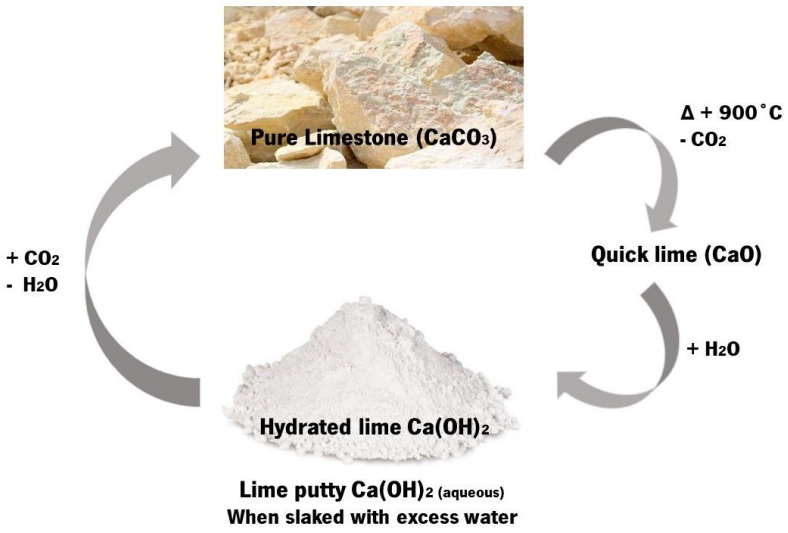

Figure 5: Illustration of the lime cycle

If excess water is added to lime, the process is referred to as slaking (wet process). It results in the formation of lime putty and has been described as 'suspension of calcium hydroxide crystals in water' [2]. Traditionally, it was more common to use lime in the form of putty because it could be stored underwater for long periods (up to 3 years) and this would lead to an improvement of its properties [2]. It has been found that mortars with lime putty result in better workability due to higher water retention and viscosity of the same volume of material used compared to hydrated lime [2, 9]. Rodriguez-Navarro *et al.* [44], report that this happens because as lime putty ages, pre-existing micrometer-sized prismatic calcium hydroxide crystals get modified to sub micrometer-sized plate-like crystals, due to preferential dissolution of the prismatic faces and secondary crystallization. These new plate-like crystals which are generated on the original prismatic crystals offer a larger specific surface area.

Both lime putty and hydrated lime are non-hydraulic binders, that harden by absorbing carbon dioxide (CO_2) and result in the formation of calcium carbonate or $CaCO_3$ once again [41]. This process, called carbonation of lime is a diffusion-dissolution mechanism, dependent on carbon dioxide, and to a great extent dependent on the pore structure of the resulting mortar and the amount of water in it [2]. The first step involves the dissolution of calcium hydroxide crystals in the capillary pore water, which also tends to raise the pH to around 12.8 [2]. The rate of this dissolution has been reported to depend on the specific surface area, solid-liquid interfacial area, and concentration of hydroxide ions, and the size of the crystals of calcium hydroxide (smaller crystals have higher solubility than larger crystals) [45, 46]. The process of carbonation though, is really slow because atmospheric carbon dioxide has to diffuse into the pores of

the material, after the removal of excess water from the mix [47]. Simultaneously, another process occurs which is the diffusion of carbon dioxide through the pores of the mortar, as pore water dries and evaporates [47]. Diffusion of carbon dioxide gets hindered in saturated conditions because diffusivity of carbon dioxide drops by almost 10,000 times in water compared to that in the air [48, 49]. However, since the controlling factor of carbonation reaction is the dissolution of calcium hydroxide crystals in the aqueous medium of the reaction, the presence of some minimum amount of water is necessary [47]. Based on experimental data, it was reported that the optimum range of relative humidity required for carbonation is between 40% to 80%, in which vapor and liquid form of water co-exist, facilitating the presence of continuous phase in the pores [2, 47]. The diffusion of carbon dioxide in water is reported to be the controlling step in carbonation [50]. Once carbon dioxide has dissolved in water, carbonate ions are formed, which react with calcium ions to form calcium carbonate [2]. The process is essentially that of nucleation and crystal growth, the kinetics of which is reported to be driven by the kinetics of transfer of ion mass [2]. It is widely accepted that carbonation reaction is affected by relative humidity and temperature, and is independent of the concentration of carbon dioxide [2, 47].

Calcium carbonate resulting from the carbonation of calcium hydroxide is known to crystallize in three different polymorphs, namely calcite, aragonite, and vaterite depending on the ambient temperature and humidity conditions, in which the reaction takes place [2]. Calcite has been reported to usually be the predominant polymorph precipitating in lime mortars, with the other two relatively unstable polymorphs eventually transforming into it [51]. Aragonite is found in different depths of mortars and is reported to precipitate at high pressures and temperatures, while vaterite, which is a metastable polymorph, is reported to precipitate in the beginning, along with amorphous calcium carbonate, in the size of nanometer crystals [52]. The formation of different polymorphs is also guided by the domination of kinetic or thermodynamic factors. If the former prevails, the polymorphs likely to be formed are aragonite or vaterite, eventually transforming into the more stable calcite form. However, in the case of thermodynamics being the prevailing factor in the carbonation reaction, it is expected that calcium carbonate will precipitate as calcite [45].

2.3 Lime-cement blended (masonry) mortars

The technical role of bedding mortar in masonry construction is often discussed with regard to properties such as deformability, workability, strength, stiffness, shrinkage, and vapor transmission [13, 53-55]. However, it is difficult for any individual binder to fulfill all requisite criteria of a suitable masonry mortar and so it is common to use more than one type of binder [8, 56-58]. Masonry mortars generally combine

binders in varying proportions, and in some cases admixtures, to overcome their shortcomings for different applications [53, 59].

Individually, air lime mortars and Portland cement mortars, are commonly used in heritage and modern constructions respectively, since they offer different benefits and limitations in terms of their aesthetics, compatibility, and mechanical properties to masonry. Typically cement mortars are associated with fast setting, high strength, and stiffness [8, 60]. Air lime mortars, on the other hand, are associated with longer setting time and lower mechanical strength good workability, an ability to accommodate deformation, and vapor permeability [8, 56]. And though the combination of air lime and Portland cement has been used on the field around the world for several years [56], the development of lime-cement blended mortars was formally recognized by ASTM only in 1951 through a standard called Specification for Mortar for Unit Masonry (C270-51) [61]. It is surprising however that in the last 70 years, there has not been consolidated research studying the effect of changing the lime-cement ratio in the binder of a mortar, on the mechanical behavior of mortar and masonry. While works have been identified, focusing on individual properties of masonry mortars, such as changes in mineralogy, strength or porosity of mortars [7, 45, 48, 56, 59, 62-67], it is difficult to draw global conclusions or make direct comparisons due to differences in the materials of the binder, or binder to aggregate and water to binder ratios of the mixes. Therefore, in this research, two of the most commonly available/used binders around the world, namely air lime and cement were selected for study at a mortar and masonry level [7].

2.3.1 Lime carbonation and cement hydration

In lime-cement blended mortars, hardening occurs as a result of both reactions, with hydration promoting early (~28 days) strength gain and carbonation contributing to evolving strength of mortars in later ages (~365 days) [59]. Cizer [2] reports that independent of moisture content in atmospheric conditions, cement hydration is the dominant reaction and takes place before lime carbonation initiates. The primary difference in the products of hydration in a cement mortar, versus a lime-cement mortar, is reported to be the presence of the C-A-H phase which appears in the latter as hexagonal plate-like crystals with a diameter of less than 1 micrometer (individually or in clusters), or as fine spherical particles in granulates [2, 68, 69]. Apart from these C-A-H phases formed, the other hydrated phases found in lime-cement mortars are reported to be the same as those found in cement mortars; C-S-H phases and AFm phases [34, 48]. In moist curing conditions (~93% RH), cement hydration is promoted such that almost all of it is completed in the first 28 days. Contrastingly, if the curing conditions are dry (~60% RH), carbonation is reported to start evolving 7 days onward and continues to progress up to at least 365 days [2].

In lime-cement blended mortars, one issue that could cause concern is the carbonation of hydrated phases, which leads to a loss of calcium from hydrated phases and could potentially affect the durability of the material [2]. Carbon dioxide is known to be capable of attacking the phases formed during hydration (CH and C-S-H phases), leading to a phenomenon called decalcification [70]. When the C-S-H phase undergoes carbonation it decomposes into calcium carbonate and a hydrous silica gel that is known to be highly porous and is accompanied by a reduction in volume due to a process called carbonation shrinkage [71, 72]. So far, however, carbonation of hydrated phases in atmospheric curing conditions has not seemed to cause any major concern in the development of mechanical properties of lime-cement mortars such as strength, in the long term [59]. The presumptive reason for this is the carbonation of free calcium hydroxide in the mortars, which leads to the formation of calcite crystals, a consequent reduction in porosity, and an increase in strength [2]. This hypothesis needs to be verified though, since the decalcification of hydrated phases, is known to cause a reduction in mechanical strength [71].

2.3.2 Workability and water retention

For any mortar to be used in construction, certain design criteria need to be satisfied [18]. Very often though, research on mortars tends to get focused on the mechanical or durability characteristics to such an extent, that essential practical factors tend to get overlooked, such as the workability of a mortar. Amongst other factors, a workable mortar must spread easily and be able to support the weight of the unit that is placed on top of it, and permit a bit of adjustment for alignment [73]. However, the concept of workability includes several other complexities such as consistency, plasticity, water retention, and time of setting and adhesion [74]. Any method that is used to measure the workability of a mortar is bound to simplify it to an extent and focus on a few of the complexities.

The standards in the EN 1015 series [75, 76] for instance, focus on consistency, defining it as the fluidity of a mortar. Consistency indicates how deformable a fresh mortar would be when subjected to certain types of stresses. Two methods are proposed to measure it, namely the flow table test and the plunger penetration test [75, 76]. Other tests that are used often for such purposes include the ball drop test and the cone penetration test both of which are based on the depth of penetration [9]. The flow table test is one of the most widely used methods to measure consistency due to the simplicity and accessibility of the method. It is based on the principle of subjecting a predefined volume to vertical impacts, allowing it to fall freely through a certain height and then measuring its mean diameter (Figure 6). In the work of Hendrickx [9] an international panel of six masons qualitatively assessed the suitability of freshly prepared batches of mortar. Mixes were categorized as light, lean, dry or fluid, and so on. Light meant that the

mortar was easy to stir and to apply to the bricks, lean referred to a mortar that was poor in the binder, dry referred to the mix being too viscous while fluid implied too much water content. Parameters such as the mortar 'sticking to the brick', 'easy to spread on the mortar bed', and 'not stiffening too fast due to loss of water' were also discussed [9]. The mixes approved by the masons (which included lime-cement mortars, among others) were found to have flow values ranging between 155 and 185 mm.

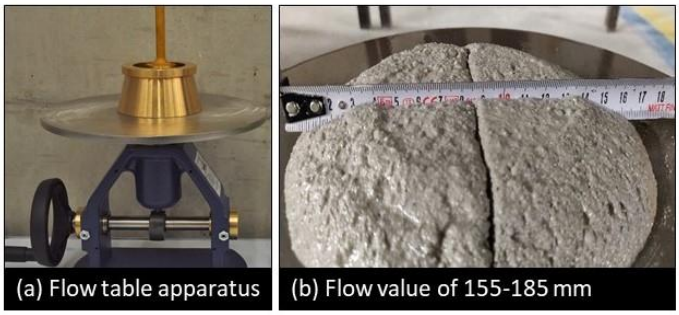

Figure 6: Flow value between 155-185 mm for a lime-cement mortar, measured on a flow table according to EN 1015-3 [75]

Different researchers have shown that the addition of hydrated lime improves the workability of mortars, compared to natural hydraulic lime or Portland cement [74, 77-79]. Concerning application in construction sites, it has been observed that masons tend to prefer the use of lime in mortars because it provides the 'right ease of applicability' compared to cement mortars which are often described as 'too stiff' to work with [9, 10]. Hydrated lime has also been reported to contribute to the plasticity of mortars [10, 74, 79, 80]. Plasticity is associated with permanent deformations on the application of stresses, that are higher than yield stress values [9]. Apart from consistency and plasticity, another aspect of workability that deserves attention is water retention, described in terms of a concept called desorptivity which characterizes the ability of fresh mortars (slurries) to retain water [9]. Desorptivity is measured by applying pressure on the mortar using an inert gas (such as nitrogen), typically equivalent to what would be expected from the capillary suction of a substrate [81]. Low desorptivity or high water retention is a highly desirable property in a mortar since it ensures good adhesion to the substrate and consequently good bond strength [82, 83]. Water retention decreases with increasing quantities of water-binder ratio, B/Ag ratio as well as the particle size of the aggregate [84]. The type of binder used also affects the water retentivity of a mortar, decreasing in the order of hydrated air lime, hydraulic lime, and Portland cement [84, 85]. The common practice of using an air-entraining admixture in a cement mortar (composition 1:5) was tested for water retentivity and compared with a lime-cement mortar with composition 1:1:6. The latter had a much lower value of desorptivity compared to the cement mortar with admixture [86]. In the same study, a lime mortar with 1:3 B/Ag composition performed better than the 1:1:6 lime-cement

mortar, reaffirming that air lime contributes to better water retention. Some of the earliest experiments on water retention of mortars from as far back as 1934 have also shown lime-cement mortars to perform better than only cement mortars [80, 87, 88].

2.3.3 Mechanical strength and ultrasound pulse velocity (UPV)

Mechanical strength is arguably one of the most important properties of mortars that is used in the design of unreinforced masonry. Eurocode 6 [18] uses the compressive strength of mortar as one of the parameters to estimate the strength of masonry in compression and flexure (parallel and perpendicular to the bed joints). Besides this, the compressive strength of mortar is often correlated with other important properties of mortars such as open porosity, tensile and flexural strength, and E-modulus which plays an important role in determining the mechanical response of a material [89-92]. In fact, in the case of concrete, building standards allow the determination of E-modulus based on the compressive strength of the material, such as in Eurocode 2 [93]. The compressive strength of lime-cement molded mortar specimens is measured in Europe according to EN 1015-11 [16]. Prisms (160×40×40 mm^3) are subjected to a three-point bending test to measure the flexural strength, following which the broken halves are used to measure the compressive strength, which is the maximum force obtained divided by the area subject to the load (40×40mm^2). Since this is a relatively easy test to perform and the results tend to have a lower scatter, compared to other properties, numerous articles in the literature may be found studying the strength of mortars [48, 59, 62, 94-96]. Commonly acknowledged trends include an increase in the strength of mortar with decreasing quantity of lime in the lime-cement binder, higher B/Ag ratio, and curing time [2, 59, 95, 97].

While it is recognized that mixes with greater quantities of lime in them, exhibit lower strength [59], there seems to be a lack of consensus on the quantitative correlation between the strength of the mortar and the quantity of lime in the binder. Macharia [95] states that a 30% addition of lime in a cement mortar leads to a 70% difference in strength compared to a cement mortar. However, Cizer [2] found that a 30% addition of lime leads to only a 40% decrease in the strength of the mortar. If the data presented by Haach *et al.* [11] is analyzed, it is possible to note that 50% substitution of cement by lime, leads to approximately 50% change in the strength of the mortar. This lack of consensus observed, is likely due to differences in the types of lime, cement, and aggregates used, and water to binder ratio, and therefore there is a need for an extensive, systematic campaign that uses consistent conditions and raw materials to quantify trends in lime-cement mortars. It may also be observed from existing literature, that by the age of 7 days cement-lime mortars gain more than 75% of their total strength [48, 59], though it is not explicitly quantified.

Such observations open windows for quantifying the gain of strength, concerning the age of the mix and composition of the binder. Furthermore, the observations also provide ground to explore the correlation of strength with other important properties such as stiffness, which were found to be scarce in literature [62]. The influence of aggregates on mechanical strength of lime-cement mortars is far less debated compared to other aspects [98]. It is fairly well accepted that an increase in the quantity of aggregates leads to an increase in water-binder ratio and a reduction in strength of the mortar [59, 96, 99]. However, a quantitative discussion on this subject was not found.

Quantitative values of ultrasound pulse velocity (UPV) by themselves are not of much significance in assessing the behavior of a given material. However, UPV may be put to good use in quality control by correlating it with other properties of materials, such as density, compressive strength, and E-modulus [91]. Its potential has been particularly well explored in the field of concrete and cement mortars, with several studies focusing on using UPV to predict values of compressive strength based on empirical observations, as well as theoretically developed expressions [100-103]. Similarly, empirical correlations between UPV, tensile and compressive strength of granite stones may be found in the work of Vasconcelos [104]. Even if the values of exponents and constants of proportionality used in correlations presented by different authors vary, the basis of these correlations following the laws of physics should theoretically apply to most materials. For instance, body wave velocities (P-compressional/primary wave and S-secondary/shear waves) are inversely proportional to the square root of the density of the material in which the wave is passing through, and directly proportional to the square root of the dynamic Young's modulus of the material [105]. It is therefore surprising that the relationship between UPV and compressive strength (with or without bulk density) has not been studied extensively for lime-based mortars, especially if one accounts for the fact that often lime-based mortars are associated with historic constructions, where very little/no material is available for destructive tests [106, 107]. Little work was found to focus specifically on UPV measurements of lime-cement mortars, far less so, correlating those values with other parameters like mechanical strength or density [108, 109]. The work of Palomar *et al.* [110] explored some of these aspects for one lime-cement mix with composition 1:1:6 concerning porosity, UPV, and thermal conductivity but focused primarily on the presence of fibers and clay. It may, therefore, be worth investigating the relationship between UPV and compressive strength for lime-cement mortars in the current research.

2.3.4 Stiffness at early and later ages

E-modulus is an extremely important parameter for mortars since compatibility between its stiffness and that of the unit determines the ability of masonry to respond to stresses without cracking [111]. The serviceability and even failure of masonry, when composed of unit and mortar, depends on the deformability, strength, and thickness of its components and their interaction. Under the assumption that no sliding occurs between the two components, different empirical formulae proposed to explain the failure modes of masonry, employ the difference in elastic stiffness of unit and mortar as a guiding criterion [112, 113]. However, static modulus of elasticity (E-modulus) is not an easy property to measure on-site, compared to dynamic E-modulus [114]. Furthermore, most of the studies that exist on the measurement of E-modulus are focused on different types of concretes [115], the methods of which may have to be adapted for lime-based materials due to lower mechanical strength and greater fragility of the latter [116]. Indeed, one of the most commonly used methods to measure E-modulus is the cyclic compression test meant for hardened concrete and based on EN 12390-13 [117]. It is based on averaging the slopes obtained from the stress-strain curves of cyclic loads, where the maximum load applied equals one-third of the compressive strength of the specimen (Figure 7).

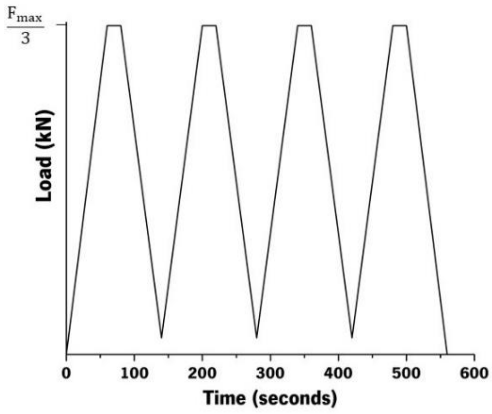

Figure 7: Cyclic compression, typically used to measure E-modulus

Haach *et al.* [11, 65, 96] used this method to test lime-cement mortars with different water-binder ratios (2:1:9, 1:1:6, and 1:2:9) and found E-modulus to range between 3 and 9 GPa, with stiffness reducing as lime content in the binder was increased. Other works [48, 118] confirm this trend but were found to compare the E-modulus of lime-cement mortars versus cement mortars, through the slopes of stress-strain curves obtained from compression tests. Arandigoyen *et al.* [59] found that lime-cement mortars with a high amount of cement in them (>50% of binder) have a linear slope almost until maximum capacity, whereas mortars with a greater quantity of lime in them, exhibit a significant plastic zone. It

appears that there is a general agreement on E-modulus decreasing with an increasing quantity of lime in binder, however similar to the tendencies observed for compressive strength, there is a lack of quantitative correlations in the literature.

Furthermore, studies have been almost universally focused on the behavior of mortars, which have gained adequate maturity, generally accepted as 28 days for cement-based materials and at least 90-180 days for lime-based materials [119-121]. Based on the literature review conducted, no research was found to focus on the behavior of lime–cement mortars specifically between 0 and 7 days of curing age. This knowledge is important to bridge the research gap concerning gain of mechanical strength and stiffness in masonry and consequently stresses developed, in early ages. However, E-modulus in early ages is not easy to measure using the cyclic compression test, even for cement-based mortars, mostly for practical reasons such as the material not possessing adequate strength to be tested [122, 123]. For early age testing, other approaches, based on ultrasound wave transmission, bender-extender elements, or resonant frequency identification have been adopted by different researchers, mostly for cement-based materials [124]. Some of the alternatives follow the same principle of cyclic loading but allow tests without demolding the specimens, such as BTJASPE (BéTon au Jeune Age, Suivi de la Prise et du module d'Elasticité) [125] and TSTM (Temperature Stress Testing Machine) [126]. Amongst these, a method that may relevant for monitoring E-modulus in early ages is EMM-ARM (Elasticity Modulus Measurement through Ambient Response Method)) [127]. This technique has been successfully employed in cement and lime-based stabilized soils since it is capable of measuring the changes in stiffness of any material that can be cast into a mold and undergoes significant changes in stiffness with time [128]. The method is based on continuous modal identification of the first flexural resonant frequency of composite beams (specimens of materials to be tested, cast in cylindrical molds), based on vibrations naturally occurring in the environment [124]. The evolution of resonant frequency identified during the experiment can be directly correlated with the E-modulus by using the dynamic equation of motion, and appears to provide values of E-modulus similar to those obtained from the classical cyclic compression tests [115, 129]. The potential of this method has been explored in this research to assess its suitability for lime-cement mortars.

2.3.5 Deformability and Poisson's ratio

Static Poisson's ratio, defined as the ratio of lateral to longitudinal strain, is a parameter that is widely recognized as needed in assessing the deformability and deflection properties of different materials [130, 131]. While it is not a primary factor that influences design decisions, it is important to investigate

Poisson's ratio of mortars because it is also known to influence the failure mechanisms of masonry [132, 133]. It is common to use values of E-modulus and Poisson's ratio of both unit and mortar to determine stresses in the different components of masonry [134]. Usually, units are stiffer than the mortar used in masonry, meaning that the unit restrains the mortar when subjected to compressive loads, causing triaxial compression in the mortar and a state of biaxial tension-compression in the brick [135, 136].

Research conducted on the behavior of mortars subjected to triaxial stresses suggests that the failure mechanism of mortars varies based on the type or quantity of binder used, as well as the lateral stresses applied on the mortars [133, 137]. Hayen *et al.* [138] tested mortars with different compositions (lime putty, hydraulic lime, and lime-cement binders) in triaxial compression and found that the response of mortars is independent of their respective composition, and is influenced primarily by the ratio of lateral to vertical stress (k). Contrastingly, the experimental work of Mohamad *et al.* [118, 133] indicates that the failure mechanism of mortars under triaxial compression may be dependent on the type and quantity of binder used. From their work on lime-cement mortars, it is possible to observe that as lateral stresses increase, weak mortars (1:1:6, 1:2:9) exhibit an exponential decrease in Poisson's ratio, whereas strong mortars (4:1:12, 2:1:9), exhibit a linear decrease. And the reason for this difference has been attributed to higher porosity and differing void sizes in the 'weaker' i.e., lime based mortars. A linear decrease in values of Poisson's ratio with increasing lateral stresses, has been confirmed for cement mortars by other authors [139]. In the context of concrete, Ottosen [140] had proposed that Poisson's ratio remains constant until a stress/strength ratio (β) of 0.8, after which, it increases up to failure. Based on the experimental results obtained by Mohammad *et al.* [118] a modification to Ottosen's model was proposed (Figure 8), for two different cases of failure types in mortars. Here, the symbol (β) represents the lateral stress to strength ratio. In both cases, the value of Poisson's ratio of mortar decreases with increasing stress/strength ratio, up to a threshold value. The behavior thereafter, depends on the strength of the mortar. If the mortar is strong, the Poisson's ratio increases gradually corresponding to shear failure, marked as (a) in the figure. While in the case of the weak mortar, the Poisson's ratio increases suddenly, corresponding to pore collapse, marked as (b) in the figure. In general, if the Poisson's ratio of mortar is less than that of the unit, variations in it are not expected to affect the strength of masonry [141].

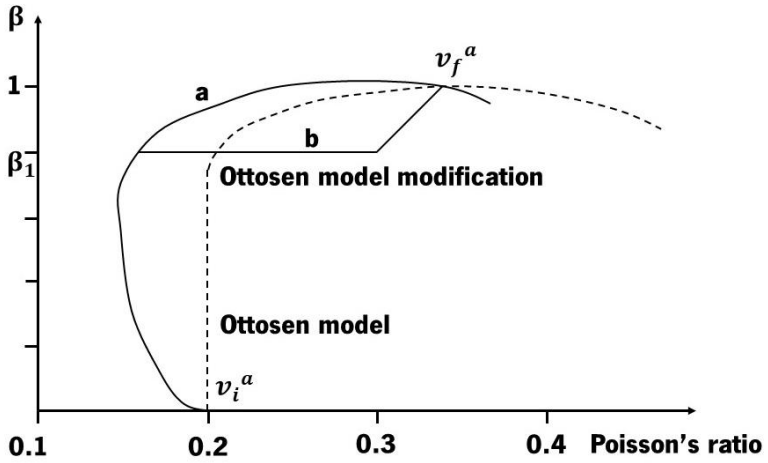

Figure 8: Ottosen model and modification [118]

Considering the contradictory observations in the little data available on this subject, it is important to systematically assess the influence of different factors on Poisson's ratio of mortars. Experimental values of static Poisson's ratio of mortars have not been widely researched, authors usually employ average or representative values for analytic expressions [141-143]. It is also possible to find studies focused on measuring dynamic Poisson's ratio of mortars [144, 145]. However, in the absence of a standard or widely accepted method of correlation between dynamic and static values of Poisson's ratios, these studies remain at best, only an indication of static values of Poisson's ratios. The value of Poisson's ratio usually used for concrete is around 0.2 [146, 147]. And it is possible to observe from literature, that the general range of Poisson's ratio obtained/used for mortars (lime, cement, or blended) is around 0.2 as well, often ranging between 0.15 to 0.25 [134, 148-150].

2.3.6 Fracture energy and crack propagation

Fracture energy may be defined as the energy required for crack propagation, or to create one unit area of a crack [151, 152]. One of the most famous mathematical descriptions has been provided by Griffith applicable for homogenous, brittle materials under uniaxial tensile stresses, which relies on an energy balance approach and links the extent of plastic deformation associated with the crack extension to a quantitative figure, shown in (Equation 1) [153-155]. Here, 'a' indicates the size of the smallest crack that can be detected where 'γ' is the surface energy, σ is the associated stress level and E is the E-modulus.

$$\sigma = \sqrt{\frac{2E\gamma}{\pi a}} \qquad 1$$

While in brittle materials, the energy is released from rupturing of chemical bonds along the plane of cracking, in more ductile materials this energy is associated with plastic flow near the crack tip [152]. Since Griffith's model was based on balancing surface energy and total strain energy released per unit volume upon the development of the crack; it was found unsuitable in the case of ductile materials [155]. Irwin *et al.* [156] modified the equation to account for the energy dissipated due to plastic flow in the proximity of the crack tip introducing the parameter critical strain energy release rate G_f, shown in (Equation 2).

$$\sigma = \sqrt{\frac{2EG_f}{\pi a}} \qquad 2$$

In this approach, the assumption is that a unit area of crack is formed when the energy released G_f is greater than or equal to the energy absorbed [157]. This critical energy that causes crack propagation can be determined by experimentally obtaining the corresponding critical load that is required to fracture a specimen with a pre-defined crack length (a), typically in a three-point bending test [155, 158]. While several advanced analytical concepts have been proposed over time by different authors for determining fracture energy, the most commonly used method to determine fracture energy in mortar and concrete is the three-point bending tests of samples with a pre-defined notch in them, based on the recommendations of RILEM, which relies on calculating fracture energy as a ratio of work done during the test to the area of the ligament of the specimen being tested as shown in (Equation 3) [158, 159]. W is the work done during the test, b is the width of the specimen, d is the depth and a is the size or length of the notch. In the RILEM recommendation itself, the work done is calculated as a sum of the area under the force-displacement curve and a factor associated with the mass of the setup.

$$G_f = \frac{W}{b(d-a)} \qquad 3$$

Elices, Planas, and Guinea [160-162] put forward a series of three articles discussing the influence of different factors such as the experimental procedures being used, the tail of the force-displacement curve, and energy dissipation during the test, and finally put across a more refined expression built on what was proposed by RILEM [158]. The modified expression took into account measured and unmeasured work that was done due to the force-displacement tail, in the numerator (W_m+W_{um}) and has been used by different authors since to evaluate fracture energy of specimens. Garijo *et al.* [94] used these modified expressions to evaluate the fracture energy of hydraulic lime mortars with different water-binder ratios and found values to range between 4 to 13 N/m. The fracture energy of air lime mortars was found to

range around 5 N/m in the literature [163]. In the case of lime-cement mortars, fracture energy is reported to decrease as the quantity of lime in the binder increase, with values ranging between 7 and 44 N/m for lime-cement mortars with B/Ag ratio 1:6 and 75%, 50% and 25% lime in the binder [164]. Not surprisingly, fracture energy is yet another parameter that has been much more extensively studied in the case of concrete or cement-based mortars, over lime-based materials [165, 166]. From reviewing the tendencies found in the fracture energy of concrete it is known that increasing the size of the aggregates or the specimen, decreasing the water/binder ratio, or decreasing the ratio of the predefined notch to the depth of the beam specimen, lead to an increase in fracture energy [159, 166]. The presence of fiber reinforcements leads to an increase in the fracture energy of the concrete, though this depends on the type of fiber used [166, 167]. In this regard, the presence of fiber reinforcements has also been found to increase the fracture energy of lime-based materials [168]. Broadly though, most studies on fracture energy were found to focus on concrete [159, 169, 170]. Adequate data could not be found to spot contradictions or specific trends on fracture energy as a function of lime content in the binder.

2.3.7 Open porosity

Porosity is commonly used to discuss the pore structure of a given material and refers to the volume of void space of a material, as a function of its total volume [171]. It is usually linked with the strength and durability of mortars and the amount of water in the pores not only influences both carbonation and hydration but also affects mechanical properties such as stiffness and shrinkage [172-175]. Furthermore, porosity has been reported to be affected by the type of binder used, the water binder ratio in the mortar, the B/Ag ratio, the mineralogical nature of the aggregate used, its particle size distribution as well as the ambient environment of the mortar [172].

Unless otherwise specified, porosity that is usually referred to, is ‘open porosity’, versus total porosity which is a combination of open and closed porosity. These two types refer to the interconnectivity of pores, with the word ‘open’ implying permeability to gases and liquids, while ‘closed’ refers to isolated pores that do not connect to the main pore structure of the material [172]. The methods that are widely used to measure open porosity and pore size distribution are the water immersion method and mercury intrusion porosimetry (MIP) respectively. The former involves, placing specimens in a vacuum for a predefined period, followed by complete immersion in water, under vacuum [176]. Porosity is then calculated as a function of the saturated weight of the specimen, measured in water and air, and the dried weight of the specimen expressed in percentage. MIP is a technique [176], that involves pressurizing mercury into the pores of the material being tested. Larger pores are expected to fill initially, followed by

smaller pores getting filled as the applied pressure increases. This method is capable of providing information on the porosity, pore size distribution, and pore volume of a given material [56, 66]. Porosity in this method is calculated as a function of the volume of mercury that penetrates the specimen, and the weight and bulk density of the specimen.

Silva *et al.* [7], reported that for the same binder-aggregate ratio (1:3), the pore size distribution of lime mortars is bimodal (with peaks at 0.5 and 30 mm) and that of cement mortar is unimodal (with peaks at 0.3 mm). On mixing the two binders, this clear demarcation begins to blur and there is a shift observed in the size of the pores as well as their distribution curves. With increasing hydraulic content in the binder, there is an increase in pores with less than 0.01 mm size and a decrease of pores with 10 mm size. The pore sizes mentioned will vary based on the quantity and type of aggregates used, even if the binder remains unchanged. While increasing the quantity of aggregates leads to an increase in the porosity of cement mortars, in the case of lime mortars, the highest quantity of binder exhibits the highest porosity as well [58, 177].

In lime-cement mortars an increase in open porosity of blended pastes and mortars corresponded with increasing quantities of lime in the binder [2, 45]. However, the literature on the effect of lime or cement in blended mortars is not unanimous. Cizer *et al.* [48] report that the porosity of mortars increases with increasing quantities of lime in the binder and ranges between 18% and 28%. Contrastingly, Arandigoyen *et al.* [59] found the open porosity of mortars (around 20%) to be independent of the lime-cement proportion in the binder. This is unexpected since the same research group found the porosity of lime-cement pastes to increase with increasing quantities of lime [45, 66, 67]. Yet another trend, was reported by Macharia [95], who found the values of porosity of lime-cement mortars to range between 20% and 30%, with an increase in porosity only up to 45% lime in the binder by mass, followed by a subsequent decrease in values of porosity. This suggests that in lime-cement mortars, there might be a desirable or optimum ratio with regard to porosity and pore structure. However, there is a lack of unanimity in trends and quantitative values of porosity of lime-cement mortars.

2.3.8 Drying shrinkage

ASTM C596-01 [178] defines drying shrinkage as the change in length of a specimen due to a sum of factors excepting any external applications of force, instated conditions of temperature, relative humidity, and evaporation rates. Drying shrinkage is also associated with volume changes in materials, typically reduction when it is exposed to drying [179]. This phenomenon is of relevance because when it occurs

in the presence of external restraints imposed on the material, tensile stresses may develop and lead to cracking [179]. In the case of concrete, where members might be several centimeters thick, moisture gradience between the surface and the bulk of the specimen also plays a role in the development of stresses, however, in the case of mortars in masonry, this factor usually is not of great concern [62, 179]. In cement-based materials, drying shrinkage along with autogenous shrinkage has been extensively researched in the last few years, since it is linked with studies of moisture transfer, porosity, and ultimately durability of the material [180-183]. However, the same attention has not been provided to the drying shrinkage of lime-based mortars [184, 185]. This is surprising since, drying shrinkage can happen in any mortar and the corresponding cracks are bad for the durability of the materials because they allow the ingress of moisture and possibly unwanted harmful chemical salts [186, 187]. For cement mortars, the values of drying shrinkage found in the literature were found to stabilize by 30 days and were in the range of 700-1200 μm/m, depending on their compositions and the incorporations of admixtures [188-190]. One of the articles that were found to discuss lime-cement mortars reported drying shrinkage to reduce in the order of air lime mortar, lime-cement blended mortar, and hydraulic lime mortar, with values in the range of 6000, 2000, and 1500 μm/m respectively [62]. The general range of drying shrinkage values of lime-cement mortars (800-1200 μm/m) was found to be higher than those of cement mortars (600-900 μm/m) [185, 191]. Furthermore, within lime mortars, lime putty is reported to exhibit more shrinkage than hydrated lime powder [192]. To the best of the author's knowledge, no work was found discussing the impact of the quantity of lime in the binder on the drying shrinkage of lime-cement mortars.

2.3.9 Summary

The literature on the impact of lime in mortars was found to be primarily focused on strength, stiffness, and porosity. In the case of the former, despite established trends, there is a lack of quantitative assessment [48, 59] and in the case of the latter, there is contradictory information [48, 59, 95]. Based on the review, one may however expect that an increase in lime in a lime-cement mortar would lead to lower strength and stiffness [48, 118][48, 118][48, 118][34, 110] and higher porosity [48, 59]. Regarding stiffness, no work was found discussing the E-modulus of lime-cement mortars in early ages (< 7 days).

Regarding properties such as Poisson's ratio, fracture energy, and drying shrinkage, adequate literature on lime-based mortars was not found to permit discussion on trends or contradictions in them. However, a general range of expectable values was found for each of these properties, either from tests on predominantly cement-based mortars or scattered works on lime-based mortars. For Poisson's ratio of

mortars, values were found to lie between 0.15 and 0.25 [134, 148-150]. In the case of fracture energy, values found varied in the range of 7 – 44 N/m, with values decreasing as the quantity of lime in the mortar increased [164]. And finally drying shrinkage for lime-cement mortars was reported to be around 600 – 900 μm/m [185, 191].

Furthermore, since this collective information comes from multiple sources, with different materials and operators involved in each case, direct comparison becomes difficult. There is a clear lack of a comprehensive study that uses the same materials and protocols to test several mechanical properties focusing on the lime-cement ratio in the binder. Results obtained from such experiments will also serve as useful inputs for numerical modeling. There is also scope for exploring the correlation between different parameters, which could optimize the number of tests required for a given set of materials or serve as a method to cross-check results obtained.

2.4 Influence of lime-cement mortars on the mechanical behavior of unreinforced masonry

Masonry elements primarily resist loads in the vertical direction but are also often subject to lateral loads such as wind pressure and earthquakes (Figure 9). The weakness in such cases usually lies at the interface of unit and mortar, and therefore, good bond strength is crucial to ensure adequate resistance of masonry to shear and tension [193]. The influence of mortar on the mechanical behavior of masonry has been addressed in the literature, but most studies discuss the behavior of masonry in compression [13], with a few of them focusing on bond strength [194-196]. However, there is a lack of knowledge on the influence of lime in the mortar on these properties of masonry. Because of this, regarding different lime-cement ratios, there is also a gap in the correlation of different scales of study, from the mortar level to the bond between brick and mortar to wall panels to full scale structures. And this information is crucial to optimize the choice of mortar for a given unit, not just to satisfy design requirements for masonry but also to obtain the best combination possible of strength, porosity, workability and shrinkage characteristics of the mortar [8, 197]. This segment, therefore, discusses the contribution of mortar to the compressive strength, stiffness, flexural resistance, and bond strength of masonry, focusing on the presence of lime in the binder. It also addresses the in-plane shear resistance of masonry wall panels.

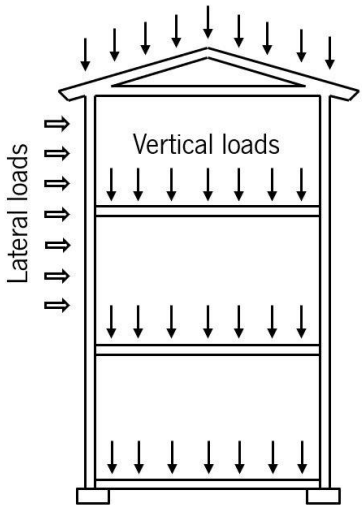

Figure 9: Vertical and lateral loads on masonry

2.4.1 Masonry in vertical compression

2.4.1.1 Strength

Compressive strength of masonry is a parameter that has been investigated widely by researchers and is measured in Europe according to EN 1052-1 [17] which recommends dividing the maximum vertical load applied on the specimen without restraint or eccentricity, by the loaded cross-section of the specimen. Compressive strength is known to be affected by a variety of factors such as the type of unit and mortar used, the relative strength and stiffness of the components, and it naturally also depends on the bond between the unit and mortar [135, 195, 198-207]. The type of masonry bond, i.e. the arrangements of the units and the texture, greatly influences the response of masonry to compressive loads [148, 201, 208]. It has also been reported that the compressive strength of masonry decreases as its height to thickness ratio increases [209-211]. Results on the effect of joint thickness on strength of masonry are conflicting, with some researchers suggesting an optimal thickness of 2 cm [212], while others suggest that strength of masonry consistently decreases as the thickness of joint increases [150, 213, 214]. The use of thinner mortar joints is recommended based on mechanics, since they are expected to reduce lateral tensile stresses in the units and increase the stress confinement in the mortar, consequently increasing its strength [215]. Indeed, it is common to find masonry with joint thickness around 10-12 mm [12, 13, 216], providing this is sufficient to accommodate the geometric tolerance of the masonry units.

In addition to these factors, the anisotropic and inhomogeneous nature of masonry provides additional complexity [217]. Different researchers have tried to estimate the compressive strength of masonry based on the properties of its components [136, 193, 218, 219]. One of the earliest attempts at this

quantification was made in 1971 by assuming linear elastic behavior of masonry [150]. Since then, considerable development has taken place in this field with the use of non-linear micro-mechanical models, artificial neural networks, and fuzzy logic to predict the behavior of masonry in compression [148, 220-224]. The bottleneck in this development is the need for a wide range of experimental data to calibrate the models [220, 223]. So until these models start producing reliable results for different cases, simple analytic expressions, estimations, and trends are essential to understand the behavior of masonry. From the experiments in the literature, on various units and mortars, it may be also be concluded that the strength of the masonry is dependent on the strength of the unit to a much larger extent than that of the mortar. For joint thicknesses of 10 and 15 mm, an increase in the strength of mortar by 150% leads to an increase in the strength of masonry of only 16% and 36% respectively [225]. In tests on filled and unfilled concrete masonry prisms, an increase in mortar strength of 250% led to an increase in strength of only 35% [11]. It has been shown that in the case of ungrouted prisms, increasing the compressive strength of mortar by almost 72% led to an increase in the strength of masonry by only 20% [226].

One of the most commonly used expressions to estimate the strength of masonry involves the strength of the unit and the strength of mortar and is of the nature as shown in (Equation 4).

$$f_k = K f_b^{\alpha} f_m^{\beta} \qquad 4$$

Here, f_b is the compressive strength of bricks and f_m that of the mortar, while the values of K, α, and β vary based on the experimental data being used. A summary of these values, from some of the most frequently appearing works in the literature, has been presented in Table 1. From this data, it is possible to observe that almost all the expressions have a higher value of exponent for the strength of unit than the strength of mortar. Only one work uses the same value of exponent 0.5 for unit and mortar [227].

Table 1: A summary of values of K, α, and β (Equation 4) as presented by different authors

K	α	β	Source
Variable (~0.55)	0.7	0.3	Eurocode 6 [18]
0.83	0.67	0.33	Mann [228]
0.25	1.03	0.28	Sajanthan *et al.* [229]
.275	0.5	0.5	Dayaratnam [227]
0.63	0.49	0.32	Kaushik *et al.* [13]
0.3	1	-	Bennet *et al.* [230]

.317	.866	.134	Gumaste *et al.* [216]
.35	.65	.25	Christy *et al.* [231]
.69	.6	.35	Kumavat *et al.* [232]
.317	.531	.208	Hendry *et al.* [233]
.886	.75	.18	Sarhat *et al.* [234]
.75	.75	.31	Lumantarna *et al.* [235]
0.9	.67	.33	Rostampour [236]

Studies have shown that in addition to their strength, the volume fractions and the height to thickness ratio of mortar and unit, may also be important contributors to the compressive strength of masonry [237, 238] [201]. Expressions accounting for such parameters, obtained from regression data of over 200 tests, have been compared with equation 4 [201], and interestingly both have led to good estimations [201], especially the one presented by Kaushik *et al.* [13]. Similarly, in comparison with results from artificial neural networks [220] feeding on data of 96 masonry specimens, equation 4 was found to predict the compressive strength of masonry well, especially the expression of Mann [228]. The commonality in the expressions of Kaushik *et al.* [13] and Mann [228] is the exponent used for the strength of mortar, 0.32 and 0.33 respectively (Table 1). And while the value of this exponent appears to vary from 0.18 to 0.5, the average appears to be around 0.3 (Table 1).

2.4.1.2 Stiffness

Even if the mortar is not the main contributor to the strength of masonry, it does appear to play an important role in the deformation capacities of masonry, especially governing its non-linear behavior [239-241]. Due to differences in stiffness of unit and mortar, there is bound to be an unequal distribution of deformations and stresses in the two components, compared to masonry as a whole [143]. Furthermore, in a state of uniaxial compression of masonry, the difference in stiffness of the unit and mortar also results in a state of triaxial compression in the mortar and compression-biaxial tension in the unit [113, 199] (Figure 10). However, this state of stress would only happen when the unit is adequately stiffer than the mortar, causing the weaker mortar to exhibit non-linear deformation early in the loading process and consequently causing the unit to undergo plastic deformation only later on [134]. Since triaxial compression leads to an increase in strength of the mortar while the unit is being subjected to lateral tensile stresses, it would typically be the unit failing first in tension, with little damage occurring in the mortar joint [242].

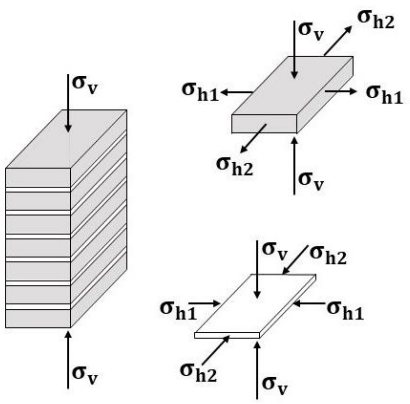

Figure 10:Depiction of stresses in masonry when unit is stiffer than the mortar [129]

When the mortar is stronger and stiffer than the unit, the mortar joint is subjected to a state of compression-biaxial tension, causing damage to it [143]. However, once again the failure of masonry is guided by the unit, this time crushing under compression. And if the mortar is stiffer but weaker than the unit, it is still the unit that is expected to fail by crushing in compression [143]. This implies, that regardless of the relative strength and stiffness of unit and mortar, the compressive strength of masonry is guided by the strength of the unit, whereas the mortar guides the deformation and failure mode of masonry [136], as was also proposed by Atkinson *et al.* [136]. Indeed, depending on the strength of the mortar, and possibly the type of binder used, the failure mechanism may vary [133]. While experimental evidence of this behavior at the mortar level has been shown through triaxial tests, at the masonry level, the influence of the type of mortar used, has also been investigated by a few researchers [12, 134, 243]. The most relevant of which for this research, is probably the work of Kaushik *et al.* [13], who studied two cement mortars of composition 1:3 and 1:6 and one lime-cement mortar 1:2:9, the strength of which lay between that of the two cement mortars. They observed that while the strength of masonry with different mortars was in the descending order of 1:3, 1:2:9 and 1:6, the failure strain or ductility did not follow the same order. It was the mortar with lime in its binder, 1:2:9 that led to maximum ductility of the three mortars, with almost 50% greater ductility compared to masonry with 1:3 cement mortar, while the strength was only 13% lower [13]. This is a great starting point for further investigation of the presence of different quantities of lime in the binder of the mortar, on the strength, stiffness, and deformation behavior of masonry. The presence of lime in the binder (1:1:6), compared to a cement mortar (1:3) leading to increased deformability of masonry, and lower strength has been confirmed by other researchers as well [11]. Beyond a point, the use of a strong and stiff mortar is unlikely to cause an increase in the strength of masonry [12, 13].

Another observation is that as the strength of the mortar reduces, the stress-strain relationship of masonry becomes increasingly non-linear [12]. This is particularly relevant in the discussion of the stiffness of masonry, since almost all the experimental data available in the literature on E-modulus of masonry, is obtained from the slope of the stress-strain curve of masonry in the form of secant modulus assuming linear behavior until 33% or 50% of its maximum capacity [11, 12]. Indeed EN 1052-1 [17] recommends assessing E-modulus as the secant modulus at 33% of the maximum compressive strength, from the stress-strain curve of masonry. There is not much work available in the literature, that evaluates the E-modulus of masonry through cyclic compressive loading, even in studies where the behavior of masonry has been studied extensively [244, 245]. In studies where the cyclic compressive behavior of masonry is studied, it is done so with cycles of imposed vertical displacements that increase gradually, aimed at understanding the seismic response of masonry [246, 247]. Therefore, in the absence of data on E-modulus obtained from cyclic loading, what is more easily available is a correlation between compressive strength and secant E-modulus of masonry [13]. Many international standards allow for the estimation of the E-modulus of masonry from the value of compressive strength, such as the International Building Code [248] and Eurocode 6 [18] which recommend E-modulus to be assessed as 700 and 1000 times the compressive strength, respectively. However, this value varies widely in the literature and could be anywhere between 200 and 1700 [13, 249] [243]. In the case of lime-based mortars, experimental data shows that this value varies between 80 and 230 with the value increasing, with the hydraulicity of the mortar [12]. Researchers have also explored the possibilities of non-linear relationships between compressive strength and E-modulus of masonry (polynomial [12] and parabolic [250]). Evidently, there is not much consensus on how to estimate the E-modulus of masonry as a function of compressive strength. And if one is to account for the wide variation in mortars and units used, the complexity only gets compounded, not to forget that this discussion is based in the context of secant modulus of elasticity. There is not much literature available for comparison on E-modulus obtained from cyclic loading.

2.4.1.3 Stress-strain relationship

Eurocode 6 [18] suggests that the stress-strain relationship in masonry is non-linear in nature, and presents a parabolic curve as a typical curve for any unit used while allowing idealizations of parabolic-rectangular shapes as well as linear or rectangular for design purposes. Different researchers have presented analytic expressions to estimate the stress-strain relationship of masonry and concrete [131, 245, 251-255]. One of the most commonly used expressions is a dimensionless form of the stress-strain curve of masonry corresponding to a parabolic shape [256] and has been shown in equation 5. Here, σ

and ε correspond to stress and strain in masonry, while f and ε_m correspond to peak stress and corresponding strain respectively. The application of this expression extends up to 90% of the peak stress (f) in the post-peak part of the curve.

$$\frac{\sigma}{f} = 2\frac{\varepsilon}{\varepsilon_m} - \left(\frac{\varepsilon}{\varepsilon_m}\right)^2 \quad 5$$

Kaushik *et al.* [13] used equation 5 to describe the pre-peak part of their experimentally obtained stress-strain curves, as well as the post-peak behavior until the peak stress (f) is reduced to 90% of its value. Thereafter, a linear path was proposed from $0.9f$ to ($2.75\varepsilon_m$, $0.2f$) and ($2\varepsilon_m$, $0.2f$) for mortars with and without lime in their binder respectively, based on regression of experimental data. This approach has also successfully been used by other researchers [12, 257], for the comparison of experimental and analytical data including compressive tests on masonry with hydraulic lime, air lime, and lime-cement mortars.

To estimate values of strain corresponding to peak stress, expressions have been proposed either only as a function of strength and mortar [198] or involving the strength and stiffness of masonry (Equation 6) [13]. While in some cases equation 6 has led to severe underestimation of experimental results (-80% to -90%) [12], in other cases it was adapted successfully by modifying the values of constants [257].

$$\varepsilon_m = \frac{0.27\, f}{f_m^{0.25} E_{masonry}^{0.7}} \quad 6$$

2.4.2 Flexural strength

One of the biggest vulnerabilities of unreinforced masonry is its response to out of plane, lateral loads, which becomes especially prominent during earthquakes [258-260]. This inherent weakness has been attributed to masonry being weak in tension [261-263]. And while in the last few decades, several strengthening techniques have been proposed and attempts have been made at numerical modeling of the out of plane behavior of masonry, it has been shown that further research is necessary in understanding the influence of different parameters on flexural strength of masonry, to improve the seismic response of buildings [264, 265]. The type of bending depends to a large extent on the support conditions of the wall, with one-way vertical bending (i.e. flexure parallel to bed joints) occurring when the vertical edges are free, and the top and bottom edges are supported [194]. Meanwhile, if the vertical edges are supported and the bottom of the wall is not too restrained, horizontal bending occurs (i.e. flexure perpendicular to bed joints) [194]. Finally, if all sides of the wall are supported, two-way bending

tends to occur, leading to a greater capacity. The response of masonry in bending is much better in the horizontal direction (perpendicular to the bed joints) compared to the vertical direction (parallel to the bed joints) because in the former case, the resistance stems from the friction between bed joints as well as from the bond strength of the head joints, while in the latter case, resistance is known to usually rely only on the bond strength of the bed joints [261].

Eurocode 6 [18] recommends the design of laterally loaded walls, by providing bending moment coefficients based on a yield analysis method, and relies on flexural strength of masonry [266]. The yield line analysis method assumes the collapse mechanism to be composed of rigid blocks and rotations to be along crack lines where deformations are concentrated, at the ultimate stage. And when bending moment reaches yield value, along any crack line it stays so until all contributing cracks attain the yield moment capacity [261]. While several researchers have argued against the use of the yield line analysis method, since the formation of plastic hinges or yield lines is not possible in non-ductile masonry [267, 268], experiments have shown that when failure in the two orthogonal directions happens simultaneously, the yield line theory predicts the failure load quite well, though it is unable to do so when cracking precedes failure [269].

The bending moment calculated in Eurocode 6 [18] is from the characteristic value of flexural strength, which may be obtained from a table that categorizes values based on the strength of mortar and the type of unit used. Alternatively, it may be obtained through experiments of four-point bending tests (Figure 11) according to the recommendations of EN 1052-2 [270].

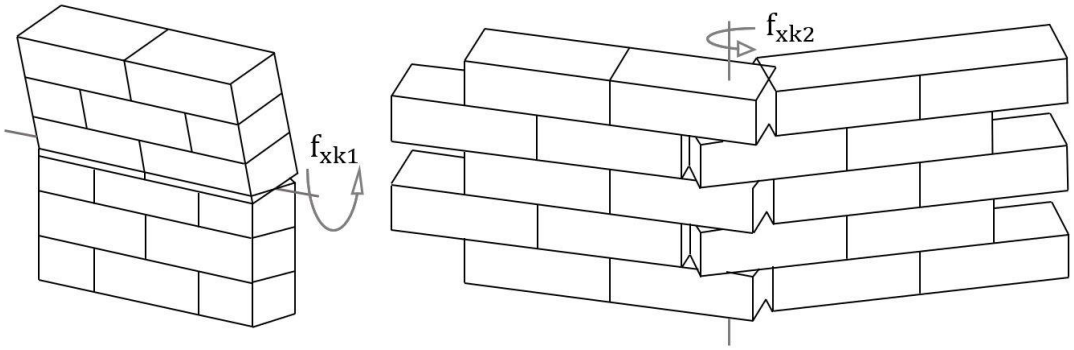

Figure 11: Flexural strength of masonry parallel (f_{xk1}) and perpendicular (f_{xk2}) to bed joints [271]

It is reported that with regard to out-of-plane behavior, material properties do not influence the lateral strength and corresponding displacement capacity as much as factors such as geometry, applied vertical force and boundary conditions do [272]. Openings in the walls are also reported to play a role in the out-of-plane response, regarding both, their positions as well as dimensions [273, 274]. Van der Pluijm [275]

investigated the influence of test methods and sizes of specimens, and also highlighted that flexural strength is a structural property, rather than material. There have been various studies investigating flexural strength, to understand the influence of different types and combinations of mortars and units, as well as the effect of reinforcements [276-278]. One can also find studies focusing on the influence of factors such as cementitious composites and FRP laminates [279, 280]. However, to the best of the author's knowledge, studies focused on investigating the presence of lime in the binder on the flexural strength (f_{xk1} and f_{xk2}) of masonry could not be found [240, 270]. However, it is possible to find studies on the impact of lime in mortars on the flexural bond strength of masonry [14, 195].

Flexural bond strength may be measured using the bond wrench test (Figure 12), according to EN 1052-5 [281]. It is reported to increase with increasing strength of the mortar, with values ranging from 0.002 to 0.215 MPa [195]. Experiments performed on burnt clay bricks and stabilized mud, as well as soil-sand blocks, also confirm that the strength of the mortar contributes to an increased flexural bond strength in masonry [14]. When different lime-cement mortars were tested, flexural tensile bond strength, in general, was found to increase with increasing cement in the binder [282]. This is expected since increasing cement in the binder, also leads to an increase in the strength of the mortar. However, it was interesting to note that when a lime-cement mortar (1:1:10, f_c 3.3 MPa) was compared with a cement mortar (1:6, f_c 3.6 MPa), the bond strength obtained was better with the former, despite having a lower compressive strength at the mortar level. It is possible, therefore, that while the compressive strength of the mortar is an important indicator of flexural bond strength of masonry, it is not adequate by itself, and the effect of using different materials would merit further investigation.

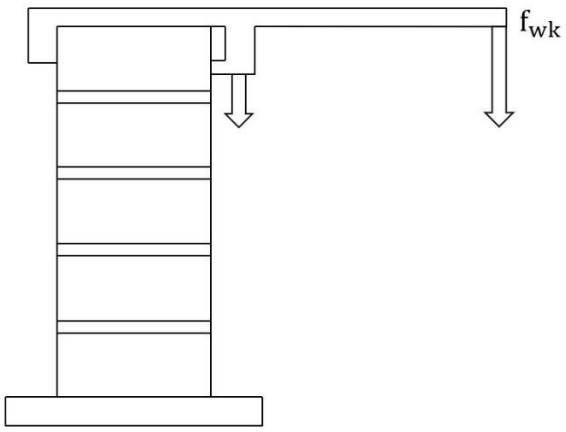

Figure 12: Flexural bond strength of horizontal bed joints in masonry using a bond wrench [195]

The possibility of a correlation between flexural bond strength measured using the bond wrench test [281] and flexural strength (parallel to bed joints) from the four-point bending test [270], has been explored by

some researchers [283]. Experimental values of flexural bond strength are reported to be higher than flexural strength (parallel to bed joints) obtained from prisms, which in turn are higher than those obtained from wallets [275]. Furthermore, when tested in bending, the strength of masonry also depends on the number of joints in pure flexure. Based on the weakest link theory, masonry specimens are often treated as beams in bending with joints of different strengths, and since one of them is bound to fail first, the strength of the beam is determined by the strength of its weakest joint [284, 285]. Van der Pluijm [275] showed using order statistics that for a coefficient of variation of 25%, the flexural strength obtained from a masonry specimen with 4 joints in pure flexure, would be 0.7 times the value of flexural bond strength in the joints.

2.4.3 Shear bond strength

Shear bond strength is an extremely important parameter of masonry and has been studied by different researchers [195, 286]. It is typically investigated through experiments using couplet or triplet specimens, with the latter being more common [287-289]. In Europe, shear bond strength is tested through triplet specimens and is done according to the recommendations of EN 1052-3 [290]. It involves the application of three distinct levels of perpendicular pre-compression, while a lateral load is applied to shear the unit-mortar joint (Figure 13). The maximum shear strength obtained is recorded for each level of perpendicular pre-compression, and experimental data are analyzed to obtain values of initial shear strength or characteristic shear strength of the materials being tested. This method involves the use of Mohr-Coulomb law to describe failure, which establishes a linear relationship between normal stress (σ) and shear stress (τ) (Equation 7) [291]. Here, c is cohesion, also known as initial shear strength (f_{vo}), and tan ϕ is the coefficient of friction. This relationship is valid for only low and moderate normal stresses since at higher values, crushing and cracking of the unit is possible [291].

$$\tau = c + \tan\phi . \sigma \qquad 7$$

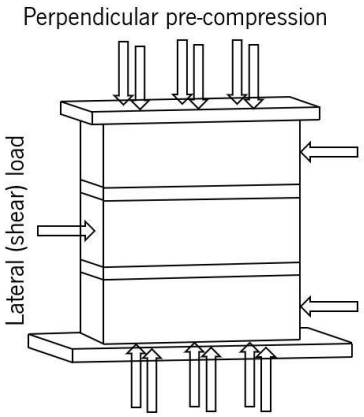

Figure 13: Triplet masonry specimens used to determine the initial shear strength of masonry

EN 1052-3 [290] allows the determination of initial shear strength by testing specimens in the absence of normal stresses, this however implies that information about friction between unit and mortar is lost. Another parameter associated which is often studied, in association with shear bond strength is the angle of dilatancy (ψ), the tangent of which ($\tan\psi$) is defined as the ratio of normal to shear displacement [286, 292]. It is an indication of the volume change associated with inelastic shearing deformation and is known to linearly decrease with increasing pre-compression [275, 286].

It is possible to find research [196] focusing on the effects of pre-compression on the peak shear stress on (wire-cut, clay) brick masonry and cement mortars of different strengths (10-30 MPa). Shear stress increases with an increase in normal stress, and the relationship tends to become non-linear above 1 MPa of vertical pre-compression. The values of cohesion increase with increasing strength of mortar, and also depended on other factors such as surface roughness and water absorption properties of the unit [196]. On the other hand, a relationship between internal friction and strength of mortar was not established, since the former was found to be independent of the latter to a large extent. The angle of friction was found to be around 45˚ by some researchers [196] but accompanied by significant variation. Initial shear strength has been tested for different lime-cement mortars and concrete blocks [293], with the primary focus being on the relative strength between mortar and units. It was found that both, the strength of mortar and unit contributed to an increase in cohesion, with higher values obtained the quantity of cement in the binder was increased. Another study reached similar conclusions by testing lime-cement mortars (1:2:9, 1:1:6 and 4:1:12) with different types of units, molded clay brick, extruded clay brick and concrete blocks, in triplet specimens. A higher quantity of cement in the binder led to higher shear bond strength for all types of units [282]. However, in both these studies, no vertical pre-compression was applied and therefore, there is a lack of information on the coefficient of friction. Values

of initial shear strength for lime-cement mortars were found to vary widely, ranging between 0.07 to 1 MPa [282, 293]. For lime-based mortars, the values of initial shear strength and coefficient of friction were found to lie between 0.15 to 0.43 MPa and 0.8 to 0.92 respectively [294].

Compared to flexural strength, information on the initial shear strength of masonry is more widely available in the literature, though not many of them focus on the influence of lime-cement ratios in the binder on the bond strength of masonry [282, 293, 294]. Even in the cases where different lime-cement ratios are compared, it is unfortunate that the tests were performed in the absence of vertical pre-compression and so information on friction, and the effect of lime on it is absent [200, 282].

Research has also highlighted a good correlation between initial shear strength and compressive strength of masonry, emphasizing that good bond strength would lead to an improvement in the compressive strength of masonry [200]. However, there is contradictory information on this, since some researchers found a poor correlation between the two properties through their experimental data [294]. Initial shear strength is also often correlated with flexural tensile bond strength of masonry across different units, with the former being approximately 1.2 times the latter [282]. The Australian standard AS 3700 [295] also recommends a correlation of shear bond strength being equal to 1.25 times the flexural bond strength. Other researchers have also found this to be true [288].

2.4.4 In-plane shear strength (combined vertical and horizontal loading)

Masonry typically fails in shear, when it is subjected to a combination of vertical and horizontal loads, as often happens in earthquakes [296]. And its response may be studied through quasi-static cyclic tests or dynamic shaking table tests [104]. Compared to dynamic tests, quasi-static cyclic tests may be a more suitable option for testing unreinforced masonry, because they facilitate accurate damage measurements, even if dynamic tests are capable of simulating seismic forces more accurately [297]. Quasi-static cyclic tests are also more conservative compared to dynamic tests because they lead to lower lateral capacities and greater damage in the specimens being tested [104]. The lateral strength capacity of unreinforced masonry is an important parameter, however, to evaluate the response of a structure to seismic loads, factors such as stiffness and strength degradation, energy dissipation, and overall ductility are also crucial. A high ductility factor in masonry indicates better non-linear deformation capacity and thereby better performance of masonry under seismic loading [104]. Usually, deformations are compared by accounting for a parameter called lateral drift which is expressed in percentage and is the ratio of lateral displacement and the height of the wall [104]. Energy dissipation is also an important indicator for evaluating the

seismic performance of a structure because high energy dissipation implies a potential reduction in demand for ductility [298]. In earthquakes since the direction of lateral loads reverses constantly, typically cyclic tests are designed to simulate the alternating direction of loads [206, 299-301]. The in-plane response of unreinforced masonry walls is known to depend on its geometry, vertical loads, boundary conditions and its mechanical characteristics as well as those of its constituents [296]. Furthermore, it is known that different failure modes are possible, based on the vertical load, quality and bond strength of unit and mortar (Figure 14) [302].

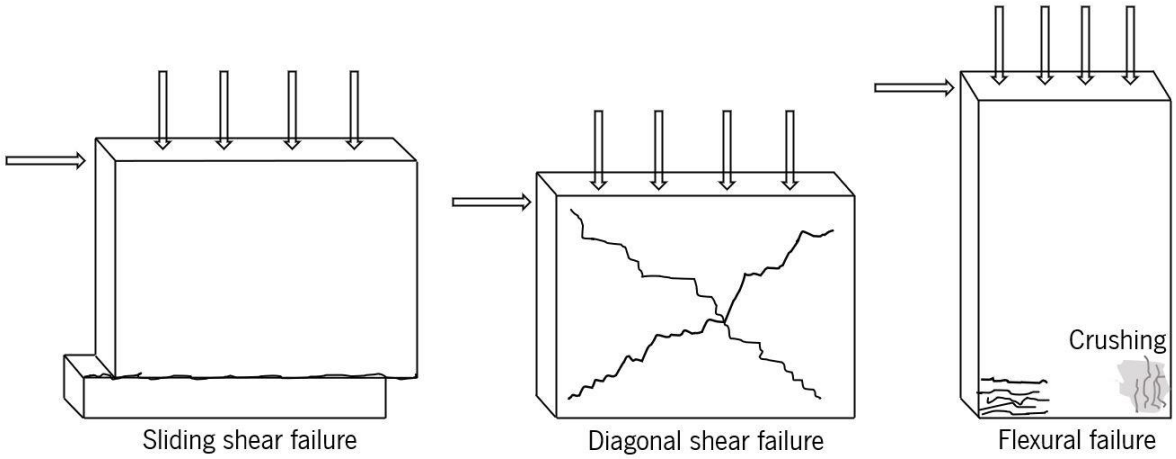

Figure 14: In-plane failure mechanisms of masonry subject to combined vertical and horizontal loading

The first type is known as sliding failure, which occurs as a result of low vertical stresses and typically poor mortar quality, causing the wall to shear into two and the sliding occurs between the two parts [303]. The characteristics of this type of failure mode are that it is stable, results in large displacements and energy dissipation, and is usually observed in the upper parts of buildings since they are subjected to lower vertical stresses compared to the bottom parts [296, 303]. The second failure mode is called diagonal shear failure and occurs when the principal tensile strength of masonry is surpassed by the principal stresses (in-plane) generated in it [303]. This failure mode is characterized by the development of diagonal cracks, low displacement capacity and relatively fast dissipation of strength and stiffness, and average energy dissipation, and is typically observed in the bottom part of masonry buildings. The formation of cracks through mortar joints, units, or both depends on the quality of the individual components [296]. The third mode of failure is called rocking-flexural failure and is usually associated with slender walls where the moment to shear ratio is high, low vertical stresses, high displacement capacity, and very little strength degradation and average energy dissipation in hysteresis. The final failure takes place with masonry being crushed at the corners [303].

Usually, in cyclic tests performed in the laboratory, flexural mechanisms develop in the beginning due to the low axial tensile strength of masonry and must not be mistaken as the final failure mode [296]. Development of horizontal tensile cracks in the bottom part of the specimens takes place near the supports, potentially accompanied by crushing of corners, but the resistance of the wall usually increases until it fails in shear. It is also important to remark that the first failure mode discussed above, that of sliding failure, is linked with shear bond strength, i.e., a function of cohesion and friction between the unit and mortar joints. The second mode of shear failure mechanism is guided by principal tensile strength [296, 304], and may be expressed analytically (Equation 8) by assuming that masonry behaves in an isotropic, elastic manner until failure [304, 305]. Here, σ is the vertical compressive stress, τ_{max} is the shear stress in the wall corresponding to maximum lateral load capacity and r is a factor that considers the ratio of height to length of the wall.

$$f_t = \sqrt{\left(\frac{\sigma}{2}\right)^2 + (r\,\tau_{max})^2} - \frac{\sigma}{2} \qquad 8$$

This failure could occur through the formation of a single diagonal crack, or two of them, and could pass through only the mortar joints, only the units (less common), or involve both mortar joints and units [306-308]. Even after the formation of diagonal cracks, the wall is usually expected to have some remaining bearing capacity, especially if it is composed of units and mortar of good quality [309]. Balasubramanian *et al.* [304] have presented a review of analytic formulae presented by different authors to estimate the shear capacity of masonry subjected to cyclic loads, categorized according to failure modes, which is useful for comparison of experimental results with analytical data. Eurocode 6 [18] recommends the determination of design value of shear resistance based on the Mohr-Coulomb law, and global strength parameters of masonry, with the initial shear strength of masonry depending on the strength class of the mortar and coefficient of friction for the wall equal to 0.4 (Equation 9.1), where l_c is the length of the wall under compression. However, it may be argued that this expression (Equation 9.1) is specific to shear failure due to sliding and has no relation with the tensile strength of masonry [206]. Another expression, that is frequently used to express the shear resistance of masonry has been presented by Magenes *et al.* [310] and is valid for failure through mortar joints (equation 9.2). It employs local (i.e. joint) material properties of cohesion and coefficient of friction, also accounting for the shear ratio (effective height/length of the wall) and influence of head joints (Equation 9.2). To account for the failure which may be initiated by shear-tensile cracking of bricks, equation 9.3 may be considered based on a proposal of Mann *et al.* [311]. For the rocking-flexural failure mode, one of the most commonly used analytic

expressions is based on equilibrium (equation 9.4) and has been proposed by Calvi and Magenes [310]. Here, j accounts for the vertical stress distribution at the compressed toe and usually has a value of 0.85, based on the assumption of an equivalent rectangular stress block. In all the analytic expressions presented, some accuracy has been sacrificed to permit speed and simplicity, however, this simplification allows the evaluation of relative importance of different parameters that contribute to the shear response of unreinforced masonry [297].

$$V_d = \frac{(f_{vko} + 0.4\,\sigma)\,t\,l_c}{\gamma_m} \qquad 9.1$$

$$V_d = l\,t\,\tau_{max} \text{ where } \tau_{max} = \min(\tau_c, \tau_w)$$
$$\tau_c = \frac{1.5c+\mu\sigma}{1+3c\alpha_v/\sigma} \text{ where } \alpha_v = \frac{h_o}{l}$$
$$\tau_w = \frac{c + \mu\sigma}{1 + \alpha_v} \qquad 9.2$$

9

$$V_d = lt\frac{f_{tb}}{2.3(1+\alpha_v)}\sqrt{1+\frac{\sigma}{f_{tb}}} \qquad 9.3$$

$$V_d = \frac{l\,t\,\sigma}{2\alpha_v}\left(1 - \frac{\sigma}{jf_u}\right) \qquad 9.4$$

Many researchers have investigated the response of masonry to cyclic loads with different types of reinforcements such as glass fiber reinforced polymers (GFRP) and fiber-reinforced cementitious matrices (FRCM) to study how different retrofitting techniques improve the lateral strength and energy dissipation capacity of masonry [306, 308, 312-314]. The response of masonry (stone) to in-plane cyclic loads has also been studied as a function of distinct textural typologies. Ductility was found to decrease as the irregularity of bonds in the masonry walls increased [315]. In lime-based unreinforced masonry, the performance of three lime mortars with B/Ag ratios 1:1, 1:2, and 1:3 was compared in quasi-static cyclic loading and it was found that parameters such as energy dissipation and stiffness increased, and ductility reduced with an increase in the compressive strength of the lime mortar used [307]. The general range of maximum drift capacity (%) for clay brick unreinforced masonry walls in the literature is reported to be between 0.43% and 1.06%, with an average value of 0.6% [316]. Furthermore, maximum drift capacity is known to decrease with increasing values of vertical loads applied [104, 316]. Regarding the maximum lateral capacity of clay brick unreinforced masonry walls, values were found to range between 0.3 and 0.5 MPa [296]. However, to the best of the author's knowledge research on this topic, focusing specifically on the influence of lime-cement mortars, could not be found.

2.4.8 Summary

Regarding masonry in vertical compression, it is known so far that including lime in the mortar leads to greater deformability, lower strength, and stiffness of masonry [12, 13]. However, it is also reported that, in general, while mortar does not contribute majorly to altering the strength of masonry, it does significantly influence its stiffness and deformation capacity [11]. In the case of flexural strength, not much research was found to directly focus on the influence of lime on the resistance of masonry parallel and perpendicular to the bed joints, however, there is consensus on flexural strength increasing with an increase in the strength of mortar [275]. Furthermore, it is also widely acknowledged that flexural strength in the perpendicular direction is higher than in the parallel direction to the bed joints [285]. Concerning flexural tensile bond strength, values are reported to increase with increasing strength of the mortar [14, 195]. However, some research has shown that this may not necessarily be true. A lime-cement mortar with lower compressive strength than a cement mortar was found to result in improved flexural bond strength [282]. It is evident, that there is need for more experimental research on this topic.

Initial shear strength of unreinforced masonry is a very important property that relies on the bond of materials of the mortar and unit and is often correlated with the flexural bond strength and compressive strength of the material [200, 282, 288]. Values of initial shear strength are reported to increase with the strength of the mortar, and range between 0.07 to 1 MPa in the case of lime-cement mortars [282, 293, 294]. However, the focus of these works is not on the influence of the lime-cement ratios, and even in the cases where different lime-cement ratios are compared the tests were performed in the absence of perpendicular pre-compression and so information on friction, and the effect of lime on it is absent [200, 282]. Finally, the failure of unreinforced masonry walls, subjected to combined in-plane vertical and horizontal loads is important to understand their mechanical behavior when subject to seismic action [104]. While studies specifically focusing on the influence of using different lime-cement ratios in the mortar on this aspect of masonry were not found, the general range of maximum drift capacity (%) for clay brick URM was found to be between 0.43% and 1.06% [316]. This is a wide range, and there is a need for not only deformation capacity, but also for factors, such as lateral strength capacity, stiffness and strength degradation and energy dissipation, to be assessed as a function of different materials used in the mortar.

From the discussion above, it is possible to conclude that the influence of lime in mortar on the behavior of masonry in compression has been relatively well explored compared to the behavior of masonry in flexure or shear, and especially under quasi-static cyclic loads [13, 240]. This is not ideal, since masonry

is designed to resist loads not just in vertical compression, but also in tension and shear. In the case of seismic activity, it is also important to understand its behavior when lateral loads are reversed. Since lime and cement are commonly used for the construction of masonry around the world, it is crucial to study their impact on the behavior of masonry, to optimize design and facilitate the choice of a compatible mortar for any given unit.

3. Materials, mortar compositions & protocols

3.1 Introduction

This chapter initially highlights the choices and characteristics of the materials used in this doctoral research, then elaborates on the mortar mixes considered, and subsequently introduces the masonry specimens investigated. The aspects discussed include the mineralogical composition of the binders and aggregates, the protocols adopted to prepare the mortars and, their curing conditions, the repeatability of results, and finally the construction of masonry specimens. To give the reader an overview of the experiments performed and the samples adopted, the chapter also presents a summary of the tests conducted at the mortar and masonry level. Detailed discussions on the methodology used for each test has been discussed in subsequent chapters (Chapter 4 - mortars, Chapter 5 - masonry), within the context of results obtained from each experiment. This chapter is primarily focused on providing the reasoning behind the choices of materials and on the preparation of samples (mortar and masonry).

One of the important intents of the present research was to ensure that the mortar mixes selected were representative, in terms of their compositions. A natural consequence of this was the workability of the selected mixes. It was of utmost importance that the mortars investigated in this research program were workable, usable by masons on the construction sites, and so this factor also played a significant role in developing mortar mixes. In particular, representativity contributed to the choice of the reference cement mix. Finally, the choice of materials has been strongly influenced by the intent to ensure repeatability of results in this research campaign, as well as scientific replication and comparison by other researchers. Within the framework of the above-mentioned priorities, the choice of the unit (brick) and possible alternatives for the construction of masonry specimens have also been discussed, together with the reasons that guided the final decision.

It is also important to explicitly state the involvement of the Mortar Task Force (MTF) of the European Lime Association (EuLA), in the context of this research program, specifically pertinent to this chapter. Decisions concerning the materials (binders, aggregates, and bricks) were made based on literature review and were complemented by technical discussions between the author, the supervisors of this Ph.D. and the representatives of MTF, EuLA, taking into consideration representativeness and the ability to translate the knowledge obtained from lab work to industrial and construction sites.

3.2 Raw materials

3.2.1 Binders

The materials used as binders for the mixes were air lime and Portland cement. The type of cement chosen was Portland cement CEM I - 42.5 R. Despite the knowledge that CEM II is more commonly employed in the industry, CEM I was chosen to reduce the number of chemical variables in the mix designs and improve repeatability. The reasoning for this is the composition of different types of cement in EN 197-1 [21]. According to the said standard, CEM II in comparison with CEM I, is allowed to have 30% more variation in its constituents apart from clinker, such as silica fumes, limestone filler, fly ash, calcined Pozzolana, and burnt shale. The composition of these constituents are themselves variable, based on the geographical location they are obtained from and the method of treatment, hence in an attempt to reduce variability, CEM I was chosen. Details of the corresponding batch of cement CEM I – 42.5 R used in this campaign were obtained from the technical data sheet provided by the manufacturer Secil, namely ACM-040/2016. The density and Blaine specific surface of the material specified was 3.12 g/cm^3 and 3508 cm^2/g respectively. The clinker composition consisted of 12.6% of C_2S and 62.2% of C_3S. The chemical composition of the main components of cement has been presented in Table 2. The term LOI refers to loss on ignition and was measured based on the recommendations of EN 459-2 [317]. The apparent bulk density measured was equal to 0.93 g/cm^3.

Table 2: Chemical analysis of main components of cement CEM I - 42.5R as provided by the manufacturer Secil

LOI (%)	SO_3(%)	MgO (%)	Al_2O_3 (%)	Fe_2O_3 (%)	K_2O (%)	SiO_2(%)	CaO(%)
2.05	3.05	1.75	4.27	3.2	0.77	20.55	63.4

The type of air lime chosen for this campaign was CL90-S. Similar to the choice of cement, the selection of the type of lime was based on minimizing the variables influencing the design of mortar mixes. According to EN 459-1 [43], compared to other types of air lime, CL 90-S has the least amount of variation in its chemical composition and the maximum amount of available lime, ≥ 80% by mass, and therefore, it was selected for this research. Lime was provided by Lhoist and details of its composition were obtained from the datasheet provided by the manufacturer for the corresponding batch used; control number 90000998782. The density and BET specific surface area declared were 2.24 g/cm^3 and 150000 cm^2/g respectively. The mean value of particle size distribution was reported to be in the range of 5.5-6.5 μm. The details of particle size distribution were obtained from laser diffraction (Malvern) (Table 3). The chemical composition of lime as obtained from X-ray fluorescence (Axios Panalytical), expressed as oxide equivalent has been presented in Table 4. LOI referring to loss on ignition was based on the

recommendations presented in EN 459-2 [317]. The apparent bulk density of lime measured was 0.36 g/cm^3.

Table 3: Particle size distribution (PSD) of lime CL 90 - S as provided by the manufacturer Lhoist

Diameter of sieve refusal (µm)	2	5	10	25	32	40	50	63	80	90	125	200
Quantity (%)	90.38	60.77	30.61	10.90	8.01	5.71	3.78	2.26	1.19	0.82	0.16	0.00

Table 4: Chemical composition of lime CL 90 - S as provided by the manufacturer Lhoist

LOI (%)	SO_3(%)	MgO (%)	Al_2O_3(%)	Fe_2O_3(%)	K_2O (%)	SiO_2(%)	CaO(%)
25	0.197	0.68	0.06	0.05	0.013	0.12	74.35

The total quantity of binder material required for this research campaign was estimated to be around 200 kgs of cement and 400 kg of lime, delivered in packages of 40 kg and 20 kg each, respectively. These quantities of material were obtained altogether at the beginning of the Ph.D. and stored carefully. The same batch of binder materials (cement and lime) were used in all experiments right up to the end, to make sure that no differences in the results arose from a difference in the raw materials used. Concerning long term storage of the binders, each bag of cement and lime was wrapped in two layers of low-density polyethylene plastic bag over its original packaging and subsequently stored in simple plastic barrels (Figure 15) in the basement of the University of Minho (UMinho) laboratory (21±1˚C and 70±5% RH). Each bag of plastic was knotted at its extremity and the knots of each of the layers of packaging were placed at opposite ends, to minimize contact of the material with ambient atmosphere and humidity (Figure 15).

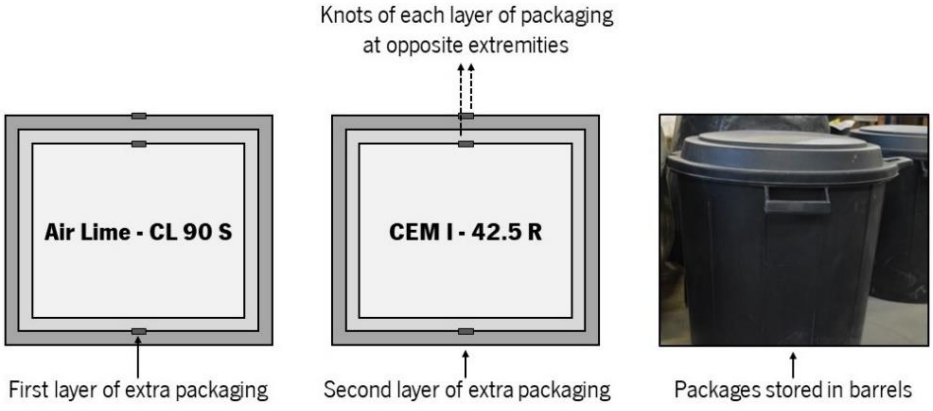

Figure 15: Packaging and storage of binders – lime and cement

Through the course of a few years, chemical changes in the materials are expected to occur, regardless of how carefully they are stored. To assess the condition of the materials after 4 years, thermogravimetric analyses (TGA) were performed on both lime and cement in February 2021. The results obtained from TGA have been presented, for both cement and lime in Figure 16 and

Table *5*. Figure 16 highlights the change in weight of the specimens with an increase in temperature, from 50˚C to 1000˚C. Both samples weighed around 22 mg (lime 22.55 mg, cement 22.72 mg) and were heated in a nitrogen atmosphere at a rate of 10 ˚C/min.

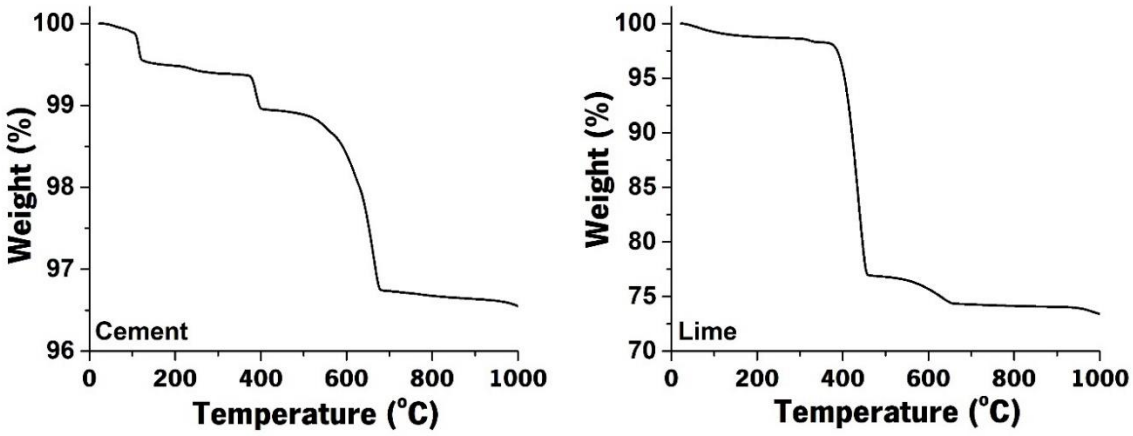

Figure 16: TGA of the binders - lime and cement, at the end of the research period

To analyze the data obtained from TGA, weight losses in the materials corresponding to specific ranges of temperature were quantified. It is known from the literature that compounds and phases decompose in characteristic temperature ranges [318-321], as has been specified in

Table *5*. These intervals of temperature were confirmed and adapted for materials tested in this research, with the help of the derivative of weight loss with respect to temperature. From the point of view of storage, in the case of lime, the important quantities to be compared involve the amount of physically adsorbed water (50-105˚C), calcium hydroxide (350-550˚C), and calcium carbonate (550-800˚C). In the case of cement, apart from the phases mentioned, chemically bound or non-evaporable water (105-350˚C) also needs to be accounted for, to evaluate the degree of hydration [318]. The method used to calculate the degree of hydration was originally proposed by Bhatty [322], also used by Monteagudo *et al.* [319], and has been presented in equation 10, expressed in percentage.

$$\text{Degree of hydration} = \frac{\text{Weight}_{\text{Chemically bound}} + \text{Weight}_{\text{Calcium hydroxide}} + 0.41\,(\text{Weight}_{\text{Calcium carbonate}})}{0.24} \qquad 10$$

Table 5: Details of TGA of binders (lime and cement) at the end of the research (Figure 16)

Weight loss corresponding to degradation of the compounds	Temperature range (˚C)	Quantities for cement (%)	Quantities for lime (%)
Adsorbed & free water	50 – 105	0.10	0.60
Chemically bound water	105 – 350	0.50	-

$Ca(OH)_2$	350 – 550	0.64	21.78
$CaCO_3$	550 – 800	2.06	2.34
Degree of hydration		8.28	-

All values in

Table *5*, have been expressed in weight % of the loss. It is possible to observe that the weight loss in the temperature range 50 – 105˚C, corresponding to free water, is small for both materials, < 1%. Furthermore, even after 4 years, not much carbonation has taken place in the lime, as only 2.34% loss of CO_2 is observed in the range of 550-800 °C, corresponding to 5.5% of $CaCO_3$, by weight. While in the case of cement, the degree of hydration is relatively small as well. It is, therefore, possible to conclude that the materials were well stored in the duration of the research program.

3.2.2 Aggregates

Aggregates for this research were ordered from the company Societe Nouvelle Du Littoral (S.N.L) in France which designs and produces different types of silica-based sands (normalized as well as custom graded) for laboratories that work with cement-based materials [323]. For research at the mortar level, the aggregate used was sand with a customized particle size range [0.063,4] mm, following the boundaries for particle sizes mentioned in EN 1200:1976, which has been superseded by EN 13139:2013 [324] (Figure 17). This was done to ensure that the grading of the aggregates was well distributed, suitable according to existing recommendations, as well as to enhance representativeness regarding actual use in constructions. The sand was siliceous and its apparent bulk density was 1.60 g/cm^3. The packing density and water absorption of the aggregate were found to be 0.68 and 0.23% respectively, measured according to the recommendations of EN 1097-3 [325] and EN 1097-6 [326].

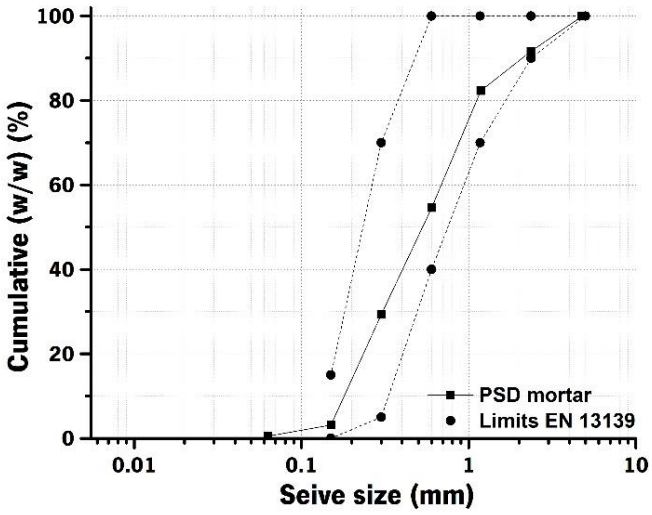

Figure 17: PSD of aggregates used in experiments for mortar level studies, the results are in Chapter 4

In the second stage of the research, which was focused on testing masonry, the particle size distribution of the aggregate was modified. This modification was necessary to obtain a cement only (reference) mortar, which was unattainable with the original PSD of the aggregates (Figure 17) because of bleeding in the cement mortar mix. A detailed description of this problem and the various solutions that were tried before modifying the particle size distribution of the aggregates may be found in Section 3.4.1. By the time the final solution was arrived at, considerable progress had taken place in the research and the mortar level studies (Chapter 4) had been completed. Furthermore, the cement mortar was particularly relevant as a reference in experiments at the masonry level. Therefore, the modified aggregates were used only for masonry level research and this was accompanied by recharacterization of selected mortars.

The modification in the particle size distribution of the aggregates was achieved through the addition of a siliceous inert filler, which had particles of size less than 63 μm. Details of the particle size distribution have been presented in Table 6, along with information on its chemical composition. In all cases in which the modified aggregate was used, 15% (by volume) of the original aggregate was substituted by the filler, which was almost 10% by weight. This resulted in a modification of the particle size distribution of the aggregate to [0,4] mm (Figure 18). The apparent bulk density of the filler was determined in the lab and found to be 1.1 g/cm^3.

Table 6: Information on particle size distribution (PSD) and chemical composition of siliceous filler added to aggregate

Size	Quantity	Compound	Quantity
>80 μm	19%	SiO_2	99.99%
106 μm	D10	Fe_2O_3	130 ppm

37 µm	D50	Al_2O_3	730 ppm
6 µm	D90	TiO_2	120 ppm
		CaO	60 ppm

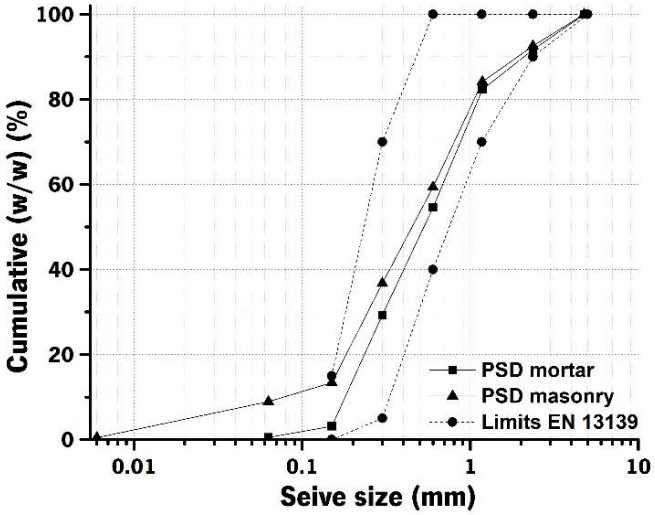

Figure 18: Modified particle size distribution of aggregate (siliceous sand) used in experiments involving masonry specimens, the results of which have been discussed in Chapter 5

3.2.3 Masonry unit

To select a unit for masonry construction, different options of units were considered, based on what was found in the literature [327-332] as well as based on deliberations with the members of the mortar task force (MTF) of EuLA (European Lime Association) [333]. It was recognized that while several different options are available in the market [330, 334, 335], either solid or hollow, including concrete blocks, calcium silicate blocks, and autoclave aerated concrete blocks, clay bricks would be a good starting point for testing lime-cement mortars. Thereafter, depending on how conclusive the results turn out to be, other units could be experimented with, possibly in another doctoral research program. Clay bricks may also be further categorized into sub-groups based on their geometry, perforations (vertical or horizontal), and method of manufacturing, including extruded or molded clay bricks, and further may be of the type solid or perforated [336].

The choice was finally narrowed down to solid clay bricks. The selection of the brick was based primarily on properties of water absorption and the initial rate of absorption (IRA). It was hypothesized that bricks with higher IRA and higher water absorption (typically molded bricks, compared to wire-cut or extruded bricks) might help better assess the differences in the binder of the mortar, through the mechanical behavior of masonry. To select the brick for this research, samples were gathered from three different

companies and tested in the laboratory for water absorption and IRA according to EN 772-21 [337] and EN 772-11 [338] respectively (Table 7, Figure 19). The values of compressive strength displayed in Table 7 were provided by the manufacturer. Options I and II were extruded clay bricks and Option III was a molded clay brick.

Table 7: Mechanical characterization of clay bricks considered as options for this research campaign

Parameter (Unit)	Type I (CoV %)	Type II (CoV %)	Type III (CoV %)
IRA (kg/m^2.min)	0.9 (33.1%)	1.5 (18.1%)	3.6 (15.6%)
Water absorption (%)	15.1 (2.9%)	9.1 (5.2%)	10.3 (7.6%)
Compressive strength (MPa)	> 28	> 30	12

Figure 19: Clay bricks considered as options for this research campaign, corresponding to Table 7

Out of the options tested, the brick finally chosen was Option III, a molded, solid clay brick with frogs supplied by Wienerberger, with size 215×102×65 mm^3 (Figure 20). As may be observed from Table 7, this brick had high IRA and water absorption characteristics, and a relatively low compressive strength. According to the technical data sheet (DoP number 152110-B1W1210) provided by the manufacturer, the configuration of the brick falls in the category of group 1, tolerance T1, range R1 and the volume of frogs has been specified as less than 20%, under the standard EN 771-1 [336]. Furthermore, the water absorption and IRA, as specified by the manufacturer are 15% and 1-5 kg/m^2.min, respectively. Mechanical characterization of the brick including compressive and flexural strength and E-modulus has been addressed in detail in Chapter 5 along with the methodology and results of different characteristics, as a subsection of the characterization of components of masonry.

Figure 20: Solid molded clay brick with frogs chosen for the project, supplied by Wienerberger

3.3 Mixes for mortar level study

3.3.1 Preparation and curing protocols

The beginning of this research aligned with the timeline of setting up new equipment in the laboratory for casting mortar mixes, especially focusing on the needs of this project (Figure 21). All of the equipment was from the company Matest and the specific models used have been indicated in Figure 21 [339-342].

The equipment included a mixer (E 093) programmed according to protocols of EN 196-1 [340]. According to the protocol, that was used to prepare all the mortar mixes, the binder should be mixed with water at low speed (rotation of 140±5 min^{-1} and planetary movement of 62±5 min^{-1}) for 60 seconds, followed by high-speed mixing (rotation of 285±10 min^{-1} and planetary movement of 125±10 min^{-1}) for another 30 seconds. Aggregate is supposed to be added to the mixture, slowly between 30 to 60 seconds. It is then recommended to bring the mixer to rest for 90 seconds. In this interval, the sides of the vessel of the mixer may be scraped to mix the mortar that may be sticking to the sides or bottom of the vessel. Finally, the contents of the mixer are supposed to be mixed at high speed for another 60 seconds, making the total mixing process 4 minutes long. Each batch of mortar was restricted in quantity based on the size of the vessel which had a capacity of 4.7 liters. The rule of thumb used for the quantities of materials, was approximately 3 kgs of aggregates for each casting so that material would not spill out during high-speed mixing. Time ‘zero’ was measured as the moment when water was first brought into contact with the binder. For all batches that were cast in this mixer, from time zero to the moment when the compacted molds were placed in the climatic chamber for curing, it took between 45-60 minutes.

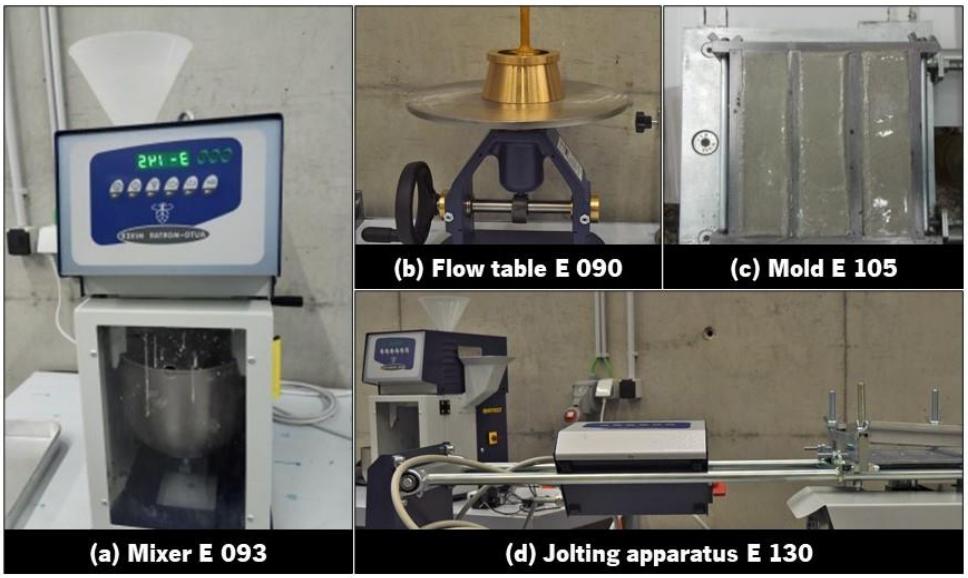

Figure 21: Equipment used in the laboratory for casting mortar mixes, from the brand Matest (a) Mixer E 093 [340]; (b) Flow table E 090 [339]; (c) Mold E 105 [341]; (d) Jolting apparatus E 130 [342];

For the studies that took place at the mortar level, raw materials were preconditioned in the same environment to avoid variation in the mortar mixes introduced from changes in temperature or humidity. In this regard, pre-conditioning protocols used by the round-robin testing program of cost action TU 1404 [343] were used as a base, since these guidelines were adopted by them to compare results from the same experiments, across different laboratories in various countries [343]. The binders (cement and lime) were stored in sealed bags at 20±1˚C, for a minimum of 7 days before the actual mixing. Additionally, before each casting, the aggregates were dried completely at 105˚C and cooled down to room temperature (20±1˚C). This was usually done over-night, corresponding to a cooling down period of approximately 15 hours, since the sand would be removed from the oven, an evening before (around 7 PM), and the mixes would be cast the next morning (around 10 AM). The water used for the mixing was also stored in the laboratory at room temperature (20±1˚C) for a minimum of 7 days before casting.

With regard to sample preparation at the mortar level, the specimens that were cast in prisms of size 40×40×160 mm^3 (molds E 105) were compacted using standard jolting apparatus (E 130 - Figure 21) specified in EN 196-1 [344]. The process consisted of partially filling the molds and jolting them 60 times in exactly 60 seconds. The mold would then be completely filled and jolted another 60 times in 60 seconds. In the case of mortars being cast in a cylindrical shape, each cylindrical specimen had a diameter of 60 mm and a height of 120 mm and was made from a polyvinyl chloride tube with a base of strong adhesive tape. Since this arrangement could not be compacted on the jolting apparatus, a vibrating table was used [345] with specifications 220-240 V, 50 Hz, complying with EN 12390-2 [346]. The

cylindrical specimens were subjected to vibration for 10 seconds twice during casting; with the mold first being half-filled and consequently completely filled to assist the removal of air bubbles. During the processes of compaction and vibration, care was taken to observe that no bleeding or segregation of water and mortar mix occurred, because then the mix would be unacceptable and the water-binder ratio would have to be readjusted.

An overview of the casting and curing processes used for mortar preparation has been illustrated in Figure 22.

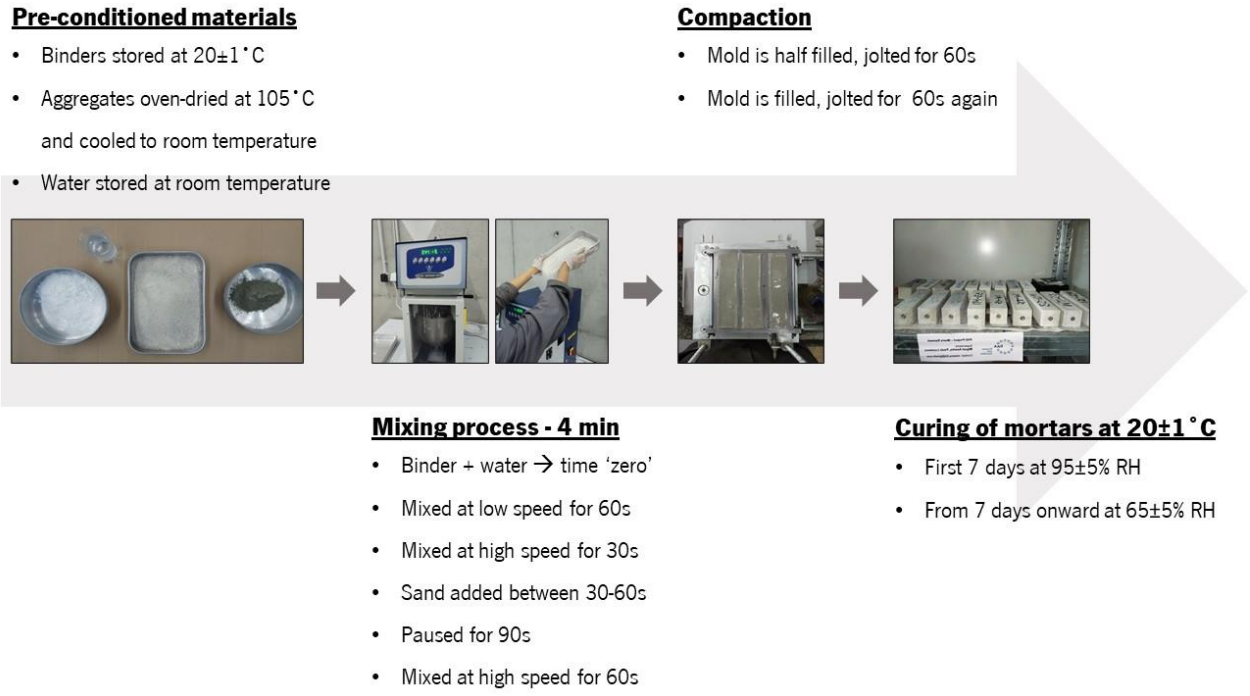

Figure 22: Overview of casting of lime-cement mortars according to EN 196-1 [344] and curing according to EN 1015-11 [16]

Curing conditions for lime-cement mixes were decided based on recommendations in EN 1015-11 [16]. All lime-cement mortar mixes were cured at 20±1˚C and 95±5% RH for the first 7 days and thereafter at 20±1˚C and 65±5% RH, up to the age of testing. Demolding of lime-cement mortar specimens was also decided based on EN 1015-11 [16], which recommends demolding after 2 days for lime-cement mixes if the amount of lime in the binder is less than 50% by mass, and demolding after 5 days if the amount of lime in the binder is greater than 50% by mass. In the case of the cement-only mix (i.e., no lime present in the binder), specimens were cured according to EN 196-1 [344]. For the first 24 hours, the molds containing cement-only mixes were covered in a plastic bag and placed in a climatic chamber with a temperature of 20±1˚C and RH of 95±5%. Thereafter, the cement-only specimens were submerged in water at 20±1˚C, up to the age of testing.

3.3.2 Mortar mix compositions

For research at the mortar level, fifteen different mortars were studied to understand the mechanical behavior of lime-cement mixes (Table 8). Binder aggregate (B/Ag) ratios of 1:3, 1:4, 1:5, and 1:6 were tested, expressed in percentage by volume as 33%, 25%, 20%, and 17% respectively, while the quantity of lime in the binder was varied from 10% to 90%, by volume. An effort was made to choose mix compositions that would be representative of what is used on the field, and not just convenient from an academic point of view. For example, the lime content in the binder could have been varied by 10% systematically for regression analyses, i.e., 60%, 70%, and so on. However, out of the lime-cement mortar mixes commonly used on the field 67% lime in the binder is more common (1:2:9), over 60% or 70%. Choosing to directly study a commonly used mix composition, would help translate the research done in the laboratory to practical applications in the field. To guide the process of selecting the most commonly used B/Ag ratios and lime-cement ratios in the binder, the MTF of EuLA was consulted [333], along with identifying the mix compositions, that appeared repeatedly in the literature [2, 9, 59, 95, 347]. Mortar compositions prescribed in the national annexes to Eurocode 6, from different countries were also taken into account [348-355]. The notations adopted, denote the proportion of different constituents of the mix by volume, for example, 1C3L12S represents a 1:3:12 mix ratio of cement C, lime L, and sand S, respectively. Furthermore, to make it convenient for the reader, all graphs and references to different mixes in the text have been provided with the quantity of lime in the binder (by volume) in parenthesis adjacent to the name of the mix, for example, 1C3L12S (75%). All proportions were converted to mass, using apparent bulk densities of cement (0.93 g/cm^3), lime (0.36 g/cm^3), and sand (1.6 g/cm^3), for the sake of consistent measurement of raw materials. The asterisk symbol (*) in Table 8 indicates, that the value lay in the range of 175±10 mm but the exact measurement was not recorded.

Table 8: Composition of blended lime-cement mortars (for 1 m^3 of mortar produced)

Nomenclature (Lime content by volume %)	Cement: Lime: Sand (Volume)	Cement (kg)	Lime (kg)	Aggregate (kg)	w/b ratio (By weight)	w/b ratio (By volume)	Flow table value (mm)
9C1L30S (10%)	9:1:30	315.2	13.4	1846.1	0.88	0.77	185
3C1L12S (25%)	3:1:12	262.7	33.4	1846.1	1.00	0.79	165
2C1L9S (33%)	2:1:9	233.5	44.5	1846.1	1.09	0.81	180
1C1L6S (50%)	1:1:6	175.1	66.8	1846.1	1.25	0.81	165
1C2L9S (67%)	1:2:9	116.8	89.0	1846.1	1.58	0.87	165
1C3L12S (75%)	1:3:12	87.6	100.1	1846.1	1.76	0.88	165

1C9L30S (90%)	1:9:30	35.0	120.2	1846.1	2.31	0.96	185
3C1L16S (25%)	3:1:16	197.0	25.0	1846.1	1.35	1.07	182.5
2C1L12S (33%)	2:1:12	175.1	33.4	1846.1	1.50	1.11	*
1C1L8S (50%)	1:1:8	131.3	50.1	1846.1	1.72	1.11	180
1C2L12S (67%)	1:2:12	87.6	66.8	1846.1	1.94	1.07	180
2C1L15S (33%)	2:1:15	140.1	26.7	1846.1	1.80	1.33	175
1C1L10S (50%)	1:1:10	105.1	40.1	1846.1	2.21	1.42	180
1C2L15S (67%)	1:2:15	70.1	53.4	1846.1	2.38	1.31	*
1C1L12S (50%)	1:1:12	87.6	33.4	1846.1	2.69	1.73	180

A key aspect of this research program was to ensure that the mixes being studied would be adequate in terms of use in the field. Therefore a target value of 175±10 mm, as per the flow table test [356], was chosen to determine water-binder (w/b) ratios of the mixes (Figure 23). This chosen interval of 175±10 mm also falls in the range of workability assessed as suitable in the work of Hendrickx [9], who presented a doctoral thesis that addresses the workability of mortar mixes, taking into account the technical experience of six international masons, which has been further elaborated on, in Chapter 2, Section 2.3.1. And therefore the water-binder ratio for all mixes was determined, to attain a flow table value of 175±10 mm. In most of the cases, on average, it took 4 trials, (ranging between 2 to 6 attempts) to obtain the desired flow table value of 175±10 mm. For each attempt, the mix was cast, and workability was tested on the flow table according to EN 1015 - 3 [356], using a hand-operated flow table (Figure 21). If the desired flow table value was not attained, the mix was discarded and a new batch of mortar was cast with a modified water-binder ratio. This process was repeated till the flow table value obtained lay in the range of 175±10 mm. The range was also considered wide enough to encompass minor variations that could arise due to changes in room temperature, water temperature or other effects.

Figure 23: Target consistency aimed for 175±10 mm, for all mortars

In this research, specifically pertaining to mortars, not all tests could be carried out on all 15 mixes. It was decided that the basic properties of mechanical strength (compression and flexure), hardened bulk density, and UPV would be measured for all mixes up to 365 days of age. Thereafter, a few mixes would be selected from the 15 mixes for other tests such as open porosity, E-modulus, and drying shrinkage.

Since different tests have been conducted on mortar specimens of various sizes and at multiple ages, an illustration has been provided summarizing the number and composition of mortar mixes that were tested for each of the different mechanical properties (Figure 24). The figure has three columns, with the first two from the left corresponding to discrete measurements, and the third one discussing continuous measurements. Within each column, there are four tiers, the first of which specifies the experiments, and the second tier indicates how many mixes were tested for each of those experiments. The third tier describes the composition of the mixes tested, grouping them by B/Ag ratio, and mentioning the quantity of lime in the binder (% by volume), in parentheses. And the final tier indicates the different ages at which each of those tests were performed, in number of days.

A more detailed description of specimen sizes, testing ages, and standards for the experiments performed at the mortar level have been presented in Table 9. All test results were obtained from an average of 3 specimens per mortar type, except for compressive strength in which 6 specimens were used per mortar type and for EMM-ARM (a method used for constant monitoring of E-modulus) in which simultaneous tests were performed on 2 specimens. The details of the methodology, along with a discussion of the results of all mortar level properties will be discussed in Chapter 4.

For research at the mortar level alone, it may be noted that results from 409 individual specimens, including prisms and cylinders, were used. Furthermore, mortar was also cast for trial tests, to obtain the right workability and to repeat some of the tests and confirm the results. If those quantities are also accounted for, a conservative estimate would be approximately 650 individual specimens which is a mortar volume of 0.246 m^3 implying around 135 batches of mortar cast.

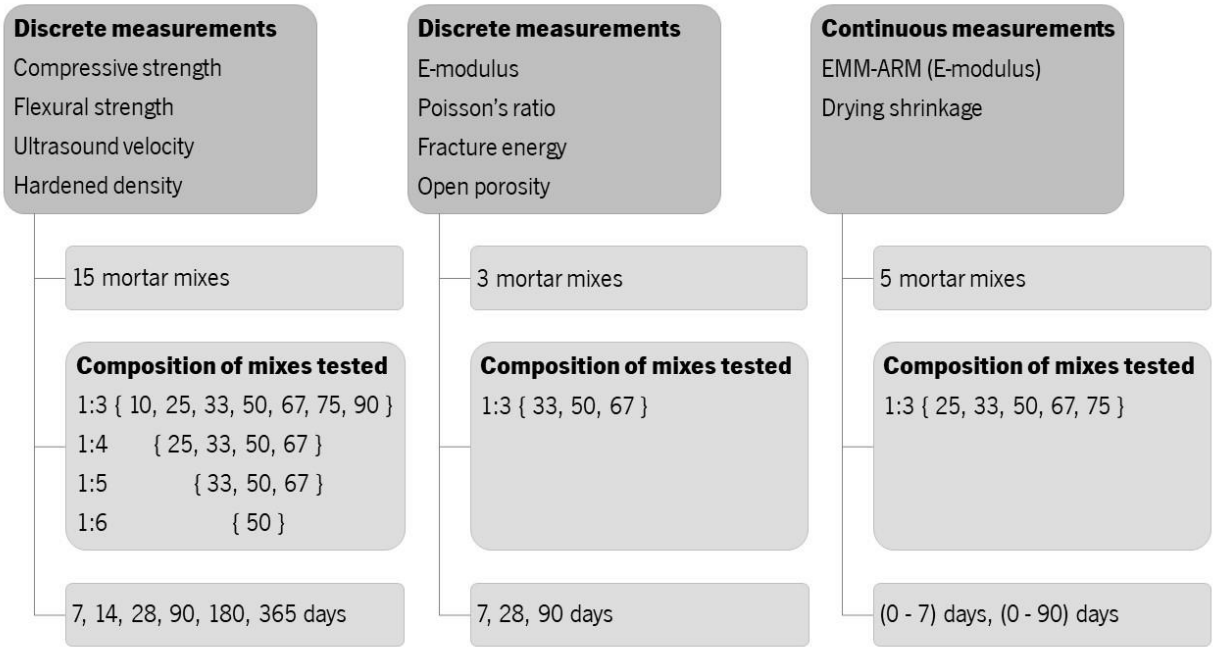

Figure 24: Summary of mixes tested for different mechanical properties, for mortar level research pertaining to Chapter 4

Table 9: Summary of tests conducted at the mortar level

Name of test	Specimens (Units in mm)	Mortars tested	Recommendations followed	Ages of testing (days)
Hardened density	Prisms 40×40×160	All mortars	Based on EN 1015-10 [357]	7, 14, 28, 90, 180, 365
UPV	Prisms 40×40×160	All mortars	-	7, 14, 28, 90, 180, 365
Flexural strength	Prisms 40×40×160	All mortars	EN 1015-11[16]	7, 14, 28, 90, 180, 365
Compressive strength	Halves of prisms from flexural strength test	All mortars	EN 1015-11[16]	7, 14, 28, 90, 180, 365
Open porosity	Prisms 40×40×160	1C2L9S (67%), 1C1L6S (50%), 3C1L12S (25%)	Based on TC 25-PEM [176]	7, 28, 90
Drying shrinkage	Prisms 40×40×160	1C3L12S (75%), 1C2L9S (67%), 1C1L6S (50%), 2C1L9S (33%), 3C1L12S (25%)	Based on EN 12617-4 [358]	0 to 90
EMM-ARM	Cylinder l 550 , ⌀ 44	1C3L12S (75%), 1C2L9S (67%), 1C1L6S (50%), 2C1L9S (33%), 3C1L12S (25%)	EMM-ARM user manual [359]	0 to 7
E-modulus	Cylinder h 120, ⌀ 60	1C2L9S (67%), 1C1L6S (50%), 3C1L12S (25%)	EN 12390:13 [117]	7, 28, 90
Poisson's ratio	Cylinder h 120, ⌀ 60	1C2L9S (67%), 1C1L6S (50%), 3C1L12S (25%)	Similar to E-modulus	7, 28, 90
Fracture energy	Prisms 40×40×160	1C2L9S (67%), 1C1L6S (50%), 3C1L12S (25%)	RILEM 50-FMC [158]	7, 28, 90

3.3.3 Assessment of repeatability

Because 15 mortar mixes were being tested for different mechanical characteristics at multiple ages, and since the capacity of the vessel in the mixer was limited to 5 liters, it was inevitable that several batches

of the same mortar would have to be cast, on the same day or different days. Therefore, two key factors were paid special attention to, from the point of view of repeatability (consistent repeated measurements under identical conditions including the same operator and machinery):

a) Repeatability of casting process of the mix, so that the same mortar was being tested for different mechanical properties.
b) Repeatability of experiments.

This was also done to acknowledge the learning curve associated with experimentation (casting mixes and testing various mechanical parameters) for the author, who was also the operator. So, experiments from which data was recorded for drawing scientific conclusions, were only accounted for after repeatability was verified. In this regard, before recording any data, there was a special period dedicated to verifying the robustness of the mixing protocol. One of the distinguishing factors involved was the adoption of guidelines from the round-robin testing program of cost action TU 1404 [343] as mentioned in Section 3.3.1, for pre-conditioning of the materials. Additionally, tests were made using two different mortar mixes (cast on different days) for the same property, at the same age, and the results obtained were compared. The parameter chosen for comparison was compressive strength, and the two mixes chosen were 2C1L9S (33%) and 1C2L9S (67%), with less than and more than 50% lime content. The mixes were tested at curing ages of 15 days and 7 days respectively. The results obtained have been shown in Table 10. The difference in the two batches of 1C2L9S (67%) was found to be 1.5% and for the mix 2C1L9S (33%), it was found to be 0.6%. The differences in the results were less than the coefficients of variation in the results. Further, these differences may also very well lie in the range of individual variation of any mortar mix tested for compressive strength even in early ages [59, 360] as will be observed in a detailed discussion on compressive strength in Chapter 4 Section 4.4.2.

Another aspect considered was that of quality control, assisted by non-destructive testing, through measurement of ultrasound pulse velocity (UPV). UPV was measured for all mortar specimens, at each age of testing and compared with ‘control specimens’ for their respective mixes, at the same age. It is also possible to observe from values of ultrasound velocity presented in Table 10, that the differences recorded were small.

Table 10: Compressive strength of mixes tested for repeatability

Mixes	2C1L9S (33%)	1C2L9S (67%)
Age of testing (days)	15	7

Room temp (˚C) and RH (%) while casting - 1	23.0˚C, 51 %	24.2˚C, 55 %
Room temp (˚C) and RH (%) while casting - 2	24.8˚C, 66 %	24.0˚C, 49 %
Compressive strength (MPa) – 1 (CoV%)	7.97 (2.4 %)	1.72 (3.7 %)
Compressive strength (MPa) – 2 (CoV%)	8.01 (4.3 %)	1.75 (3.3 %)
Difference in compressive strength (%)	0.6 %	1.5 %
Ultrasound velocity (m/s) – 1	2857	1946
Ultrasound velocity (m/s) – 2	2923	1973
Difference in ultrasound velocity (%)	2.3 %	1.4 %

To further utilize the potential of UPV as a non-destructive method to control quality, the same was used for all 15 mixes through 6 different ages, up to 365 days. The specimens that were to be tested for compressive and flexural strength at 365 days of age, were labeled as control specimens for each mix. At each age of testing and for each mix, before testing the specimens for strength, bulk density, and UPV were measured. In parallel, bulk density and UPV were also measured for the control specimens at the same corresponding age. This way, there were two sets of UPV and bulk density measurements available for each mix at each age, except at 365 days because at that age, only the control specimens were left to be tested. The aim of this was to measure the difference in UPV between the control specimens and the actual specimens that were to be tested for strength at each age, serving as a test of coherence in values from different batches of the same mix, aiding the assessment of repeatability and possibly to identify/explain outliers. This process would also serve in monitoring changes in UPV and bulk density over one year in the control specimens of each of the 15 mixes.

Amongst the mixes tested, the difference between the UPV values of the control specimens and the actual specimens to be tested at each age was mostly found to be less than 5%, in some cases extending up to 13% (for less than 10 out of 90 cases, Annex-Table 14). The difference in hardened density was also less than 5% mostly, going up to 8% in very few cases Annex-Table 14. These mixes happened to have either large quantities of lime in the binder or high binder-aggregate (B/Ag) ratios. It was thus found reliable to cast several batches of mortar mixes with the mixing protocol defined in Section 3.2.3. Due to the low variations observed, it was also found acceptable to correlate different mechanical properties of UPV, compressive strength, and hardened density of the same mixes cast in different batches.

3.4 Masonry level research

3.4.1 Modification in aggregates and reference mix for masonry level research

In alignment with the goals of this research campaign (Chapter 1, Section 1.2), one of the objectives was to compare the performance of lime-cement mortared masonry with that of cement mortared masonry. For this purpose, a reference cement mortar with composition 1:5 (Cement: Aggregate) was chosen. The decision to use a cement only mortar as a reference was based on the fact that cement mortars (with B/Ag ratios 1:3, 1:5, and 1:6) are commonly used in the construction industry [13, 361-363]. This reference cement mix 1:5 ended up becoming the reason for modifications in the aggregate.

To use this reference mix, it was necessary to find a suitable water-binder ratio that would result in a flow value of 175±10 mm (Section 3.5, Chapter 3). It was found that despite repeated trials, it was not possible to obtain a reference cement mix (1:5) that did not bleed, and yet satisfied the 175±10 mm flow value workability criterion. A mortar that bled would not lead to reliable results since the amount of water in it would always vary based on how much water bled out of it, consequently creating significant variations in the mechanical behavior. Therefore, the next step was to use a plasticizer that would help obtain a mix that would satisfy the workability criterion and prevent bleeding of the mix. For this, various options were considered and tested, the prominent one being Sika Viscocrete (650 duo A). This led to the desired workability in the mix concerning the flow table value of 175±10 mm. However, during the compaction of the mortar into molds, a considerable quantity of water was discarded (Figure 25). This was also not acceptable because there was no way to control or assess the quantity of water being discarded.

Next, potential reasons for this problem were analyzed with a special focus on the aggregate. It was possible to pinpoint, that since the aggregate was tailored for this project with a particle size distribution of [0.063,4] mm (Section 3.2.2), it was missing fines less than 63 µm in size. In the case of lime cement blended mixes, this problem of bleeding was not occurring, probably due to the presence of lime and its particle size distribution was in some way serving as fines (Section 3.2.1).

Figure 25: Water expelled (a) during compaction from a trial of the reference cement mix (b)

However, in the absence of lime in the mix, the aggregate was not adequate in preventing the observed loss of water as described above. To verify this hypothesis, natural river sand [0,4] mm was used to cast a cement mortar, with the same binder CEM I – 42.5 R. It was confirmed that it was possible to cast a cement mix with the desired workability, without the use of a plasticizer and the mix bleeding. Therefore, a siliceous filler with particle size less than 63 μm was obtained and added to the original aggregate, to obtain the modified aggregate (Figure 18). The quantity that was added, was determined by obtaining the desired cement without a plasticizer or bleeding and was found to be a 15% substitution (by volume) of the original aggregate.

It must be highlighted that it was not known at the beginning of the research that problems in finding a reference cement mortar would arise due to the aggregate. Since it was possible to obtain lime-cement mixes of different compositions relatively easily, the first suspicion for the problem was not the aggregates. It took time to experiment with different plasticizers, and finally, narrow down the cause of the problem. And so the mortar level study had progressed to a significant extent, focused on the objective of understanding patterns in mechanical properties of lime-cement mixes had been obtained, concerning varying proportions of lime and cement in the binder as well as the impact of binder-aggregate ratios. As no problems were found with such mixes, it was decided not to repeat the entire mortar level study, and the 15 mixes discussed in Section 3.3.2 remain unaffected and employed the use of the original aggregate. The modified aggregate (Figure 18) was, therefore, only introduced at the masonry level of research.

3.4.2 Composition of lime-cement mixes chosen for masonry level research

For research at the masonry level, a few relevant lime-cement mixes were selected, out of the 15 lime-cement mixes studied at the mortar level, based on the results from the mortar level study, and a review of mixes commonly used in the literature and industry. The two lime-cement mortars considered were with B/Ag ratio 1:3, by volume; with 50% and 67% lime in the binder, by volume [2, 95, 347, 364]. The choice of the reference cement mix (1:5) was also based on a review of the cement mortar mixes commonly used on the field [13, 361-363], as has been explained above. Since a prominent underlying theme in all these choices was the representativity of mixes used on the field, decisions concerning mix compositions again involved detailed discussions with the mortar task force of EuLA [333], members of which are working professionals in the construction industry.

In this stage of the research, since the aggregate was modified, the nomenclature of lime-cement mortars was also changed, to avoid confusion with the mortar level study. The mixes with composition 1:1:6 and 1:2:9 (Cement: Lime: Aggregate) have been denoted as 'L50' and 'L67' respectively, so that the mechanical properties of the two lime-cement mixes are not confused with those presented in Chapter 4 as 1C1L6S (50%) and 1C2L9S (67%). And the mix 1:5 (Cement: Aggregate) has been denoted as 'Ref'. The composition of the three mortars selected has been presented in Table 11, based on a flow table value of 175±10 mm, for all of them.

Table 11: Composition of mortars with modified aggregate (for 1 m^3 of mortar produced)

Nomenclature	Cement: Lime: Sand (Volume)	Cement (kg)	Lime (kg)	Aggregate (kg)		w/b ratio (By weight)	w/b ratio (By volume)
				Sand	Filler		
Ref	1:0:5	233.5	0	1743.6	206.4	1.2	1.12
L50	1:1:6	192.6	73.4	1726.1	204.4	1.09	0.70
L67	1:2:9	128.4	97.9	1726.1	204.4	1.3	0.71

Since at this level, the focus of the research was the characterization of mechanical behavior of masonry, the mortars were not extensively recharacterized, just adequately to support the main goal. The mechanical properties studied were mechanical strength, stiffness, hardened density, and ultrasound velocity. Furthermore, two curing conditions were adopted for the sake of comparison:

a) Standard mortars - The three mixes (Ref, L50, and L67) were cast as per the mixing protocols specified in Section 3.3.1 and cured accordingly as well. This set has been referred to as 'standard mortars', implying that the process respected the recommendations of the European standards [16, 344].
b) In situ mortars - Mortars (Ref, L50, and L67) used in masonry construction were cast in large batches, as has been described in detail in the next section (Section 3.4.3). Small quantities were taken from large batches when the mortar was being prepared for masonry construction and cured right next to the masonry specimens, subject to the same temperature and humidity conditions. This set has been referred to as 'in situ mortars'.

The two main differences in 'standard' and 'in situ' sets of mortars are the quantity of materials being cast in a batch and the temperature and humidity conditions in which the specimens were cured.

3.4.3 Construction of masonry specimens

For research at the masonry level, specimens were constructed and tested, to analyze the influence of different mortars on the mechanical performance of masonry. Based on recommendations from the literature, the thickness of mortar joints was chosen as 10 mm [12, 13, 134, 150, 365, 366]. All masonry specimens were constructed and air-cured in the basement of the laboratory of IBS at the University of Minho. The average temperature and humidity measured in the storage areas were found to be relatively stable, around 21±1˚C and 70±5% RH monitored for almost one year. The binders, sand and filler, bricks, and water were also stored in the same location, in the basement of the laboratory, before the construction of masonry specimens. The aggregates were not oven-dried, due to the large volume that was used in masonry construction. However, to make sure that the moisture level in the aggregates did not impact the composition of the mortar, samples were collected from different packages of aggregates; their weights were measured, put into the oven and dried at 105˚C, and then their weight was measured again. It was found that there was almost no difference in the two weights recorded, pre and post oven drying. This meant that the aggregates were already dry in their packages. And therefore, during masonry construction, aggregates were always used from unsealed packages. This was also convenient since the aggregates were delivered in packages of weight 10 kgs each.

Since the construction of masonry required mortars in large quantities, the preparation of mortars was done in much larger batches compared to those used for mortar level studies (Figure 26). However, the batches could also not be too large, to avoid the beginning of hardening of mortar before construction. To find the optimum size of each batch, the recommendation of RILEM LUM B1 [367] was adopted, which suggests that all batches of mortar must be used within 60 minutes of preparation. Time zero was considered as the moment when the binders came into contact with water. Therefore, for each batch of mortar prepared, approximately 13 kilos of aggregates were used, ensuring that the entire quantity of mortar cast was used for masonry construction, in less than one hour.

A professional mason associated with the civil engineering laboratory of the University of Minho, for over two decades, was in charge of the construction of masonry. For every masonry specimen constructed, the raw materials for the mortars were weighed and prepared for casting by the author. The subsequent mixing was done by the mason, and carefully timed by the author. The mixing protocol used for preparing mortars was kept similar to that used at the mortar level, to enhance uniformity in this research campaign. The binders were weighed carefully and brought into contact with water, marking time ‘zero’ (Figure 26). The contents were mixed in a barrel (Height 50 cm, Diameter 50 cm) for 90 seconds, while the aggregate

was introduced between 30-90 seconds. Mixing was then paused for 90 seconds, in which mortar was scraped from the sides and bottom of the barrel, and finally, the contents were mixed again for another 90 seconds. The mixer used was representative of what is often used in the field by masons and suitable for mixing large quantities (Figure 26). The model used was Parkside PFMR 1400 B1 with a motor power of 1400 W, a rotation speed of 700 per minute, and stirrer holder M14 [368]. In parallel, the units (clay bricks) were well dusted and soaked in water for ~30 minutes before construction, by the author. This was done to avoid suction of water from the mortar, by the bricks, which could happen if they were dry and could potentially affect the bond strength of masonry negatively [367]. Finally, the actual construction of all masonry specimens used in this research campaign was done by the mason. To give the reader an idea of the time required to construct these specimens (Figure 27), it may be approximated that to build two single leaf wallets that were five courses high and two courses wide, it took one hour and approximately one batch of mortar (Aggregates - 13 kgs). The time stamps indicated in Figure 27, are regarding 'time zero' which is when the binder first came into contact with water. For this research, over 120 masonry specimens were constructed, in total.

Figure 26: Illustration of process used to construct masonry

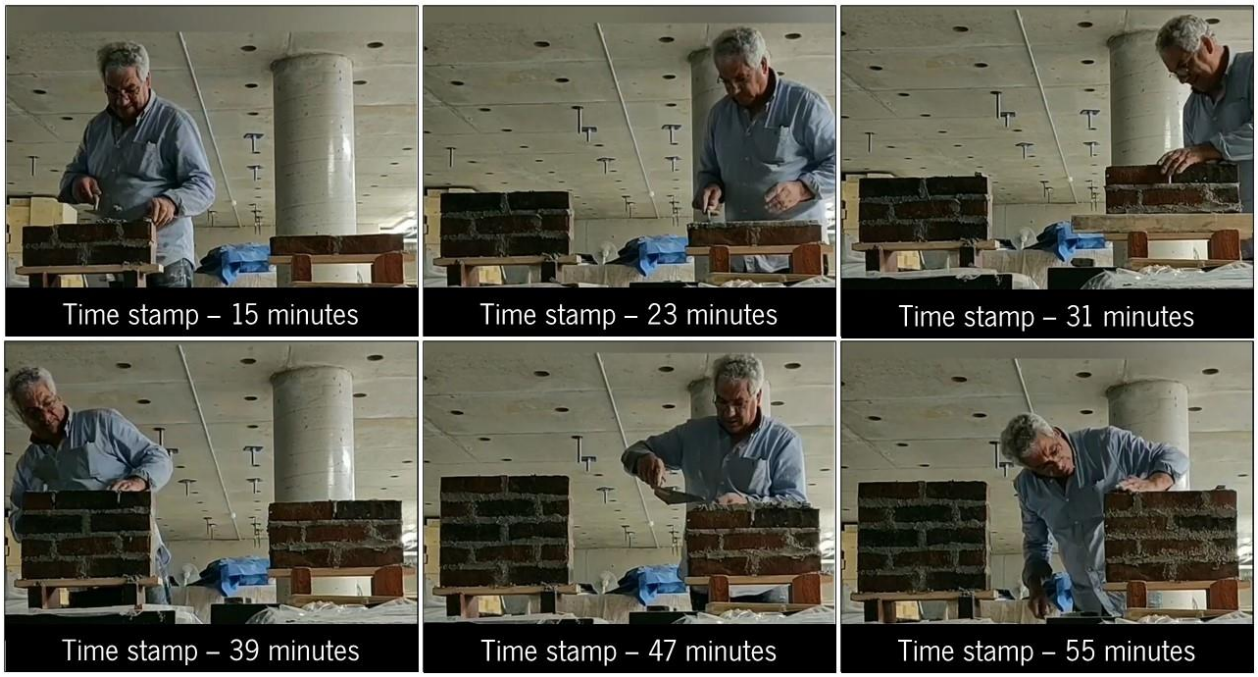

Figure 27: Time-lapse of construction of masonry specimens

Since at the mortar and masonry level research, there was a difference in the mixer used, and quantity of mortar prepared, the flow table values of the mortars prepared for masonry were re-checked and found to lie in the same range of 175±10 mm. Furthermore, qualitative validation of the workability of the mortars was also obtained from the mason. Mortar prepared in these large batches was also used to cast specimens for in situ characterization, as mentioned in the previous section (Section 3.4.2). This implied that specimens were cast in cylinders and prisms, with material taken from the batches created in large quantities for constructing masonry and cured in the same ambient conditions that masonry specimens were subjected to (Figure 28). The rationale behind this was to perform in situ characterization of E-modulus and compressive strength of mortars subjected to the same curing conditions as that of the masonry. The results obtained have been discussed in Chapter 5 and compared with the properties of the mortars prepared in standard conditions (Section 3.4.2). In standard conditions, mechanical strength was tested at 7, 28, and 90 days and E-modulus was tested at 90 days. In parallel conditions, mechanical strength and E-modulus were tested at 28 and 90 days, which are usually adopted in the case of cement and lime mixes, respectively. An illustration summarizing the tests conducted for masonry level research has been shown in Figure 29. The sizes of masonry specimens depended on the test conducted (Figure 28, Table 12), namely compressive strength, E-modulus, shear bond strength, flexural strength (parallel and perpendicular), and in-plane shear wall panel strength. For each of the tests mentioned in, 3 masonry specimens were tested and the average value was used. All tests at the masonry level were performed between 90 to 180 days after the construction of the specimens. More specifically, compressive strength,

E-modulus, and shear bond strength were tested after 90 days of aging, flexural strength (parallel and perpendicular) was tested 150 days of aging and finally, in-plane shear capacity wall strength (cyclic loading) was tested after 180 days of aging. The testing had to be phased out because only one operator (the author) was performing the tests. Furthermore, it was found in the mortar level research (Chapter 4), that the strength and stiffness of mortars remained almost the same between 90 and 180 days, meaning that phasing out the masonry tests over time was acceptable.

Table 12: Summary of tests conducted at the masonry level

Name of test	Specimens (mm) Height × Width	Recommendations followed
Compressive strength	450×440 (wallet)	EN 1052-1 [17]
E-modulus	450×440 (wallet)	Based on the concept of cyclic loading up to 0.33 f_{max}
Flexural strength - parallel	670×440	EN 1052-2 [270]
Flexural strength - perpendicular	890×440	EN 1052-2 [270]
Shear bond strength	215×215	EN 1052-3 (Three levels of vertical pre-compression) [290]
In-plane shear wall panels	900×900	Based on FEMA 461 [369]

Figure 28: Left – Mortar specimens constructed for in situ characterization with masonry | Right – Overview of masonry specimens cast for mechanical characterization

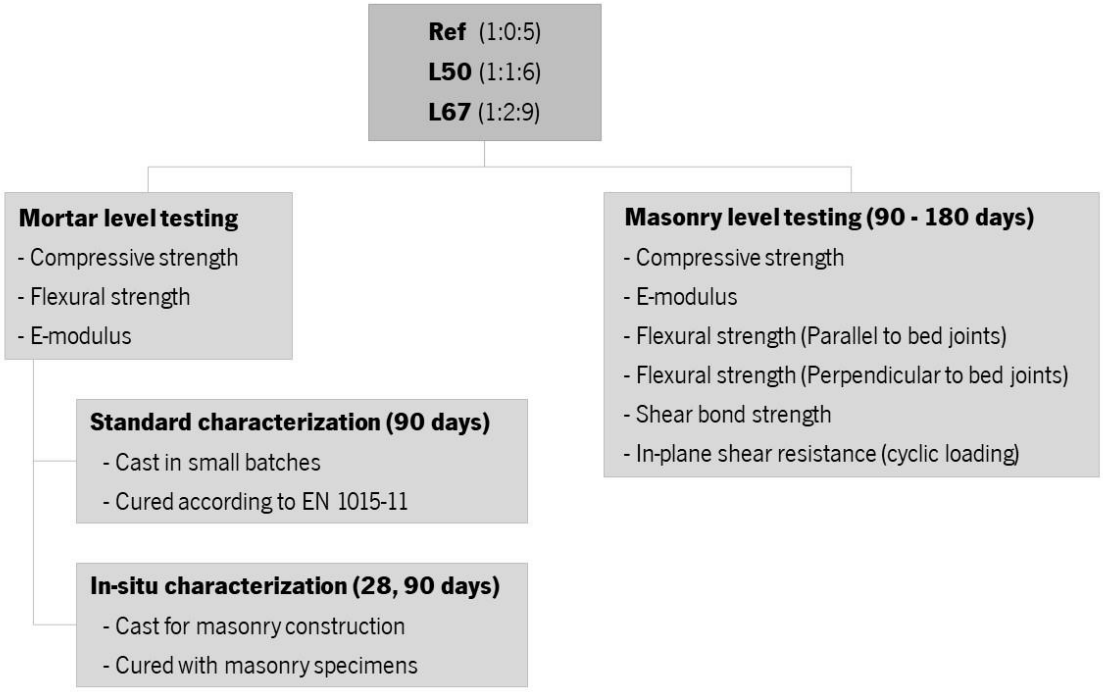

Figure 29: Illustration summarizing tests performed for masonry level research

4. Mechanical behavior of lime-cement mortars

4.1 Introduction

As discussed in Chapter 2, it is possible to find a consensus on the overall trends regarding the impact of the type of binder and quantity of aggregates on the mechanical behavior of mortars. However, there is an evident lack of systematic quantification of such an impact on the basic mechanical properties of mortars, as well as the correlation between different properties. This chapter aims to address that gap, by presenting information on the mechanical behavior of lime-cement mortars and providing a discussion on possible correlations. Following the introduction, there are ten sections (Sections 4.2 to 4.11) in this chapter that cover the methodology and results of different mechanical properties in the order of – workability and corresponding water-binder ratios, mechanical strength, hardened bulk density and UPV, E-modulus, Poisson's ratio, fracture energy, open porosity, drying shrinkage and EMM-ARM (Elasticity Modulus Measurement through Ambient Response Method). Subsequently, final remarks are presented. The sequence of the sections has been based on the type of measurements (continuous/discrete) and the number of mixes tested in each case (Detailed explanation in Chapter 3). Discrete measurements of workability, mechanical strength (compressive strength and flexural strength), hardened bulk density, and UPV were measured for 15 lime-cement mortars for 6 different ages – 7, 14, 28, 90, 180, and 365 days. The next set of results are for discrete measurements at 7, 28, and 90 days, regarding mechanical properties: E-modulus, Poisson's ratio, fracture energy, and open porosity have been discussed for three lime-cement mixes. The three mixes (B/Ag ratio 1:3) selected were, one with 50% lime in the binder (1C1L6S (50%)), one with less than 50% lime in the binder (3C1L12S (25%)), and one with more than 50% lime in the binder (1C2L9S (67%)). The choice of these mixes was made based on the selection of other researchers as well as what is often used in the industry, as has been discussed in detail in Chapter 3 [48, 59, 364]. Finally, results from two more mechanical properties, EMM-ARM and drying shrinkage have been presented (continuous measurements), the former from 0 to 7 days, and the latter from 7 to 90 days. Five mixes were studied for these two properties namely 3C1L12S (25%), 2C1L9S (33%) 1C1L6S (50%), 1C2L9S (67%) and 1C3L12S (75%). Details of the specimens and ages of testing have also been presented in Chapter 3.

It must be mentioned, that all equations and relationships presented in this chapter are valid only for the materials specified in this thesis. If the nature of any of the materials is changed (lime, cement, or sand) or if other conditions such as ambient temperature or relative humidity are varied, the equations may require recalibration. The analytic expressions presented in this chapter are intended to help better

understand the quantitative influence of different factors on mechanical properties. Furthermore, it is also hoped that a consequence of presenting these expressions could be the generalization and development of "rules-of-thumb" that could be used by practitioners in the field or the lab. These correlations could also help cross-check experimentally obtained values or allow estimation of mechanical properties without an actual test, resulting in optimization of time, money, and resources of materials and space. For example, if the strength of a mix is tested at 7 days, the strength of the mix at 365 days could be estimated.

4.2 Methodological aspects considered in statistical correlations

a) Regression analyses performed in this thesis used either Origin Pro 9.0 which is a data analysis and graphing software [370], Microsoft Excel, or Python (programming language) on the platform of Google collab [371].
b) Results of different mechanical properties are supplemented with corresponding coefficients of variation (CoV) in parenthesis, wherever applicable.
c) Wherever applicable, graphs have been supplemented with error bars that represent the standard error. Standard error was obtained by diving the standard deviation by the square root of the number of specimens used to obtain the average value of that measurement.
d) Concerning regression analyses performed in this chapter, the r-squared (R^2) value (or the coefficient of determination) was used as an indication of how well, the model or equation fit the data. It is a statistical measure that is used to explain the proportion of variation in the response variable, which can be explained by the regression model being used and varies between 0 and 1. The value 0 indicates that the regression model does not explain any variation, while values approaching 1 indicate that the regression explains most of the variance in the response variable [372].
e) Another characteristic that was taken into account while considering the suitability of the regression analyses was the p-value. A small p-value indicates that the relationship between the dependent and independent variables is not due to chance, thereby allowing the rejection of the null hypothesis. A null hypothesis in turn is the assumption that there is no relation between the dependent and independent variable. Therefore, a p-value smaller than the significance level, which is most commonly set as 0.05, in addition to an r-squared value approaching 1, validates the regression model. In this research, most results presented were found to have a p-value notably less than 0.05, indicating their statistical significance [373]. However, since the p-value is only a probability of the null hypothesis being right, it cannot be treated in isolation and must be interpreted as a part of the

entire research accounting for the sample size, sample treatment, and outcome [374]. In a few cases where regression was performed in this research with only three data points available, the p-value exceeded 0.05, by a small margin, despite reasonable R-squared values (generally > 0.94, in some cases ranging till 0.85). The data was not rejected in these cases because the p-value is dependent on sample size, and having only 3 data points would require exceptionally high R-squared values to result in p-values less than 0.05 Since inadequacy of data points in these cases could lead to unreliable conclusions based on p-values, values > 0.05 were also considered acceptable.

f) The F-critical value (also known as F-statistic) was also considered in addition to the p-value, and it is calculated as the ratio of the mean square of the fitted model and the mean square of errors [375]. It indicates if the fitted model performs better than the intercept only model, with zero predictor variables and a constant result. If the F-value obtained from the data is greater than the F-critical value, this indicates that the coefficients added to the regression model, improve the explanation of the response variable. Most often, F-value being greater than F-critical is indicated by Prob(F-statistic) or p-value, which if less than 0.05, indicates that the F-value obtained from the data is greater than the F-critical value. [372, 373, 375].

4.3 Workability and water-binder ratios

It was of utmost importance that the workability of mixes chosen was representative of what is used on the field by masons and consistent throughout the experimental program, as discussed in detail in Section 3.3.2, Chapter 3. Therefore, workability was measured following EN 1015-3 [75] and the target flow table value chosen was 175±10 mm for all mixes. The water-binder ratio (by mass) for each mix was determined experimentally, by trial and error (Figure 30).

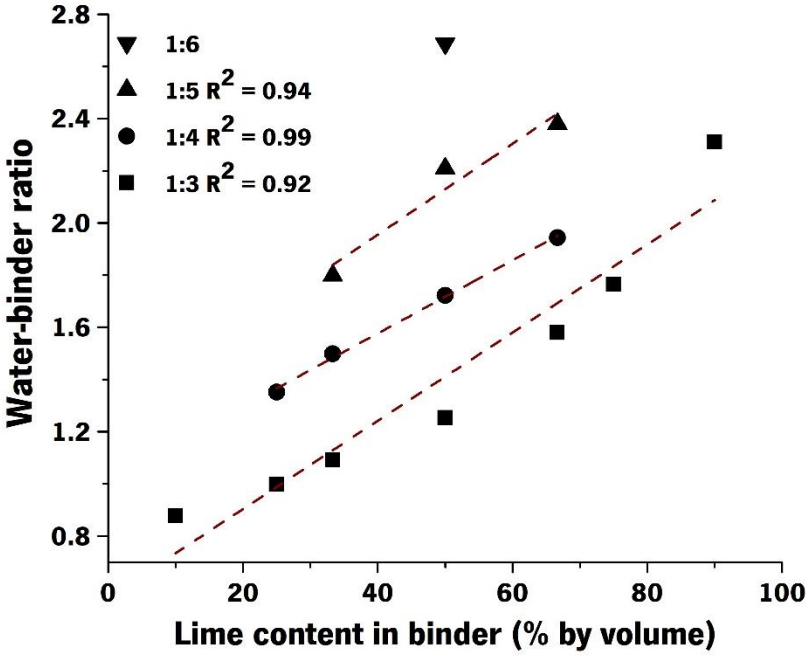

Figure 30: Water-binder ratio (by mass) of mixes expressed as a function of lime content in the binder, in the workability range of 175±10 mm, measured using the flow table test according to EN 1015-3 [75]. The values 1:3, 1:4, 1:5 and 1:6 indicate B/Ag ratios. The R-squared values shown are for individual B/Ag ratios (only one mix for 1:6).

It was observed that for the same B/Ag ratio, the requisite water for the mix changed each time the quantity of lime in the binder was varied. It was possible to identify a linear pattern that related the amount of lime in the binder (by volume) with the water-binder ratio (Figure 30). It was also discovered that each time the binder-aggregate ratio (by volume) was changed; the linear relation had to be recalibrated. If the quantity of lime in the binder was kept constant and the B/Ag ratio was changed, it was possible to observe the influence of the latter on the w/b ratio as well. Therefore, a multiple linear regression was performed and has been presented to correlate the quantity of lime in the binder (by volume) and the B/Ag ratio (by volume) with the water-binder ratio (by mass) of each mix, which resulted in an adjusted R^2 value of 0.93, and F-value of 87.08 (Prob>F-value 1.8e-7). Attempts were made to use the water-binder ratio by volume as the dependent variable for the multiple linear regression. However, a good fit was not obtained and therefore, the water-binder ratio shown is by mass or weight in Equation 11.

$$\frac{w}{b} = 2.495 + 0.0168\ (\text{Lime in binder }\%) - 0.059\ (\frac{B}{Ag}\%) \qquad 11$$

All 15 mortar mixes (Detailed in Chapter 3) were used as input for the regression performed (Equation 11). Predicted values were compared with actual values (average difference in absolute value was 7.1%),

and it was found that the difference was mostly less than 10% (Table 13) except for the mix 1C1L12S (50%) with a difference of around 12.5%, and the mix 9C1L30S (10%) with a difference of around 20%.

Since Equation 11 has three terms, a simpler expression has also been provided in equation 12 as an alternative with a common slope for all mixes, where the intercept varies as a function of the B/Ag ratio.

$$\frac{w}{b} = 0.0158\ (\text{Lime in binder \%}) + f(\frac{B}{Ag}) \qquad 12$$

The slope 0.0158 was calculated by averaging the value of slopes of all three linear regressions shown in Figure 30 and the term $f(\frac{B}{Ag})$ is the value of the intercept obtained from the average difference in different intercepts (0.357) from individual regressions, added to the intercept from B/Ag ratio 1:3 (0.567). Therefore, $f(\frac{B}{Ag})$ for 1:3 is 0.567, for 1:4 is 0.924 (which is 0.567+0.357), for 1:5 is 1.282 (which is 0.924+0.357), and for 1:6 it is 1.639 (which is 1.282+0.357).

Table 13: Water-binder ratio (by mass) for different mixes - used, predicted, and difference (%)

Mortar mixes	Lime content in binder (%)	B/Ag ratio (%)	Actual water-binder ratio	Predicted water-binder ratio		Difference (%)	
				Equation 10	Equation 11	Equation 10	Equation 11
9C1L30S	10	33.3	0.88	0.69	0.72	-20.8	-17.4
3C1L12S	25	33.3	1.00	0.95	0.96	-5.2	-3.7
2C1L9S	33.3	33.3	1.09	1.09	1.09	-0.4	0.3
1C1L6S	50	33.3	1.25	1.37	1.36	9.0	8.2
1C2L9S	67.7	33.3	1.58	1.66	1.64	5.3	3.6
1C3L12S	75	33.3	1.76	1.79	1.75	1.2	-0.8
1C9L30S	90	33.3	2.31	2.04	1.99	-11.8	-13.9
3C1L16S	25	25	1.35	1.44	1.32	6.4	-2.4
2C1L12S	33.3	25	1.50	1.58	1.45	5.3	-3.2
1C1L8S	50	25	1.72	1.86	1.71	7.9	-0.5
1C2L12S	67.7	25	1.94	2.15	1.99	10.8	2.5
2C1L15S	33.3	20	1.80	1.87	1.81	4.1	0.5
1C1L10S	50	20	2.21	2.15	2.07	-2.6	-6.3
1C2L15S	67.7	20	2.38	2.45	2.35	3.0	-1.2
1C1L12S	50	16.7	2.69	2.35	2.43	-12.6	-9.7
Average						7.1	4.9

The objective of proposing such equations, (calibrated according to the materials used) is to reduce the number of trials that would otherwise be required to determine the water-binder ratio for a targeted flow

value. The values estimated from Equations 10 and 11 and presented in Table 13 have been plotted alongside the actual water-binder ratios used in the mortar mixes, in Figure 31.

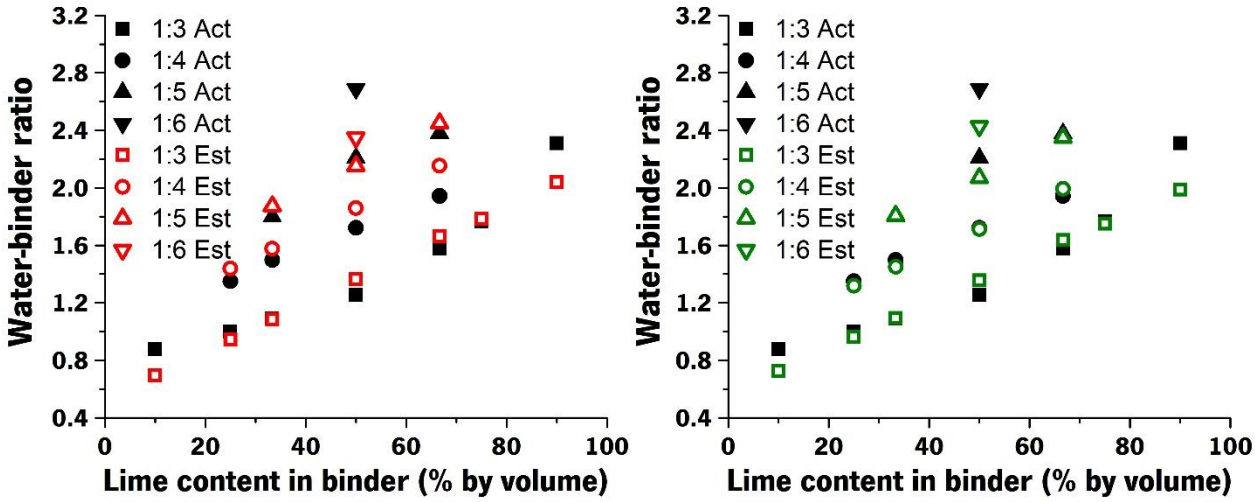

Figure 31: Experimental water binder ratios (Table 13) versus estimated according to (a) Equation 10 (b) Equation 11

4.4 Mechanical strength

4.4.1 Methodology

Compressive strength and flexural strength of the mortar mixes were measured according to EN 1015-11 [16], on a universal testing machine from the company Lloyd. Three prismatic specimens of size 40 × 40 × 160 mm^3 were used in each 3-point bending test to measure flexural strength (Figure 32 (a)). All specimens initially tested for flexural strength and were loaded by controlling the displacement, at a rate of 12 µm/s. Subsequently, the halves obtained after flexural strength testing were used for the test of compressive strength; 6 specimens/measurements contributed to the final value of compressive strength, in each case. For compressive strength, the contact area between the specimen and equipment for load application was 40 mm × 40 mm, and the height of the specimen was 40 mm (Figure 32 (b)). A pre-load of 150 N was applied on all specimens and the rate of loading was 50 N/s.

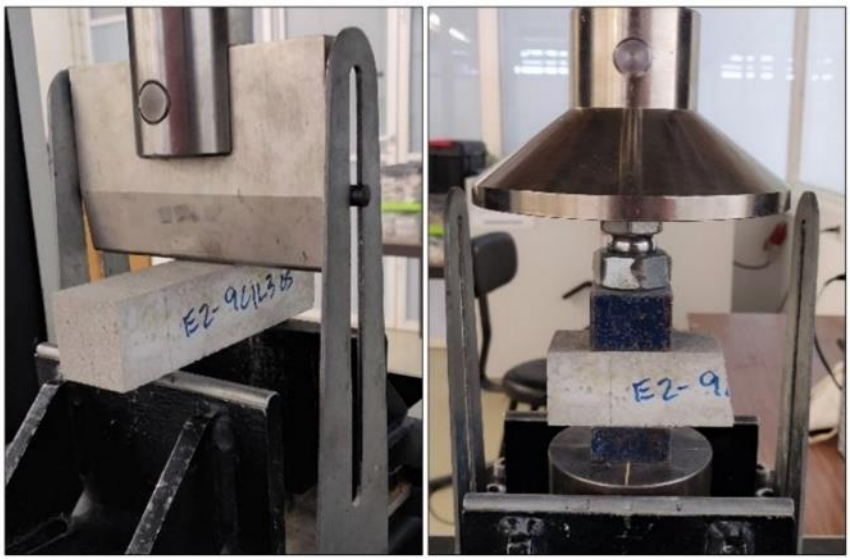

Figure 32: Images for (a) Flexural test (3-point bending) and (b) Uniaxial (unconfined) compression test for mortar specimens

4.4.2 Results of mechanical strength

Since the mechanical strength of lime-cement has been expressed as a function of common factors, the factors have been explained below along with their notations.

a) Lime content in the binder (10, 25, 33.3, 50, 66.7, 75, 90) % by volume. For example, lime content in the mix 1C2L9S has been expressed as 67% by volume of the binder.
b) Binder aggregate ratio or B/Ag ratio (1:3, 1:4, 1:5, 1:6) or (33.3, 25, 20, 16.7) % by volume. For example, the mix 1C2L9S has a binder-aggregate ratio of 1:3 or 1/3 expressed as 33% binder in the mix, by volume.
c) Curing age, (7, 14, 28, 90, 180, 365) days.

For the 15 mortar mixes specified in Chapter 3, for ages from 7 days to 365 days, values of compressive strength obtained have been presented in Table 14 and range from 0.14 MPa to 15.5 MPa, while values of flexural strength range from 0.04 MPa to 5.22 MPa as presented in Table 15.

It is recognized that a direct comparison of the values obtained here with those found in the existing literature is not possible because, among many other factors, researchers use different types of lime or cement. However, a comparison of the general range of values is feasible and must be discussed to validate the strengths obtained in this thesis. Arandigoyen *et al.* [59] present one of the widest ranges of data of compressive strength available on lime-cement blended mortars (5–13 MPa) and this is similar to the range of values obtained here (2–15 MPa). However, in some cases, the values of strength presented by them are slightly higher than the corresponding values obtained in this campaign. One of

the plausible reasons for this could be the use of a lower water-binder ratio by them due to differences in the type of cement (Type II versus Type I in this campaign) or difference in target workability for the mixes. But this is difficult to verify because the water-binder ratio used to prepare their mixes has not been explicitly mentioned. The values of compressive strength presented by Cizer [2] seem to be in the range of 5–35 MPa, considerably higher than those presented here. But the flow value targeted was between 120 and 130 mm which is likely to explain the difference, since the lower the amount of water used in the mix, the greater is the strength of the mix obtained [96]. Data on compressive strength of blended lime-cement mortars presented by Haach *et al.* was found to be similar to the values obtained in this experimental campaign for approximately the same consistency [11, 96]. Similarly, it was found that if similar consistency (flow value) is targeted, flexural strength attained in blended lime-cement mortars falls in the range of data found in the current experimental campaign, as observed from the work of Macharia [95].

Eurocode 6 [18], together with EN 998-2 [376], characterize mortars into classes based on the minimum compressive strength (in MPa) that the mortar must attain in 28 days. This categorization is based only on strength and does not discuss the composition of the mortar. However, in the different national annexes to the current version of the Eurocode 6 [18], more details are provided on how different compositions of mixes, may lead to the fulfillment of strength requirements for different mortar classes. It was found that in the cases where the same mortar mixes were tested, the strength at 28 days was in the expectable mortar class range. For example, the Polish national annex [377] suggests a mix composition of 1:2:9 in the category of 2.5 MPa. As may be observed from Table 14, the mix 1:2:9 attains a strength of 2.35 MPa in 28 days. The Belgian national annex [350] suggests mix compositions of 1:1:6 and 2:1:9 for the categories of 5 MPa and 8 MPa respectively. In this research, the mixes 1:1:6 and 2:1:9 led to strengths of 4.68 MPa and 8.13 MPa respectively (Table 14).

Table 14: Compressive strength values of lime-cement mortars from 7 days to 365 days

Mortars	fc-7 (MPa) (CoV %)	fc-14 (MPa) (CoV %)	fc-28 (MPa) (CoV %)	fc-90 (MPa) (CoV %)	fc-180 (MPa) (CoV %)	fc-365 (MPa) (CoV %)
9C1L30S (10%)	8.94 (3.6%)	10.64 (9.6%)	12.11 (4.4%)	12.22 (8.0%)	11.29 (7.4%)	15.46 (5.5%)
3C1L12S (25%)	7.66 (3.5%)	9.91 (5.0%)	9.95 (3.6%)	9.28 (0.6%)	9.92 (6.3%)	12.19 (5.3%)
2C1L9S (33%)	6.09 (2.8%)	7.36 (4.9%)	8.13 (6.6%)	8.57 (6.0%)	8.73 (9.7%)	8.65 (6.7%)
1C1L6S (50%)	4.12 (5.5%)	5.41 (8.8%)	4.68 (6.3%)	6.23 (6.9%)	6.31(3.9%)	7.01 (6.4%)
1C2L9S (67%)	1.48 (6.7%)	1.90 (2.8%)	2.39 (2.6%)	2.45 (6.7%)	2.69 (10.5%)	2.67 (6.9%)
1C3L12S (75%)	0.63 (9.0%)	1.16 (7.2%)	1.37 (3.3%)	1.53 (3.1%)	1.55 (6.7%)	1.61 (3.5%)
1C9L30S (90%)	0.14 (9.8%)	0.22 (11.8%)	0.30 (6.7%)	0.41 (3.5%)	0.45 (5.7%)	0.43 (7.6%)

3C1L16S (25%)	4.59 (6.6%)	6.46 (1.4%)	6.01 (2.1%)	7.05 (4.8%)	7.85 (3.5%)	7.77 (5.1%)
2C1L12S (33%)	3.23 (5.7%)	5.03 (3.2%)	5.09 (9.5%)	5.73 (3.5%)	6.34 (2.6%)	5.16 (5.7%)
1C1L8S (50%)	2.31 (1.1%)	3.12 (8.7%)	3.00 (8.2%)	3.53 (5.4%)	3.10 (9.6%)	3.56 (5.3%)
1C2L12S (67%)	0.77 (7.0%)	1.37 (6.6%)	1.41 (9.0%)	1.19 (12.0%)	1.45 (6.1%)	1.62 (5.7%)
2C1L15S (33%)	1.86 (13.0%)	2.83 (9.5%)	3.08 (7.6%)	3.26 (12.4%)	3.69 (10.1%)	3.26 (3.5%)
1C1L10S (50%)	1.31 (3.2%)	1.77 (15.6%)	1.59 (18.9%)	1.74 (17.9%)	1.99 (5.0%)	2.05 (17.2%)
1C2L15S (67%)	0.46 (8.0%)	0.83 (8.9%)	0.85 (7.0%)	0.86 (8.6%)	0.90 (12.8%)	0.96 (6.7%)
1C1L12S (50%)	0.85 (12.2%)	1.34 (22.2%)	1.39 (17.5%)	1.19 (12.0%)	1.34 (14.9%)	1.62 (5.8%)

Table 15: Flexural strength values of lime-cement mortars from 7 days to 365 days

Mortars	ff-7 (MPa) (CoV %)	ff-14 (MPa) (CoV %)	ff-28 (MPa) (CoV %)	ff-90 (MPa) (CoV %)	ff-180 (MPa) (CoV %)	ff-365 (MPa) (CoV %)
9C1L30S (10%)	2.67 (9.8%)	3.15 (3.6%)	3.89 (12.3%)	3.15 (12.3%)	3.75 (6.7%)	5.22 (2.0%)
3C1L12S (25%)	1.95 (6.6%)	2.58 (2.7%)	2.76 (7.0%)	3.22 (4.5%)	3.64 (4.2%)	4.60 (8.0%)
2C1L9S (33%)	1.52 (5.6%)	2.32 (0.9%)	2.60 (8.6%)	2.52 (2.6%)	3.03 (5.5%)	3.11 (6.8%)
1C1L6S (50%)	1.23 (4.8%)	1.69 (4.0%)	1.96 (6.0%)	2.14 (6.7%)	2.31 (2.0%)	2.54 (1.9%)
1C2L9S (67%)	0.41 (7.7%)	0.70 (11.3%)	0.69 (4.5%)	0.86 (6.3%)	0.99 (2.9%)	0.98 (2.6%)
1C3L12S (75%)	0.28 (4.5%)	0.44 (10.8%)	0.48 (16.0%)	0.58 (7.6%)	0.61 (10.5%)	0.52 (16.9%)
1C9L30S (90%)	0.04 (29.9%)	0.04 (28.3%)	0.19 (18.1%)	0.28 (7.7%)	0.26 (5.2%)	0.21 (4.1%)
3C1L16S (25%)	1.23 (2.3%)	1.72 (11.2%)	2.10 (6.6%)	2.35 (12.6%)	2.95 (3.4%)	2.74 (7.9%)
2C1L12S (33%)	1.12 (9.3%)	1.50 (6.4%)	2.09 (1.7%)	2.09 (2.5%)	2.26 (9.9%)	2.08 (1.4%)
1C1L8S (50%)	0.70 (10.2%)	0.95 (17.3%)	1.08 (11.9%)	1.20 (3.9%)	1.24 (4.7%)	1.17 (5.4%)
1C2L12S (67%)	0.30 (6.1%)	0.53 (8.1%)	0.52 (10.2%)	0.50 (0.5%)	0.51 (13.7%)	0.60 (11.7%)
2C1L15S (33%)	0.66 (5.0%)	0.99 (9.2%)	1.16 0.8%)	1.26 (6.8%)	1.30 (7.2%)	1.32 (2.5%)
1C1L10S (50%)	0.37 (14.7%)	0.58 (11.0%)	0.64 (3.3%)	0.66 (13.8%)	0.74 (9.0%)	0.77 (3.7%)
1C2L15S (67%)	0.21 (2.9%)	0.34 (14.3%)	0.35 (37.9%)	0.36 (10.1%)	0.39 (14.8%)	0.31 (12.3%)
1C1L12S (50%)	0.29 (3.4%)	0.42 (20.9%)	0.50 (17.3%)	0.48 (9.7%)	0.51 (11.7%)	0.60 (11.7%)

If all 15 mixes are taken into account at 6 different curing ages, there are 90 data points available for compressive strength and flexural strength each. Therefore, an attempt was made to correlate the two properties. It was found that the ratio of compressive strength to flexural strength was approximately 3 for all mixes, across all ages (Table 16). The general range of the ratios varied between 2.5 to 3.5, and therefore an average ratio was calculated for each mix across different ages and has also been presented in Table 16, along with the coefficient of variation.

Table 16: Ratio of compressive strength to flexural strength for mixes of different ages

$\frac{f_c}{f_f}$ (MPa/MPa)	7d	14d	28d	90d	180d	365d	Average	CoV (%)
9C1L30S (10%)	3.3	3.4	3.1	3.9	3.0	3.0	3.3	10.3

3C1L12S (25%)	3.9	3.8	3.6	2.9	2.7	2.6	3.3	17.9
2C1L9S (33%)	4.0	3.2	3.1	3.4	2.9	2.8	3.2	13.7
1C1L6S (50%)	3.4	3.2	2.4	2.9	2.7	2.8	2.9	12.1
1C2L9S (67%)	3.6	2.7	3.5	2.8	2.7	2.7	3.0	14.0
1C3L12S (75%)	2.2	2.7	2.8	2.6	2.5	3.1	2.7	11.0
1C9L30S (90%)	3.3	5.0	1.5	1.5	1.8	2.0	2.5	54.6
3C1L16S (25%)	3.7	3.8	2.9	3.0	2.7	2.8	3.1	15.2
2C1L12S (33%)	2.9	3.4	2.4	2.7	2.8	2.5	2.8	11.9
1C1L8S (50%)	3.3	3.3	2.8	2.9	2.5	3.0	3.0	10.6
1C2L12S (67%)	2.5	2.6	2.7	2.4	2.8	2.7	2.6	6.2
2C1L15S (33%)	2.8	2.9	2.7	2.6	2.8	2.5	2.7	6.0
1C1L10S (50%)	3.6	3.1	2.5	2.6	2.7	2.7	2.8	14.1
1C2L15S (67%)	2.2	2.4	2.4	2.4	2.3	3.1	2.5	12.5
1C1L12S (50%)	3.0	3.2	2.8	2.5	2.6	2.7	2.8	9.1

Three observations may be made from the data available in Table 16:

a) Concerning lime content in the binder - The ratio f_c/f_f (Table 16, column titled average) generally reduces with increasing lime content in the binder. For B/Ag ratio 1:3, as the quantity of lime in the binder increases from 10% to 90%, the average ratio decreases from 3.3 to 2.5.

b) Concerning B/Ag ratio - The ratio f_c/f_f (Table 16, column titled average) decreases slightly as the binder content in the mix reduces – 3, 2.9, and 2.7 for the B/Ag ratios 1:3, 1:4, and 1:5 respectively.

c) Concerning time - Between 7 and 365 days, the ratio f_c/f_f decreases in most cases. The ratio at day 7, averaged for all mortars is 3.2, while at day 365 it is 2.7.

4.4.2.1 Evolution of mechanical strength with time

From Table 14 and Table 15 it is possible to observe that all 15 mortars, generally display a coherent increment in compressive strength and flexural strength with time. Figure 33 and Figure 34 have three graphs each, displaying the evolution of compressive and flexural strength with time, respectively. The mortars have been classified according to binder-aggregate ratios, 1:3, 1:4, and 1:5. The error bars in the graphs illustrate the scatter in different data points which have been calculated from an average of 3 measurements in flexural strength and 6 measurements in compressive strength. It may be observed that the scatter is small for most data points.

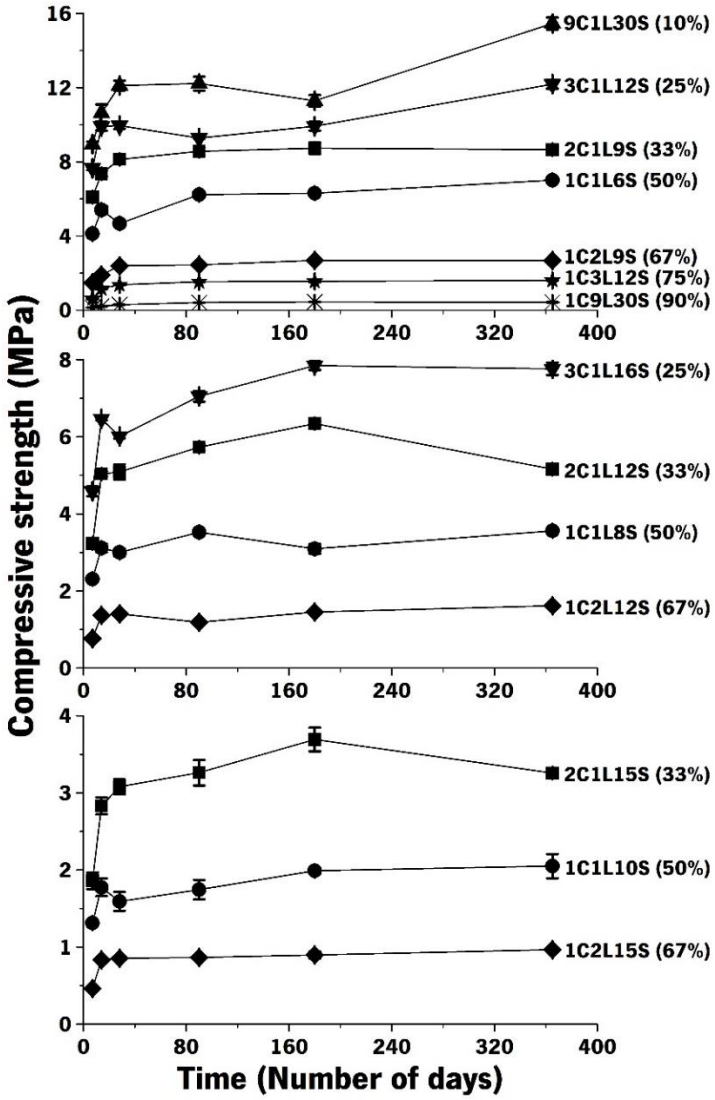

Figure 33: Evolution of compressive strength with time for different binder-aggregate ratios from 7 to 365 days

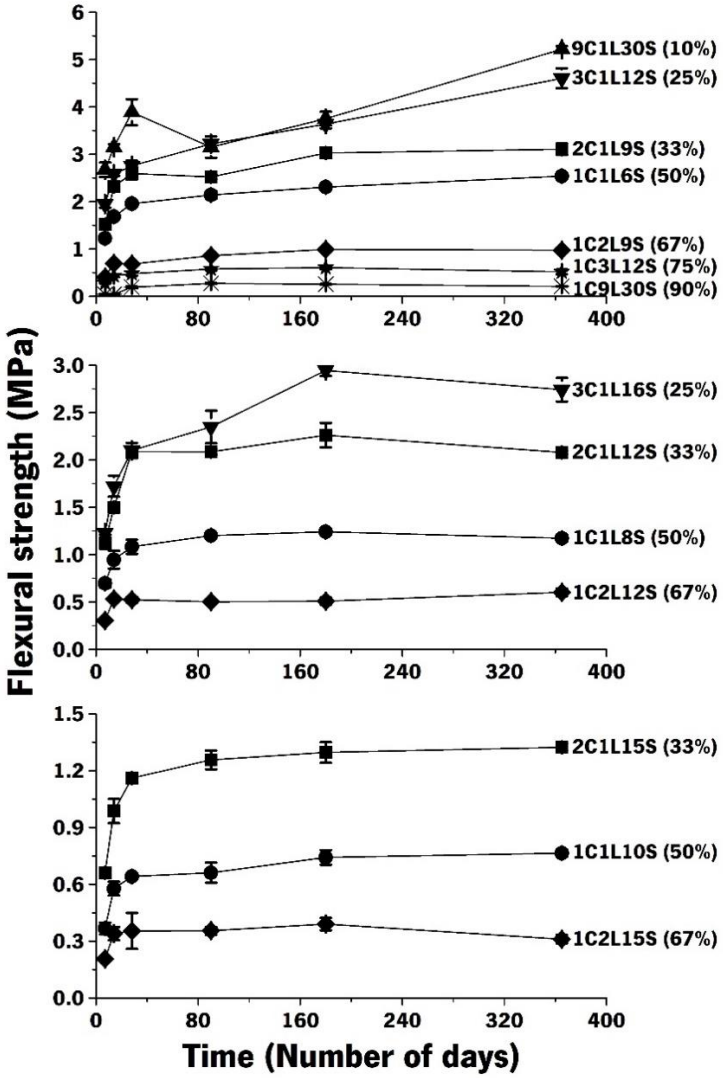

Figure 34: Evolution of flexural strength with time for different binder-aggregate ratios from 7 to 365 days

Upon observation, it was found that the strength of all mortars, seemed to evolve similarly with time, i.e. most of the strength (compressive and flexural) is gained up till 28 days of age (≥ 70%) and strength appears to increase more up to 90 days of age (≥ 90%), after which it remains approximately the same up till 365 days of age. This observation is fairly consistent with what is found in literature as the strength at 90 days is considered to be a benchmark, for mortars involving air lime in their composition [2, 12, 59]. Figure 35 and Figure 36 show the evolution of normalized values of compressive and flexural strength respectively, using the 90 days as a reference instead of 28 days for cement-based mixes. It is easy to observe that not all mixes, follow the same evolution pattern. Specifically, in the case of mortars with less than or equal to 25% lime in the binder, there appears to be a significant increase in strength between 90 and 365 days, approximately between 20-30 % in the case of compressive strength. And in the case of flexural strength, there is an increase of approximately 60% and 40% in 9C1L30S (10%) and 3C1L12S (25%) respectively. However, in the rest of the mixes, regardless of the dips and rises, the shape of most

curves appear to be similar, indicating the scope for an analytic expression for mechanical strength as a function of time.

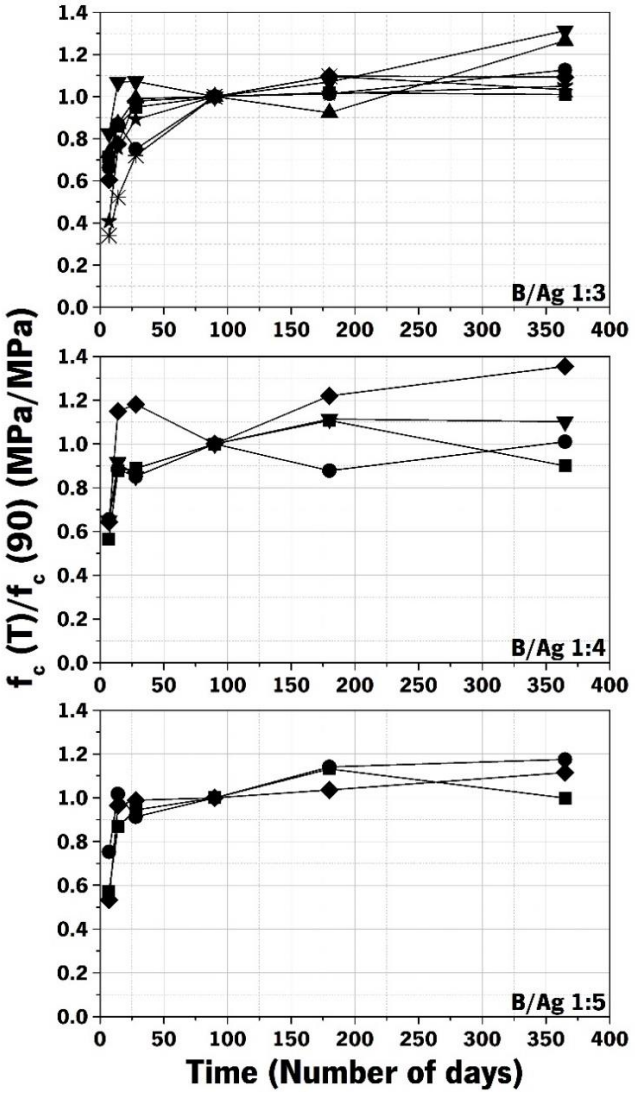

Figure 35: Evolution of normalized compressive strength with time for different binder-aggregate ratios from 7 to 365 days. Strength has been normalized with respect to compressive strength at 90 days

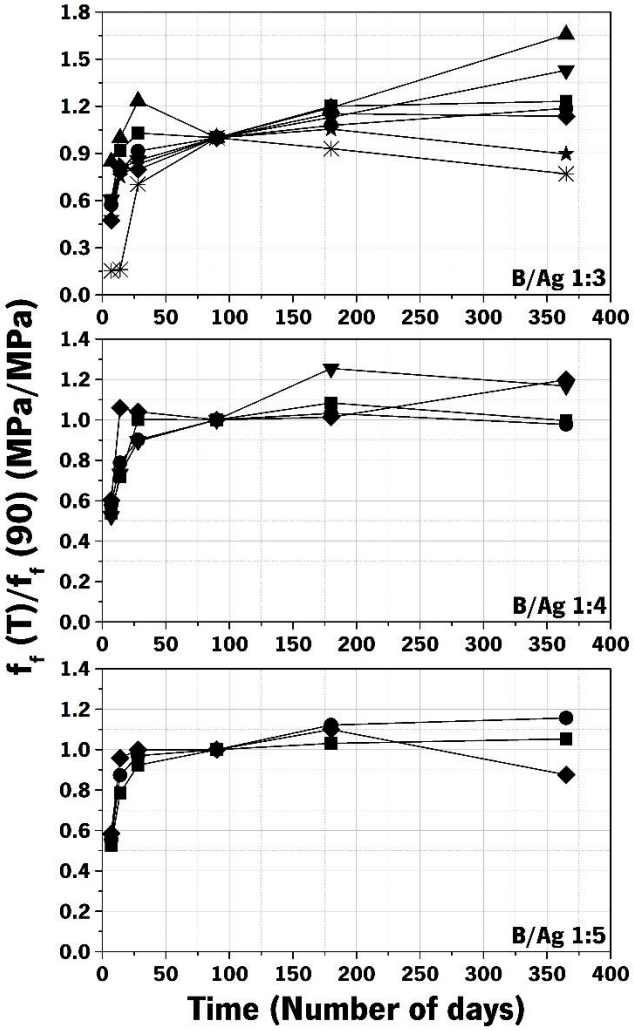

Figure 36: Evolution of normalized flexural strength with time for different binder-aggregate ratios from 7 to 365 days. Strength has been normalized with respect to flexural strength at 90 days

Thereafter, an attempt was made to identify the pattern of evolution of strength with time. It was found that different expressions could describe this evolution in strength reasonably well such as polynomial, logistic, or exponential. The goal, however, was to find an equation with as few parameters as possible. Keeping this in mind, the simplest expression that could be found has been shown in Equation 13, where T is the age of the mortar, expressed in number of days. This equation may be used to describe the evolution of strength for all 15 lime-cement mortars (Figure 37 and Figure 38), and the differences between values predicted by the equation and the experimentally obtained values have been presented in (Annex-Table 1 and Annex-Table 3). The average difference between predicted and actual values was found to be 0.2 MPa or 8% for compressive strength and 0.1 MPa or 10% for flexural strength (Annex-Table 2 and Annex-Table 4).

$$f_c(T) = ae^{\frac{b}{\sqrt{T}}} \qquad 13$$

$$f_f(T) = ae^{\frac{b}{\sqrt{T}}}$$

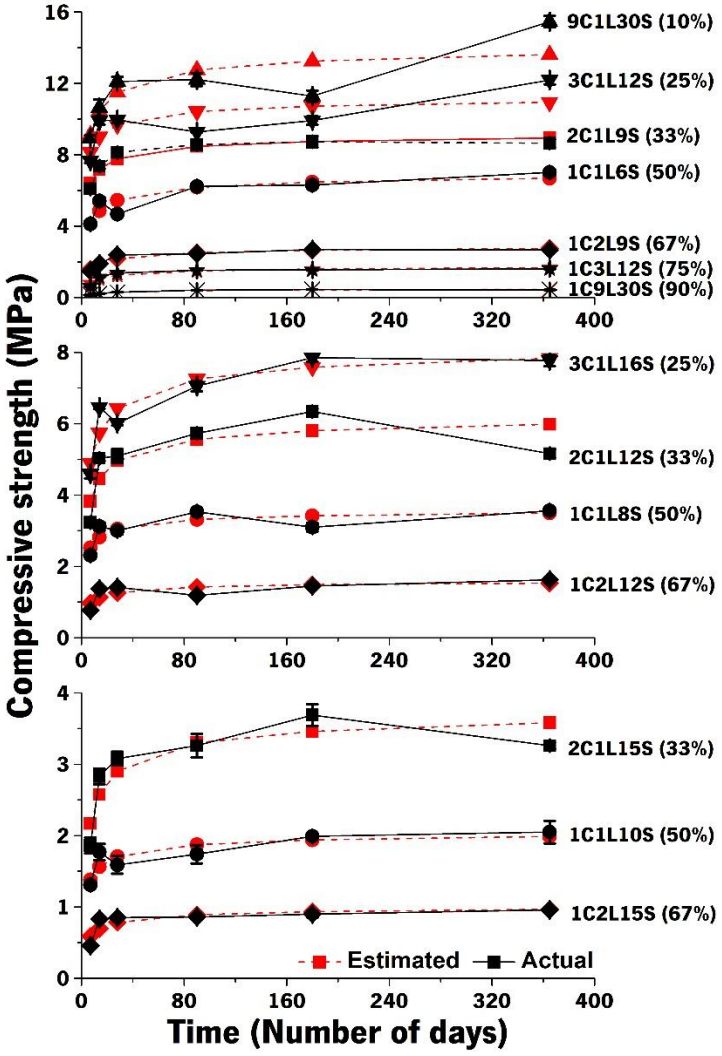

Figure 37: Evolution of compressive strength with time estimated according to Equation 13

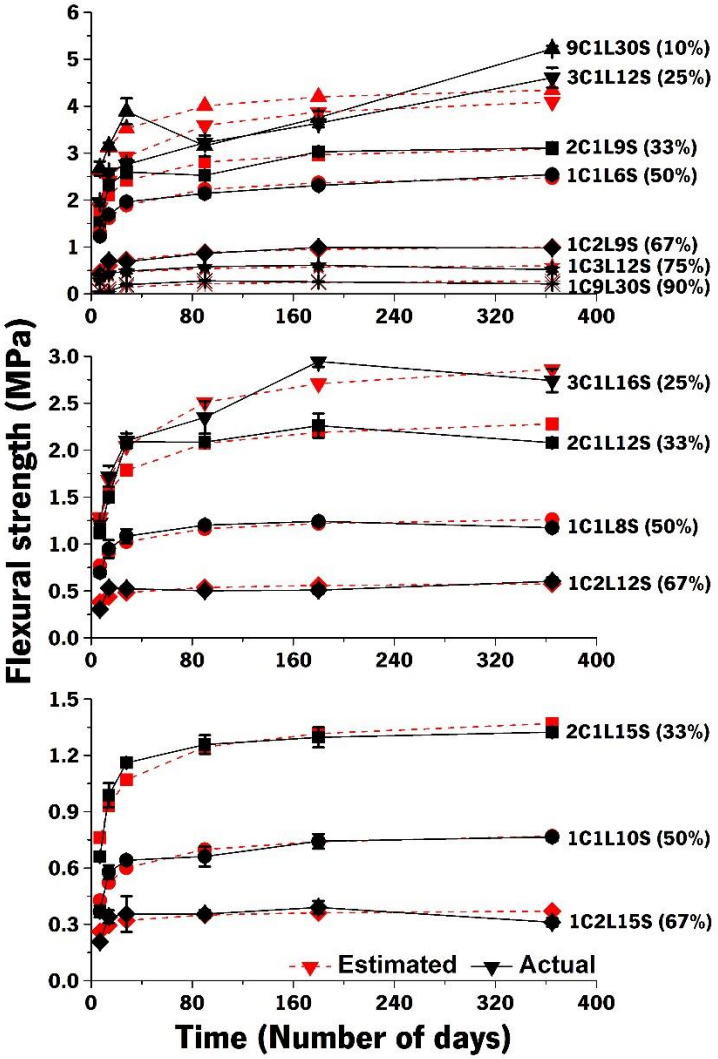

Figure 38: Evolution of flexural strength with time estimated according to Equation 13

For the proposed model, the two variables that require fitting are a and b. Based on equation 13, in the event, that time (t) tends to infinity (∞), the value of $e^{\frac{1}{\infty}}$ would tend to e^{0} which is 1, implying that fc or compressive strength would tend to the value of parameter a, which would theoretically be the strength of the mortar once it is mature, between 180 and 365 days of age, based on data presented in Table 14. Furthermore, it was found that the ratio between strength (both f_c and f_f) at 365 days of age and 7 days of age varied in the range of 1.6 to 2.5 (Annex-Table 5 and Annex-Table 6). Therefore, parameter a could be expressed in the range of 1.6 to 2.5 times, a function of the compressive strength at 7 days of the mixes. This factor ranging between 1.6 and 2.5 could potentially be generalized for different mixes. What makes that interesting is that if then, the strength of a mix is normalized with respect to its strength at 7 days, it is possible to obtain a single curve that could represent the normalized evolution of strength with time for lime-cement mixes. This was achieved through curve fitting and regression and has been shown in equation 14. This data set, therefore, included 14 mixes, at 6 different ages, which means a total of

84 data points. For this analysis, all mixes were used except for 1C9L30S (90%) since it was a clear outlier, in terms of the rate of gain of strength as well as the very small absolute values of strength at day 7. The most probable reason for this is the large quantity of lime in its binder, which makes it behave similar to an only lime binder.

$$\frac{f_c(T)}{f_c(7)} = 1.7\, e^{\frac{-1.2}{\sqrt{T}}} \quad \text{when lime in binder} \leq 50\% \text{ by volume}$$

$$\frac{f_c(T)}{f_c(7)} = 2.4\, e^{\frac{-1.7}{\sqrt{T}}} \quad \text{when lime in binder} > 50\% \text{ by volume} \qquad 14$$

$$\frac{f_f(T)}{f_f(7)} = 2.2\, e^{\frac{-1.8}{\sqrt{T}}}$$

Equation 14, therefore, allows the user to estimate the compressive strength of any of the lime-cement mixes discussed if the strength of that mix is tested at 7 days of age. Based on equation 14, if the estimated values are compared with the experimentally obtained values, it was found that the average difference was around 0.44 MPa or 11.2%, in the case of compressive strength, with the maximum difference going up to 27%, as shown in Annex-Table 7, despite low R-squared values of 0.56 and 0.60 in case of less than and greater than 50% lime in the binder, respectively. In the case of flexural strength, the R-squared value found was 0.72 and the average difference in estimated and experimental values was found to be around 10% as well or 0.15 MPa, as shown in Annex-Table 8. The evolution of compressive and flexural strength with time, based on equation 14, is illustrated in Figure 39 and Figure 40. In the cases of mixes with ≤ 25%, lime in the binder such as 9C1L30S (10%) and 3C1L12S (25%), the functions presented in equation 14 can quite significantly overestimate the strength of the mixes at certain ages, since they behave differently from the other mixes between 90 and 365 days (~up to 30% in compressive strength and even up to 60% in flexural strength Figure 35 and Figure 36). And therefore, at this stage, these equations cannot yet be safely used for extrapolation for all lime-cement mixes. It is recognized that a significantly larger data set would be required, with more mixes tested over time, to obtain better fitting and consequently higher r-squared values, which would ultimately lead to better estimations of strength. The findings reported herein seem to point in the direction of the plausibility of potential generalizations when adequate data is available.

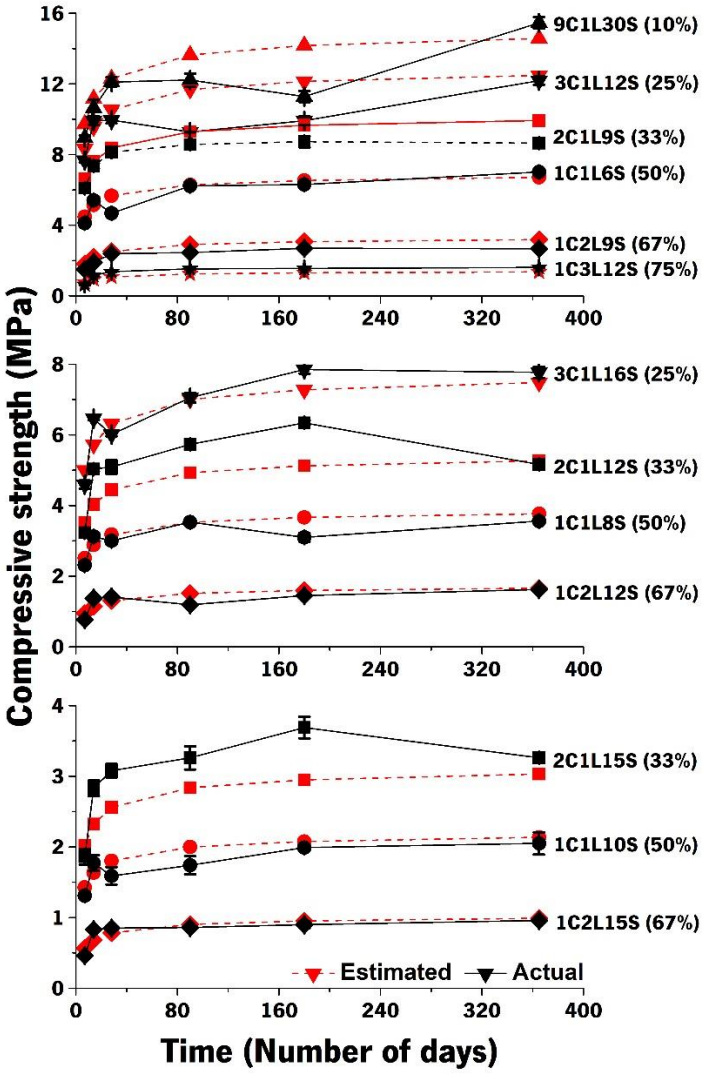

Figure 39: Evolution of compressive strength with time estimated according to Equation 14

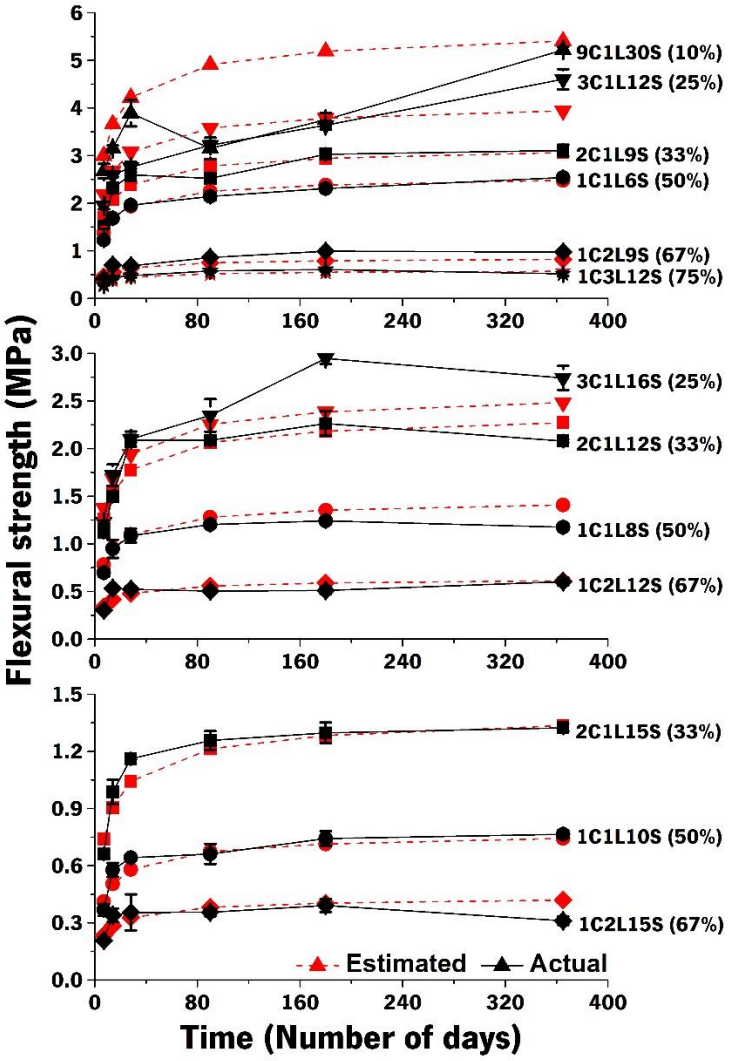

Figure 40: Evolution of flexural strength with time predicted according to Equation 14

Another observation that can be made from equation 14, is that in the case of flexural strength, only one expression was found to be adequate for all the mixes. However, for compressive strength it is possible to distinguish the normalized evolution of strength with time, depending on the mixes having more than or less than 50% lime in the binder, since the values of the constants a and b obtained were different. This has been demonstrated graphically in Figure 41. It may be noted that the two curves shown in Figure 41 do not start from the value 1 because they represent the analytic expression of equation 14, which is obtained from the best fit of the evolution of strength with time for 15 mixes. Based on the values of a and b obtained in equation 14 for the two different curves, as well as Figure 41, it is possible to conclude, that the evolution of strength in lime dominant mixes is slower, and therefore continues for longer. Their normalized growth in strength is also higher than that of cement dominant blended mixes. This may be attributed to the slow kinetics of the carbonation process in lime dominant mortars, which could take

several months or even years to progress [47], compared to the relatively faster process of cement hydration, the bulk of which takes place within the first 28 days [2, 37]. The curves in Figure 41, appear to confirm the result of the difference in kinetics of the two phenomena, which have been discussed in detail in Chapter 2.

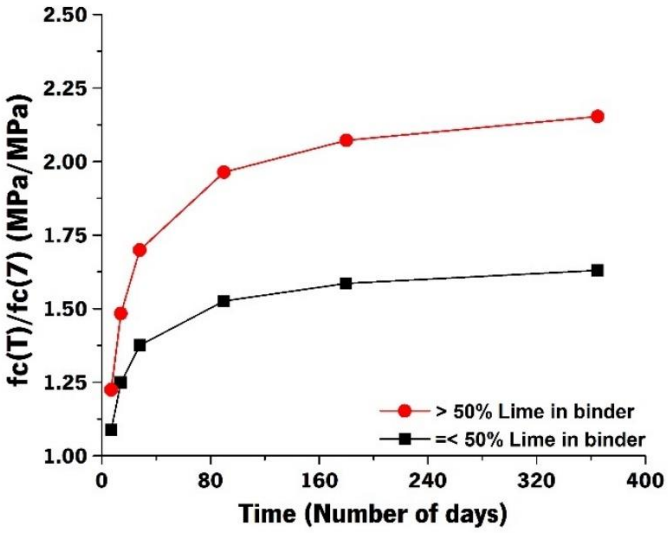

Figure 41: Graphical representation of Equation 14 – Evolution of compressive strength with time, normalized with respect to strength at day 7, for lime v/s cement dominant blended mixes

4.4.2.2 Impact of lime content in the binder on the mechanical strength of mortar

This discussion assesses the impact that lime has on the strength of the mortar by varying lime content in the binder of mixes with different B/Ag ratios (1:3, 1:4, and 1:5 by volume). To assess and quantify the influence of this factor, linear regressions were performed on data obtained at different ages. To facilitate comparison and normalization, a benchmark mortar had to be chosen, with the highest feasible strength, which is a mix with the least amount of lime in the binder (10%), for any given B/Ag ratio. Furthermore, 10% lime means 90% cement in the mix, which means it is close to the composition of a cement mortar and yet it retains the label of lime-cement masonry mortar from a practical point of view, because of the presence of 10% lime in the binder. Allowing this benchmark mix to have some amount of lime in it ensures that it is subjected to the same curing conditions, thereby reducing variables in the comparison. Based on the rationale presented, while studying the impact of lime in the binder on the mechanical performance of mortar, the benchmark mix always consists of 10% lime or 90% cement (by volume).

It was found that for a given B/Ag ratio at any age, the experimentally obtained values of compressive/flexural strength vary linearly with the quantity of lime present in the binder of the mix. To illustrate this, Figure 42 and Figure 43 show the variation of compressive and flexural strength respectively with lime content in the binder for three different mixes with different B/Ag ratios and at different ages; (a) B/Ag ratio 1:3 at day 7, (b) B/Ag ratio 1:4 at day 90 and (c) B/Ag ratio 1:5 at day 365.

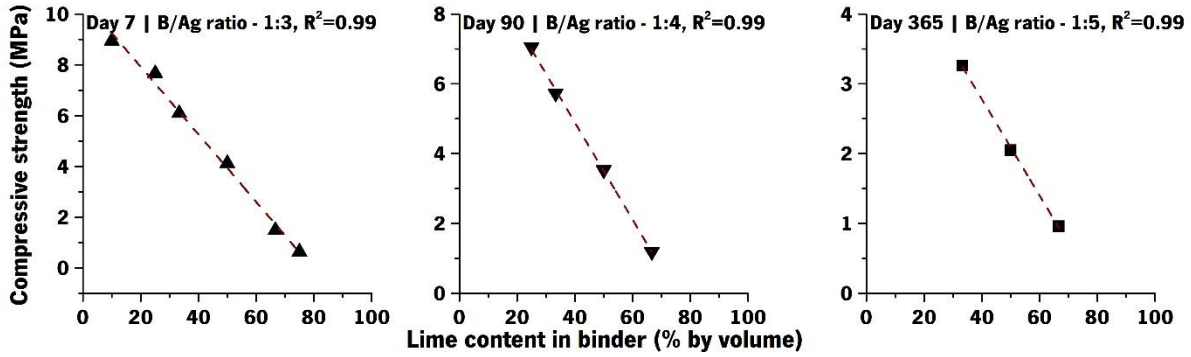

Figure 42: Illustration of a linear relationship between the compressive strength of mortar and lime content in the binder (% by volume) for different B/Ag ratios and at different ages

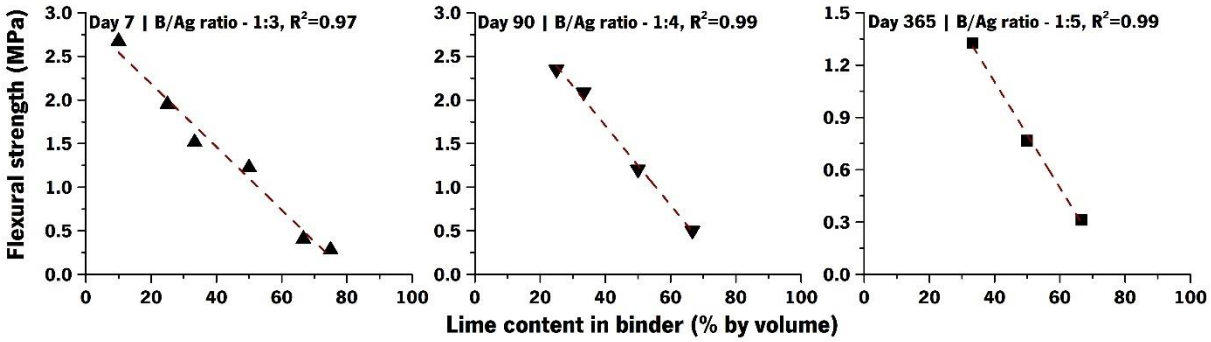

Figure 43: Illustration of a linear relationship between the flexural strength of mortar and lime content in the binder (% by volume) for different B/Ag ratios and at different ages

In a linear relationship, the slope indicates the change in the dependent variable for a unit change in the independent variable. In this context that would mean the change in compressive/flexural strength of the mix for a unit change in lime content of the binder. If the values of slope obtained are to be normalized across different B/Ag ratios, for comparison, it would be necessary to divide the value of slope by the strength of the benchmark mix and expressed as a percentage. This has been illustrated in Figure 44, using compressive strength as an example but the same is applicable for flexural strength as well. Furthermore, Table 17 and Table 18 summarize the data that was obtained from treating the variation of compressive and flexural strength respectively with lime content in the binder for all ages – days 7, 14, 28, 90, 180, and 365. This has been shown for all three B/Ag ratios 1:3, 1:4, 1:5. Table 17 and Table

18 also show the R-squared value for each case, establishing the goodness of fit for the linear relationship in each case. It may be observed that in all cases the R^2 value was 0.98 on an average, going to 0.94 and 0.93 in one case each of compressive and flexural strength. It must be noted that in the case of B/Ag ratio 1:3, the mix 1C9L30S (90%) was excluded from the linear regression for both compressive and flexural strength because it reduced the linearity of the rest of the data set, and consequently the accuracy of the estimations. Additionally, the absolute values of strength obtained for this mix were so low, that it was very sensitive to variations in estimations of strength. For example, an average absolute difference of 0.2 MPa, in estimation and actual strength could lead to more than 100% error and so 90% lime was not included in the data set for regression.

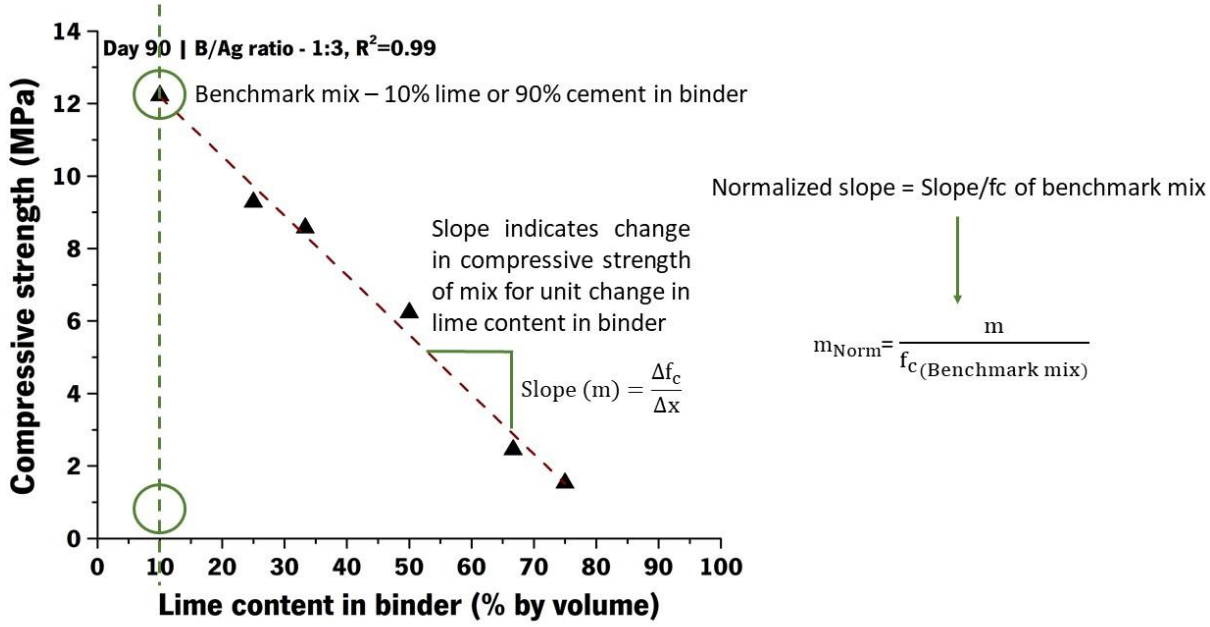

Figure 44: Illustration of calculation of normalized slope using compressive strength and lime content in the binder as an example (Also applicable to flexural strength because of the linear relationship demonstrated in Figure 43)

Table 17: Change (%) in compressive strength of lime-cement mixes for a unit change in lime content in the binder (% by volume)

Change (%) in compressive strength for every 1% change in lime content in binder | Benchmark mix has 10% lime and 90% cement in the binder						
B/Ag ratio	1:3		1:4		1:5	
Data points – lime content (% vol)	10, 25, 33.3, 50, 66.7, 75		25, 33.3, 50, 66.7		33.3, 50, 66.7	
Age (Curing days)	R^2	Δf_c(%)	R^2	Δf_c(%)	R^2	Δf_c(%)
7	0.99	-1.43	0.97	-1.50	0.99	-1.43
14	0.98	-1.38	0.99	-1.47	1.00	-1.40

28	0.99	-1.40	0.99	-1.44	0.96	-1.45
90	0.99	-1.34	1.00	-1.51	0.97	-1.46
180	0.98	-1.30	0.97	-1.55	0.98	-1.49
365	0.98	-1.40	0.94	-1.47	1.00	-1.40
Average of all ages (CoV)	0.99 (0.7%)	-1.4 (3.4%)	0.98 (2.2%)	-1.5 (2.5%)	0.98 (1.6%)	-1.4 (2.5%)

Table 18: Change (%) in flexural strength of lime-cement mixes for a unit change in lime content in the binder (% by volume)

Change (%) in flexural strength for every 1% change in lime content in binder | Benchmark mix has 10% lime and 90% cement in the binder						
B/Ag ratio	1:3		1:4		1:5	
Data points – lime content (% vol)	10, 25, 33.3, 50, 66.7, 75		25, 33.3, 50, 66.7		33.3, 50, 66.7	
Age (Curing days)	R^2	Δf_f(%)	R^2	Δf_f(%)	R^2	Δf_f(%)
7	0.98	-1.41	0.99	-1.40	0.97	-1.40
14	0.99	-1.31	0.99	-1.33	0.97	-1.35
28	0.98	-1.36	0.96	-1.43	0.97	-1.41
90	0.93	-1.23	0.99	-1.46	0.96	-1.44
180	0.96	-1.26	0.98	-1.55	0.98	-1.41
365	0.98	-1.39	0.97	-1.48	0.99	-1.48
Average of all ages (CoV)	0.97 (2.2%)	-1.3 (5.5%)	0.98 (1.5%)	-1.4 (5.2%)	0.97 (1.2%)	-1.4 (3.2%)

It was thus found that for every 1% increase in lime content in the binder (by volume), on average there is a 1.4% decrease in compressive and flexural strength of the given mix with respect to the benchmark mix (90% cement in the binder by volume), at any age and for any B/Ag ratio. This analysis makes it possible to theoretically estimate the compressive/flexural strength of any lime-cement mix with a specified quantity of lime in the binder if the strength of the benchmark mix is known.

To test if this method leads to a reasonable approximation of the strength of a mix, the compressive strength of the mix 1C2L9S (67%) at 90 days of age, is estimated as an example. The B/Ag ratio would be 1:3 and the benchmark mix would have 90% cement or 10% lime in the binder and therefore it would be the mix 9C1L30S (10%). From experimental testing (Table 14), it is known that the value of the strength of this mix at 180 days of age is 11.29 MPa, and from Table 17 it may be noted that for B/Ag ratio 1:3, at 180 days, the change in strength would be -1.30% for every 1% increase in lime content in the binder (by volume). The increase in lime content is 66.67–10 = 56.67%, therefore the change in strength should be 56.67×(-1.30) = -73.67%. The strength would then be 11.29 – (73.67% of 11.29) = 2.97 MPa. The experimental value recorded in the test was 2.69 MPa (CoV 10.5%), which means a good estimation. Using the same logic, as just presented, values of compressive strength have been estimated for different mixes using Table 17 and compared with the experimental values (Table 14) with the differences (%)

presented in Annex-Table 9. The average difference in estimation and the experimental value was found to be 7.5%, with the maximum difference going up to 27%. In the case of flexural strength (Table 15) values were estimated using Table 18 and differences have been presented in Annex-Table 10. The average difference in estimation and the experimental value was found to be 8.8% and the maximum difference was found to be 25%.

4.4.2.3 Impact of binder-aggregate ratio (B/Ag) on the mechanical strength of mortar

This section assesses the impact of the quantity of the binder present in a mix, across fixed binder compositions (33.3%, 50%, and 66.7% lime in the binder, by volume). In the case of comparison of different B/Ag ratios, out of the options available (1:3, 1:4, 1:5, 1:6), the binder-aggregate ratio of 1:3, has the most amount of binder in the mix, and for a given binder composition, is likely to result in the highest strength of the mix. And therefore, the benchmark mix would be a mortar with a B/Ag ratio of 1:3, by volume. It is also the strongest composition possible from a practical point of view of what may be used in the field. While studying the impact of binder in the mix on the mechanical performance of mortar, the benchmark mix always consists of 33% binder or binder-aggregate ratio of 1:3 (by volume). The compressive and flexural strengths of different mixes were found to vary linearly with the B/Ag ratio of different mixes (Figure 45 and Figure 46).

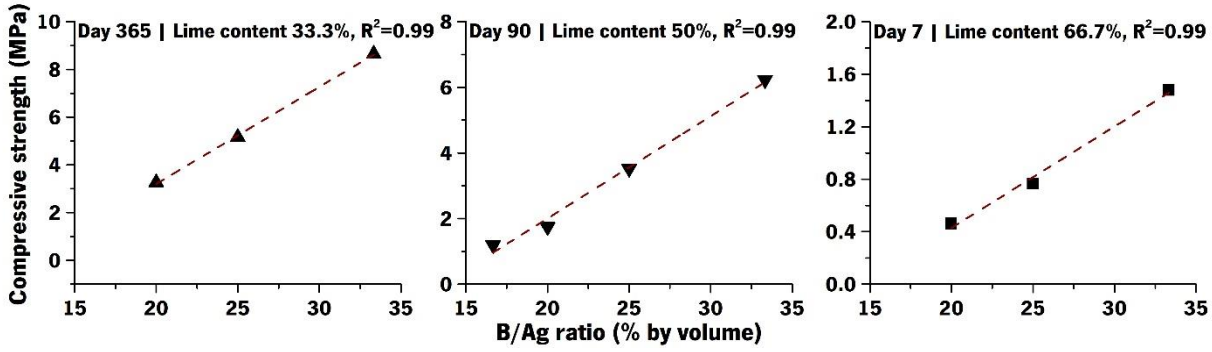

Figure 45: Illustration of a linear relationship between compressive strength of mortar and B/Ag ratio (% by volume) for lime contents in the binder and at different ages

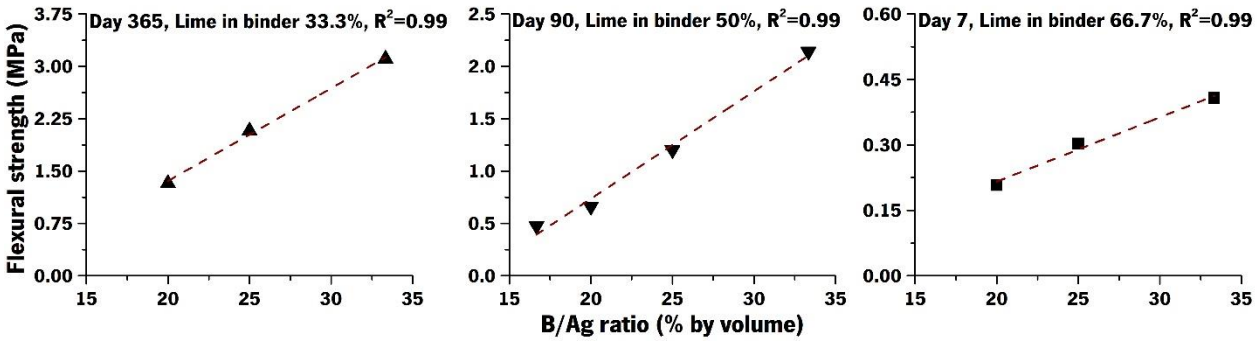

Figure 46: Illustration of a linear relationship between flexural strength of mortar and B/Ag ratio (% by volume) for lime contents in the binder and at different ages

The impact of the binder on the strength of mortar mixes was quantified similarly to how the impact of the lime content in the binder was assessed (Section 4.4.2.2). The values of slopes, indicating the change in compressive/flexural strength of the mix for a unit change in B/Ag ratio of the mixes, were normalized, using the benchmark mix and expressed as a percentage (An example has been illustrated in Figure 47 using flexural strength, but the same applies to compressive strength, because of the linear relationship exhibited in Figure 45). The data obtained from treating the variation in mechanical strength with B/Ag ratio has been shown in Table 19 and Table 20 for all ages – days 7, 14, 28, 90, 180, and 365. This has been shown for three lime-cement compositions 33.3%, 50%, and 66.7%, lime in the binder, by volume. Table 19 and Table 20 also show the R^2 value for each case, establishing the goodness of fit for the linear relationship in each case. It may be observed that in all cases the R^2 value was 0.98 on average, going down to 0.97 in case of compressive and till 0.95 in case of flexural strength.

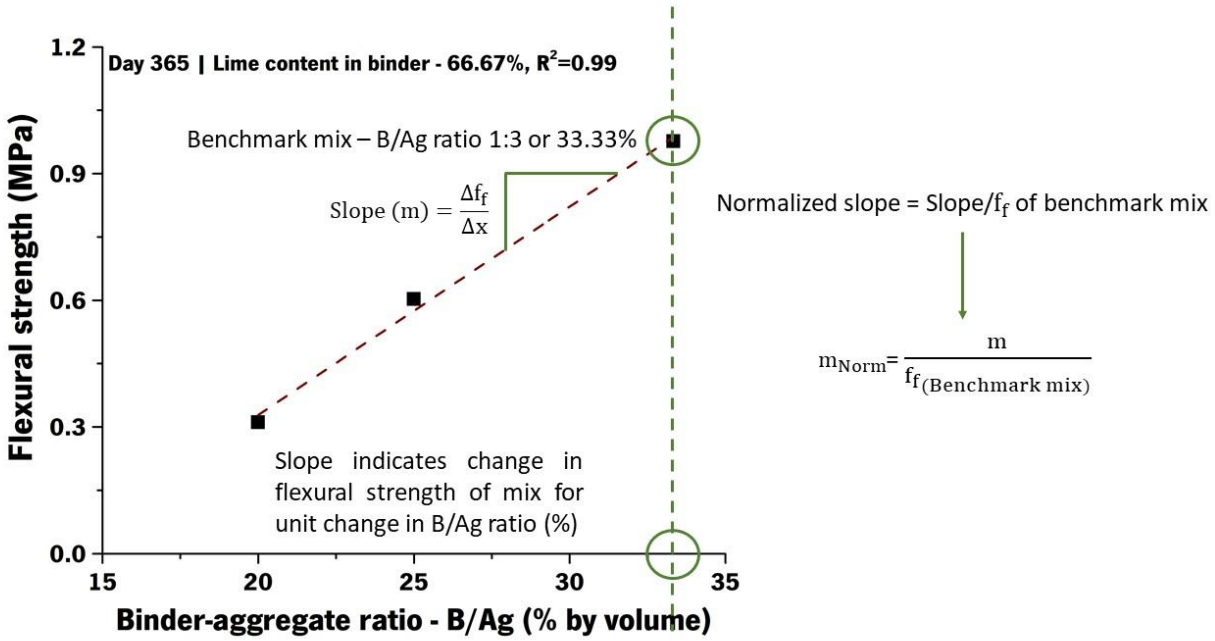

Figure 47: Illustration of calculation of normalized slope using flexural strength and B/Ag ratio as an example (Also applicable to compressive strength because of the linear relationship demonstrated in Figure 45)

Table 19: Change (%) in compressive strength of lime-cement mixes for every unit change in B/Ag ratio (by volume)

Change (%) in compressive strength for every 1% change in B/Ag ratio | Benchmark mix has 33.3% binder (1:3 B/Ag) in the mix						
Lime quantity in binder, by volume	33.3%		50%		66.7%	
Data points – B/Ag ratio	1:3, 1:4, 1:5		1:3, 1:4, 1:5, 1:6		1:3, 1:4, 1:5	
Age (Curing days)	R^2	Δf_c(%)	R^2	Δf_c(%)	R^2	Δf_c(%)
7	1.00	-5.30	0.99	-4.91	0.99	-5.30
14	0.98	-4.46	0.99	-4.73	0.98	-4.04
28	1.00	-4.63	0.98	-4.46	1.00	-4.85
90	0.99	-4.51	0.99	-5.06	0.97	-5.12
180	0.97	-4.13	0.98	-4.96	1.00	-5.10
365	1.00	-4.71	0.97	-4.93	1.00	-4.79
Average of all ages (CoV)	0.99 (1.2%)	-4.62 (8.4%)	0.98 (0.9%)	-4.84 (4.4%)	0.99 (1.4%)	-4.87 (9.2%)

Table 20: Change (%) in flexural strength of lime-cement mixes for every unit change in B/Ag ratio (% by volume)

Change (%) in flexural strength for every 1% change in B/Ag ratio | Benchmark mix has 33.3% binder (1:3 B/Ag) in the mix						
Lime quantity in binder, by volume	33.3%		50%		66.7%	
Data points – B/Ag ratio	1:3, 1:4, 1:5		1:3, 1:4, 1:5, 1:6		1:3, 1:4, 1:5	
Age (Curing days)	R^2	Δf_f(%)	R^2	Δf_f(%)	R^2	Δf_f(%)
7	0.96	4.02	0.99	4.86	0.99	3.57
14	1.00	4.29	0.99	4.70	0.97	3.67

28	0.91	3.82	0.98	4.71	0.98	3.48
90	0.90	3.47	0.99	4.88	0.99	4.52
180	0.96	4.06	0.99	4.87	0.96	4.81
365	1.00	4.24	0.95	4.92	0.99	5.01
Average of all ages (CoV)	0.95 (4.5%)	-3.98 (7.6%)	0.98 (1.5%)	-4.82 (2.0%)	0.98 (1.4%)	-4.18 (16.2%)

A 1% decrease in binder content (by volume), led to around 5% change in compressive and flexural strength of the given mix with respect to the benchmark mix (1:3 B/Ag ratio by volume), at any age and for any B/Ag ratio. The objective of this analysis is to theoretically estimate the compressive/flexural strength of any lime-cement mix with a specified B/Ag ratio if the strength of the benchmark mix is known.

As an example, the flexural strength of the mix 1C1L10S (50%) at 180 days of age, will be estimated. Since this mix has 50% lime content in its binder, the benchmark, in this case, is a mix with 50% lime in the binder as well, and a B/Ag ratio of 1:3 i.e., the mix 1C1L6S (50%). From experimental testing (Table 15), it is known that the strength of the benchmark mix at 180 days of age is 2.31 MPa, and from Table 20, the change in strength at 180 days is expected to be -4.87%, for every 1% change in binder content of the mix. The decrease in binder content is 33.33% – 20% = 13.33%, therefore the change in strength should be 13.33×(-4.87) = -64.92%. The strength would then be 2.31 – (64.9% of 2.31) = 0.81 MPa. The actual value (Table 15) recorded from the test was 0.74 MPa (CoV 9.0%), which accounts for a difference of only 9.5% in estimation.

Using the same method, values of compressive strength and flexural strength have been estimated for different mixes, using Table 19 and Table 20, and compared with experimental values (Table 14 and Table 15). In the case of compressive strength (Annex-Table 11), the average and maximum differences in estimated and experimental values were found to be 7.2% and 23% respectively. While for flexural strength (Annex-Table 12) the average and maximum differences were found to be 9.2% and 27% respectively.

4.4.2.4 Mechanical strength as a function of lime in binder, B/Ag ratio, and time

It has been shown in each of the three previous sections, how parameters of time, lime content in the binder, and B/Ag ratio influence the mechanical strength of different mortar compositions (Sections 4.4.2.1, 4.4.2.2, and 4.4.2.3 respectively). An attempt was therefore made to express mechanical strength as a function of all these parameters (Equation 15). To obtain such an equation, 14 out of 15 mixes (Chapter 3) were used for regression; the mix 1C1L12S (50%) was not used, since it was the only mix with a B/Ag ratio of 1:6 and would cause an imbalance in the factors for the global regression. The

dependent variable could correspond to compressive strength (f_c) or flexural strength (f_f), while the independent variables include lime content in the binder (10, 25, 33.3, 50, 66.7, 75, 90) in % by volume and expressed as x, B/Ag ratio (1:3, 1:4, 1:5 or 33.3, 25, 20) in % by volume expressed as y and time (7, 14, 28, 90, 180, 365) days expressed as T. The nature of the equation is similar for compressive and flexural strength, what changes are the values of the coefficients - p, q, and r for x, y, and T respectively, as shown in Table 21.

$$f_c \text{ or } f_f = \gamma\,(px + qy + r\sqrt{T}) \quad x \leq 50\%$$
$$f_c \text{ or } f_f = \gamma\,(px^{1.5} + q\sqrt{y} + \frac{r}{\sqrt{T}}) \quad x > 50\% \qquad 15$$

The symbol γ represents a correction factor, which ensures a conservative value of strength for more than 95% of the data points. Without this factor, Equation 15 corresponds to the best fit of the available data such that the difference in predicted and actual values are both positive and negative. But if equation 15 is to be used for estimation of strength, then the predicted value should be less than the experimental value and therefore it was necessary to introduce the correction factor. Table 21 also specifies the minimum and maximum absolute errors for each case and a comparison of predicted and experimental values (without the correction factor γ) has been depicted in Figure 48. The R^2 values, along with the low p-values (~approaching 0) and high F-values in all cases, indicate the goodness of the fit of the proposed equations. Values of mechanical strength predicted by equation 15, are available in Annex-Table 13.

Table 21: Values of coefficients corresponding to equation 15

Coefficient | Notation	f_c when $x \leq 50\%$	f_c when $x > 50\%$	f_f when $x \leq 50\%$	f_f when $x > 50\%$
p	-1.419E-1	-6.028E-1	-4.267E-2	-1.886E-3
q	3.555E-1	1.001E+0	1.042E-1	3.324E-3
r	1.290E-1	-2.144E+0	6.766E-2	-8.431E-1
Minimum error (MPa)	-1.83	-0.18	-0.72	-0.01
Maximum error (MPa)	2.57	2.39	0.90	0.85
γ	.75	.8	0.7	0.75
R^2	0.94	0.93	0.89	0.89
F-value	3549	1577	2184	1256
p-value	3e-50	7e-27	9e-45	2e-25

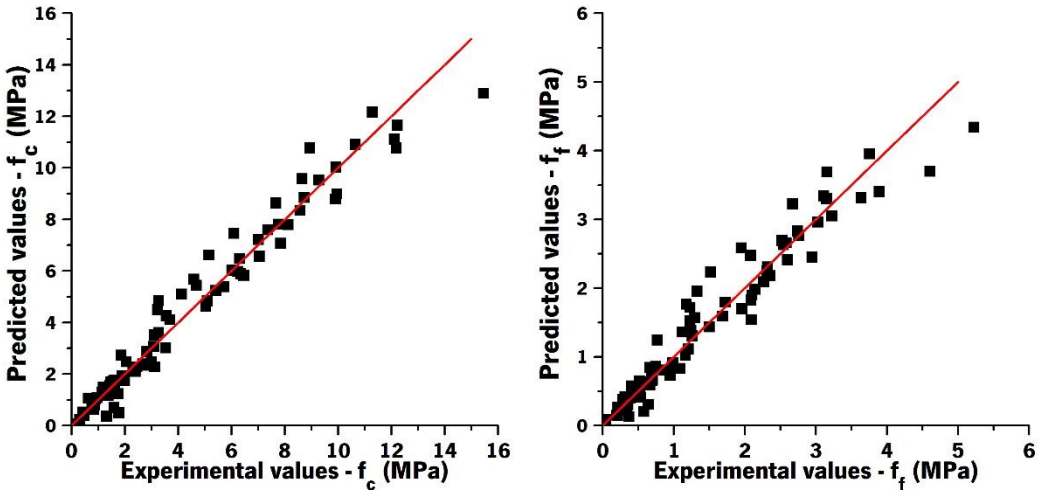

Figure 48: Predicted versus experimental values for mechanical strength, corresponding to Equation 15 without the correction factor: (a) f_c compressive strength (b) f_f flexural strength

4.5 Hardened bulk density and ultrasound velocity (UPV)

4.5.1 Methodology

Bulk density was calculated by measuring the weight of different mortar specimens and dividing it by their volume (40×40×160)mm^3; an average of three values was used in each case. Ultrasound velocity (UPV) was measured using Pundit Lab by Proceq [378]. All measurements were made along the length of the prismatic mortar specimens, 160 mm (Figure 49). Probes of 25 mm diameter were used for the emission and reception of P-waves with 150 kHz frequency. It is recognized that by itself UPV may not lead to a quantitative assessment of the stiffness of the material being tested. However, it could be used as a good complementary method to follow the trends in setting or hardening kinetics of different mortar mixes [109, 114].

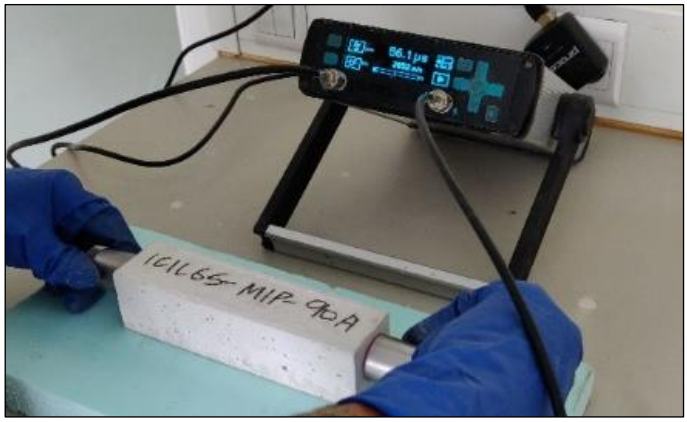

Figure 49: Depiction of measurement of ultrasound velocity (UPV) along the length (160 mm) of a mortar specimen

As mentioned in Section 0, Chapter 3, UPV was measured on the 'control specimens' of each mortar mix. The control specimens for each mix corresponded to the specimens to be tested at 365 days of age; this allowed measurement of UPV values on the same specimens through time from 7 to 365 days. These properties were attained by averaging results from the same set of three specimens over time. Values of UPV for the mix 1C9L30S (90%) are not available, because it was not possible to record consistent values in these specimens. Since this mix has 90% lime, it would be expected to have high porosity and low density. It is also known that the speed of P-waves reduces in air voids, compared to that in solids [2, 110], and so the equipment possibly did not have enough sensitivity to record UPV values for this mix.

4.5.2 Results of bulk density and UPV

4.5.2.1 Evolution of bulk density and UPV with time

For different mixes, the evolution of bulk density with time has been shown in Figure 50 and the values have been provided in Annex-Table 14. It is possible to make two observations:

a) Mixes with greater cement content have higher bulk density. This can be expected since the bulk density of cement (0.93 g/cm^3) is greater than that of lime (0.36 g/cm^3) as specified in Section 3.2.1, Chapter 3.

b) In almost all the mixes, the average density of the specimens would decrease till 28 days of age and then either stabilize or would increase slowly with time. This initial drop in bulk density is expected since mortar specimens exhibit loss of weight due to drying [62, 177] on account of change in curing conditions from 95±5% RH to 65±5% RH. The subsequent increase in density, especially prominent in the mixes with more than 50% lime in the binder, by volume, may be credited to carbonation since, in this phenomena, the molar mass of the final products is heavier than that of the reactants [2].

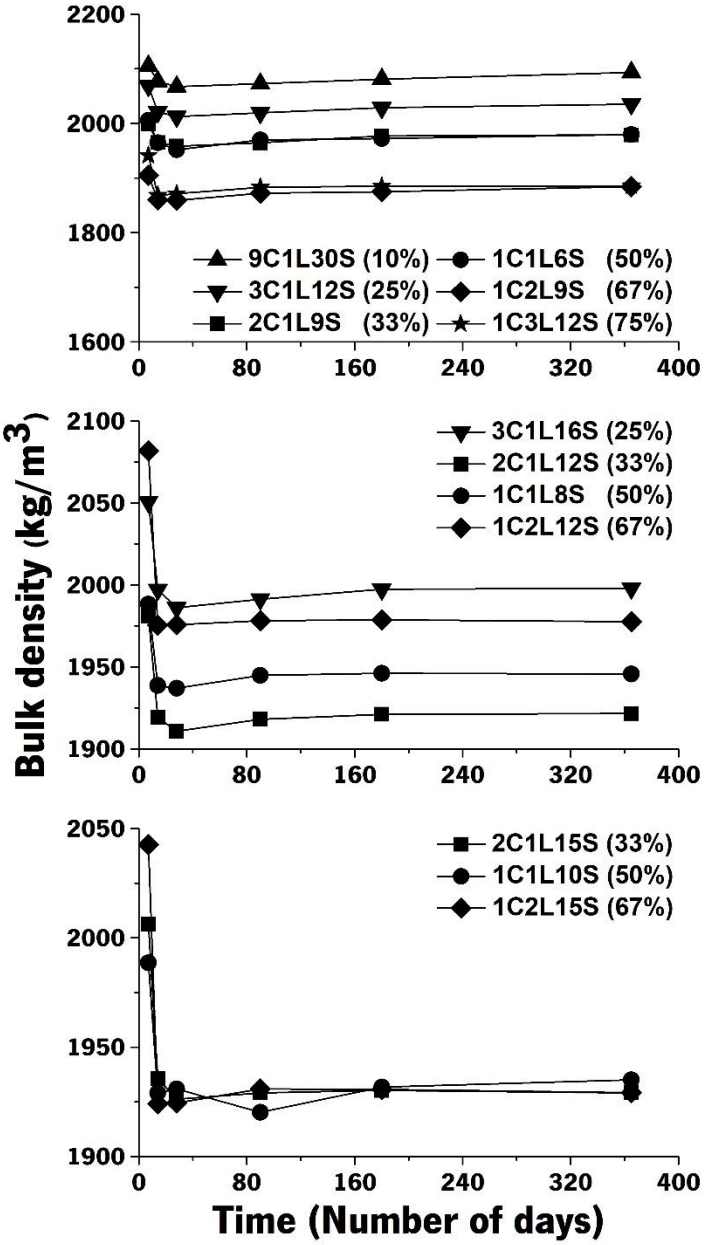

Figure 50: Evolution of bulk density with time for different lime-cement mixes

The evolution of UPV values for 14 lime-cement mixes has been shown in Figure 51. It is possible to observe that UPV values tend to decrease with increasing quantities of lime in the binder and decreasing B/Ag ratio. This may be attributed to the decrease in density of the mixes, with an increase in lime. This trend is also similar to the pattern of compressive strength (Figure 33). Despite the similarities, a direct correlation could not be found between only UPV and compressive strength.

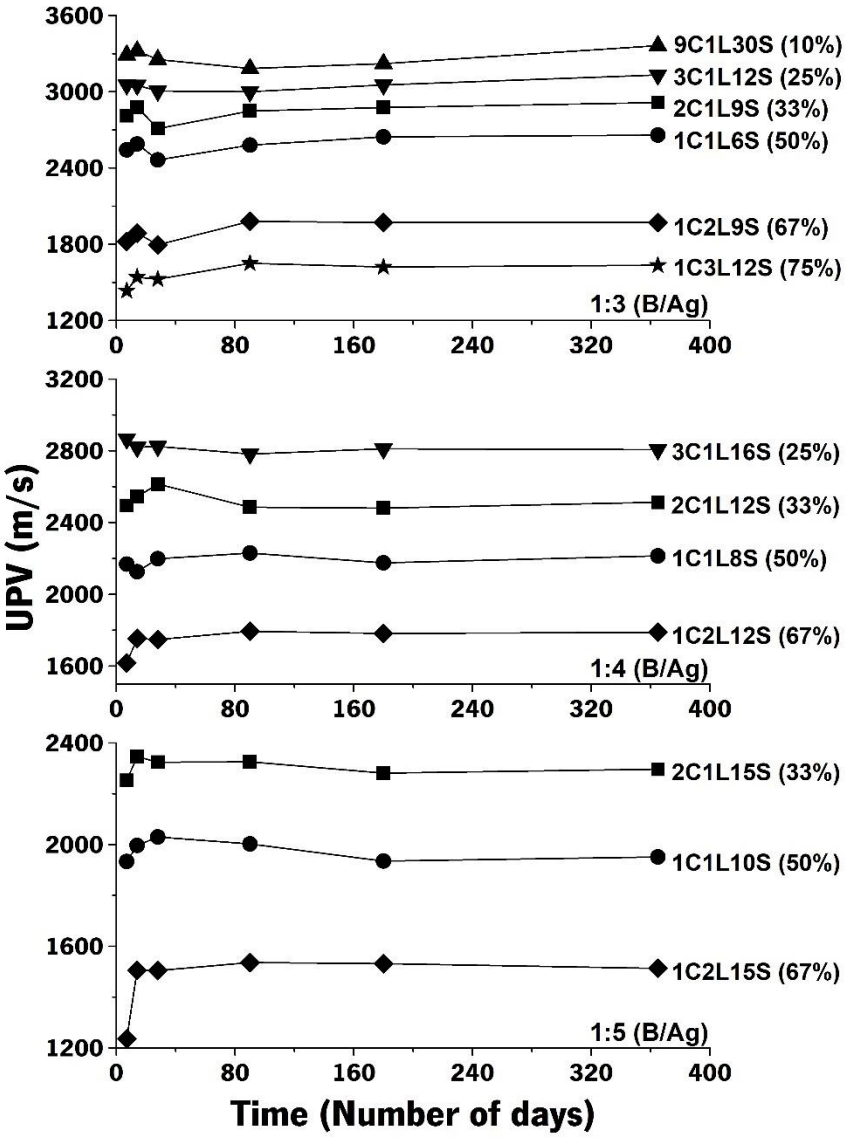

Figure 51: Evolution of ultrasound pulse velocity (UPV) with time for different lime-cement mixes

4.5.2.2 Correlation of UPV, bulk density, and compressive strength

It is known from mechanics that the square of UPV is directly proportional to Young's modulus (E-mod) [105]. Furthermore, from studies of the mechanical behavior of concrete, it is known that a product of density and compressive strength $\rho^a f_c^{\ b}$ is also proportional to E-mod, where the values of a and b may vary based on the experimental data, but are often equal to 0.5 [379, 380]. Based on this, a linear relationship was found between a function of UPV (m/s) and a function involving bulk density (kg/m^3) and compressive strength (MPa) (Equation 16).

$$UPV(T)^2 = k.\rho(T)^{1.5} f_c(T)^{0.5} \quad (16)$$

The symbol T is time and the symbol k is a constant of proportionality. Since for a given B/Ag ratio, compressive strength decreases linearly with an increase in lime content in the binder (Figure 42), and UPV and density also appeared to decrease with an increase in lime content in the binder, equation 16 was plotted graphically, to check if it had a relation with lime content in the binder for any given B/Ag ratio. An example has been illustrated in (Figure 52) for a B/Ag ratio of 1:3, where the y-axis corresponds to $\mathrm{Y(T)} = \mathrm{UPV(T)}^2$ and the x-axis corresponds to $\mathrm{X(T)} = \rho(\mathrm{T})^{1.5}\mathrm{f_c(T)}^{0.5}$ and T is equal to 28 days. The R^2 value of 0.97 obtained, verifies the linearity of the relationship.

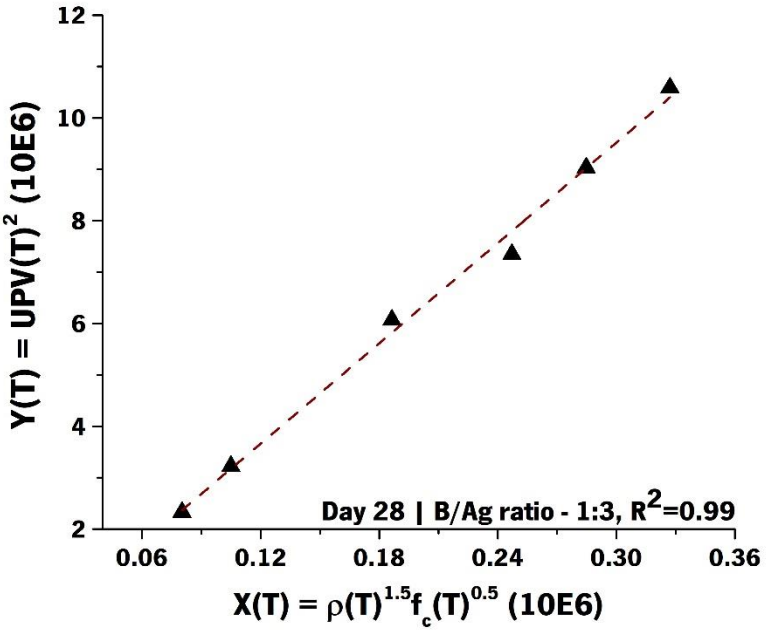

Figure 52: Correlation between ultrasound velocity and a function of density and compressive strength for varying lime content in the binder (10, 25, 33.3, 50, 66.7, 75) % by volume, for B/Ag ratio 1:3

Keeping the B/Ag ratio constant, this linear relationship was thereafter verified for different curing ages. Subsequently, it was tested for different B/Ag ratios as well, and all cases were found to be linear, with high R^2 values; the lowest R^2 value being 0.96 (Table 22). To assess, whether the linearity would be valid if the binder composition was kept constant and the B/Ag ratio was varied, linear regressions were performed for fixed lime-cement compositions as well (Table 23). In this case, as well, high R^2 values were obtained, with the lowest going down to 0.85. It may thus be concluded, that equation 16 has the potential to provide a relatively simple, non-destructive method to estimate the compressive strength of mixes without actually testing them since the measurement of UPV is quite simple and so is the measurement of weight of mortar specimens. For this purpose, however, the value of the constant k would have to be established for a given set of materials, which is possibly not an easy task. Once that is

done, equation 16 may even be used for estimating the strength of mixes at later ages, with a reasonable error range. More importantly, this method could serve as an easy technique for quality control in some cases.

Table 22: R-square values obtained from linear regression performed on mortars with varying lime contents, at different curing ages from 7-365 days and varying cases of fixed B/ag ratios

R^2 values obtained from equation 16 applied to different mixes, with varying lime contents			
Age | B/Ag ratio	1:3	1:4	1:5
Data points (Lime content %)	10, 25, 33.3, 50, 66.7, 75	25, 33.3, 50, 66.7	33.3, 50, 66.7
7	0.99	0.99	0.99
14	0.99	0.99	1.00
28	0.99	0.99	0.96
90	0.99	0.99	0.98
180	1.00	0.98	1.00
365	0.99	0.99	0.99

Table 23: R-square values obtained from linear regression performed on mortars with varying B/Ag ratios, at different curing ages from 7-365 days and varying cases of fixed lime-cement ratios in the binder

R^2 values obtained from equation 16 applied to different mixes, with varying lime contents			
Age | Lime content %	33%	50%	67%
Data points (Lime content %)	1:3, 1:4, 1:5	1:3, 1:4, 1:5, 1:6	1:3, 1:4, 1:5
7	0.99	0.99	0.99
14	0.98	0.96	0.98
28	0.87	0.95	0.92
90	0.85	0.99	0.95
180	0.95	1.00	0.99
365	0.99	0.99	1.00

4.6 Static E-modulus (Unconfined cyclic compression test)

4.6.1 Methodology

Static E-modulus was measured using the recommendations of EN 12390-13 [117] adapted for mortars (Figure 53). For this test, the specimens used were cylinders with 60 mm diameter and 120 mm height. The final value of E-modulus was computed by averaging results from three specimens. To have a smooth

surface for even application of load during the test, epoxy resin was used to cap the specimens. A hydraulic actuator with a capacity of 25 kN was used to apply an axial pre-load of 50 N and four continuous loading and unloading cycles.

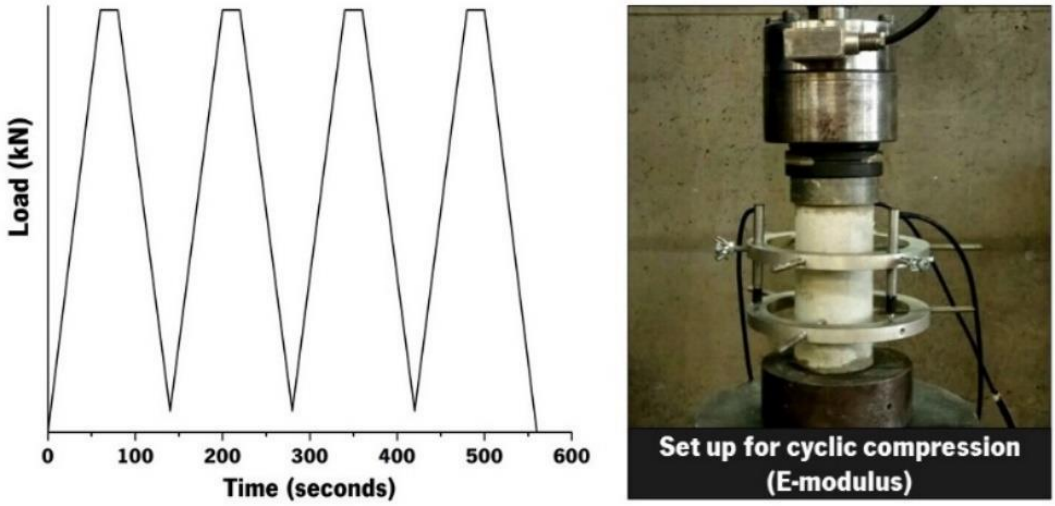

Figure 53: Unconfined cyclic compression test for measurement of static E-modulus: (a) Load cycle (b) Setup of specimen

The maximum load applied in the test equaled approximately one-third of the maximum compressive strength of the mortar at that age. This value of maximum uniaxial unconfined compressive strength was attained by testing three additional cylindrical specimens at each age before measuring E-modulus, using displacement control at a rate of 0.012 mm/s. This loading rate/velocity was determined such that the loading cycle would take 60 seconds, followed by a constant ramp of 20 seconds, and then the unloading ramp would take 60 seconds as well (Figure 53 a). The slope of the (stress/average strain) of each of the ascending branches was calculated. Then the average of the second, third, and fourth cycles was used to calculate the E-modulus of the specimen. The setup of the LVDTs adopted was similar to that used by Silva [128] for testing soil specimens stabilized by cement and has been shown in Figure 53 b. Three mixes were tested using this method 3C1L12S (25%), 1C1L6S (50%), 1C2L9S (66.7%) at curing ages of 7 days, 28 days, and 90 days.

4.6.2 Results

4.6.2.1 Evolution of static E-modulus with time, as a function of lime in the binder

Evolution of E-modulus, measured by the cyclic compression test, for the mixes 3C1L12S (25%), 1C1L6S (50%), and 1C2L9S (66.7%) has been shown in Figure 54. The global trend observed in mechanical strength concerning the quantity of lime in the binder was found true for E-modulus as well. An increase in the quantity of lime in the binder leads to a decrease in the value of the E-modulus of the mortar, at all

ages. This observation was found to be consistent with the literature [271]. Naturally, more products of cement hydration are formed, when the quantity of cement in the binder is greater. One of the most abundant products of this reaction of cement hydration reaction is calcium silicate hydrate (C–S–H) crystals. Networks of C–S–H crystals form strong connections with the solid phase, binding discrete compounds into a cohesive whole and contributing to an increase in the overall strength and stiffness of hydrated cement [24]. While stiffness of all the mixes is observed to evolve with time, the mixes with greater quantities of cement in them seem to gain most of their stiffness in the first 7 days (Figure 54, Table 24).

Table 24: Values of E-modulus as obtained from the cyclic compression test

Mortars	E-mod (GPa) Day 7	CoV (%)	E-mod (GPa) Day 28	CoV (%)	E-mod (GPa) Day 90	CoV (%)	Increase (%) (Days 7 to 90)
1C2L9S (66.7%)	4.8	8.5	5.5	7.7	6.2	4.6	27.1
1C1L6S (50%)	9.8	7.0	10.9	2.6	11.7	10.8	19.0
3C1L12S (25%)	16.3	15.0	16.6	3.5	17.5	1.8	6.8

The increase in stiffness of the mixes between day 7 and day 90 is found to be 7%, 19%, and 27% for the mixes 3C1L12S (25%), 1C1L6S (50%), and 1C2L9S (67%) respectively. One may, therefore, conclude that the greater the amount of lime in the binder of the mix, the larger is the continued increase in stiffness, up to the age of 90 days. The most plausible explanation for this increase in stiffness over time may be attributed to stiffening induced by carbonation of the lime since hydration processes are expected to have been almost completed by 28 days of curing age [2]. While the feasibility of the general range of values obtained could be validated from literature (3 to 24 GPa), existing data classifying E-modulus of the mortar as a function of lime content in the binder could not be identified for a direct comparison [11].

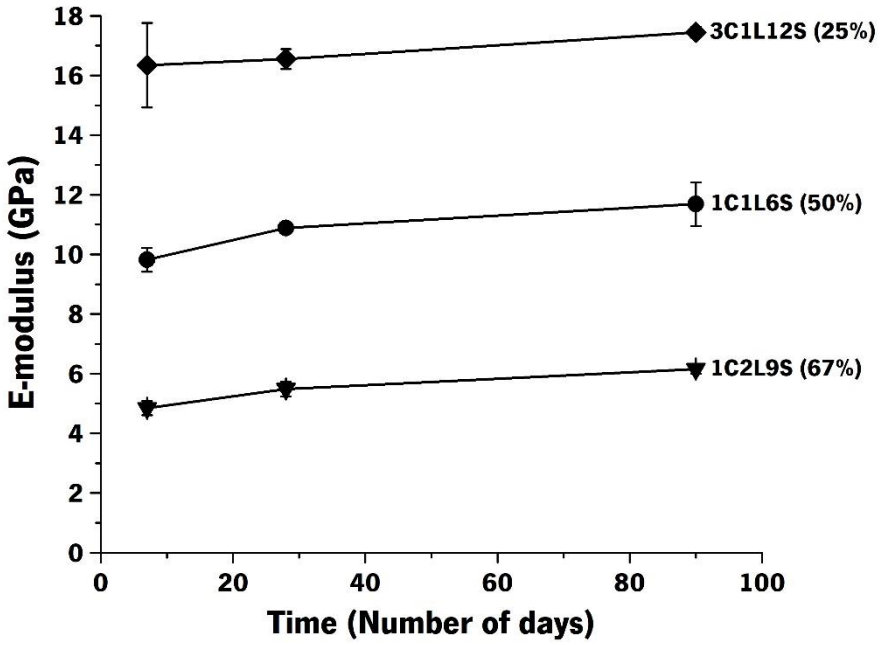

Figure 54: Evolution of E-modulus with time, as measured by cyclic compression test (B/Ag 1:3, by volume)

4.6.2.2 Correlation of E-modulus (cyclic compression test) and compressive strength

The evolution of the ratio of E-modulus to compressive strength (E/fc) with time, for cylindrical specimens, has been plotted in Figure 55. This ratio was found to lie in the range of 1300-3000, which was similar to the ratios found in the literature [243]. Only one value of the ratio for mix 1C2L9S (66.7%) at day 7 was found to reach 4650 (Figure 55). Mortars with a greater quantity of cement in them, exhibit a lower E/fc ratio. From an engineering perspective, a valid question regarding cracking and capacity to accommodate movements is whether the E/fc or the absolute value of E is more relevant. Given the low values of stresses applied to masonry, the absolute value of E seems more relevant for this purpose. It is also interesting to note that with time, the difference in values of E/fc ratios decreases, and by 90 days, the ratios for all three mortars fall in the range of 1300-2300 which means that the increase of strength with time, is much larger than an increase of stiffness with time.

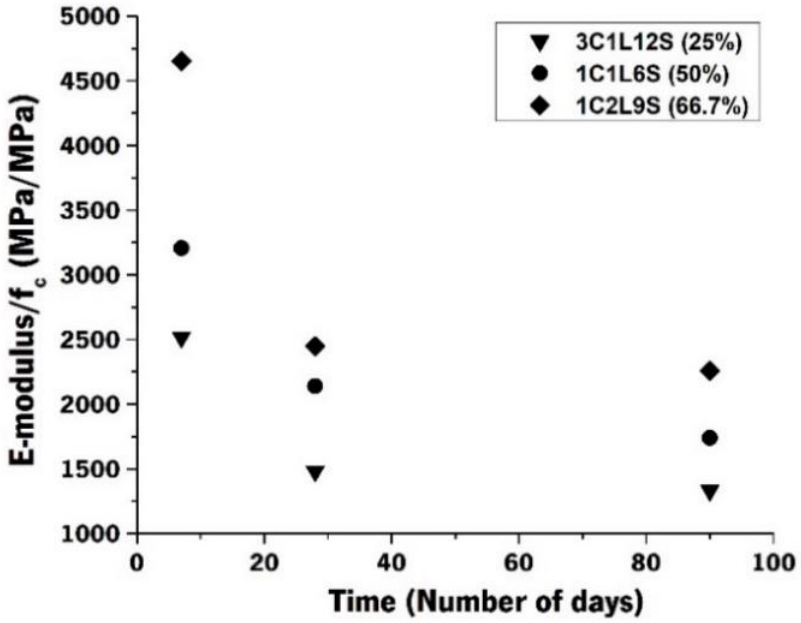

Figure 55: Evolution of ratio of E-modulus to compressive strength (E/fc) with time

4.7 Poisson's ratio

4.7.1 Methodology

The experimental conditions used for Poisson's ratio were similar to the one used for E-modulus (cyclic compression) (Section 4.6.1, Figure 53). The test of Poisson's ratio was conducted on the same specimens that were used for E-modulus. However, separate tests were required to accommodate the vertical and horizontal layouts of the LVDTs. Cylindrical specimens with 60 mm diameter and 120 mm height were used for the test and the mixes tested had binder-aggregate ratio 1:3 and lime contents 25%, 50%, and 67%. The loading cycles were also the same as that used for E-mod. Since Poisson's ratio is defined as lateral strain divided by longitudinal strain, the longitudinal strain was measured by the set-up of E-modulus with 3 LVDTs (Figure 53) and the lateral strain was measured by a metallic ring with a hinge, fastened at the center of the specimen with an LVDT attached in the horizontal direction (Figure 56). The final value of Poisson's ratio was also computed by averaging results from three specimens for each mix.

Figure 56: Measurement of Poisson's ratio - Set up of the specimen with the horizontal layout of LVDT

4.7.2 Results

Poisson's ratio was recorded for the different mixes and has been displayed along with the individual coefficient of variation of each observation, adjacent to it, in percentages (Table 25). All values were observed to be in the range of 0.13 to 0.23. The global average was found to be 0.18 with a scatter of 18%, regardless of the age or lime content in the binder. Shear modulus (G) for each of the mixes was also calculated using the value of E-modulus (E) and Poisson's ratio (υ) measured (Equation 17).

Table 25: Values of Poisson's ratio and shear modulus for lime-cement mortars (7, 28, and 90 days of age)

Property	Poisson's ratio (COV %)			Shear modulus (GPa)		
Mix/Age (Days)	1C2L9S (67%)	1C1L6S (50%)	3C1L12S (25%)	1C2L9S (67%)	1C1L6S (50%)	3C1L12S (25%)
7	0.20 (18.2)	0.20 (20.2)	0.18 (12.5)	2.0	4.1	6.9
28	0.19 (10.8)	0.15 (7.4)	0.21 (14.0)	2.3	4.8	6.8
90	0.16 (21.6)	0.13 (3.8)	0.23 (7.9)	2.7	5.2	7.1

It was possible to observe that the greater the quantity of lime in the mix, the lower was the value of shear modulus obtained (Table 25). It may also be noted that the value of shear modulus increased with time for almost all mixes, regardless of binder content. However, the quantity of lime in the binder of the mix was found to influence the extent of the increase in values of shear modulus recorded. For instance, between day 7 and day 90 of curing age, the shear modulus was found to increase by 24%, 21%, and 3% in the mixes 1C2L9S (67%), 1C1L6S (50%), and 3C1L12S (25%) respectively.

$$G = \frac{E}{2(1+\upsilon)} \qquad 17$$

Finally, it is worth noting that Poisson's ratio is a parameter that is difficult to measure very accurately and tends to have high values of dispersion, due to the precision and sensitivity of the setup and

instrumentation involved. Coefficients of variation between 8 and 20% have been found, with higher dispersion at 7 days. At 28 and 90 days, it was consistently the mortar with the greatest quantity of cement that exhibited the largest Poisson's value.

4.8 Fracture energy

4.8.1 Methodology

Fracture energy was measured in prismatic specimens of size 40×40×160 mm (Figure 57), with a trapezoid-shaped precast notch; 5 mm in depth, equal length of non-parallel sides inclined at an angle of 15˚ and the shorter parallel side being 2.5 mm in length, according to RILEM recommendation 50 FMC [381]. Displacement control was used at 0.006 mm/s with a preload of 50 N.

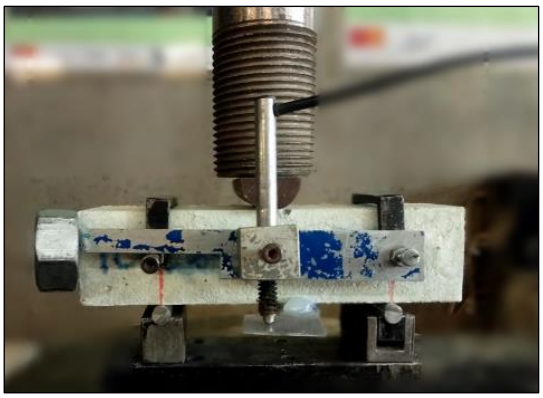

Figure 57: Set up used to measure fracture energy

If fracture energy, were to be calculated using the recommendation of RILEM 50 FMC [381], fracture energy would be dependent on the weight of the specimen as well as the portion of the force-displacement curve that is usually not recorded in experiments. The value of fracture energy G_f was therefore obtained using equation(s) 18, a method originally proposed by Elices, Guinea, and Planas [160-162] which eliminates the above-mentioned variations.

$$G_f = \frac{W_m + W_{um}}{b(d-a)}$$

$$W_{um} = \frac{2A}{d_u} \qquad 18$$

$$F = A\left(\frac{1}{{d_0}^2} - \frac{1}{{d_u}^2}\right)$$

Here W_m represents the measured energy and is the area under the experimental force-displacement curve, W_{um} is the unmeasured energy and represents the work that is not recorded because the test is stopped before complete failure of the specimen (Figure 58). The symbol b refers to the width of the

prismatic specimen, d refers to the height of the prismatic specimen and a refers to the depth of the notch in the prismatic specimen. The exact procedure for such calculations has been based on the work done by Fallahnejad *et al.* [382] and Garijo *et al.* [94]. W_{um} was calculated based on the ultimate displacement of the specimens in the test and a constant A. The constant A was calculated by fitting the tail end of the experimental curve, at displacement d_0 corresponding to a force that is 10% of the maximum load and a displacement d_u corresponding to load/force of 0 N. Since, it is desirable to have the same value of ultimate displacement for all specimens, the value of ultimate displacement (d_u) chosen was 0.2 mm. Typically W_{um} is reported to be < 10% of W_m and was found to be true in this experimental campaign as well [94].

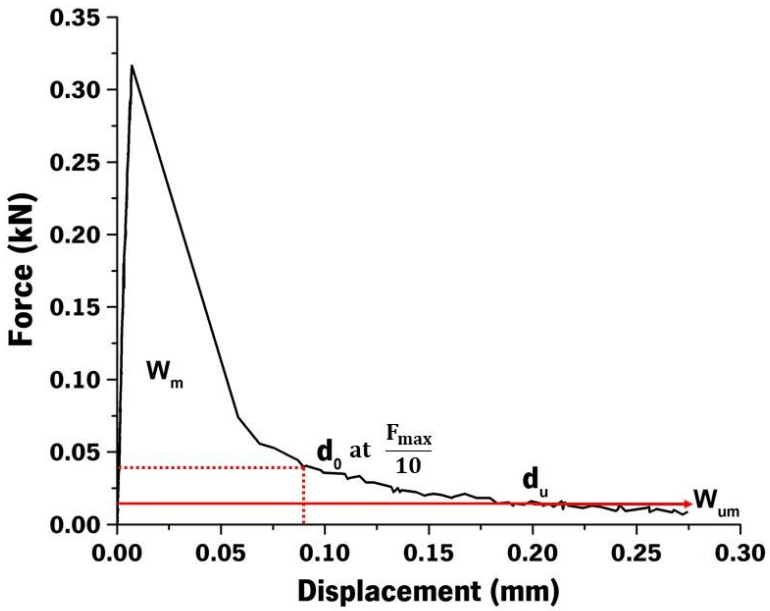

Figure 58: Illustration of calculation of fracture energy

4.8.2 Results

The results of fracture energy obtained have been displayed in Table 26, for the mixes 1C2L9S (67%), 1C1L6S (50%), and 3C1L12S (25%) for 7, 28, and 90 days. It may be observed that values of fracture energy tend to increase with time for the mixes 1C2L9S (67%) and 1C1L6S (50%). This was expected since fracture energy is usually found to increase with time for concrete and cement-based mortars [164, 383-385]. However, in the mix 3C1L12S (25%), there appears to be an increase in fracture energy from 7 to 28 days, followed by a drop in 90 days. The reason for this behavior is neither known nor expected. Therefore, a conservative approach has been adopted and no conclusions regarding trends in fracture energy have been drawn.

Table 26: Values of fracture energy for lime-cement mortars (7, 28, and 90 days of age)

Property	Fracture energy (N/m) (COV %)		
Mix/Age (Days)	1C2L9S (67%)	1C1L6S (50%)	3C1L12S (25%)
7	4.7 (18.8%)	11.5 (52.6%)	34.6 (7.7%)
28	8.9 (14.4%)	24.7 (11.8%)	83.8 (1.4%)
90	10.0 (13.1%)	24.5 (6.6%)	62.0 (2.1%)

It is common to present the values of characteristic length along with fracture energy [94]. Characteristic length (l_{ch}) was a parameter originally presented by Hillerborg *et al.* [157], which is used as an indication of the brittleness of a material and is evaluated using fracture energy (G_f), E-modulus (E), and tensile strength (f_t) (Equation 19).

$$l_{ch} = \frac{EG_f}{{f_t}^2} \quad 19$$

The higher the value of characteristic length, the more dominant is the brittle nature of the material expected to be [94]. Therefore, this parameter was also considered. However, since the tensile strength of lime-cement mortars has not been measured directly in this experimental campaign, it was derived as a function of flexural strength (f_f) of the mortars, based on an expression (Equation 20) adapted from the Model Code 2010 [386] for concrete where h is the height of the specimen tested. The values have been presented in Table 27.

$$f_t = \left(\frac{0.06h^{0.7}}{1 + 0.06h^{0.7}}\right) f_f \quad 20$$

It was found that the characteristic length of the mortars 1C2L9S (67%) and 1C1L6S (50%) decreased with time, indicating an increase in brittle nature with time. Once again, it was found that the mix 3C1L12S (25%) acted differently, showing an increase between 7 to 28 days, followed by a decrease between 28 and 90 days. At all ages, the lowest characteristic length could be associated with the mix 1C1L6S (50%). However, patterns in the characteristic length of mortars, concerning the amount of lime in the binder could not be found.

Table 27: Derived values of tensile strength and characteristic length for lime-cement mortars

Property	Tensile strength (MPa)			Characteristic length (mm)		
Mix/Age (Days)	1C2L9S (67%)	1C1L6S (50%)	3C1L12S (25%)	1C2L9S (67%)	1C1L6S (50%)	3C1L12S (25%)
7	0.18	0.54	0.86	700.8	382.4	760.9
28	0.30	0.87	1.22	530.6	354.7	932.4

90	0.38	0.91	1.43	426.9	344.5	532.4

4.9 Open porosity

4.9.1 Methodology

Open porosity was measured at 7, 28, and 90 days of curing age for three mixes with binder-aggregate ratio 1:3 and lime content 25%, 50%, and 67%. The principle of measurement was based on the RILEM recommendations by RILEM TC 25-PEM (1980) for deterioration of stone [387], which recommends subjecting oven-dried specimens to vacuum for a specified period. Water is then slowly introduced into the vacuum chamber and the specimens are allowed to remain immersed and in a vacuum for the same amount of time. However, the duration of subjecting the specimens to vacuum and immersion in water was modified to 3 hours from 24 hours based on the recommendations (tailored for mortars) by the University of Beira Interior [388], often used in Portugal.

4.9.2 Results

Open porosity was also measured for three lime-cement mixes 3C1L12S (25%), 1C1L6S (50%), 1C2L9S (66.7%) (Table 28).

Table 28: Values of open porosity for lime cement mixes (7, 28, and 90 days)

Mortars | Open porosity (%)	Day 7	CoV (%)	Day 28	CoV (%)	Day 90	CoV (%)
1C2L9S (66.7%)	27.4	1.1	26.0	0.9	25.8	1.4
1C1L6S (50%)	27.0	0.6	24.2	0.7	24.1	0.3
3C1L12S (25%)	25.7	1.7	25.5	1.6	23.3	2.1

While globally the values seemed to vary little and lay between 23% and 27% it was possible to identify two trends. First, that open porosity decreases with age for all mixes, this trend has been verified by other authors and may primarily be attributed to carbonation in mixes 1C2L9S (66.7%) and 1C1L6S (50%), and mostly to hydration in the mix 3C1L12S (25%) [95]. The second trend is the increase in porosity with an increase in the lime content of the binder, which seems to align with the conclusions of Cizer [2]. The reason for this has been attributed to an increased specific surface area of lime compared to cement particles, which increases the demand for water to achieve the same consistency of the mix.

4.10 Drying shrinkage

4.10.1 Methodology

Drying shrinkage was measured for 5 lime-cement mixes (3C1L12S (25%), 2C1L9S (33.3%), 1C1L6S (50%), 1C2L9S (66.7%), 1C3L12S (75%)) from 7 days to up to approximately 90 days of curing age. The apparatus used was a length comparator with a digital dial gauge of 12 mm and a precision of ±0.001 mm and each measurement was an average of readings from three prismatic specimens 40×40×160 mm^3 (from the same batch), measured from either end of the length of the specimen. Shrinkage was calculated by dividing the change in length of the specimen by the effective gauge length. Measurements were recorded from day 7 onward when all samples were moved to an environment with 65±5% RH to ensure uniformity in the test since some of the mixes with more than 50% lime in the binder (by mass) had to be subjected to different demolding conditions [16].

4.10.2 Results

Drying shrinkage was measured for lime-cement mortars with B/Ag ratio 1:3 and lime content varying from 25% to 75% up to 90 days of curing age [Figure 59]. Most values seemed to be low and range between 550-750 micro strains. The mix 1C2L9S (67%) had its final value of shrinkage in the range of 800 micro strains. Additionally, almost all mixes seemed to stabilize by attaining their maximum values between 15-20 days from the time of casting, corresponding to the initial steepness of the curve. The quantity of lime in the binder did not seem to have a major impact on the extent of drying shrinkage. This is puzzling since it was possible to observe patterns as a function of the quantity of lime-cement ratio in the binder in open porosity, as shown in the previous section.

In the absence of direct literature on drying shrinkage of lime-cement mortars [62], the pore size distribution of lime-cement mixes available in literature was studied instead. Mosquera *et al.* [7, 389] stated that the binder composition had an impact on the pore size distribution of the mortar while it was the binder-aggregate ratio that had an impact on total porosity, which has also been mentioned by Arandigoyen *et al.* [59]. For the same binder-aggregate ratio (1:3), if the pore size distributions of mixes with only cement and only lime are considered, the former displays a unimodal distribution with a peak around 0.3 μm and the latter shows a bimodal distribution with peaks at 0.5 and 30 μm [7]. While the absolute values of the pore sizes where the peak occurs may vary with the measurement apparatus and based on the type of lime and cement used, the nature of distribution and the range of values of the pore size distribution are well established [56]. At a constant binder-aggregate ratio, when cement is added to lime in increasing proportions, there is a continuous reduction in the pore size of the lime mortar, possibly

due to cement filling up the larger pores present in lime. The bi-dispersion is reported to tend towards uni-dispersion [7]. It has further been reported that with increasing quantities of cement in a lime-cement mix, there is an increase in the number of pores of size less than 0.1 μm and greater than 10 μm [7]. However, while this transition implies a distinct change in the size of pores for the different mixes; most of the lime-cement compositions still tend to retain a similar pore distribution in the range of sizes in between 0.1-10 μm which is directly relevant for drying shrinkage, i.e. mesopores 1.25 – 25 μm [390]. Furthermore, this pore size distribution has been reported as being pretty heterogeneous [59]. This may serve as a reason for the stated absence of any specific pattern in drying shrinkage of the mixes as a function of lime content in the binder.

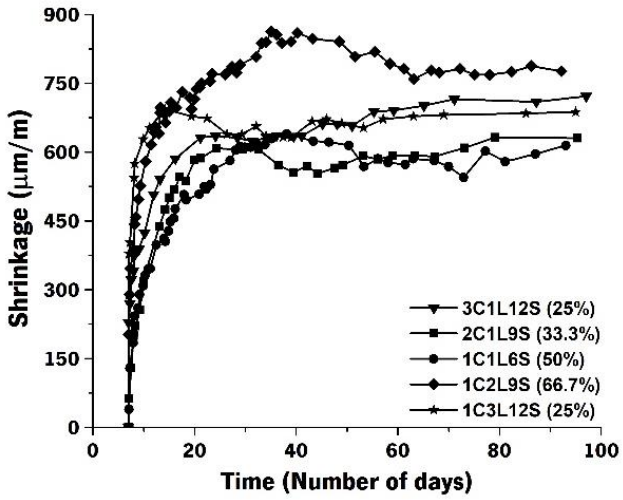

Figure 59: Evolution of drying shrinkage with time for lime-cement mortars (B/Ag 1:3, by volume)

4.11 EMM-ARM

4.11.1 Methodology

EMM-ARM (E-modulus Measurement through Ambient Response Method) is a method that was introduced in 2009 by Azenha *et al.* [391], used to measure the development of stiffness of concrete, mortar, and cement paste mixtures (Figure 60). A detailed description of the method and its principles may be found in the Ph.D. thesis of Granja [115]. Specifically, Appendix-A of the thesis is a user-guide for the EMM-ARM method (Version 2.0.1). Concerning mortars, and taking into account the most recent developments of EMM-ARM, a PVC mold was used filled with the mortar to be tested, and placed horizontally in simply supported conditions (Figure 60 d) and subjected to forced vibrations at mid-span [129]. This external excitation is provided electromagnetically with an actuator and a magnet placed under the specimen, without any direct contact and the response is measured with the help of accelerometers.

The accelerometer measurements are then fed into the system through a data logger, to perform modal identification. The acquisition sampling rate used was 1250 Hz, acquisition time per sample was 300 s, and the time between two sampling events was 720 s. Even though the nature of the measurement is technically discrete, because of the frequency at which data was obtained (every 12 minutes), from a global perspective it may be considered almost-continuous. The expected frequency at the start of the procedure was set to 60 Hz. The evolution of the first flexural resonant frequency of the composite mold was assessed, as it was a function of the increasing stiffness of the mortar cast inside of it. Continuous estimations of Young's modulus were obtained employing the dynamic equation of motion, according to the principles set forward in [129, 392]. An overview of the test preparation and set up has been illustrated through images in Figure 60.

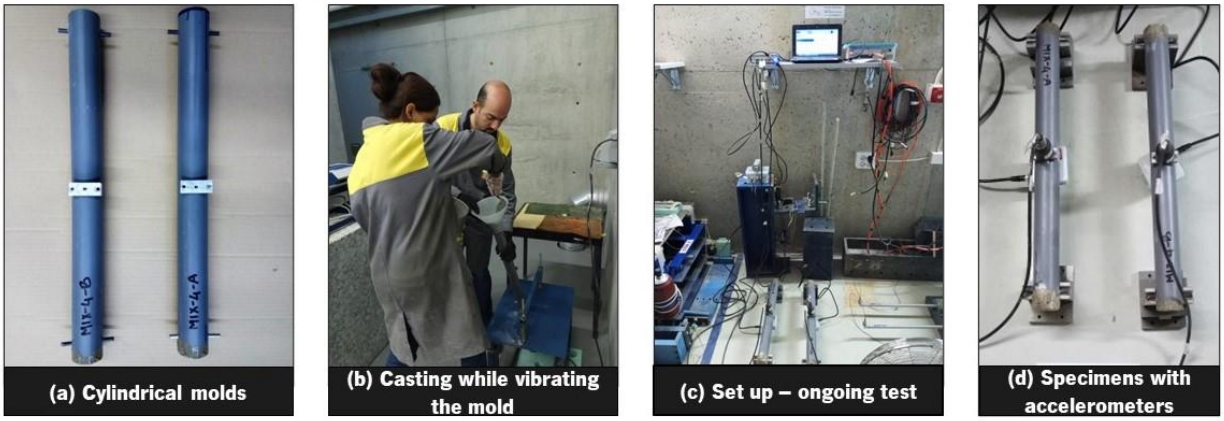

Figure 60: Illustration of the preparation for and set up of EMM-ARM to measure E-modulus (continuous monitoring)

The molds had the dimensions of 550 mm in length, and 44 mm internal and 50 mm external diameter (Figure 60 a). Two steel rods of 6 mm diameter and 85 mm length were required to be drilled into the PVC tube to act as supports for a span of 500 mm. After the mortar was cast into the mold (Figure 60 b), the specimen was sealed from both ends using 20 mm thick polystyrene cylinder caps [115]. Since the specimens were completely sealed in this test, relative humidity may be considered as 95±5%, comparable with the curing conditions specified in EN 1015-11 [16] for the first seven days. However, it must be noted that the moisture-curing conditions are not the same since in standard conditions, the mortar specimens were demolded after 2 days and exposed to air curing in 95±5% RH. The ambient room of the temperature where the test was conducted was maintained at 20±2˚C. This method of EMM-ARM was used to monitor the evolution of stiffness of 5 different mortars - 3C1L12S (25%), 2C1L9S (33.3%), 1C1L6S (50%), 1C2L9S (66.7%), 1C3L12S (75%), from the time of casting up to 7 days of age.

4.11.2 Results

4.11.2.1 Evolution of E-modulus with time, measured by EMM-ARM

The evolution of E-modulus measured through the method EMM-ARM has been shown for 5 different lime-cement mixes with B/Ag ratio 1:3 (Figure 61). Tests for the mixes were conducted with two specimens simultaneously and the resulting curves presented are an average, with a coefficient of variation between (2-12)% in all cases. Only the mix 2C1L9S (33.3%) was conducted with one specimen due to a technical problem with one of the accelerometers.

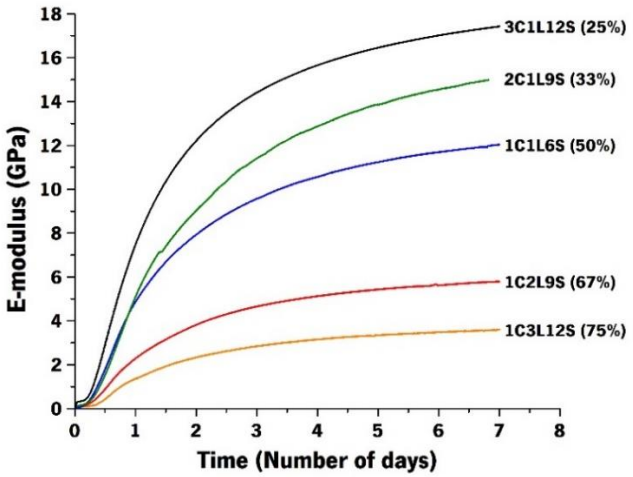

Figure 61: Evolution of E-modulus of lime-cement mortars obtained from EMM-ARM test (B/Ag 1:3, by volume)

On day 7, consistent with results of E-modulus obtained from the classical cyclic compression test (Section 4.6.2.1), an increase in the quantity of lime in the binder leads to a lower value of E-modulus of the mortar. Between 0 and 7 days as well, this trend appears to be similar. Cizer [2] has reported that competition between hydration and carbonation is almost non-existent in early ages (~7 days), under atmospheric conditions, i.e., cement hydration is faster and a significant part of it takes place before carbonation begins to contribute to gain in strength or stiffness of the mortar.

To quantify the effect of lime in the binder of the mortar, values of E-modulus were compared every 24 h, from 1 to 7 days (Figure 62 a). Based on the seven linear regression analyses performed for values from day 1 to day 7, a correlation could be established. Corresponding to an increase in time from day 2 to day 7 the values of adjusted R-sqaured consistently increased from 0.96 to 0.98, F-value increased from 80 to 210, and the p-value decreased from 2.96E-03 to 7E-04. Day 1 exhibited a relatively weaker correlation with values of adjusted R^2 equal to 0.91, F-value of 40, and p-value of 7.8E-02. The mix

9C1L30S (10% lime in the binder by volume) was used as a benchmark for normalization. It was found that at all curing ages, day 1 to day 7: every 1% increase in the quantity of lime in the binder led to a corresponding 1.3% decrease in stiffness of the mortar. It is also possible to observe that all mortars, regardless of the quantity of lime in the binder, appear to gain approximately 40% of their total stiffness in the first 24 hours, and 80% in the first 72 h hours. After the fourth day, the increase in stiffness of all the mortars was found to be 5% or lesser.

Furthermore, stiffness was normalized for the corresponding values attained at day 7 for all mortars and plotted together (Figure 62 b). One may conclude that the dormant period in cement hydration that occurs in the first 3-4 hours, appears to be similar in all the mortars. It may also be observed that curves of almost all the mortars tend to overlap, indicating that the kinetics of hardening between the different mortars is similar. Concerning kinetics of stiffness evolution, it is reported in the literature [2] that cement hydration is the dominant reaction in the first few days since the casting of a lime-cement mix, and therefore, the expectation would be that the greater the quantity of cement in the binder, the faster would be the kinetics of hardening. However, a small difference may be observed in the mix 2C1L9S (33.3%), which exhibits the slowest kinetics, which is contrary to expectation, since it does not have the least amount of cement in the binder. The conclusion may be that the mix 2C1L9S (33.3%) behaves somewhat as an outlier in this test. External factors such as ambient curing temperature or minor differences in the setup may have led to slightly slower kinetics. However, since a significant difference in the environment or procedure of the test was not observed by the operator, there may be other mechanisms at play and this matter would, therefore, merit further investigation. Especially because minor differences in the rate of cement hydration, due to the presence of hydrated lime have been reported in the literature [393, 394]. Fourmentin *et al.* [393], state that the presence of lime accelerates the process of cement hydration, reducing its dormant period, but to a negligible extent. This phenomenon has been attributed to the high specific surface area of lime, which possibly provides a larger surface area for precipitation of the C–S–H crystals formed during cement hydration. These authors further state that this accelerating effect of lime saturates after a certain quantity. Another explanation is that lime destroys Al–O bonds networks (corresponding to oxides of Aluminium) in tricalcium aluminates, which are formed as a product of cement hydration; resulting in an increase in alkalinity of the mix, consequently accelerating the reaction [2]. It is, therefore, not possible to conclude with certainty whether the mix 2C1L9S (33.3%) is an outlier or it represents a mechanism that is not well understood as of now.

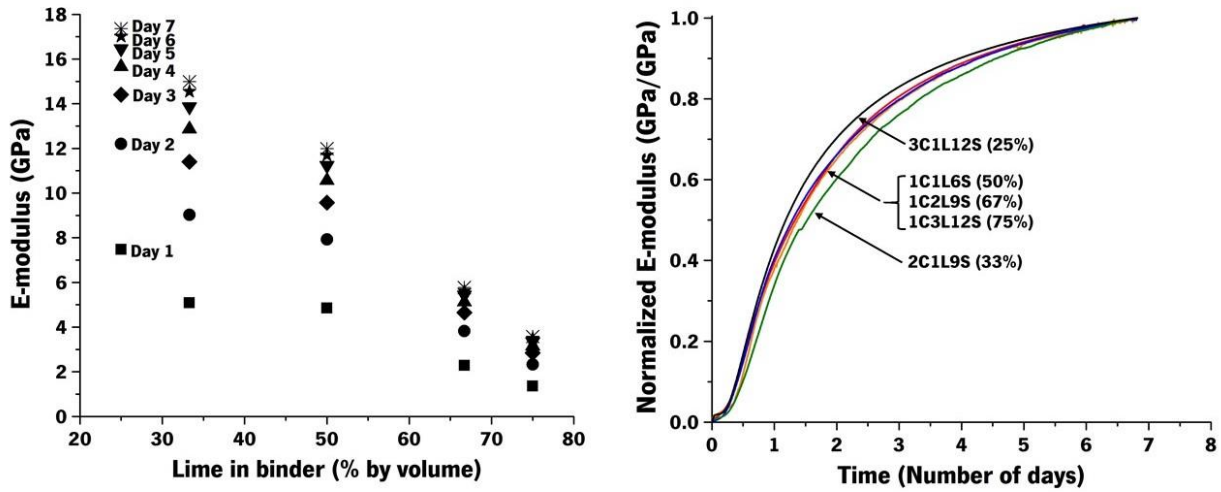

Figure 62: (a) E-modulus versus lime content in the binder, % by volume (b) Normalized evolution of E-modulus with time for lime-cement mixes (B/Ag 1:3, by volume)

4.11.2.2 Comparison of E-modulus values from EMM-ARM & cyclic compression test

Since values of E-modulus of the mortar after 7 days of curing were obtained from 2 different methods, they were compared. A direct comparison is not possible because of differing moisture curing conditions, since, in the EMM-ARM test, the specimens were kept sealed throughout, while for the cylinders tested using the cyclic compression test, the specimens were demolded and exposed to 90% RH between 2 to 7 days. Regardless, it was expected that the values would be in the same range (Table 29, Figure 63), and was found to be true. All the mixes showed a slightly higher E-modulus value from the test of EMM-ARM and this may be expected due to two reasons. First, the sealed specimens in EMM-ARM, provide greater RH, promoting conditions for cement hydration [2, 24]. The second reason is that in the cyclic compression (static) test, even though loads applied are in the linear range, deformations do take place, possibly causing micro-changes/damages in the microstructure which does not happen in a dynamic test (EMM-ARM) [395].

Table 29: Comparison of E-modulus (GPa) at 7 days of age, obtained from EMM-ARM and cyclic compression test

Mortars	Cyclic compression | E-mod (GPa)	EMM-ARM | E-mod (GPa)	Diff (%) using cyclic compression test as a reference
1C2L9S (66.7%)	4.8	5.8	19.1
1C1L6S (50%)	9.8	12.0	22.0
3C1L12S (25%)	16.3	17.4	6.2

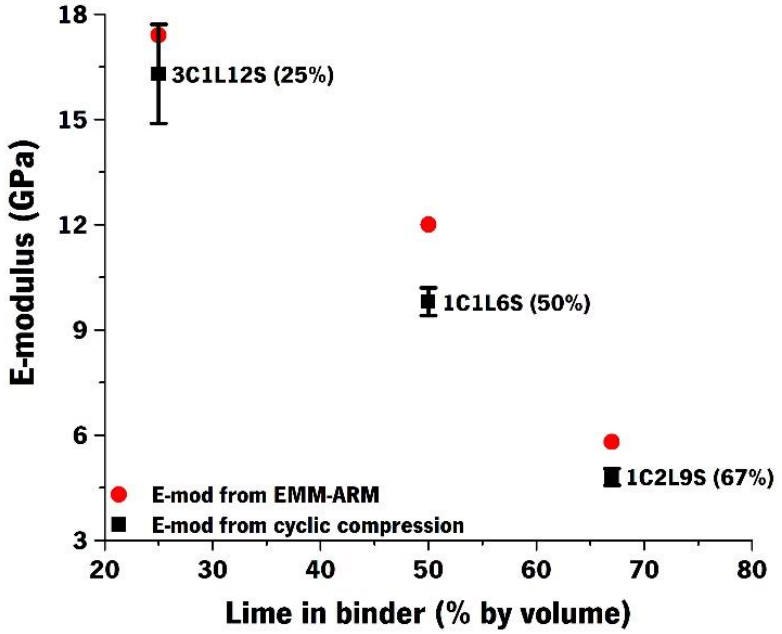

Figure 63: Comparison of values of E-modulus (GPa), obtained from EMM-ARM and cyclic compression test at 7 days of age

To facilitate a comparison of E-modulus from the classical cyclic compression test and EMM-ARM, with similar moisture curing conditions, one mix was chosen 1C1L6S (50%). Six cylindrical specimens were kept sealed up to the time of testing (6.5 days) by the method of cyclic compression (Section 4.6.2.1) - three for compression and three for E-modulus. E-modulus obtained from EMM-ARM (average value) corresponded to 11.8 GPa and that from cyclic compression test corresponding to 10.9 GPa (obtained from an average of three specimens with a coefficient of variation of 0.2%). The difference of 7.4% in the results was considered acceptable since up to 10% variation was found common in the measurement of static Young's modulus of mortars, as observed in this research (Table 24) as well as in literature [11].

4.12 Final remarks

This chapter focuses on the characterization and correlation of basic mechanical properties of different lime-cement mortars, including – workability, mechanical strength (compression and flexure), UPV & bulk density, stiffness measured by EMM-ARM as well as the cyclic compression method, fracture energy, Poisson's ratio, drying shrinkage and open porosity. The following key points summarize the findings of this chapter:

1) For a target workability, the requisite water-binder ratio increases linearly with increasing lime content in the binder, as well as with decreasing B/Ag ratio of the mix. An equation has been presented to

estimate the requisite water binder ratio for a given mix, as a function of the composition of the mix (lime-cement ratio, B/Ag ratio), within a 10% error margin (Section 4.3).

2) The evolution of mechanical strength (compression and flexure) with time has been expressed in equations that are a function of the strengths of the corresponding mixes at 7 days (Section 4.4.2.1).
3) It was found that for B/Ag ratios 1:3, 1:4, and 1:5, every 1% increase in the quantity of lime in the binder (by volume), led to a 1.4% reduction in the mechanical strength (compression/flexure) of the mix, with respect to the benchmark mix – with 10% lime or 90% cement in the binder (Section 4.4.2.2).
4) It was found that for binder compositions with 33.3%, 50%, and 66.7% lime in the binder, every 1% decrease in B/Ag ratio (by volume), led to a 5% reduction in the mechanical strength (compression/flexure) of the mix, with respect to the benchmark mix – B/Ag ratio 1:3 (Section 4.4.2.3).
5) Mechanical strength (compression/flexure) could be expressed in an equation as a function of lime content in the binder, B/Ag ratio, and curing age (Section 4.4.2.4)
6) Bulk density was found to decrease till 28 days for almost all the mixes and then stabilize or increase slowly with time (Section 4.5.2.1). UPV values were found to decrease with increasing lime content in the binder and decreasing B/Ag ratios of lime-cement mixes. Furthermore, it was found that the square of UPV $(\mathrm{UPV(T)}^2)$ and a product of density and compressive strength $(\rho(\mathrm{T})^{1.5}\mathrm{f_c(T)}^{0.5})$ varied linearly with lime content in the binder and B/Ag ratios (Section 4.5.2.2).
7) E-modulus measured by the cyclic compression test was found to be in the range of 4-18 GPa for mixes 1C2L9S (67%), 1C1L6S (50%), and 3C1L12S (25%) between 7 to 90 days. The increase in stiffness of the mixes between day 7 and day 90 was found to be 7%, 19%, and 27% for the mixes 3C1L12S (25%), 1C1L6S (50%), and 1C2L9S (67%) respectively (Section 4.6.2.1). Furthermore, for these mortars, the ratio of E-modulus to compressive strength for cylindrical specimens was found to vary from 1300 to 2300 at 90 days of age (Section 4.6.2.2).
8) For the mortars 3C1L12S (25%), 1C1L6S (50%), and 1C2L9S (67%), Poisson's ratio was found to vary from 0.13 to 0.23 between 7 to 90 days of age, with a global average of 0.18 (18% CoV). (Section 4.7.2).
9) For the mortars 3C1L12S (25%), 1C1L6S (50%), and 1C2L9S (67%), fracture energy was found to range from 5 to 83 N/m depending on the quantity of lime in the binder (Section 4.8.2).
10) Open porosity was measured for the mixes 3C1L12S (25%), 1C1L6S (50%), and 1C2L9S (67%) at 7, 28, and 90 days of age. The value decreased with age for all mixes and increased with the amount

of lime content in the binder. The general range of values was found to vary only slightly between 23% and 27% (Section 4.9.2).

11) Drying shrinkage was measured for lime-cement mortars with B/Ag ratio 1:3 and lime content varying from 25% to 75% up to 90 days of curing age. The quantity of lime in the binder did not appear to have an impact on the extent of drying shrinkage. Most values ranged between 550-750 micro strains (Section 4.10.2).

12) E-modulus was measured for lime-cement mortars with B/Ag ratio 1:3 and varying lime content in the binder (25%, 33%, 50%, 67%, 75%) from time 0 to 7 days of age using the method EMM-ARM. Results from the EMM-ARM test indicate that at all curing ages, day 1 to day 7: every 1% increase in the quantity of lime in the binder led to a corresponding 1.3% decrease in stiffness of mortars. It was also observed that all mortars, regardless of the quantity of lime in the binder, appeared to gain approximately 40% of their total stiffness in the first 24 hours, and 80% in the first 72 hours. After the fourth day, the increase in stiffness of all the mortars was found to be 5% or lesser (Section 4.11.2).

5. Influence of lime-cement mortars on the mechanical behavior of masonry

5.1 Introduction

The goal of this chapter is to describe and discuss the findings of an experimental program, aimed at better understanding how the mechanical behavior of masonry changes when it is constructed with different types of mortars: lime-cement and cement only. All masonry specimens were constructed with solid-frogged clay brick units, chosen according to the reasoning presented in Section 3.2.3, Chapter 3. In total, three mortars were used for this stage of the research; the reference mortar is made of cement with a composition of 1:5 (B/Ag, by volume), while the other two had a B/Ag ratio of 1:3 by volume and 50% and 66.7% lime in the binder, by volume. It may be noted that these mortars are different in composition, from the corresponding mortars in Chapter 4, because of the change in the particle size distribution of the aggregate. This was done to obtain the cement reference mortar (Detailed explanation in Section 3.4.1, Chapter 3). Therefore, to avoid confusion, the mortars used for research on masonry will be referred to as Ref, L50, and L67 corresponding to the compositions 1:5 (Cement: Aggregate), 1:1:6 (Cement: Lime: Aggregate), and 1:2:9 (Cement: Lime: Aggregate), all proportions by volume.

Section 5.2 discusses the mechanical characteristics of the components used to construct masonry; the three selected mortars (Ref, L50 and L67) and brick. Section 5.2.1 discusses the mortars used to construct masonry and a study of their mechanical properties including mechanical strength (compression and flexure) and E-modulus, while section 5.2.2 characterizes the mechanical properties of the brick used to construct masonry, such as mechanical strength, E-modulus, IRA and water absorption.

Subsequently, sections 5.3 to 5.6 study the contribution of mortar to masonry by addressing different mechanical properties; compressive strength and E-modulus, flexural strength, shear bond strength and in-plane shear wall strength of masonry. Section 5.3 addresses the compressive strength and E-modulus of masonry, as well as compares the strains at peak and ductility under compression. Section 5.4 presents the flexural strength of masonry, in two directions – parallel to the bed joints and perpendicular to the bed joints. Section 5.5 presents the shear bond strength of masonry, and the coefficients of friction. Finally section 5.6 presents results of masonry wall panels subject to combined normal and lateral in-plane cyclic loading, and discusses energy dissipation, stiffness degradation and drift capacities. Masonry specimens have been referred to, based on the mortars used to construct them, i.e., Ref, L50 and L67.

To measure displacements in the masonry specimens, linear variable differential transformers (LVDTs) from RDP were used [396]. Those with a linear range of ±2.5 mm were of the type D6/02500ARA with a sensitivity of 375 mV/V and linearity of 0.07%. Others with a linear range of ±5 mm were of the type D6/05000A, and had a sensitivity of 700 mV/V and linearity of 0.13%. Further, all surfaces of masonry specimens that came into contact with steel plates were rectified for even distribution of the loads applied, using a bitumen based polyester resin (Sotinco 67-120 [397]). For attaching the LVDTs to the surface of masonry specimens, small metallic plates were used as an interface, along with a thermoplastic adhesive which is commonly referred to as hot glue, known for fast bonding, low costs and ease of availability [398].

5.2 Components used for masonry construction

5.2.1 Mortars used for masonry construction

The rationale behind choosing the three mortar mixes 1:0:5 or (1:5), 1:1:6 and 1:2:9, has been presented in detail in Chapter 3. This decision was based on results obtained from the 15 lime-cement mixes studied in Chapter 4, and a review of compositions that were found to be commonly used in the literature and industry [2, 95, 347, 364]. The reference mortar (1:0:5) has been denoted as 'Ref', while the other two mortars (1:1:6 and 1:2:9) have been denoted as 'L50' and 'L67' corresponding to 50% and 67% lime (by volume) in their respective binders.

5.2.1.1 Characterization of mechanical strength of mortars used in masonry

As mentioned in Chapter 3, two different curing conditions were adopted for the mortars, and were assigned the nomenclature of standard and in situ. 'Standard' implies that the process respected the recommendations of the European standards, for both mixing protocols as well as curing conditions. 'In situ' refers to mortars that were cast in large batches for masonry construction. Samples were taken from the large batches and cured next to the masonry specimens in the same temperature and humidity conditions.

(a) Standard mortars

Mechanical (compressive and flexural) strength was tested on days 7, 28, and 90 and the results have been presented in Table 30 and Figure 64. By day 90, the reference mix has the highest compressive and flexural strength, closely followed by the mix L50 with a compressive strength that is 17% lower and

almost the same flexural strength. The mix L67 on the other hand has a compressive strength 58% lower than the reference mix and a flexural strength 47% lower than the reference.

Table 30: Mechanical (compressive and flexural) strength of standard mortars

Property	Compressive strength (MPa)			Flexural strength (MPa)		
Mortars/Age	fc-7 (CoV %)	fc-28 (CoV %)	fc-90 (CoV %)	ff-7 (CoV %)	ff-28 (CoV %)	ff-90 (CoV %)
L67 (1:2:9)	2.28 (7.9)	4.35 (10.8)	4.69 (2.1)	0.85 (6.5)	1.88 (5.0)	1.88 (4.5)
L50 (1:1:6)	5.80 (4.9)	9.35 (5.1)	9.28 (5.7)	1.88 (3.9)	3.93 (0.7)	3.42 (3.5)
Ref (1:0:5)	7.77 (5.2)	10.27 (7.3)	11.21 (2.7)	2.46 (3.5)	3.14 (2.4)	3.53 (7.1)

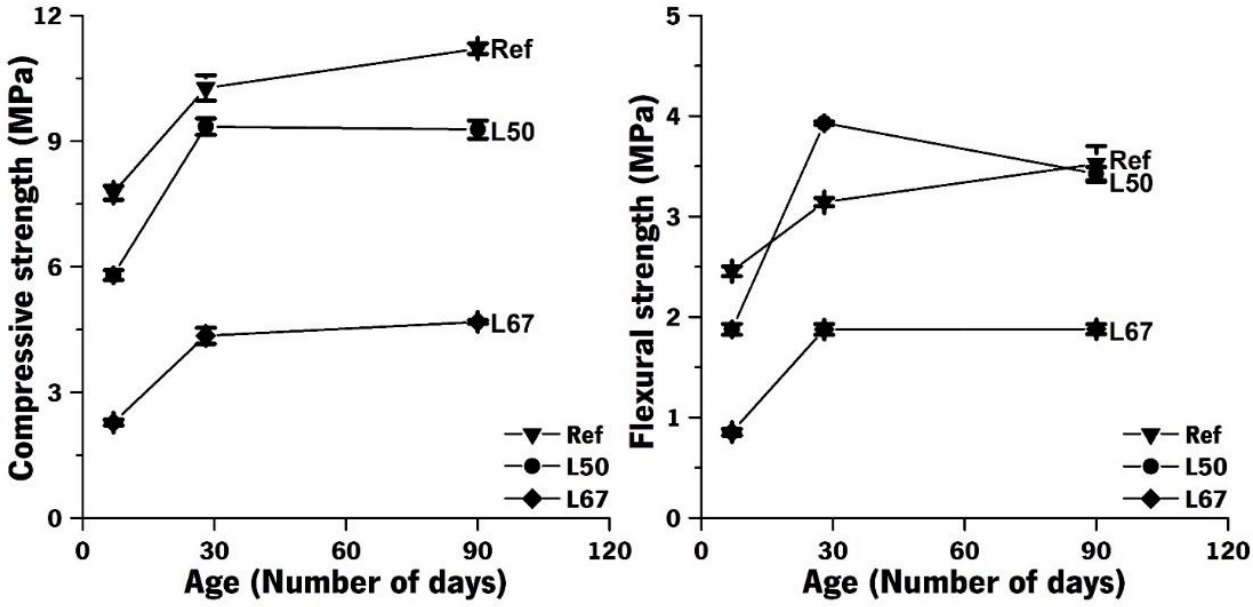

Figure 64: Mechanical strength of mortars (standard conditions) used for research on masonry

Mortars L67 and L50 in standard conditions were tested according to EN 1015-11[16] and have compositions similar to 1C2L9S (67%) and 1C1L6S (50%) respectively, that were studied in Chapter 4. A comparison of their performance in terms of mechanical strength at days 7, 28, and 90 have been presented in the Annexes (Annex-Figure 1), since it would help understand the impact of changing the particle size distribution of the aggregates, on the mechanical strength of mortars.

(b) In situ mortars

Mechanical (compressive and flexural) strength was tested on days 28 and 90 and the results have been presented in Table 31 and Figure 65. It may be seen that by day 90, the compressive and flexural strengths of all the mortars are slightly higher than in the standard conditions (Figure 66). The global trends, however, remain similar. Once again, on day 90, the reference mix has the highest compressive and flexural strength, closely followed by the mix L50 with a compressive strength that is 17% lower and almost the same flexural strength. And the mix L67 has a compressive strength 56% lower than the reference mix and a flexural strength 49% lower than the reference.

Table 31: Mechanical (compressive and flexural) strength of in situ mortars

Property	Compressive strength (MPa)		Flexural strength (MPa)	
Mortars	fc-28 (CoV %)	fc-90 (CoV %)	ff-28 (CoV %)	ff-90 (CoV %)
L67 (1:2:9)	4.12 (3.4)	5.30 (5.2)	1.57 (3.5)	1.95 (2.1)
L50 (1:1:6)	9.75 (7.6)	10.07 (8.5)	2.99 (9.3)	3.55 (7.8)
Ref (1:0:5)	10.88 (8.9)	12.08 (6.0)	3.04 (1.0)	3.78 (11.3)

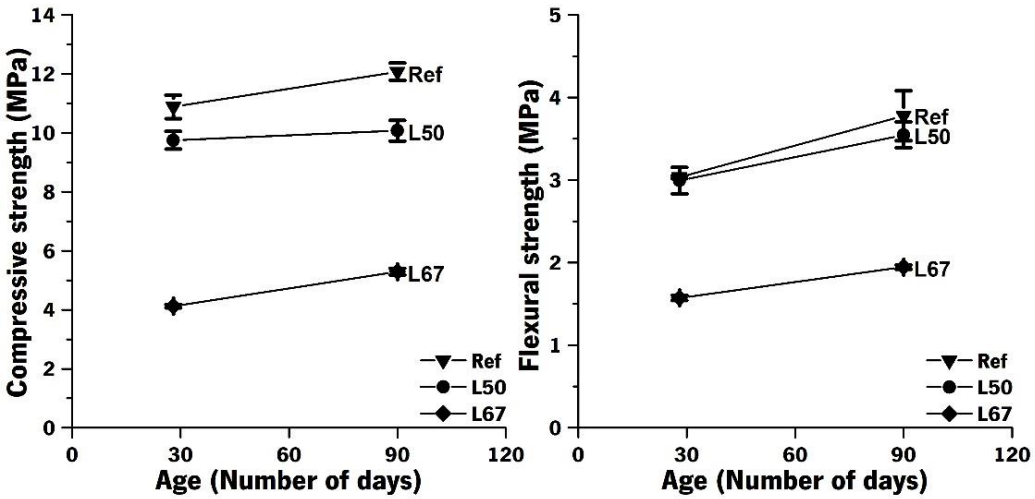

Figure 65: Mechanical strength of mortars (in situ conditions) used for research on masonry

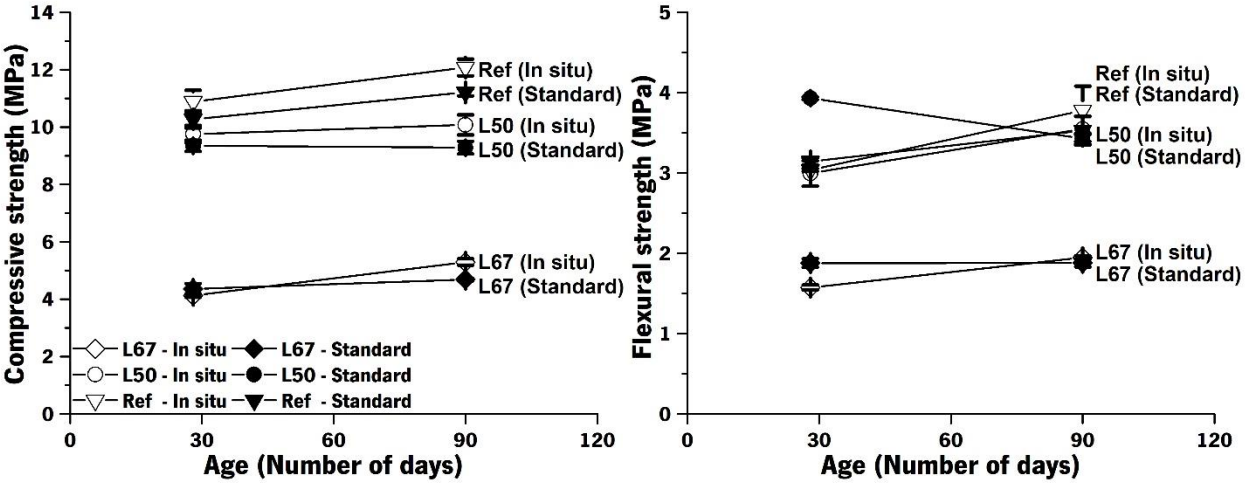

Figure 66: Comparison of mechanical strength of mortars, used in masonry specimens in standard (Table 30) and in situ (Table 31) conditions at 28 and 90 days of curing age

5.2.1.2 Characterization of E-modulus of mortars used in masonry

E-modulus for the in situ mortars was measured using the cyclic compression test, at ages 28 and 90 days. For the sake of comparison and characterization in standard conditions, E-modulus was also measured for standard mortars at 90 days of age. All results have been shown in Table 32 and Figure 67. If experimental scatter is accounted for, the values of E-modulus between day 28 and day 90 for the in situ conditions may be considered the same. Similarly, considering the coefficient of variation at day 90, if the values of E-modulus are compared for in situ and standard conditions, the values are once again in the same range except for the reference mix. This is expectable since, in the standard conditions, the reference mix is immersed in water until testing which favors cement hydration [24], as opposed to the in situ conditions, in which the reference mix is exposed to the same atmosphere as masonry.

Table 32: E-modulus for mortars (standard and in situ)

Category	In situ		Standard
Mortars	E-mod - 28 (GPa) (CoV %)	E-mod - 90 (GPa) (CoV %)	E-mod - 90 (GPa) (CoV %)
L67 (1:2:9)	6.94 (15.7)	7.90 (5.3)	8.54 (1.2)
L50 (1:1:6)	16.47 (16.8)	15.97 (17.5)	14.86 (2.2)
Ref (1:0:5)	16.53 (7.6)	15.21 (5.1)	19.47 (10.5)

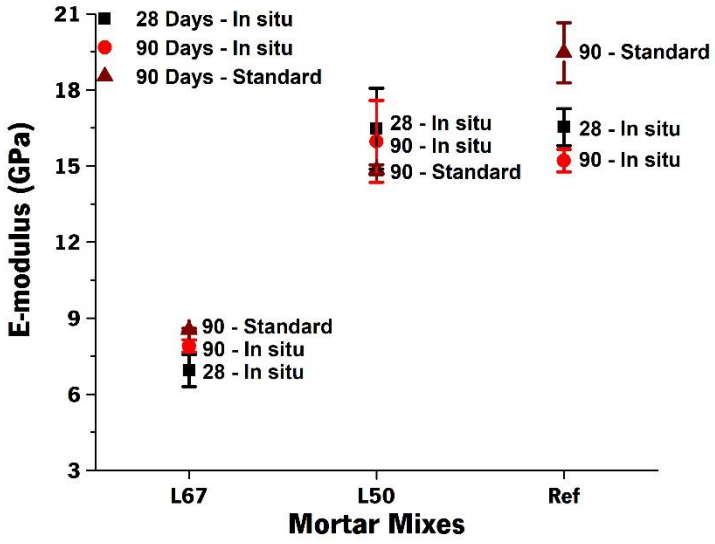

Figure 67: E-modulus for mortars (standard and in situ)

Comparison of E-modulus at 90 days of curing age for mortars L67 and L50 in standard conditions, with 1C2L9S (67%) and 1C1L6S (50%) (studied in Chapter 4) has been presented in the Annexes (Annex-Figure 2), since it would help understand the impact of changing the particle size distribution of the aggregates, on the mechanical stiffness of mortars.

5.2.2 Mechanical characterization of bricks used for masonry construction

The brick selected for this research came with a datasheet that specified some of its mechanical properties (Chapter 3). However, a few properties such as the E-modulus and flexural strength of the brick were not specified. While performing the said tests, it decided to also measure the compressive strength, water absorption, and IRA in the scope of this Ph.D. work. The values finally used for the research were those that were measured in the laboratory and have been presented here in Section 5.2.2.2.

5.2.2.1 Methodology for different tests used to characterize the bricks

All specimens used for characterization were first oven-dried at 105±5˚C and subsequently cooled down to room temperature before testing. The criterion of drying used was similar to that used for mortar specimens. If the difference in the weight of the specimen was less than 1% between two subsequent measurements taken in one hour, then the specimen was considered to be dry.

Compressive strength

The compressive strength (Figure 68 a) of the brick was measured using 6 specimens that were rectified on the top and bottom surfaces, such that the final height of the specimens after rectification was greater than 40 mm and the height to width ratio was also greater than 0.4, according to EN 772-1 [399]. The process of rectification was carried out using standard laboratory equipment which involved the specimens coming into contact with water and therefore the specimens were oven-dried after rectification. The frogs in the bricks were not filled, since the net loaded area of the brick was greater than 35% of the bed face, as per EN 772-1 [399]. The force applied on the specimen was increased using a hydraulic actuator with a capacity of 1000 kN and displacement control was used at a speed of 5 µm/s. Thereafter, based on the height to width ratio of each of the specimens, shape factors from EN 772-1 [399] were used to obtain normalized compressive strength of the bricks.

E-modulus

For E-modulus, six cubic specimens of size 50×50×50 mm^3 were used. The set up consisted of two metallic pieces of size 50×50×50 mm^3, placed on the top and bottom of the specimen, which supported the rings that held the 4 LVDTs used, one for each face of the specimen (Figure 68 b). A hydraulic actuator with a capacity of 25 kN was used to apply an axial pre-load of 100 N and four continuous loading and unloading cycles. The maximum load equaled approximately one-third of the maximum compressive strength obtained from tests on eleven cubic brick specimens of the same size 50×50×50 mm^3. Similar to the methodology adopted for mortars, the duration of each loading and unloading cycle was designed to be 60 s, with a constant ramp of 20 s in between. Finally, the slopes (stress/average strain) of the ascending branches were averaged and used to calculate the E-modulus for each specimen.

Flexural strength

The flexural strength of prismatic brick specimens of size 40×40×160 mm^3 was measured in a way similar to that of mortar specimens, using the three-point bending test (Figure 68 c). The supports were placed at a distance of 96 mm from each other, 32 mm from either end. Five specimens were used in total and the test was performed using displacement control at a rate of 6 µm/s.

Water absorption and IRA

Water absorption (Figure 68 d) was measured on 6 prismatic specimens of size 40×40×160 mm^3 according to EN 772-21 [337]. Specimens were cooled down to room temperature after oven drying and were immersed in water for 24±0.5 hours. The mass of each specimen was noted before and after

immersion, the difference of which was expressed as a function of the original dry mass to obtain the amount of water absorbed by the specimens. The final value obtained was a value averaged from six specimens, and expressed in percentage.

The initial rate of absorption (IRA) (Figure 68 e) was also measured on 6 prismatic specimens of size 40×40×160 mm^3 according to EN 772-11 [338]. The procedure involved immersing each specimen in water, up to a depth of 5±1 mm, for one minute and noting down the corresponding differences in mass. The difference in mass was then divided by the product of, the area of the specimen exposed to water, and time (one minute).

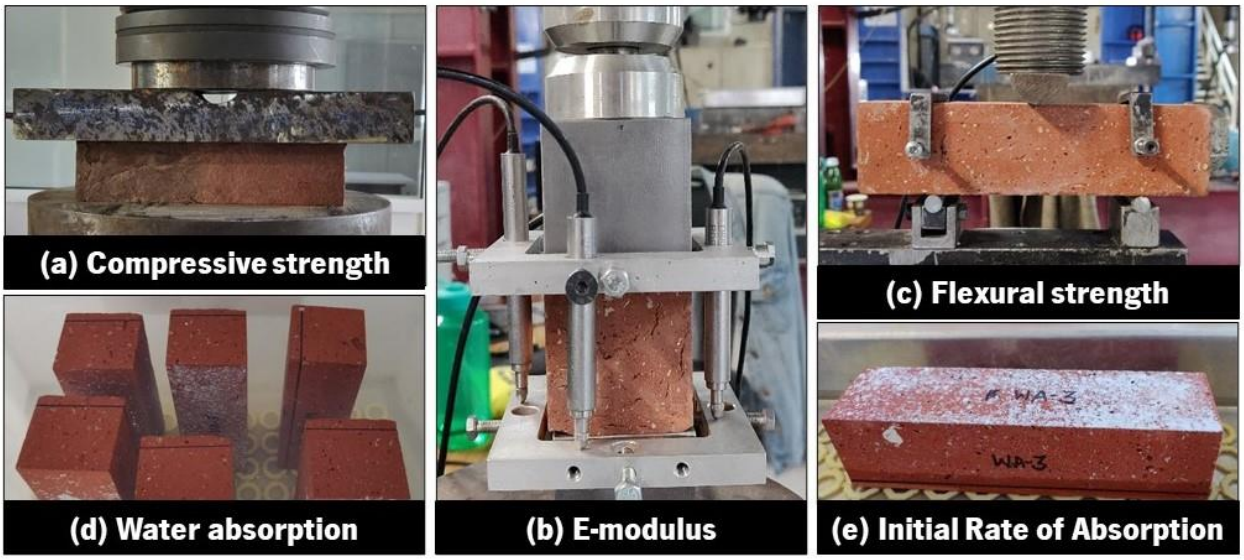

Figure 68: Different tests performed to characterize the mechanical properties of bricks

5.2.2.2 Results of mechanical and physical characterization of brick chosen

The results obtained from different mechanical characterization tests performed on bricks have been presented in Table 33. All values have been supplemented with their respective scatter in terms of coefficient of variation. In the case of compressive strength, average values obtained from the whole brick as well as cubic specimens have been presented. For cubic specimens, the mean compressive strength obtained was 25.9 MPa, with a coefficient of variation of 22.7%. This average result or arithmetic mean was then multiplied by a factor of 0.85 to obtain the normalized compressive strength, based on the height and width (50 mm × 50mm) of the specimens [399]. The final value of normalized compressive strength, 22.03 MPa has been shown in Table 33. In the case of the whole brick being tested, the average value obtained was 26.2 MPa. Since each specimen, had a slightly different height to width ratio (varying between 0.55 to 0.66), the appropriate shape factors were used for each of them and the average of the

normalized compressive strength has been presented in Table 33. It may be observed that the normalized values of compressive strength obtained from testing the whole brick, versus the cubic specimens are similar, with a difference of 4.2%. However, it must be noted that the minimum value of compressive strength presented in the datasheet provided by the manufacturer is 12 MPa, which is much lower than the values found here. Further, it may be observed from the experimentally obtained values, that E-modulus is 222 times the compressive strength. The experimentally obtained value of IRA of 3.55 kg/m^2.min lay in the range specified in the datasheet, of 1 to 5 kg/m^2.min. In the case of water absorption, the experimental value found was 10.3% and the value presented in the datasheet was 15%.

Table 33: Mechanical characterization of bricks used to construct masonry

Property	Compressive strength* (MPa)		E-modulus	Flexural strength	Water	IRA
	Complete brick	Cubic specimen	(GPa)	(MPa)	absorption (%)	(kg/m^2.min)
Average (CoV %)	22.03 (22.7%)	21.15 (13.7%)	4.9 (15.7%)	5.41 (21.0%)	10.3 (7.6%)	3.55 (15.6%)

* Normalized value obtained by multiplying average value with shape factor according to EN 772-1 [399]

5.3 Compressive strength and E-modulus of masonry

5.3.1 Methodology

Compressive strength for masonry was tested according to the recommendations of EN 1052-1 [17]. Each specimen was composed of a single leaf of bricks, with a height of 450 mm (6 courses of bricks) and a width of 440 mm (2 bricks in each course), and has been shown in Figure 69. At the time of testing, the specimens had been cured for 90 days. A hydraulic actuator with a capacity of 1000 kN was used to perform the test using the method of displacement control at a speed of 3 μm/s. To measure deformation in the specimens, four LVDTs were used in total for each specimen and were set up as shown in Figure 69, two on each of the wider faces of the specimen (2 in the front and 2 at the back). The horizontal distance between two LVDTs on each face was 260 mm and the vertical height covered by each of the LVDTs was 230 mm. The LVDTs were fastened to aluminum plates which were attached to the specimens using hot glue. The distances measured with respect to the LVDTs were calculated from the center of each of the plates they were attached to. For each type of mortar, to calculate the final value of compressive strength, 3 masonry specimens were tested. Additionally, prior to starting the actual tests, one masonry specimen of each mortar type was tested, to assess the requirement of conditions such as the capacity of the actuator, speed of testing, and value of cyclic loads to be applied on the specimens to measure E-modulus. This extra specimen used in each case was not included in the final results.

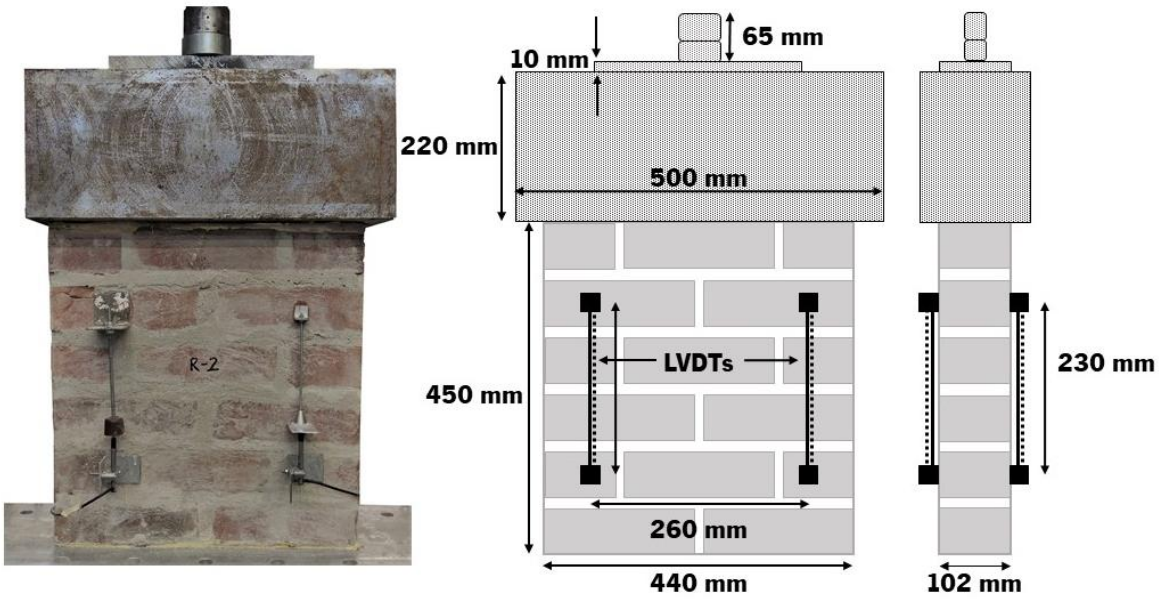

Figure 69: Schematic representation of set-up used for testing compressive strength and E-modulus of masonry specimens

Prior to testing compressive strength, the method of cyclic compression was used on each specimen to obtain the E-modulus. The maximum load equaled approximately one-third of the maximum compressive strength measured from the masonry specimen; an average of 80 kN was selected as one-third of the maximum force for all specimens. Four cycles were used in total, with the duration of each loading and unloading cycle designed to be 120 seconds, with a constant ramp of 60 seconds in between. Finally, the slopes (stress/average strain) of the ascending branches were averaged and used to calculate the E-modulus for each specimen. A total of 3 specimens were used to measure E-modulus, for each mortar type.

5.3.2 Results

5.3.2.1 Compressive strength and E-modulus

Compressive strength and E-modulus obtained from testing masonry wallets with different types of mortars have been shown in Table 34 and Figure 70. The highest compressive strength of masonry is observed in the case of the reference mortar (Ref), followed by the mortar with 50% lime in the binder (L50) and then the mortar with 67% lime in the binder (L67). Since the same type of brick was used for all specimens, the results obtained are expectable, with the strength of masonry increasing slightly in correspondence with the strength of mortars used to construct them (Ref, L50, and L67 respectively). Characteristic values of compressive strength were obtained by dividing the experimentally obtained mean compressive strength of masonry by a factor of 1.2, as specified in EN 1052-1 [17]. The ratio of E-

modulus to compressive strength for masonry was in the range of 600-650 and 725-775 for all mortar types using the average and characteristic values of strength respectively, and no trend was observed in this regard.

Table 34: Compressive strength and E-modulus of masonry wallets

Mortar type	Compressive strength (MPa)		Coefficient of variation (%)	E-modulus (GPa)	Coefficient of variation (%)	E-mod/fc	
	Average	Characteristic				Average	Characteristic
L67 (1:2:9)	6.02	5.01	6.9	3.88	11.3	645	774
L50 (1:1:6)	6.65	5.54	11.8	4.02	12.5	605	726
Ref (1:0:5)	7.18	5.98	6.1	4.46	19.3	621	746

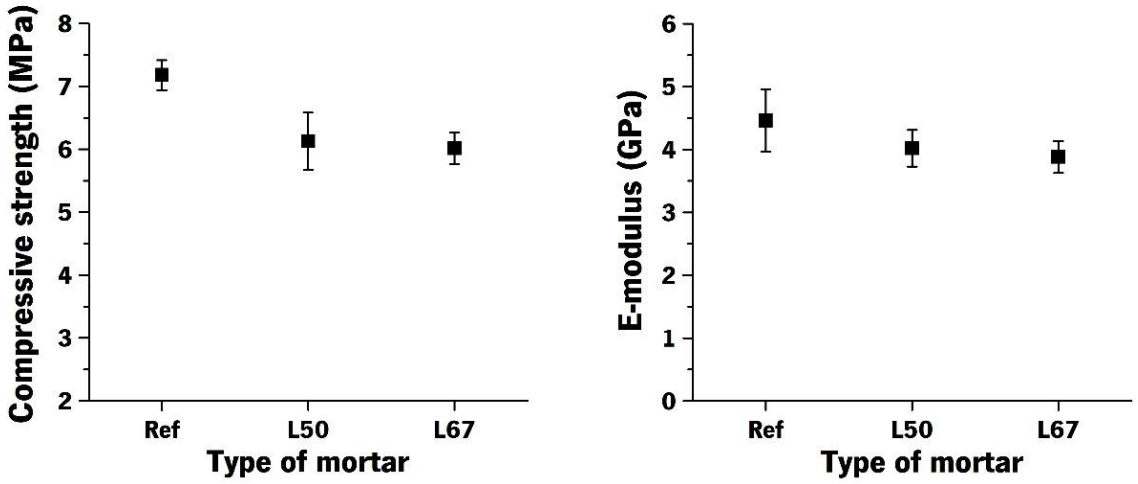

Figure 70: Compressive strength and E-modulus of masonry wallets

5.3.2.2 Compressive strength and E-modulus of masonry with regard to the corresponding properties of mortars

Since the same brick has been used in all the masonry specimens, the difference in behavior should stem from the type of mortar used. Therefore, to assess the impact of the mortar on the strength of masonry, the strength of mortar, measured in standard conditions at 90 days of age (Table 30) was compared with the data of compressive strength of masonry (Table 34):

a) Ref and L50 – At the mortar level, the difference in compressive strength is 17%, while the difference in strength at the masonry level is only 7%.
b) Ref and L67 - At the mortar level, the difference in compressive strength is 58%, while the difference in strength at the masonry level is only 16%.

Based on this analysis of the strength of masonry and mortars, it is confirmed that while the strength of the mortar does influence the strength of masonry, the effect is not linear. It appears that for a small increase in the strength of masonry, the corresponding increase in the strength of mortar has to be significantly greater (Figure 71). This is in alignment with Eurocode 6 [18] in which the compressive strength of mortar affects the compressive strength of masonry by an exponent of 0.3. This means that according to Eurocode 6 [18], the decrease in masonry strength would be 5% and 23% for L50 and L67, respectively when compared with Ref (see Section 5.3.2.3 below).

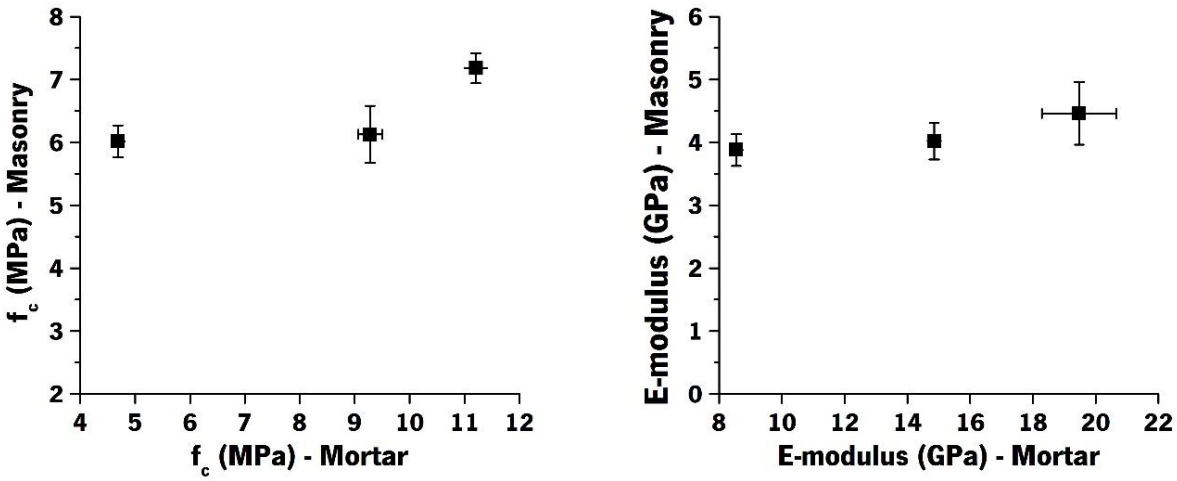

Figure 71: (a) Compressive strength – Masonry v/s mortar; (b) E-modulus – Masonry v/s mortar

In the case of E-modulus measured, a trend similar to that of compressive strength was observed, with values descending in the order of Ref, L50, and L67. Once more, the stiffness of mortar, measured in standard conditions at day 90 (Table 30) was compared with the stiffness of masonry (Table 34):

a) Ref and L50 – At the mortar level, the difference in E-modulus is 24%, while the difference in E-modulus at the masonry level is only 10%.
b) Ref and L67 - At the mortar level, the difference in E-modulus is 56%, while the difference in stiffness at the masonry level is only 13%.

It appears that similar to what was observed in compressive strength, to obtain an increase in the value of the E-modulus of masonry, a mortar with significantly higher stiffness would be required (Figure 71). This is again in alignment with the recommendations of Eurocode 6 [18] in which the E-modulus of masonry is a linear function of the compressive strength masonry (with a multiplication factor of 1000), while the values found here were in the range of 725-775 (Table 34).

5.3.2.3 Recommendations of Eurocode 6: Compressive strength of masonry as a function of the strength of brick and mortar

In terms of optimizing resources of time, finances, and materials, since it is easier to test the compressive strength of brick and mortar individually, compared to testing a masonry specimen, the relationship between these variables was assessed. Eurocode 6 [18] suggests the use of the strength of the individual components of masonry; brick and mortar, to determine the strength of masonry (Equation 21). In such expression, f_k indicates the characteristic compressive strength of masonry, while f_b refers to the normalized mean compressive strength of bricks and f_m refers to the mean compressive strength of the mortar. Since the brick used in this research falls in the category of group 1, the value of K is 0.55 and for general purpose mortars, the values of a and b specified are 0.7 and 0.3. It is also recognized that the values of coefficients K, a, and b will change depending on the type of bricks and mortars used, and indeed different researchers in literature have provided different values for these coefficients [13, 198, 230, 400].

$$f_k = K f_b^{\alpha} f_m^{\beta} \qquad 21$$

The values of compressive strength of mortar and brick were used with Equation 21 to obtain the compressive strength of masonry (Table 35) and compared with experimentally obtained values for characteristic compressive strength of masonry. Table 35 incorporates predicted values based on the coefficients suggested by Eurocode 6, and it may be seen that the predicted values consistently overestimate the compressive strength of masonry, in a 50% to 70% margin. However, if instead of characteristic values of compressive strength, the comparison is performed with mean values of compressive strength of masonry (Table 34), the difference between Eurocode 6 predictions and experimental values reduces to 27 to 41%.

Kaushik *et al.* [13] performed experimental studies on clay brick masonry in compression, with different combinations of strengths of brick and mortar, as discussed in Section 2.4.1, Chapter 2. They suggested values of K, α and β based on regression performed on their results, and also used those values to predict the average experimental strength of masonry from 9 different studies and showed that the predictions worked in an error range of (0 - 40)% for the strength of brick < 26 MPa. Since, the strength of brick used in this research is also less than 26 MPa, those values of K, α and β have been shown in the second set presented in Table 35. It may be noticed that those values consistently underestimated the strength of

masonry obtained in this research, by a margin of 29% to 37%. Even though the predictions were comparable with that of Eurocode 6 because of the underestimation, they were on the safer side.

Table 35: Values of coefficients for Equation 21 and comparison with Eurocode 6

K	α	β	Mortar	Masonry strength (MPa)		Difference (%)
				Predicted	Experimental	
0.55	.7	.3	Eurocode 6 [18]		Experimental (Characteristic value)	
			L67	7.65	5.01	52.5
			L50	9.38	5.54	69.4
			Ref	9.93	5.98	66.0
.55	.7	.3	Eurocode 6 [18]		Experimental (Average value)	
			L67	7.65	6.02	27.0
			L50	9.38	6.65	41.1
			Ref	9.93	7.18	38.3
0.63	.42	.32	Kaushik *et al.* [13]		Experimental (Average value)	
			L67	3.79	6.02	-37.0
			L50	4.72	6.65	-29.0
			Ref	5.02	7.18	-30.2

5.3.2.4 Ductility and vertical strains of masonry specimens

The stress-strain curves of different masonry specimens have been shown in Figure 72. At first glance, it is possible to observe that the maximum stresses tend to decrease from left to right, i.e., in the order of Ref, L50, and L67, as has been discussed in the previous sections. Additionally, it may also be noticed that the strain at peak load tends to increase from left to right in the image, i.e., Ref, L50, and L67. To be able to observe this more clearly, 7 points were chosen for each specimen and averaged for each mortar type. The points corresponded to different percentages of the respective peak stresses - 0%, 33.3%, 50%, 70%, 90%, 100% (peak), 90% (post-peak), 70% (post-peak), and all of their corresponding strains (Figure 73). Additionally, another graph has been presented on the right side of Figure 73, which has vertical strains on the x-axis and on the y-axis values, compressive stresses have been presented, normalized with respect to peak compressive strength of the respective mortars. It is evident that increasing the quantity of lime in the mortar, leads to an increased vertical strain capacity of masonry, prominent from 70% of peak stress onward.

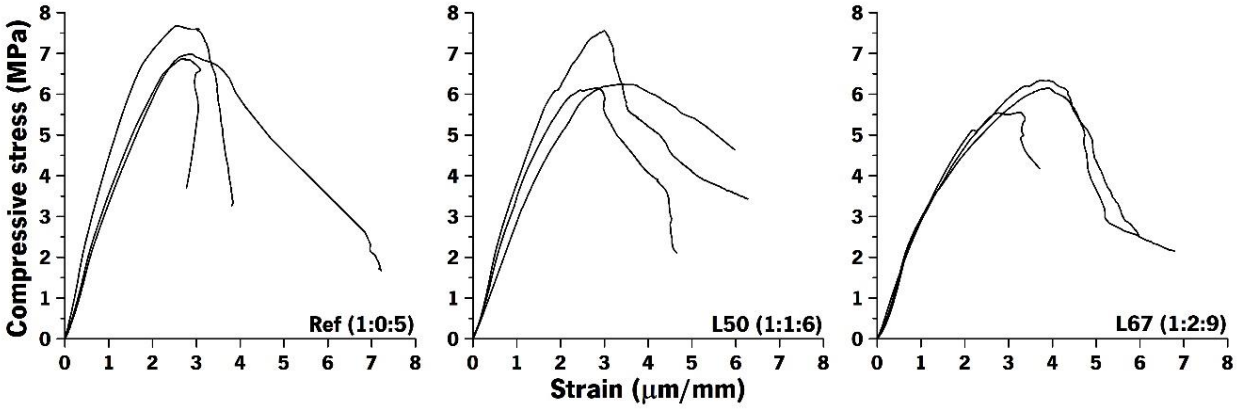

Figure 72: Stress-strain curves for masonry specimens constructed with different mortars

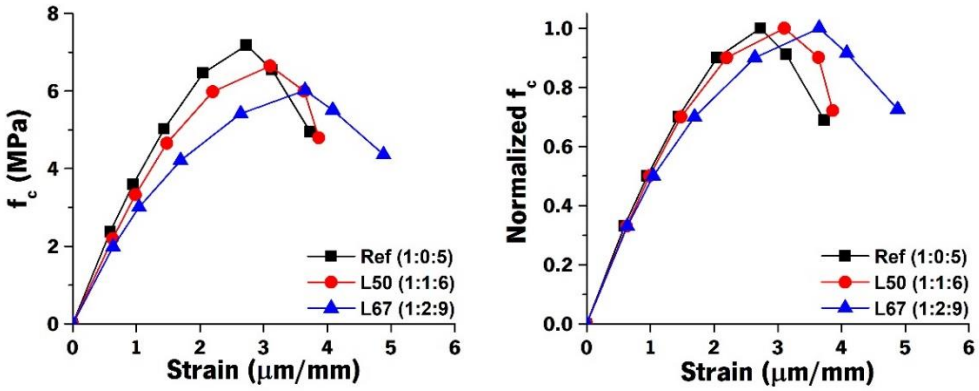

Figure 73: (Left) Averaged stress-strain curves; (Right) Normalized stress – averaged strain curves

To quantitatively compare the strain at peak load (ε_m), the corresponding secant stiffness (K_m) and ductility of different specimens, values were tabulated and have been presented in Table 36. Secant stiffness at any given point of the stress-strain curve is defined as the ratio of stress to strain between that point and the origin (0,0) [401, 402]. Pre-peak ductility is defined here as the ratio of strain, at peak load and 70% of peak load (typically the onset of inelastic strain) based on the experimental data from this research as well as recommendations from the literature [403, 404]. It may be observed that all properties specified in Table 36 exhibit a trend. Average values of strains at peak load, at 70% of the peak load, and pre-peak ductility increase in the order of Ref, L50, and L67. At the same time, values of secant stiffness at both peak load and 70% of the peak load, decrease in the order of Ref, L50, and L67.

Table 36: Peak strain, corresponding secant stiffness, and ductility of different specimens

Mortar	Strain at peak load ε_m $(\frac{\mu m}{mm})$	Strain at 70% peak load ε_y $(\frac{\mu m}{mm})$	Secant stiffness at peak load K_m (GPa)	Secant stiffness at 70% peak load K_y (GPa)	Ductility μ $(\frac{\varepsilon_m}{\varepsilon_y})$
L67 – 1	3.75	1.73	1.69	2.56	2.16

L67 – 2	3.92	1.82	1.57	2.36	2.15
L67 – 3	3.28	1.52	1.69	2.56	2.16
L67 – Avg (CoV%)	3.65 (9.1%)	1.69 (9.2%)	1.65 (4.3%)	2.49 (4.6%)	2.16 (0.2%)
L50 – 1	3.45	1.68	1.81	2.65	2.05
L50 – 2	3.01	1.49	2.51	3.54	2.01
L50 – 3	2.85	1.30	2.16	3.31	2.19
L50 – Avg (CoV%)	3.10 (9.9%)	1.49 (12.7%)	2.16 (16.2%)	3.16 (14.6%)	2.08 (4.5%)
Ref – 1	2.91	1.59	2.40	3.08	1.83
Ref – 2	2.74	1.46	2.51	3.29	1.88
Ref – 3	2.53	1.27	3.03	4.24	2.00
Ref – Avg (CoV%)	2.73 (6.9%)	1.44 (11.5%)	2.65 (12.8%)	3.54 (17.5%)	1.90 (4.5%)

In Figure 74, the vertical strain corresponding to maximum compressive strength has been plotted against maximum compressive strength of masonry wallets, exhibiting absolute values as well as relative values, normalized with respect to the strength peak deformation/vertical strain of the reference mix. The strength of L50 is 7.4% lower and its strain is 13.7% higher than Ref. In the case of L67, the strength is 16.2% lower, while the strain is 33.7% higher than Ref. Furthermore, L67 has 9.5% lower strength and 17.6% higher strain compared to L50. The commonality in all these quantities is that for every 1% decrease in strength of the masonry wallets, the strains corresponding to peak strength appear to increase by approximately 2%.

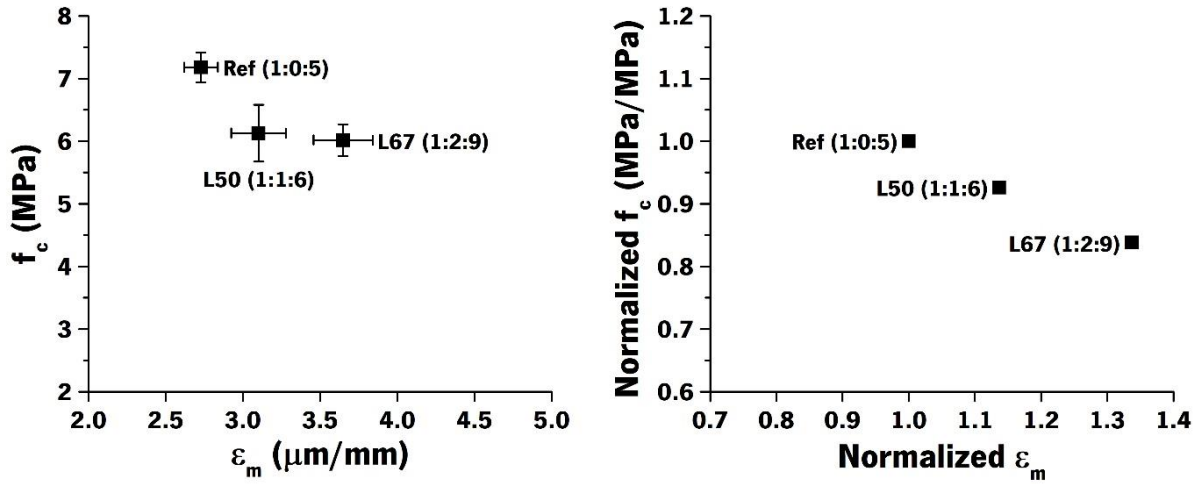

Figure 74: Vertical strain at peak stress v/s maximum compressive strength of masonry (Absolute and normalized values)

Vertical strains obtained in the masonry wallets (corresponding to peak, and 70% peak loads) have also been plotted with respect to the type of mortar used (Figure 75). It is clear, that at both peak and 70% peak loads, the vertical strains in the masonry wallets reduces, as the quantity of lime in the binder increases. The mortar L50 results in 14% and 7% higher strain masonry, with respect to Ref at peak and

yield compressive strength, respectively. While the mortar L67 results in 34% and 22% higher strain in masonry, compared to Ref, at maximum and yield compressive strength, respectively. Values of pre-peak ductility of masonry (Table 36), follow a trend similar to that of strain corresponding to peak or yield load, i.e., they increase as the quantity of lime in the binder increases. L50 results in 9% higher ductility in masonry, compared to Ref. While L67 results in 13% higher ductility in masonry compared to Ref and a 3% increase compared to L50.

From the data presented in this section, it may be tempting to conclude that using a mortar with lower strength is the prominent factor contributing to the increase in deformation capacity of masonry. It is important to point out that in this research post-peak response is not addressed, and mortars with lime in them (L50 and L67) also have lower strength than the reference cement mortar (Ref). And so to separate those two factors – the presence of lime in the binder and compressive strength of the mortar, the work done by Kaushik *et al.* [13] has also been taken into account. In their work, two mortars with composition 2:1:9 (Cement: Lime: Sand) and 1:0:6 (Cement: Sand) are compared at the mortar level, with the former being stronger. And while the stronger mortar 2:1:9, leads to great strength at the masonry level, it also leads to greater ductility, compared to the cement mortar 1:0:6. Therefore, the work of Kaushik *et al.* [13], along with the results presented here, seems to indicate a slightly larger deformation capacity in the masonry with lime. Yet, this is not evident when E-modulus is compared with the compressive strength in the present research, as similar values have been found for the different compositions of mortars.

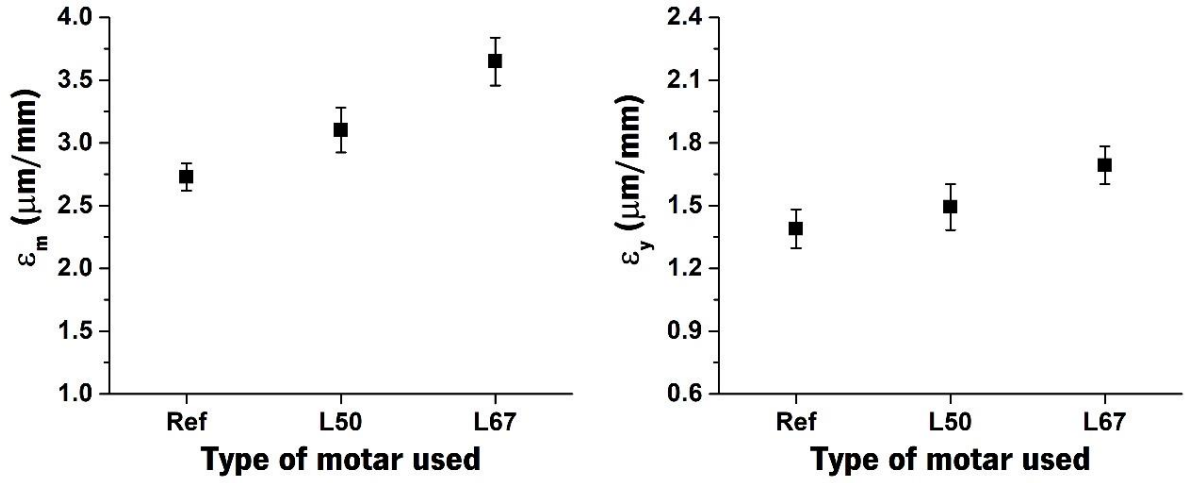

Figure 75: Vertical strain (corresponding to peak and yield stresses) v/s strength of mortars used

Furthermore, Kaushik *et al.* [13], proposed an expression, to estimate the strain in masonry corresponding to peak stress (ε_m) using the strength (f) and E-modulus ($E_{masonry}$) of masonry, as well as the strength of mortar (f_m) used, as shown in equation 22.

$$\varepsilon_m = \frac{0.27f}{f_m^{0.25} E_{masonry}^{0.7}} \quad 22$$

This is useful to estimate the strain at peak load, accounting for the type of mortar used in masonry, and so equation 22 was adopted to estimate the peak strain of masonry and was compared with experimental data obtained in this research, as has been shown in Table 37. Average values of strength and stiffness were used for each type of mortar, and it was found that the equation could predict well the experimental values of the strain of masonry at peak load, within a 10% margin.

Table 37: Estimated (equation 22) and experimental values of strain at peak stress

Mortar type	f_c – Mortar (MPa)	f – Masonry (MPa)	E-modulus – Masonry (GPa)	Strain at peak load ε_m $(\frac{mm}{mm})$		
				Predicted ($\times 10^{-3}$)	Experimental($\times 10^{-3}$)	Diff (%)
L67	4.69	6.02	3.88	3.649	3.394	-7.0
L50	9.28	6.65	4.02	3.102	3.084	-0.6
Ref	11.21	7.18	4.46	2.728	2.955	8.3

5.4 Flexural strength (Parallel and perpendicular to bed joints)

5.4.1 Methodology

Flexural strength for masonry was tested according to the recommendations of EN 1052-2 [270], in both directions; parallel to the bed joints, referred to as 'parallel', and perpendicular to the bed joints, referred to as 'perpendicular'. A hydraulic actuator with a capacity of 300 kN was used to perform the test using displacement control at a speed of 3 μm/s. In both cases, parallel and perpendicular, there were 2 LVDTs used to measure the out-of-plane deformation and were set up on either side of each specimen (Figure 76).

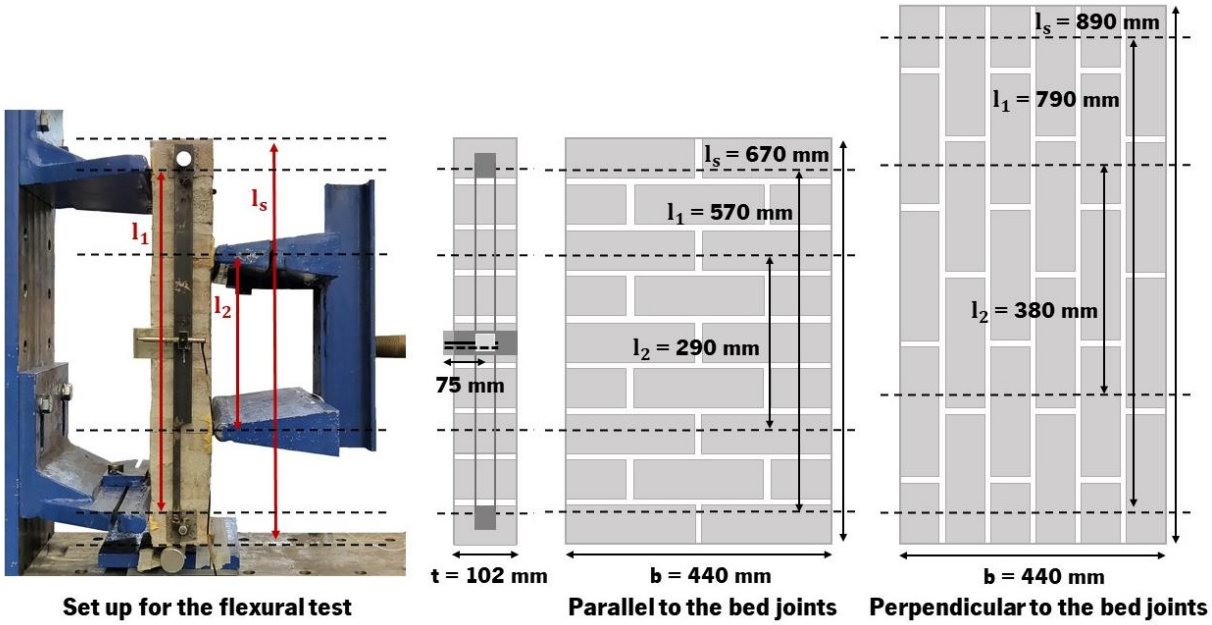

Figure 76: Set up used for the flexural test of masonry (Parallel to the bed joints and perpendicular to the bed joints)

For the parallel case, the specimens were single leaf and had 9 courses of bricks, with 2 bricks in each course. The height of each specimen was 670 mm and the width was 440 mm (Figure 76). EN1052-2:1999 [270] provides recommendations for the length of the specimen in the direction of the span (l_s), the spacing of the supports (l_1), and the spacing of the inner bearings (l_2) for the application of load. The values used for the parallel case were as follows; l_s - 670 mm, l_1 - 570 mm, l_2 - 290 mm. For the perpendicular case, the specimens were single leaf as well, but had 6 courses of bricks, with 4 bricks in each course. The height/length of each specimen was 890 mm and the width was 440 mm (Figure 76). For the perpendicular case, l_s was 890 mm, l_1 was 790 mm and l_2 was 380 mm.

5.4.2 Results of flexural strength test

The values of flexural strength presented have been calculated according to the recommendations of EN 1052-2 [270]. However, the equation was modified to consider the self-weight of the specimens. The factor of $0.5\rho g l_s$ corresponds to stresses at the center of the specimen due to self-weight where ρ denotes density [194]. The value of stresses due to self-weight was found to be 0.006 and 0.008 MPa for specimens tested in the parallel and perpendicular directions respectively, which are rather low. The final equation used has been shown in Equation 23. $F_{i,max}$ refers to the maximum recorded load in each test. The symbols used in equation 23 denote the following; l_s is the length of the specimen/span, l_1 is the length of the outer bearings, l_2 – is the length of the inner bearings, b is the width of the masonry specimen, and t is the thickness of the specimen.

$$f_f = \frac{3F_{i,max}(l_1 - l_2)}{2bt^2} - 0.5\rho g l_s \quad 23$$

The results of the flexural strength tests have been presented for the different mortars in Table 38, in the directions parallel and perpendicular to the bed joint. The first observation is that the values of flexural strength are higher in the perpendicular direction compared to the parallel direction, which is common and has been reported in the literature [275, 405]. The force-displacement responses for different masonry specimens have also been shown in Figure 77 and Figure 78, corresponding to flexural loading in parallel and perpendicular directions.

It is possible to observe that the strength of the mortar influences the flexural strength of masonry in both directions – parallel and perpendicular, to bed joints. The mix L67 with the lowest strength at the mortar level, also results in the lowest flexural strength in masonry, in both parallel and perpendicular directions. Similarly, the two mixes L50 and Ref that have similar strength at the mortar level, appear to result in similar values of flexural strength in masonry as well. An increase in flexural strength of masonry due to the use of mortar with higher compressive strength has been observed in the literature as well [406]. With regard to the presence of lime in the binder, it wasn't possible to draw any conclusion, since, in the parallel direction, L50 has a slightly higher value, while in the perpendicular direction Ref has a slightly higher value.

Table 38: Values of flexural strength of masonry in the directions parallel and perpendicular to the bed joints

Mortar type	Parallel (MPa)	(CoV %)	Perpendicular (MPa)	(CoV %)
L67	0.10	18.4	0.78	5.7
L50	0.23	3.8	1.11	3.8
Ref	0.19	8.5	1.12	14.0

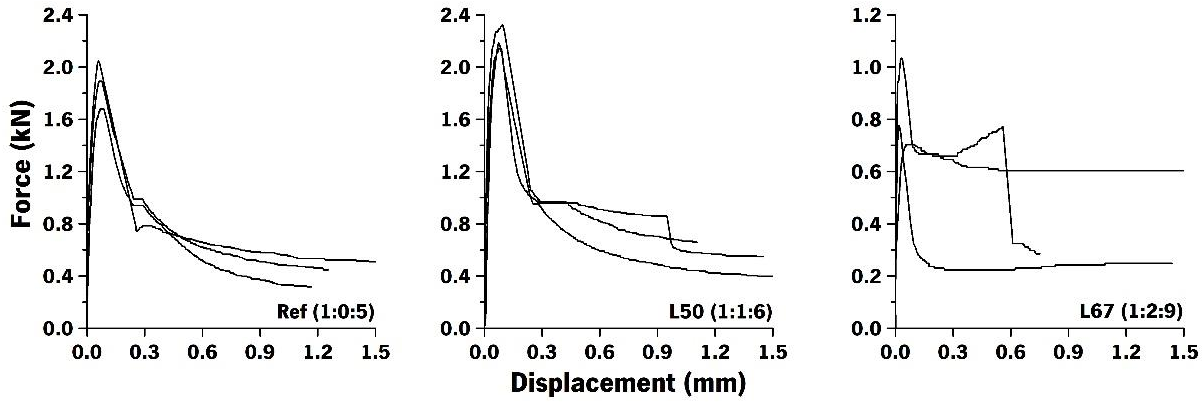

Figure 77: Force-displacement curves for masonry specimens with different mortars, parallel to bed joints (Note the different vertical scales in the graphs)

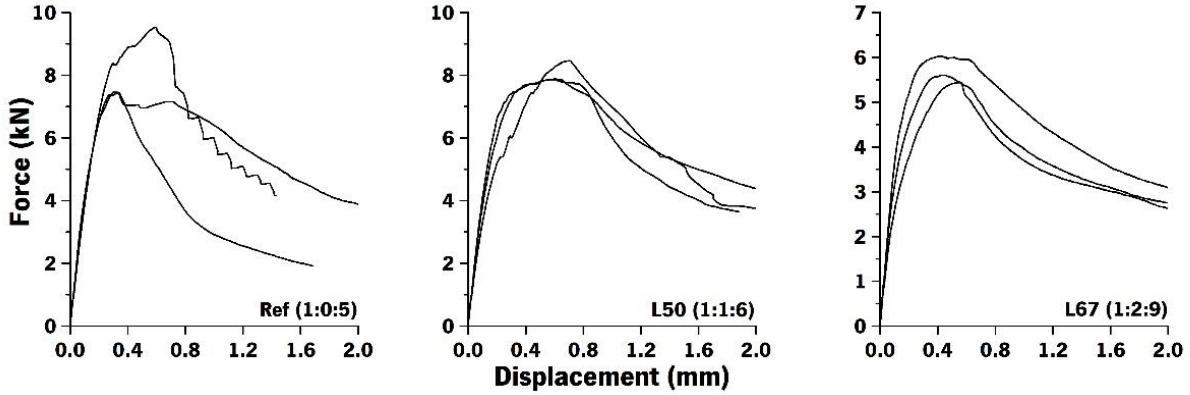

Figure 78: Force-displacement curves for masonry specimens with different mortars, perpendicular to bed joints (Note the different vertical scales in the graphs)

Eurocode 6 [18] recommends values of characteristic flexural strength of masonry, based on the type of unit and strength of mortar. Based on the units and mortars used in this research, the category of the unit would be clay brick, and the category of mortar would be ≥ 5 MPa for Ref and L50 and < 5 MPa for L67 (Table 30). Furthermore, data obtained in this research (Table 38) for flexural strength has been indicated for average values. To make a comparison with the recommendation of Eurocode 6, characteristic values would have to be used, and therefore, based on the recommendations of EN 1052-2 [270], the experimentally obtained values were divided by a factor of 1.5 (Table 39). Note that the values from standard mortars at 90 days are used to follow the prescriptive values of Eurocode 6, i.e. with no calculation. However, if the values from in situ mortars at 90 days were to be used, all mortars fall in the category of ≥ 5 MPa.

According to Eurocode 6 [18], flexural strength in the direction parallel to bed joints should be considered as 0.1 MPa, regardless of the strength of the mortar. It may be seen that L67 mortar leads to a flexural

strength of less than 0.1 MPa, whereas for L50 and Ref, the values obtained are higher. For flexural strength in the perpendicular direction, all mortars lead to values much higher than the recommendations of the code.

Table 39: Characteristic values of flexural strength and recommendations of Eurocode 6

Mortar	Compressive strength of mortar (MPa)		Flexural strength–parallel (MPa)		Flexural strength–perpendicular (MPa)	
type	Experimental	In Eurocode 6	Experimental	Eurocode 6	Experimental	Eurocode 6
L67	4.69	< 5	0.06	0.1	0.52	0.2
L50	9.28	≥ 5	0.15	0.1	0.74	0.4
Ref	11.21	≥ 5	0.13	0.1	0.75	0.4

5.4.3 Tensile bond strength derived from the experimentally obtained value of flexural strength of masonry (parallel to bed joint)

While the flexural strength of masonry in the perpendicular direction depends on factors such as fracture energy of the head joints as well as bricks, cohesion and friction between bed joints and bricks, the flexural strength of masonry in a direction parallel to the bed joints occurs, in general, primarily due to the failure of tensile bond strength between brick and masonry [285, 407]. The tensile (flexural) bond strength of masonry may also be measured using a bond wrench test [281], which was not adopted in this research. However, it is possible to estimate the value of tensile bond strength from the flexural strength of masonry in the parallel direction.

Lourenco *et al.* [285] suggested treating the masonry specimen as a beam composed of a discrete number of joints, each of which may possess a different tensile capacity. Since masonry is not a homogenous material and has inherently high variability, any of the joints subjected to pure flexure in the four-point bending test could fail first, consequently leading to the failure of masonry as a whole [275]. Therefore, it is possible to relate the flexural tensile strength of a joint, the number of joints, and the flexural capacity of masonry (treated as a beam) based on the Weibull weakest link theory (Equation 24) [194, 285]. The values of coefficients k_1 and k_2 are dependent on the number of joints that are subject to pure flexure in the masonry specimen and were suggested by Mosteller *et al.* [284].

$$\mathrm{f}_{\mathrm{f,beam}} = \mathrm{f}_{\mathrm{f,joint}} - \mathrm{k}_1 \times \mathrm{stdev}_{\mathrm{f,joint}}$$
$$\mathrm{stdev}_{\mathrm{f,beam}} = \mathrm{k}_2 \times \mathrm{stdev}_{\mathrm{f,joint}} \qquad 24$$

In this research, the flexural test on masonry performed parallel to the bed joints, subjected 4 joints to pure flexure (Figure 76). Therefore, k_1 would be 1.03 and k_2 would be 0.696. Therefore, the flexural

tensile capacity of masonry with different mortars could be estimated along with the respective values of standard deviation and this data has been presented in Table 40. It may be noticed that the flexural tensile strength of a joint is always higher than the flexural strength of masonry and that the values are almost the same for Ref and L50 but lower for L67. As stated before, an increase in the strength of the mortar appears to contribute to increasing the tensile bond strength of masonry, similar to what has been observed in the literature as well [195].

Table 40: Values of flexural tensile bond strength of joint estimated from flexural strength measured parallel to bed joints

Mortar type	Parallel (MPa) $f_{f,beam}$	Standard deviation (MPa)	Tensile strength of joint (MPa)	Standard deviation (MPa)	(CoV %)
L67	0.10	0.018	0.12	0.025	20.8
L50	0.23	0.008	0.24	0.012	5.1
Ref	0.19	0.016	0.22	0.023	10.8

5.5 Shear bond strength

5.5.1 Methodology

Shear bond strength was measured based on the recommendations of EN 1052-3 [290]. For each type of mortar 9 masonry specimens (triplet) were tested, and therefore 27 specimens in total were considered (Figure 79). Each type of mortar was subjected to three levels of perpendicular pre-compression: 0.2 MPa, 0.6 MPa, and 1 MPa, three specimens being tested for each case. A manually operated hydraulic pump (supplied by Inegi, Portugal), with a capacity of 100 kN was used to apply a constant pre-compressive load, with an average maximum variation of ≤ 0.9 kN across different tests. The shearing load was applied using another actuator with a capacity of 200 kN and an acquisition frequency of 4 Hz, using displacement control at a speed of 3 μm/s. Two LVDTs were used, one across each mortar joint, on either side of the specimen (front and back), to measure the relative slip between the bricks and mortar joints (Figure 79).

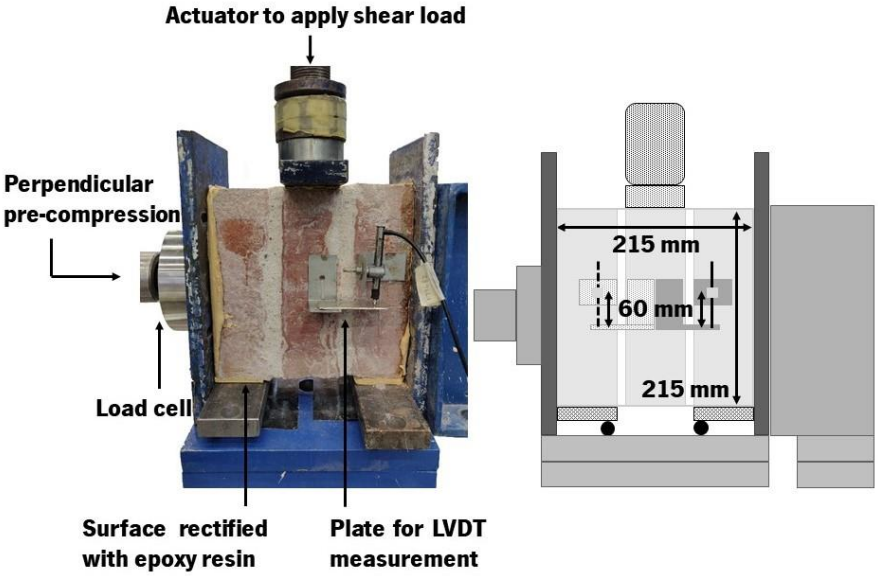

Figure 79: Setup for testing shear bond strength of masonry

5.5.2 Results of shear bond strength

Since each specimen tested in shear had two LVDTs monitoring the relative slip between the bricks, Figure 80 shows shear stress v/s relative slip, measured by both LVDTs, for each of the three mortars. For the illustration, one specimen has been chosen from each pre-compression level of each mortar type.

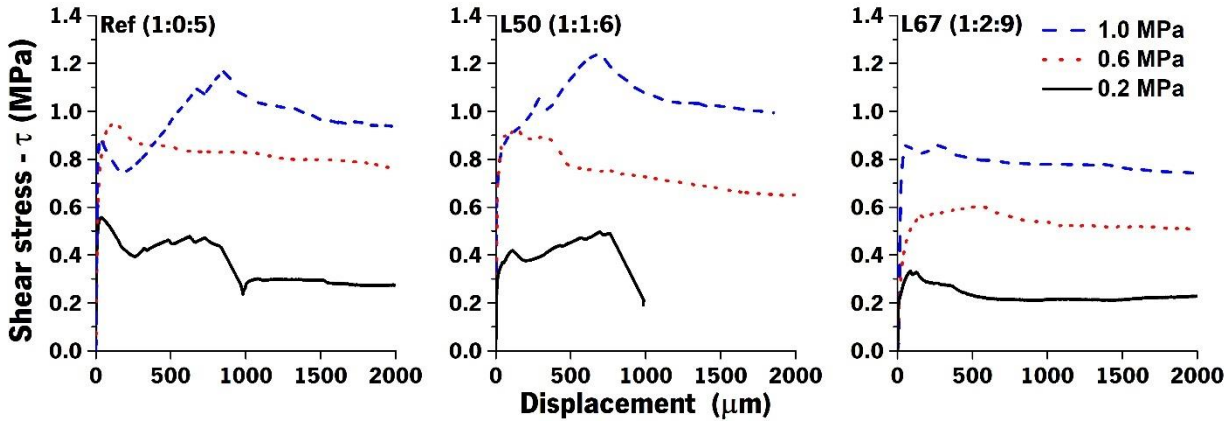

Figure 80: Shear stress versus relative slip for different masonry triplets

In all the specimens, as expected, an increase in perpendicular pre-compression tends to increase the maximum shear capacity. From Figure 80, it may also be observed that while specimens with mortar L67 exhibit lower values of shear stress, masonry with mortars Ref and L50 exhibit relatively similar values of shear stress for each level of pre-compression. To compare quantitative values, Table 41 presents the maximum shear stress with coefficients of variation for each type of mortar at three levels of

vertical/normal pre-compression (σ); 0.2 MPa, 0.6 MPa, and 1MPa. Each value of maximum shear stress (τ) presented is an average of three different specimens, for the corresponding level of pre-compression.

Table 41: Values of maximum shear stress obtained for masonry specimens for varying levels of vertical pre-compression

Mortar/Shear	Vertical pre-compression/Normal stress - σ (MPa)					
stress – τ (MPa)	0.2	(CoV %)	0.6	(CoV %)	1.0	(CoV %)
L67	0.37	9.8	0.73	15.9	0.83	4.0
L50	0.43	14.7	0.87	7.3	1.12	8.9
Ref	0.54	8.2	0.89	7.2	1.11	7.5

To obtain values of parameters like the coefficient of friction and cohesion, normal stress (or vertical pre-compression) was plotted versus shear stress for each mortar type (Figure 81).

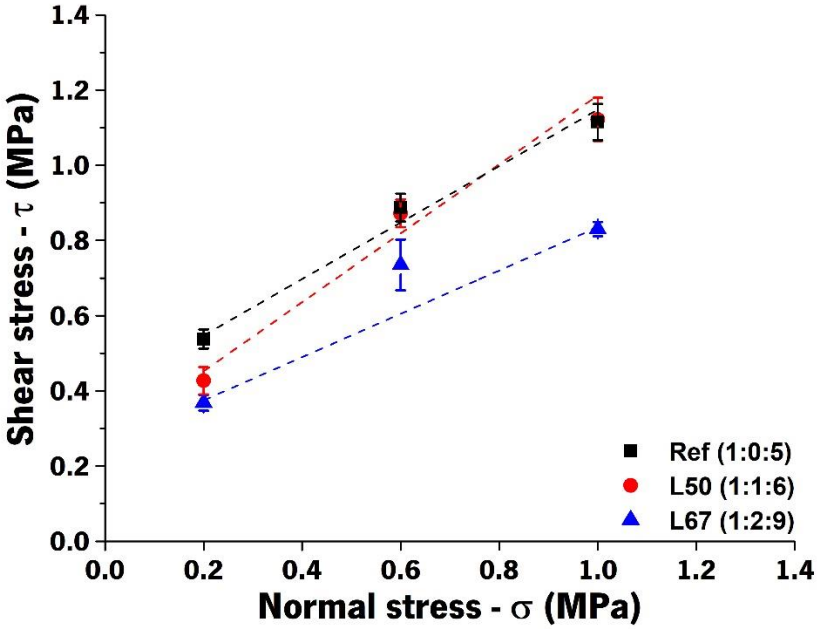

Figure 81: Normal stress versus shear stress for masonry triplets with different mortars

Additionally, to ensure that the Mohr-Coulomb criterion could be adopted, the linearity of the relationship between normal stress and shear stress had to be confirmed, for each mortar type. Linear regression was performed and R^2 values were found to be 0.99, 0.97, and 0.90 for the mortars Ref, L50, and L67 respectively, thus making it acceptable to use the Mohr-coulomb equation. Tan ϕ or refers to the coefficient of friction, c refers to cohesion or initial shear stress, (τ) denotes shear stress, and (σ) normal stress or vertical pre-compression. The values of the obtained parameters for each of the mortar types have been displayed in Table 42.

Characteristic values, of shear strength (f_{vko}) and coefficient of friction (tan ϕ) are calculated based on the suggestion of EN 1052-3 [290], multiplying the mean values by a factor of 0.8 in both cases. Eurocode 6 [18] recommends values of cohesion or initial values of shear strength (f_{vko}) based on the compressive strength of the mortar class, and type of unit. In Eurocode 6 [18], the recommended value of cohesion for mortars with strength 2.5 to 9 MPa, (L67 and L50) is 0.2 MPa, and for mortars with strength 10 to 20 MPa (Ref) is 0.3 MPa. As may be observed from Table 42, all mortars have values of cohesion greater than recommended by Eurocode 6 [18].

Table 42: Joint characteristics for different types of mortars used with brick masonry

Type of mortar	Cohesion (MPa) - c	Characteristic shear strength (MPa) - f_{vko}	Angle of friction (ϕ)	Coefficient of friction (tan ϕ)	Characteristic coefficient of friction (tan ϕ)
L67	0.30	0.24	30.0	0.58	0.46
L50	0.29	0.23	41.0	0.87	0.69
Ref	0.41	0.33	35.8	0.72	0.58

Regarding cohesion, a specific trend could not be confirmed by the data obtained in this research (Table 42), because while the value of cohesion of L50 is lower than that of Ref, surprisingly it is also lower than that of L67. Further, the coefficient of friction of L50 is higher than both Ref and L67. It is suggested in the literature [196, 287, 296], that apart from the type of mortar used, cohesion and internal friction are dependent on other factors such as surface roughness, water absorption, and mechanical strength of the bricks used, and therefore these factors merit further experimental investigation. In terms of maximum shear stress capacity at different pre-compression levels, L50 consistently exhibits higher values compared to the mix L67 (Table 41). Ref exhibits slightly higher values compared to L50 at levels of pre-compression of 0.2 MPa and 0.6 MPa, and almost the same at 1 MPa. And since at the mortar level, L50 has a much higher strength than L67 and in turn, Ref has a slightly higher compressive strength than L50, it appears, therefore, that the compressive strength of the mortar may be an indicator of maximum shear bond stress in masonry. To illustrate this graphically, Figure 82 shows the maximum shear stress of masonry as a function of the compressive strength of the mortar used. This relationship may be confirmed from literature as well, where using a mortar with higher compressive strength leads to higher shear bond strength in triplet specimens [195].

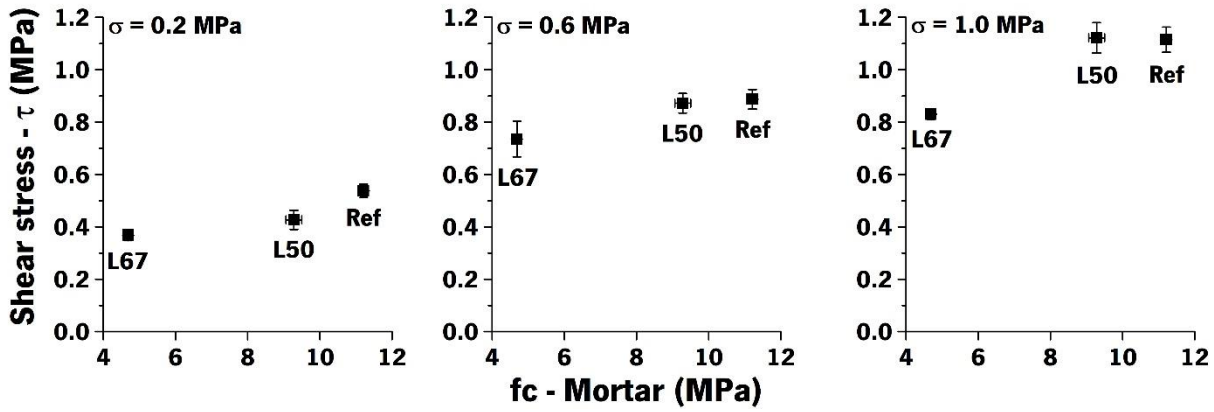

Figure 82: Maximum shear stress of masonry triplets as a function of compressive strength of mortar

From the data presented in Table 42, it may be observed that L67 and L50 have similar values of cohesion, which is lower than the cohesion of Ref. This is unexpected since the compressive strength of the mortar is often used as an indicator of cohesion, for example in Eurocode 6 [18]. Since the compressive strength (in standard conditions) of mortars L50 and Ref are in the same range (9.28 and 11.21 MPa), and L67 has a lower compressive strength (4.69 MPa), it would be expected that cohesion of L50 and Ref would be in the same range and that of L67 would be lower. From the linear regression performed on the different mortars (Figure 81), it appears that for L67, maximum shear stress at 1 MPa is less than what was expected. However, no anomalies were observed during the experiments. Therefore, to analyze the experimental data from a different perspective, a single linear regression was performed (Figure 83) using all the data from Table 41 except for one data point, shear stress of L67 at 1 MPa. The r-squared value obtained was 0.94, and the coefficient of friction obtained was 0.85. From this, values of cohesion were obtained for each mortar and found to be 0.21 MPa, 0.30 MPa, and 0.34 MPa for L67, L50, and Ref respectively (Table 43). This trend aligns with the values of compressive strength of the mortars as well as the flexural strength of masonry (Table 38).

Table 43: Values of cohesion obtained for different types of mortars, using the same coefficient of friction for all

Type of mortar	Cohesion (MPa) - c	Characteristic shear strength (MPa) - f_{vko}	Angle of friction (ϕ)	Coefficient of friction (tan ϕ)
L67	0.21	0.17		
L50	0.30	0.24	40.4	0.85
Ref	0.34	0.27		

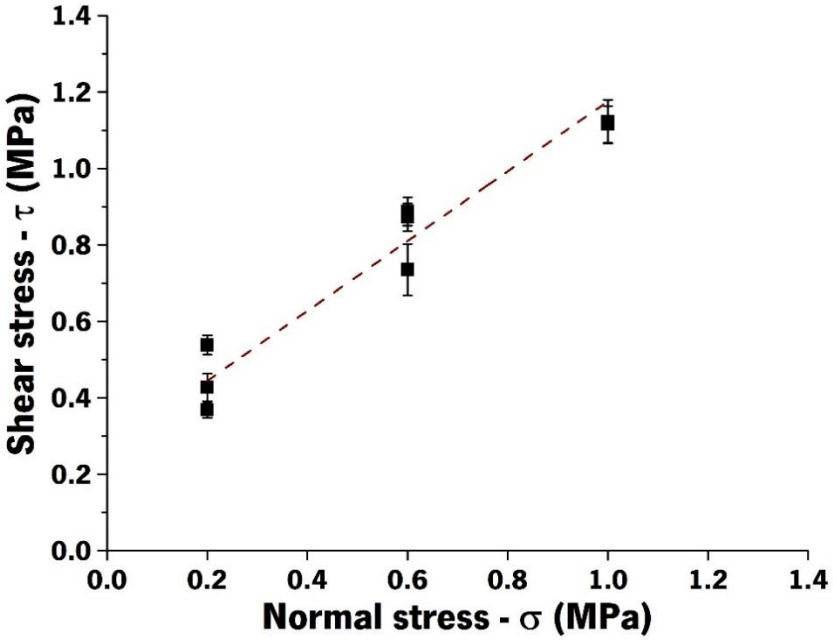

Figure 83: Normal stress versus shear stress for masonry triplets with different mortars, common linear regression

5.6 In-plane cyclic loading

5.6.1 Methodology

Tests of in-plane cyclic loading were carried out on specimens of size 900×900×102 mm^3 (Figure 84). The specimens were single leaf, 4-bricks wide, and 12 courses tall, and were tested approximately 6 months after construction. The top and bottom surfaces of the specimens were rectified to ensure even load distribution. This was done using rapid hardening cement (Mapei Lampocem [408]). Each specimen was lifted using two wide straps and a crane and lowered down onto a layer of freshly mixed cement. After a few hours, the top of the specimen was also rectified using the same rapid hardening cement, a beam, and a level. Once this process was completed, each specimen would be transported across the laboratory using the crane, to the frame and prepared for the test, the setup of which has been schematically illustrated in Figure 85. The bottom course on either side of each specimen was glued to steel angles (60 mm×300 mm×20 mm, height, width, thickness) using polyester resin. The steel angles were tied to each other using two steel rods (⌀ 10 mm) at the front and back of the specimen and were also bolted down to the base of the steel frame in which the test took place. This was done, to ensure that the specimen did not move horizontally at the bottom. The vertical pre-compressive load applied on the specimen was 72 kN, corresponding to a stress of 0.78 MPa. This level of pre-compression was also found acceptable since it accounted for about 12% of the compressive strength of masonry and was also found to be in the range of values usually used in the literature [104, 409, 410]. This was distributed

along the length of the specimen using steel beams. The actuator in the vertical direction was anchored to the solid frame on which the set-up rested, using two steel rods, to center the vertical load on the specimen as it moved horizontally. The horizontal displacements were imposed by an actuator (capacity of 200 kN, sensitivity of 2mV/V), which was placed at a height of 600 mm from the base of the specimen, and connected through a hinge to a rigid vertical beam, connecting to the rigid horizontal beams on the top of the specimen. This height, combined with the vertical load, was adopted to ensure shear failure. The LVDTs used on the specimens to measure deformation have been illustrated in the schematic set up in Figure 85, marked L1 to L7. LVDT 1 on the top was used to measure the resulting drift in the specimen, while LVDT 2 was placed horizontally in the bottom of the specimens, second layer of bricks from the last to monitor the possible opening of flexural cracks. The other 5 LVDTs (L3-L7) were used on the back of the specimen, to obtain more information of the deformations, wherever required.

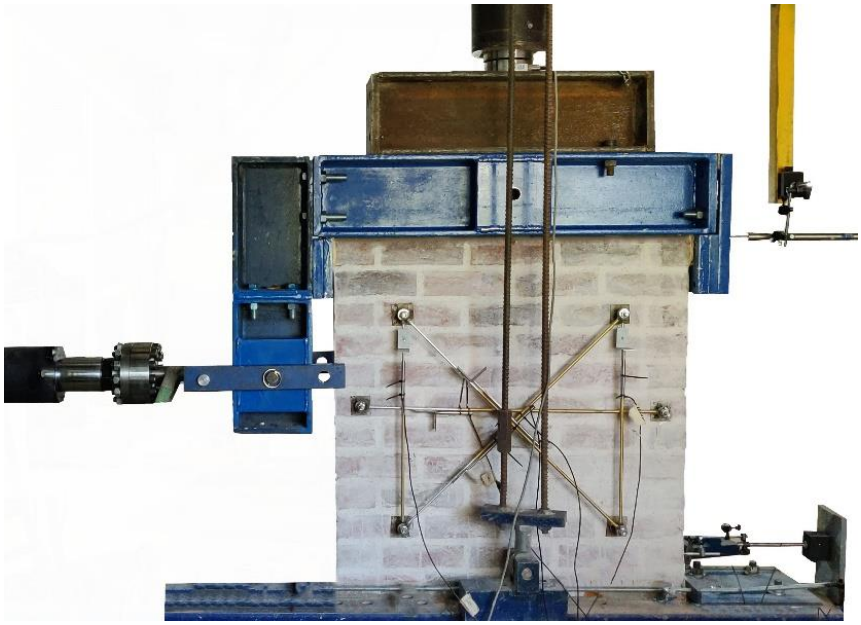

Figure 84: Setup used for in-plane cyclic loading of masonry specimens (Image from the laboratory, UMinho)

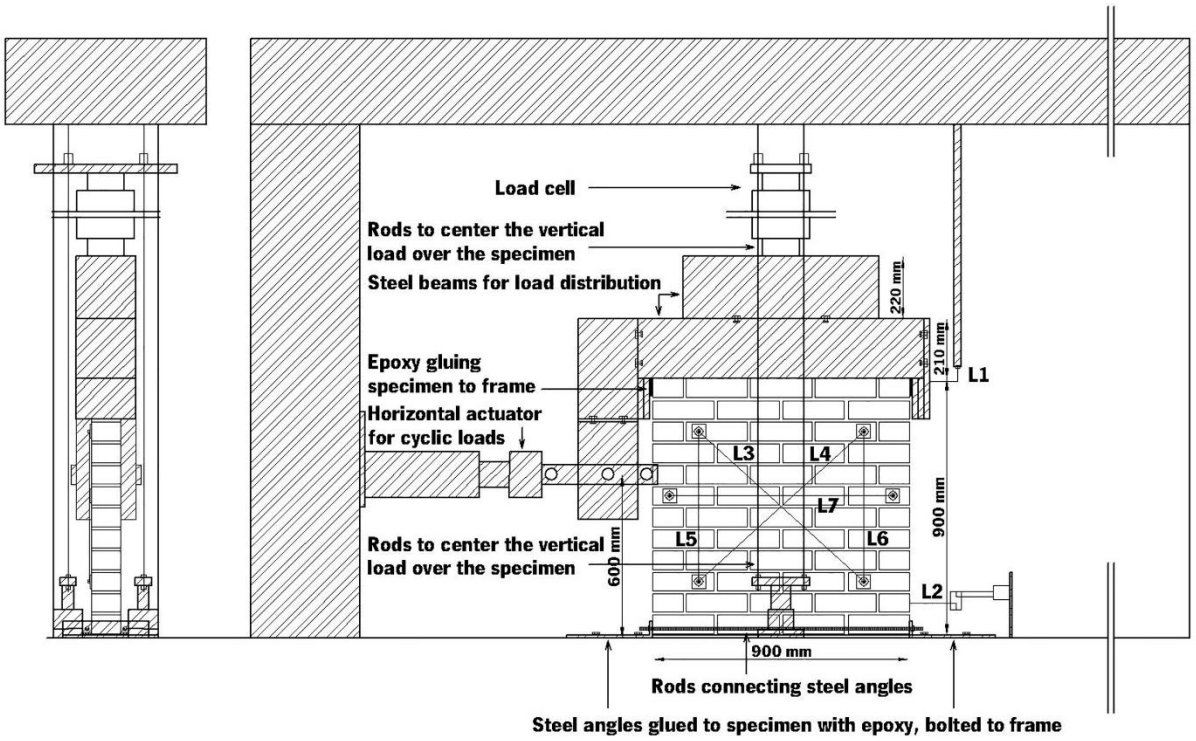

Figure 85: Illustration of setup used for in-plane cyclic loading of masonry specimens

The front of the specimen was painted with white paint and black specks to perform DIC (Digital Image Correlation). The camera used to perform DIC was Cannon EOS, M50, and was placed at a horizontal distance of approximately 1.3 m from the specimen. The settings used were aperture F 3.5, 1/40 shutter speed, and shots were taken at an interval of 5 seconds. The open-source software used to process DIC results was GOM Correlate. It may be noted that in this work, DIC as a method has only been used as a qualitative aid, to indicate the principal strains which represent the cracks in the masonry specimens.

The horizontal displacements were imposed in a ramp format through the lever, according to the recommendations of FEMA-461 [369]. The amplitude for each step was 1.4 times the value in the previous step. The starting drift was 0.05% and the maximum drift considered was 1.5%, if the failure was not reached before this level. For each amplitude, the cycle was repeated three times (Table 44, Figure 86). The speed was adapted along the test for different amplitudes, such that dynamic effects were negligible and the duration of the test was not excessive.

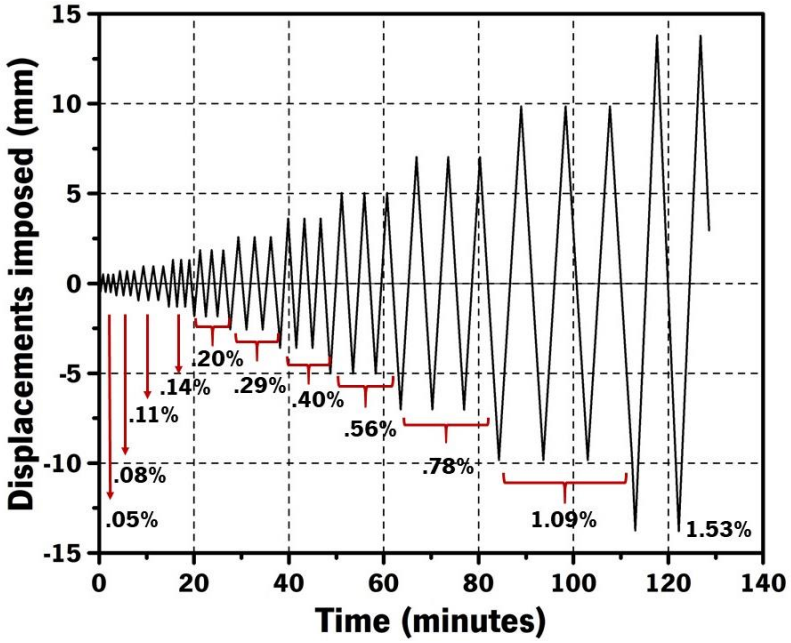

Figure 86: Horizontal deformations imposed for in-plane cyclic loading test, labelled with drift (%)

Table 44: Deformations imposed in the horizontal direction on specimens for in-plane cyclic loading

Drift (%)	0.05	0.08	0.11	0.14	0.20	0.29	0.40	0.56	0.78	1.09	1.53
Amplitude (mm)	0.49	0.68	0.95	1.30	1.84	2.57	3.59	5.02	7.02	9.83	13.77
Speed (mm/s)	0.03	0.03	0.03	0.05	0.05	0.05	0.07	0.07	0.07	0.07	0.1

5.6.2 Results

5.6.2.1 Failure modes and hysteresis diagrams

Almost all specimens tested failed by a shear mechanism, which is characterized by the formation of diagonal cracks. Typically, this happens when the principal stresses generated due to a combination of horizontal and vertical loads, exceed the tensile strength of masonry [296]. The lateral force v/s lateral displacement (LVDT 1) diagrams for all nine specimens that were tested have been shown in Figure 87. It may be observed that the range of lateral displacements is similar in all the specimens except for Ref-3. Even the shape of the hysteresis diagram is slightly different for this specimen. This was because in Ref-3 failure occurred due to horizontal sliding in the two bottom-most bed joints (Figure 88). After failure, the test was allowed to continue for longer, until the values of measured displacements clearly exceeded the range of what was observed in other specimens.

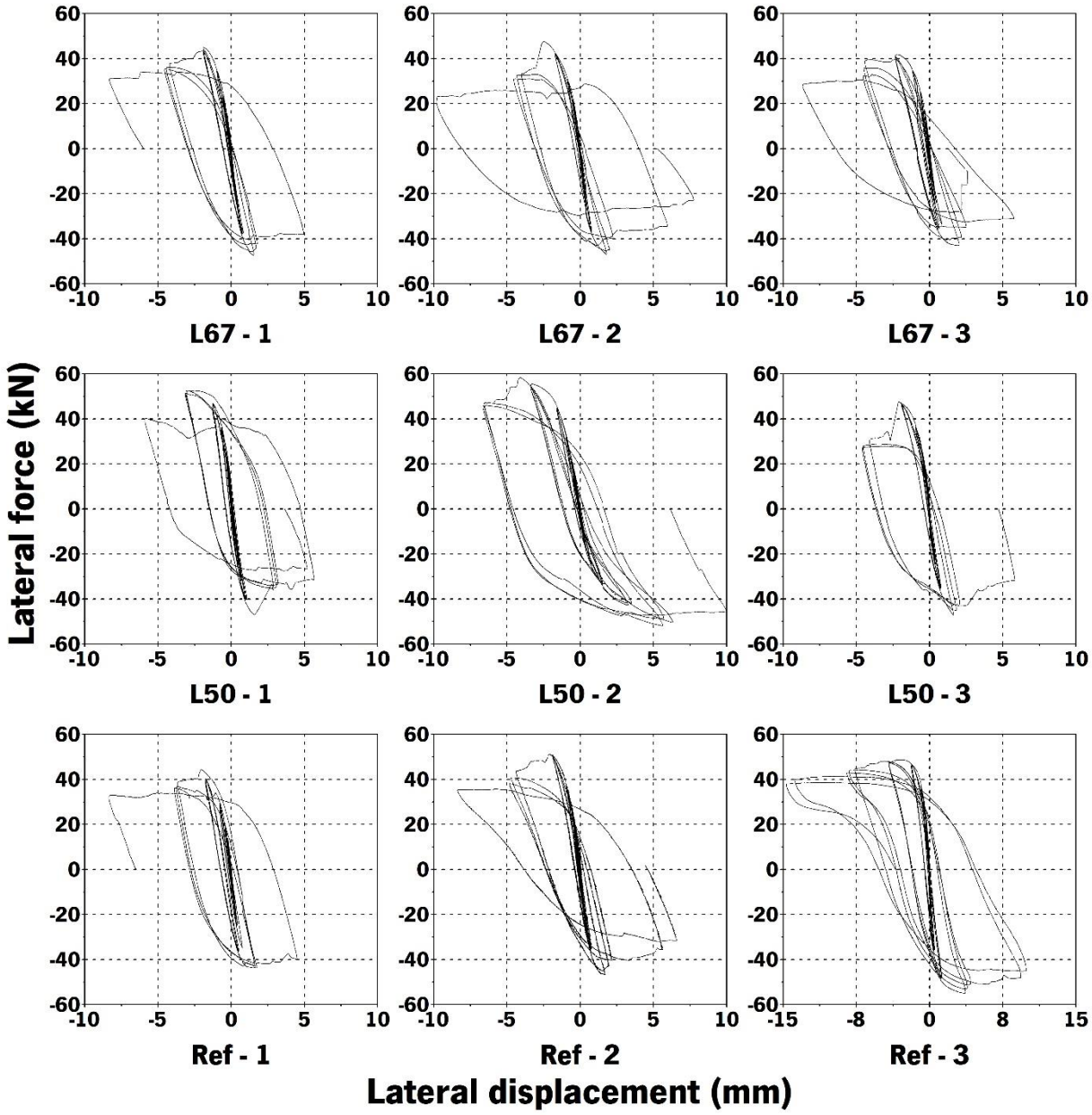

Figure 87: Lateral force versus lateral displacement in different masonry specimens subjected to in-plane cyclic loads

As may be observed, all the images in Figure 88 indicate the final crack patterns observed in the specimens. The values of principal strains were obtained from DIC. In general, the range of values obtained for principal strain appears to be similar to what has been recorded for unreinforced masonry in the literature [410].

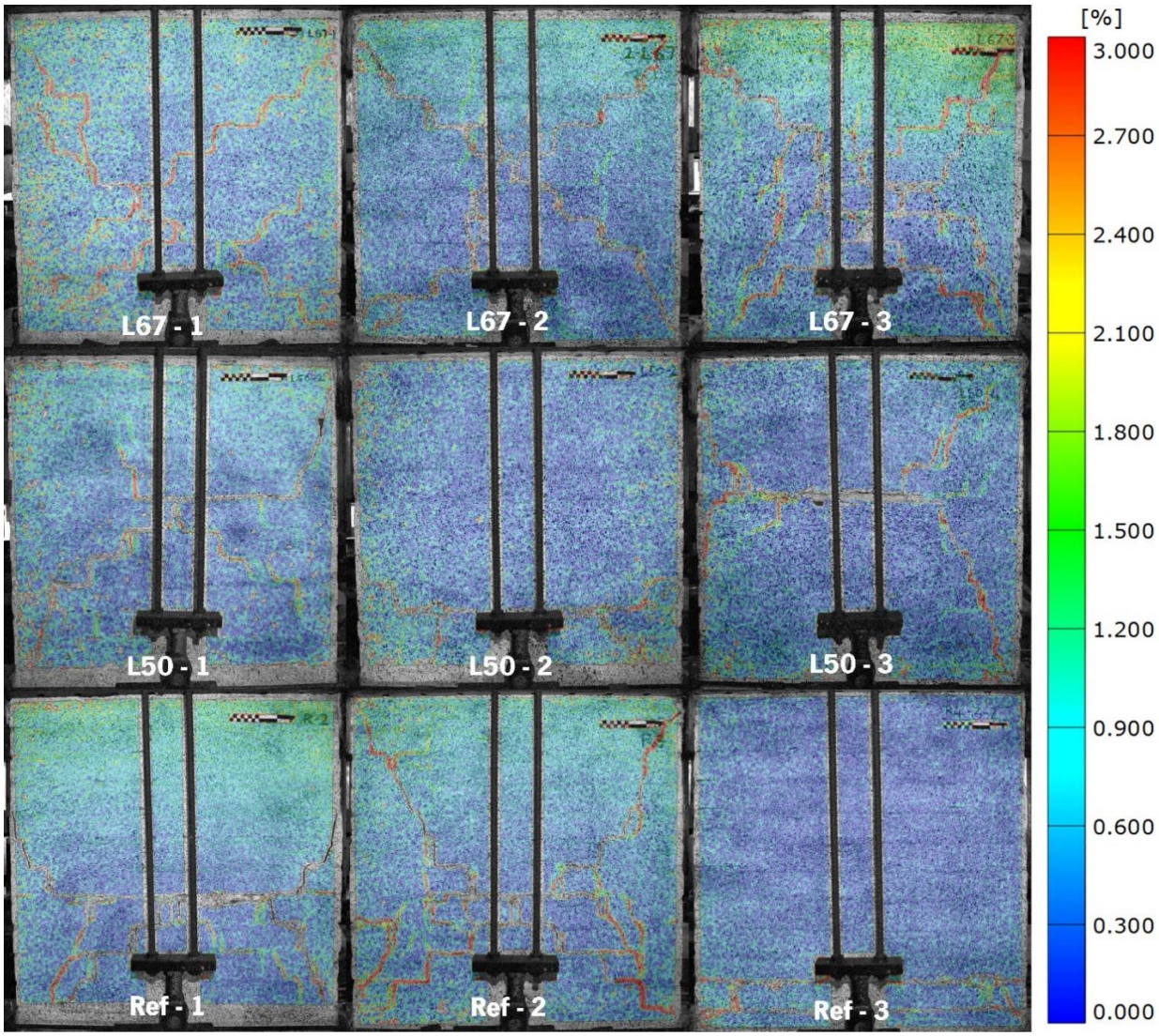

Figure 88: Final crack patterns observed in masonry specimens with the same brick and different mortars subjected to in-plane cyclic loads, indicated by principal strains from DIC

Visually, the pattern of cracks at failure (Figure 88), observed in L67, appears to be similar to each other in the form of diagonal steps. For L50, while there were X shaped cracks as well, there was also a horizontal crack running through one of the bed joints in the specimens, almost in the center for L50-1 and L50-3 and more towards the bottom in L50-2. This horizontal crack along with the diagonal ones may be observed in Ref-1 and Ref-2 as well. Ref-3 has only two horizontal cracks in the bottom, with no diagonal cracks at all, since the failure in this specimen was not due to the diagonal shear mechanism.

5.6.2.2 Experimental envelopes and corresponding bilinear idealization

In order to evaluate and compare the performance of different masonry specimens, the hysteresis diagrams were first converted to experimental envelopes, in the positive direction (push of the lateral actuator) as well as the negative direction (pull of the actuator) (Figure 89).

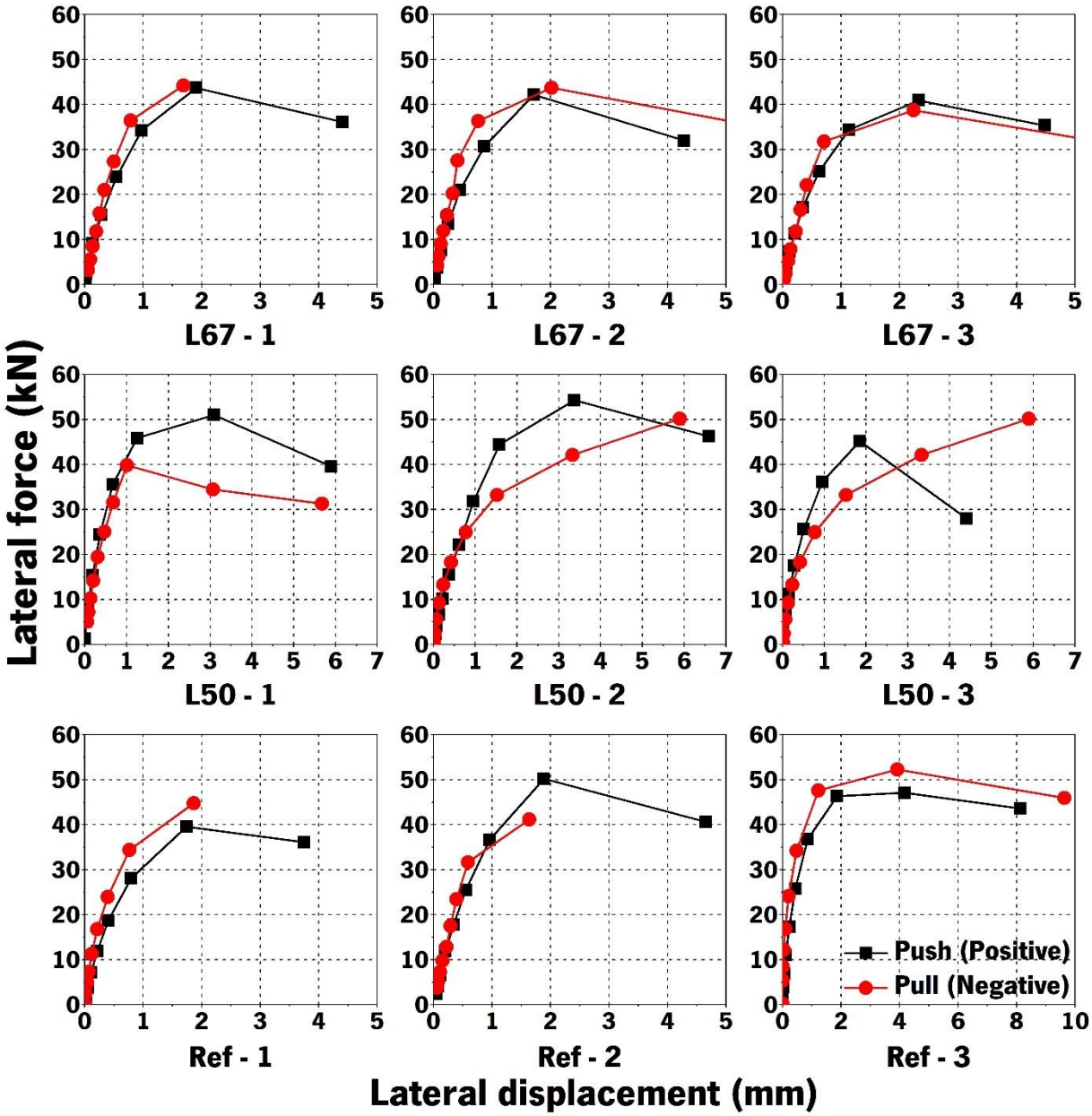

Figure 89: Experimental envelopes of lateral force v/s lateral displacements for the specimens tested

To obtain this envelope, the maximum lateral displacement was recorded from each loading cycle of the specimens, along with the corresponding force [104, 411]. Each point on the envelope is an average of the values obtained from three cycles of the same amplitude/imposed displacements, and the positive direction of the specimens was considered. The negative direction was not considered in the average,

because in this direction, the post-peak behavior was not recorded for all specimens since the test had to be stopped prior to collapse. Thereafter, in order to idealize the experimental envelopes and obtain bilinear envelopes, a method frequently used in literature was applied to evaluate parameters such as deformation capacity, strength, and stiffness of masonry subjected to cyclic loading [104, 206, 296, 410, 412]. To assess the performance of different specimens, three characteristic points have been defined in each curve (Figure 90), as suggested by Tomaževič [206].

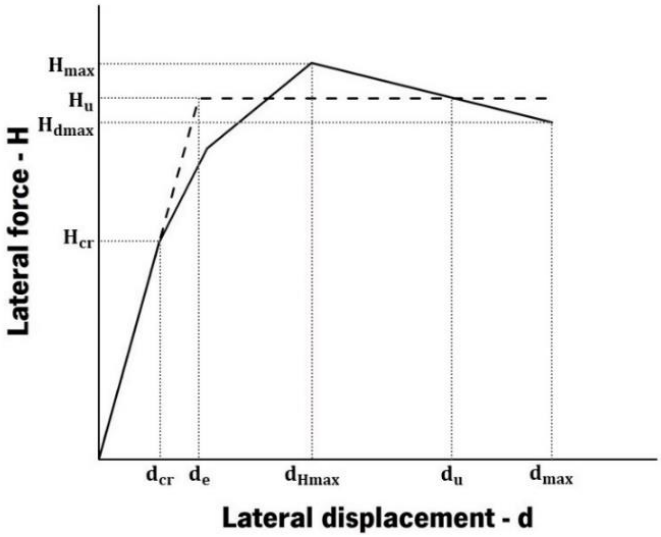

Figure 90: Bilinear idealization of the experimental force-displacement curve

The first is the crack limit state, corresponding to (H_{cr}, d_{cr}) and is recognized as values of force and displacement recorded as the point in the idealized curve, when the initial slope (secant stiffness) K_e changes. Theoretically, it is also the point at which the specimen first shows significant cracks. The second point is maximum resistance and corresponds to (H_{max}, d_{Hmax}) and the third point is associated with the maximum displacement of the specimen, corresponding to (H_{dmax}, d_{max}). Since, maximum displacement attained in the tests varied depending on when the test was stopped for different specimens, for the sake of quantitative comparison, it was defined as the post-peak displacement corresponding to 85% of the peak lateral load, similar to the criterion adopted by Deng *et al.* [314]. It must be mentioned that in the case of specimen Ref-1, the test stopped at approximately 91% of the post-peak lateral capacity and did not reach 85%, because the specimen was close to collapsing completely. Therefore, for the sake of uniform comparison, the post-peak branch of the experimental envelope was extrapolated to 85% of its lateral capacity and the value of ductility was calculated. Values of forces, displacements, corresponding to these three characteristic points of each experimental envelope, have been shown in Table 45.

Table 45: Data obtained from experimental envelopes corresponding to three characteristic points; cracking (H_{cr}, d_{cr}), maximum resistance capacity (H_{max}, d_{Hmax}) and maximum displacement (H_{dmax}, d_{max})

Specimen	H_{cr} (kN)	H_{max} (kN)	H_{dmax} (kN)	d_{cr} (mm)	d_{max} (mm)	d_{hmax} (mm)
L67 – 1	23.9	43.7	37.2	0.54	1.91	4.06
L67 – 2	21.0	42.2	35.9	0.46	1.72	3.31
L67 – 3	25.2	40.9	34.8	0.63	2.33	4.71
L50 – 1	35.6	51.0	43.4	0.67	3.09	4.97
L50 – 2	31.8	54.3	46.1	0.96	3.37	6.64
L50 – 3	25.6	45.2	38.4	0.51	1.85	2.86
Ref – 1	18.8	39.5	33.6	0.40	1.74	5.19
Ref – 2	25.4	50.2	42.7	0.55	1.89	4.06
Ref – 3	25.7	47.1	40.0	0.44	4.17	12.21

Furthermore, A_{env} is the area measured under the idealized envelope, and H_u is the ultimate resistance which is defined as the point which ensures equal energy dissipation from (a) the idealized envelope and (b) the actual experimental curve [104]. Finally, d_e is the idealized elastic displacement, which is the point at the intersection of the actual experimental curve and the idealized bilinear curve [104]. Tomaževič [206], provided equations to obtain quantitative values for K_e H_u and d_e and these have been shown in Equation 25.

$$K_e = \frac{H_{cr}}{d_{cr}} \quad (25.1)$$

$$H_u = K_e\left(d_{max} - \sqrt{d^2{}_{max} - \frac{2A_{env}}{K_e}}\right) \quad (25.2)$$

$$d_e = \frac{H_u}{K_e} \quad (25.3)$$

(25)

Using equation 25 and the experimental envelopes (Figure 89) obtained from the different specimens, parameters corresponding to the bilinear idealized envelopes were obtained for each specimen and have been displayed in Table 46. Typically, ductility μ_p is defined as the ratio of d_u to d_e [104]. However, since this ratio only addresses post-peak behavior, another parameter was introduced, μ_e to understand ductility before the specimen reached its maximum capacity. This was defined as the ratio between d_{hmax} and d_{cr}, indicating the deformation capacity between the occurrence of the first significant cracks in the specimen and when it finally reaches its maximum capacity. K_{max} is the secant stiffness at maximum capacity, and has been defined as the ratio of H_{max} to d_{Hmax}.

Table 46: Parameters used to describe the bilinear idealized envelopes

Specimen	H_u (kN)	d_u (mm)	d_e (mm)	K_e (kN/mm)	K_{max} (kN/mm)	$\frac{H_{cr}}{H_{max}}$	$\frac{H_u}{H_{max}}$	μ_e	μ_p
L67 – 1	39.8	3.20	0.90	44.1	22.9	0.55	0.91	3.5	3.6
L67 – 2	37.6	2.85	0.82	45.9	24.6	0.50	0.89	3.7	3.5
L67 – 3	37.6	3.65	0.94	40.1	17.6	0.61	0.92	3.7	3.9
L50 – 1	47.8	3.90	0.90	53.0	16.5	0.70	0.94	4.6	4.3
L50 – 2	49.7	5.15	1.50	33.1	16.1	0.59	0.92	3.5	3.4
L50 – 3	40.8	2.48	0.81	50.3	24.4	0.57	0.90	3.6	3.1
Ref – 1	35.7	3.95	0.77	46.3	22.7	0.47	0.90	4.3	5.1
Ref – 2	45.2	3.35	0.99	45.9	26.6	0.51	0.90	3.4	3.4
Ref – 3	43.9	7.80	0.75	58.3	11.3	0.55	0.93	9.4	10.4

In general, it is possible to observe from Table 45 and Table 46 that the general range of values obtained for different parameters is similar across different specimens. To compare the performance of different mortars, it is necessary to consider the average values of specimens with different mortars and this information has been presented in Table 47. All averaged values have been accompanied by the corresponding coefficient of variation in parenthesis. It must be noted, that because of failure due to sliding in Ref-3, the deformations were much larger than other specimens, and therefore this specimen has not been included in any deformation related averaged value. Additionally, displacements at cracking d_{cr}, maximum capacity d_{Hmax} have been presented as drifts (%), i.e., lateral deformation (LVDT 1) divided by the height of the specimen (900 mm) and expressed in percentages.

Table 47: Averaged values of different parameters for in-plane cyclic loading test

Mortar type	H_{max} (kN)	H_{cr} (kN)	K_e (kN/mm)	K_{max} (kN/mm)	$Drift_{cr}$ (%)	$Drift_{Hmax}$ (%)	$Drift_u$ (%)	$\frac{H_{cr}}{H_{max}}$	$\frac{H_u}{H_{max}}$	μ_e	μ_p
L67	42.3	23.4	43.4	21.7	0.06	0.22	0.36	0.55	0.91	3.7	3.6
CoV (%)	3.3	9.0	6.8	16.9	15.5	15.8	12.4	10.5	1.5	3.3	6.1
L50	50.1	31.0	45.5	19.0	0.08	0.31	0.43	0.62	0.92	3.9	3.6
CoV (%)	9.2	16.2	23.7	24.7	31.9	29.3	34.8	11.4	1.8	15.3	18.1
Ref	45.6	23.3	46.1	24.6	0.05	0.20	0.41	0.51	0.91	3.9	4.3
CoV (%)	12.0	16.9	15.2	11.0	22.0	5.9	11.6	7.1	1.9	16.3	28.7

The first observation concerning maximum lateral capacity (H_{max}) is that L50 exhibits slightly higher strength, followed by Ref and subsequently L67. This is partly unexpected when compared with results obtained from the previous tests (compressive strength, flexural strength, and bond strength). Secondly,

with regard to the capacity at which the first significant cracks tend to take place (H_{cr}), L50 once again has the highest value (in this case 33% more than Ref), while Ref and L67 appear to have almost the same values. This is also evident in the ratio of H_{cr} to H_{max}; L50 exhibits the first set of significant cracks at only 62% of its maximum capacity, followed by L67, which shows it at 55% of its maximum capacity, and finally, Ref shows it at 51%. For the different mixes, these trends in lateral strength capacity do not match with the trend of strength at the mortar level, which is Ref, L50, and L67 (Table 30). For secant stiffness, both initial and maximum, Ref seems to exhibit the highest values. Overall, it appears that L50 offers good lateral capacity, with relatively lower values of secant stiffness, compared to the other two mixes.

It is also worth noting that the ratio of H_u to H_{max} is almost the same for all mixes; 91%, which has also been observed by other researchers, from experimental results of over 60 masonry walls [206]. The ratio of H_{cr} to H_{max} was found to vary between 0.5 to 0.6, which was typically slightly less than what has been reported in the literature (0.6-0.8) or is often considered as a thumb rule, around 0.7 [296, 310]. Though not explicitly mentioned, if ratios of H_{cr} to H_{max} are evaluated from the work of Vasconcelos [104], they tend to range around 0.5. This range of 0.5 ratios can also be found in the work of other authors in literature [413].

In terms of the drift capacity corresponding to both, the state of cracking as well as maximum resistance capacity, the trend is similar to that of the ratio of H_{cr} to H_{max}; i.e., the highest drift capacity is offered by L50, followed by L67 and then Ref. In terms of the drift capacity at ultimate state corresponding to the displacement d_u, L50 still displays the highest value, followed by Ref and then L67. The general range of values for the state of ultimate drift capacity, averaged at 0.4% appears to be similar to what has been observed for unreinforced brick masonry walls at 0.5%, from two different sets of experimental studies performed in JRC Ispra and the University of Pavia in Italy, reported by Magenes *et al.* [310]. In terms of post-peak ductility, Ref seems to perform the best, followed by similar values of L50 and L67. While in terms of pre-peak ductility, Ref and L50 have similar values followed by L67. It must also be mentioned, that the differences observed here are small.

5.6.2.3 Performance: Drift capacity, stiffness degradation, and energy dissipation

In terms of drift capacity, Abrams [414] defined three performance levels for unreinforced masonry walls; IO – Immediate Occupancy, LS – Life Safety, and CP – Collapse Prevention. IO would typically correspond to the initiation of shear cracks, which usually occur at around 90% of the maximum lateral capacity [104,

310]. Since H_u in this research was around 0.9 H_{max}, the corresponding pre-peak displacement d_e was used to evaluate the drift. LS would correspond to drift at d_{Hmax}, indicating maximum lateral capacity and CP would correspond to d_{max} since theoretically that would imply the collapse of the structure [414]. The values of IO, LS, and CP obtained in this research have been shown in Table 48. Once again, Ref-3 was not included in the averaged values since it did not fail with a shear mechanism. The average value of IO was found to be around 0.10% for all mortars Ref, L50, and L67. This value is in alignment with what has been reported at IO for unreinforced masonry buildings in the literature [415]. The average values of LS and CP were found to be similar for al mortars and in the range of 0.2% to 0.3%, and 0.45% to 0.55%, respectively.

Table 48: Performance-based drift levels (%) obtained for unreinforced brick masonry walls with different mortars

Performance	IO	LS	CP	IO - Avg	LS - Avg	CP - Avg
Specimen	$Drift_e$ (%)	$Drift_{Hmax}$ (%)	$Drift_{max}$ (%)	$Drift_e - Avg$ (%)	$Drift_{Hmax} - Avg$ (%)	$Drift_{max} - Avg$ (%)
L67 – 1	0.10	0.21	0.45			
L67 – 2	0.09	0.19	0.37	0.10 (6.8%)	0.22 (15.8%)	0.45 (7.3%)
L67 – 3	0.10	0.26	0.52			
L50 – 1	0.10	0.34	0.55			
L50 – 2	0.17	0.37	0.74	0.12 (35.0%)	0.31 (29.3%)	0.54 (39.3%)
L50 – 3	0.09	0.21	0.32			
Ref – 1	0.09	0.19	0.58			
Ref – 2	0.11	0.21	0.45	0.10 (17.3%)	0.20 (5.9%)	0.51 (17.3%)
Ref – 3	0.08	0.46	1.36			

The performance of the different specimens may be observed in Figure 91. The left side of the image indicates normalized lateral forces (with respect to maximum capacity) versus corresponding lateral drift of different specimens. The right side of the image indicates the degradation of lateral stiffness versus the corresponding drift of the specimens. The secant stiffness of each cycle was estimated by considering the slope of the line that connects the maximum and minimum strength of each cycle [104].

In the case of normalized experimental envelopes (Figure 91 a), three specimens exhibit high lateral strength capacity for the drift of 0.8%; one corresponds to Ref which is Ref-3 which failed by sliding mechanism and the other two correspond to L50-1 and L50-2. The rest of the specimens seem to behave similarly. In the case of stiffness degradation (Figure 91 b), which is also indicative of the damage in the specimen [314], almost all the specimens behave similarly. L50-2 is the only specimen that has a little

higher stiffness at 1.1% lateral drift. The other prominent difference is in the curve which shows the highest value in the beginning and corresponds to Ref-3 (sliding failure mechanism) but eventually ends up in the same range of stiffness as that of the other specimens.

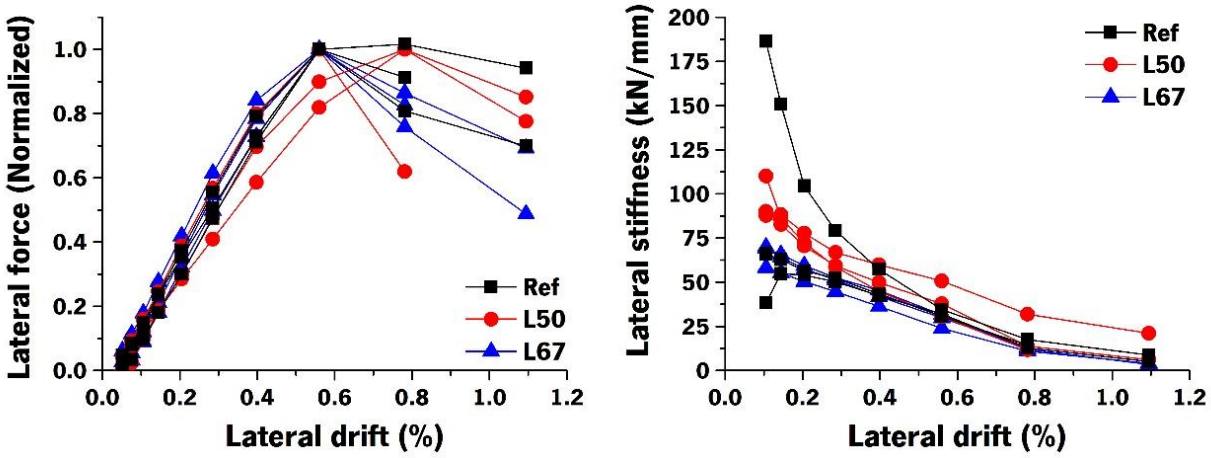

Figure 91: (a) Lateral resistance, normalized with respect to maximum capacity v/s lateral drift (b) Stiffness degradation versus lateral drift

A parameter that deserves attention is the energy dissipation of a structure, which helps reduces the amplitude of the seismic response of a structure, subsequently lowering the demands of ductility as well [298]. The energy dissipated by the specimens was measured by the area under the force hysteresis loop for each cycle. Since the global energy depends on factors such as the amount of vertical pre-compression applied [104], Shing *et al.* [298], proposed the so-called cumulative normalized energy which uses parameters from the idealized bilinear envelope to normalize the quantity of dissipated energy, for comparison. Vasconcelos used Equation 26 [104], to calculate the parameter cumulative normalized energy (E_N), which has also been used in this research. The term n in the equation refers to the load cycles.

$$E_N = \frac{1}{H_u d_e} \sum_{i=1}^{n} E_{i,dissipated} \qquad 26$$

Furthermore, it is also interesting to compare the work done by the horizontal actuator, measure in the form of energy input with the energy dissipated by the specimen [316]. Energy input is the energy required to impose lateral deformation on the specimens and was measured by considering the sum of complete areas under the hysteresis loop of each cycle. Figure 92 shows the amount of energy dissipated, the cumulative normalized energy, and the ratio of dissipated energy to the amount of energy input by each specimen. In terms of energy dissipated, both absolute and normalized, it is hard to spot a trend.

Essentially, all specimens behave similarly. In terms of the ratio of the amount of energy dissipated to the energy input, as the lateral drift increases or as the number of cycles progress, the ratio increases, tending towards 1, but never reaching it. It is clear that the introduction of damage increases the ratio of dissipated to input energy. In particular, there is a noticeable jump in the ratio of dissipated to input energy, between 0.6% to 0.8% and this coincides with the change in the lateral capacity of specimens from approximately 90% to 100% (H_u to H_{max}) as may be observed in Figure 91 a, which is when the shear cracks tend to appear.

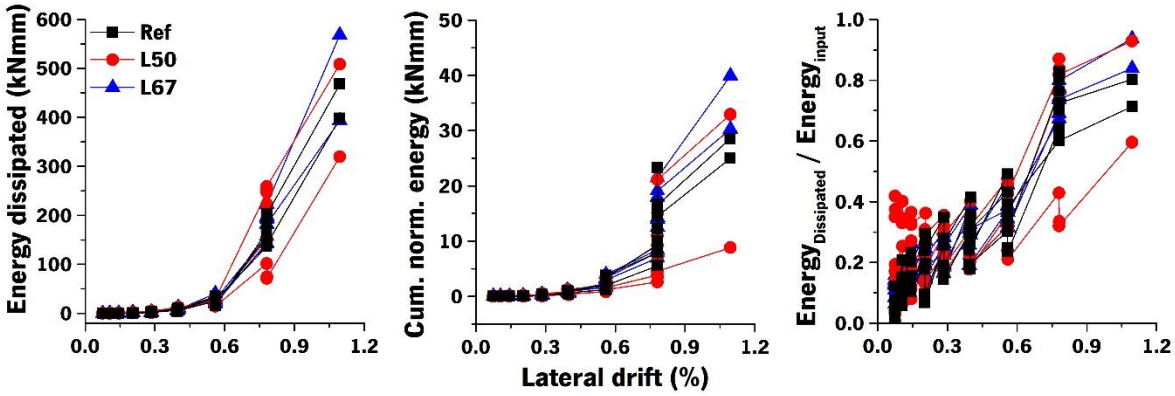

Figure 92: Energy dissipated v/s lateral drift for unreinforced masonry specimens with different mortars

5.6.2.4 Comparison of analytic and experimental data

In-plane shear strength of masonry is a complicated phenomenon, and it is evident that it is an experiment that consumes significant time and resources. Over time, simplified formulations have been presented by different researchers, which are also required by masonry design codes, and those predictions have been compared with values obtained in this research, to judge their applicability. Balasubramanian *et al.* [304], have presented a review of different formulations used for the three failure modes associated with in-plane shear behavior of unreinforced masonry, including sliding, rocking, and shear cracking. Out of the three failure modes, the one that applies to this research is shear cracking. Within said failure mode, the formulations that were found to be relevant, have been presented herein Equation 27.

$V_d = f_{vk} t\, l_c$ where $f_{vk} = f_{vko} + .4\sigma$ — Eurocode 6 [18] — 27.1

$V_d = l\, t\, \tau_u$ where $\tau_u = \min(\tau_c, \tau_w)$ — Magenes et al. [310] — 27.2

$\tau_c = \frac{1.5c+\mu\sigma}{1+3c\alpha_v/\sigma}$ where $\alpha_v = \frac{h_o}{l}$

$\tau_w = \frac{c+\mu\sigma}{1+\alpha_v}$ — 27

$H_f = \frac{l^2 t}{6h_o}(\sigma + f_{jt})$ — Vasconcelos [104] — 27.3

The symbol f_{vk} is the characteristic shear strength of masonry, obtained from cohesion and perpendicular compressive stress. The symbols t and l_c represent the thickness of the specimen and the length of the specimen under compression. τ_u is the ultimate or maximum shear strength and in the equation proposed by Magenes et al. [310] (equation 27.2), it is equal to τ_c corresponding to the cracked section or τ_w corresponding to the whole section, whichever is smaller. α_v is the shear ratio and is calculated by dividing the effective height (h_o) of the specimen by the length (l), and f_{jt} is the tensile strength of the bed joint. V_d refers to the maximum lateral capacity and H_f refers to the lateral capacity at which the first flexural crack is expected to appear and is initiated by the loss of tensile bond between the unit and mortar [104]. Since this would expectably, cause a change in stiffness of the specimen or masonry, it is expected to indicate the force at which the specimen first cracks, experimentally, corresponding to H_{cr}, assuming a linear distribution of stresses [104]. The comparison between analytically obtained values of equation 27 and experimentally obtained values (Table 47), for masonry with different mortars, has been presented in Table 49.

Table 49: Comparison between analytic and experimental values of in-plane shear capacity of masonry with different mortars

Mortar type	H_{max} (kN)					H_{cr} (kN)		
	Experimental (CoV %)	EC-6 [18]	Diff(%)	Magenes *et al.* [310]	Diff (%)	Experimental (CoV %)	Vasconcelos [104]	Diff (%)
L67	42.3 (3.3%)	50.7	19.9	41.4	-2.0	23.4 (9.0%)	20.7	-11.6
L50	50.1 (9.2%)	49.8	-0.8	53.4	6.4	31.0 (16.2%)	23.4	-24.5
Ref	45.6 (12.0%)	58.9	29.2	52.7	15.5	23.3 (16.9%)	23.0	-1.5

Equation 27.2 by Magenes *et al.* [310] provides a better estimation of maximum lateral capacity than Eurocode 6 [18]. The analytical expression of the appearance of the first crack by Vasconcelos [104] tends to underestimate the experimental values (equation 27.3).

5.7 Conclusions

This chapter addresses the mechanical behavior of masonry as a function of the different mortars used. The properties studied were compressive strength, flexural strength in directions parallel and perpendicular to the bed joint, shear bond strength and response to in-plane combined shear cyclic loading. The benefit of the presence of lime in the binder of the mortar was not very evident from the results, which have been summarized below concerning each property:

1. Compressive strength: Compressive strength (Section 5.3.2.1) of masonry with three different mortars L67, L50, and Ref was found to increase in be in the range of 6.0 to 7.2 MPa, while E-modulus was found to be in the range of 3.8 to 4.5 GPa. The ratio of E-mod to fc was found to be between 600 and 650. The presence of lime in the binder contributed to greater vertical deformation capacity at peak loads, and also contributed to lower stiffness and strength of masonry.

Between the mortars Ref and L50, Ref had a 17% higher strength and 24% higher stiffness at the mortar level, however, at the masonry level, the difference in strength and stiffness is higher by only 7% and 10% respectively. Furthermore, at peak load L50 exhibits 14% more deformation capacity and 9% higher pre-peak ductility compared to Ref.

Between the mortars Ref and L67, Ref had 58% higher strength and 56% higher stiffness at the mortar level, however, at the masonry level, the difference in strength and stiffness is higher by only 16% and 13% respectively. Furthermore, at peak load, L67 exhibits 34% more deformation capacity and 13% higher pre-peak ductility compared to Ref.

Estimation of the strength of masonry by Eurocode 6 based on the strength of its components, brick and mortar, resulted in values significantly higher than experimental results, by a margin of 50% to 70%.

2. Flexural strength (parallel and perpendicular): As expected, flexural strength (Section 5.4.2) of masonry with all mortars was found to be higher in the perpendicular direction (0.8 – 1.2 MPa) compared to the parallel direction (0.1 – 0.23 MPa). The strength of the mortar influenced the flexural strength of masonry in both directions. The mix L67 with the lowest strength at the mortar level, also results in the lowest flexural strength in masonry, in both parallel and perpendicular directions. Similarly, the two mixes L50 and Ref that have similar strength at the mortar level, appear to result in similar values of flexural strength in masonry as well. All experimentally obtained values were found to be greater than the recommendations of EC6, except for L67 in the parallel direction, the characteristic value of which was found to be less than 0.1 MPa.
3. Shear bond strength: Shear bond strength (Section 5.5.2) of masonry triplets with different mortars was tested for three different levels of vertical pre-compression – 0.2, 0.6, and 1 MPa. As expected, it was found that the maximum shear stress increases with increasing values of vertical pre-compression. Concerning cohesion (0.29 – 0.41 MPa) and coefficient of friction (0.58 – 0.87) of masonry, the values seemed to be influenced by the strength of the mortar used, but a clear trend

was not observed. All experimentally obtained values of cohesion were found to be greater than the recommendations of EC6.

4. In-plane combined cyclic shear loading: Horizontal lateral displacements were imposed on masonry specimens subjected to a vertical pre-compression of 0.78 MPa (Section 5.6.2). From the force-displacement hysteresis diagrams obtained, idealized bi-linear envelopes were developed and subsequently different parameters were compared to assess the performance of different mortars.

The maximum lateral capacity was found to be the highest for L50 (0.55 MPa), followed by Ref (.50 MPa) and L67 (0.46 MPa), respectively. Values of lateral forces ranged between 40 and 50 kN.

Interestingly, the secant stiffness at maximum load was found to be the lowest for L50 (19 kN/mm), followed by L67(22 kN/mm), and Ref (25 kN/mm).

Drift % at cracking was the highest for L50 (0.08%) followed by L67 (0.06%) and Ref (0.05%). Similarly drift % at peak capacity followed the same order of L50, L67 and Ref, with values of 0.31%, 0.22% and 0.20% respectively.

The ratio of $\frac{H_{cr}}{H_{max}}$ which indicates at what % of its maximum capacity does masonry begin to first crack, was the highest for L50, followed by L67 and Ref, with values of 0.6, 0.55, and 0.51 respectively. Finally, the ratio of $\frac{H_{u}}{H_{max}}$ was found to be approximately 0.91 for all specimens.

Energy dissipation and stiffness degradation were found to be similar for all specimens.

Eurocode 6 tends to overestimate the lateral capacity of masonry with different mortars, while the analytical expression by Magenes *et al.* [310] provides a good estimation of the in-plane shear capacity of masonry, with a difference of less than 15% between analytic and experimental values. Still, the experimental values found for Ref are lower than expected and a clear reason for this result could not be given.

6. Conclusions and future recommendations

6.1 General conclusions

This doctoral research contributes to the experimental knowledge on lime-cement mortars in unreinforced brick masonry. The existing literature on this subject is mostly limited to the behavior of mortars and masonry in compression, with scattered information on other mechanical properties. Therefore, a comprehensive approach was adopted to bridge this gap systematically by testing different mix compositions at the mortar level.

At the mortar level, some trends could be identified when the quantity of lime in the binder was increased, such as a decrease in mechanical strength and stiffness, decrease in ultrasound pulse velocity (UPV) and bulk density, and increase in porosity. However, in drying shrinkage, fracture energy, and Poisson's ratio specific trends could not be found, and only a general range of values was obtained. Analytic expressions were presented to estimate the compressive strength of lime-cement mortars as a function of (a) strength of the mix at 7 days (b) lime content, binder/aggregate (B/Ag) ratio, and time. A method based on non-destructive techniques was presented to estimate the compressive strength of mortar by using only UPV and bulk density.

Subsequently, for masonry level research, two lime-cement mixes were selected and a reference cement mortar was introduced to be tested at the masonry level. Different mechanical properties of masonry were tested such as compressive strength, E-modulus, flexural strength in both directions (parallel and perpendicular), and shear bond strength. Mean values obtained were converted into characteristic values and compared with the recommendations of Eurocode 6. The behavior of masonry wall panels subject to in-plane shear cyclic loads was also studied. The impact of lime in the binder of the mortar was not too evident in most of the properties tested. Rather than lime in mortar, it was found that the compressive strength of the mortar was a better indicator of flexural strength and shear bond strength of masonry. In compression, the increased quantity of lime in mortar resulted in lower strength and stiffness and higher pre-peak ductility of masonry, but the differences were found to be minor. Finally, in the response of masonry wall panels to in-plane cyclic shear loads, trends could not be identified regarding lime in a binder or compressive strength of the mortar.

Based on this research, it appears that using a lime-cement mortar, compared to a cement mortar, with comparable strength at the mortar level, does not lead to a significant difference in mechanical behavior

at the masonry level. It is noted that the optimal conditions of testing may not be representative of the actual site conditions, e.g. factors related to prewetting bricks or the working life of the mortar. The findings in this thesis will aid further research in the field of lime-cement mortars and their impact on the mechanical behavior of masonry. In parallel, the quantification of trends is expected to be of use to practitioners and researchers to develop rules of thumb, and aid the choice of a compatible mortar for masonry construction. Specific findings of this research have been highlighted at the mortar and masonry level, in the next section.

6.2 Specific findings

6.2.1 Mortar level

At this scale, the focus of the research was to investigate, and quantify whenever possible, the effects of lime-cement ratio on the various mechanical properties of mortars. The results obtained for different mechanical properties have been summarized below:

- 15 lime-cement mixes: B/Ag ratios (1:3, 1:4, 1:5, 1:6), Lime content (10, 25, 33, 50, 67, 75, 90) %, Ages-days (7, 14, 28, 90, 180, 365)
  1) For a target workability, the requisite water-binder ratio increases linearly with increasing lime content in the binder, as well as with decreasing B/Ag ratio of the mix. An equation was presented to estimate the requisite water binder ratio for a given mix, as a function of the composition of the mix (lime-cement ratio, B/Ag ratio), within a 10% error margin.
  2) For B/Ag ratios 1:3, 1:4, and 1:5, every 1% increase in the quantity of lime in the binder (by volume), led to a 1.4% decrease in the mechanical strength (compression/flexure) of the mix, with respect to the benchmark mix – with 10% lime or 90% cement in the binder.
  3) For binder compositions with 33.3%, 50%, and 66.7% lime in the binder, every 1% decrease in B/Ag ratio (by volume), led to a 5% decrease in the mechanical strength (compression/flexure) of the mix, with respect to the benchmark mix – B/Ag ratio 1:3.
  4) The ratio between compressive strength and flexural strength was approximately 3, for all the mixes. The ratio was found to decrease with increasing lime content in the binder, decreasing B/Ag ratios, and an increase in curing age.
  5) Bulk density was found to decrease till 28 days for almost all the mixes and then to stabilize or to increase slowly with time. UPV values were found to decrease with increasing lime content in the binder and decreasing B/Ag ratios of lime-cement mixes. Furthermore, it was found that the

square of UPV $(\mathrm{UPV(t)^2})$ and a product of density and compressive strength $(\rho(t)^{1.5}f_c(t)^{0.5})$ varied linearly with lime content in the binder and B/Ag ratios.

- 3 lime-cement mixes: B/Ag ratios (1:3), Lime content (25, 50, 67) % Ages-days (7, 28, and 90), Compositions 3C1L12S (25%), 1C1L6S (50%), and 1C2L9S (67%)

1) E-modulus measured by the cyclic compression test was found to be in the range of 4 - 18 GPa for mixes 1C2L9S (67%), 1C1L6S (50%), and 3C1L12S (25%) between 7 to 90 days. The increase in stiffness of the mixes between day 7 and day 90 was found to be 7%, 19%, and 27% for the mixes 3C1L12S (25%), 1C1L6S (50%), and 1C2L9S (67%) respectively. Furthermore, for these mortars, the ratio of E-modulus to compressive strength for cylindrical specimens was found to vary from 1300 to 2300 at 90 days of age.
2) Poisson's ratio was found to vary from 0.13 to 0.23 between 7 to 90 days of age, with a global average of 0.18 (18% CoV).
3) Fracture energy was found to range from 5 to 83 N/m depending on the quantity of lime in the binder.
4) The value of open porosity decreased with age for all mixes and increased with the amount of lime content in the binder. The general range of values was found to vary between 23% and 27%.

- 5 lime-cement mixes: B/Ag ratios (1:3), Lime content (25, 33, 50, 67, 75) %, Ages-days (up to 90 days)

1) Drying shrinkage was studied up to 90 days of age, and it did not appear to be impacted by the quantity of lime in the binder. Most values ranged between 550-750 micro strains.
2) Results from the EMM-ARM test indicate that at all curing ages, day 1 to day 7: every 1% increase in the quantity of lime in the binder led to a corresponding 1.3% decrease in stiffness of mortars. It was also observed that all mortars, regardless of the quantity of lime in the binder, appeared to gain approximately 40% of their total stiffness in the first 24 hours, and 80% in the first 72 hours. After the fourth day, the increase in stiffness of all the mortars was found to be 5% or lesser.

6.2.2 Masonry level

Based on the experiments performed in this research, the impact of lime in the binder of the mortar was not evident in the mechanical behavior of masonry. Masonry specimens were constructed with the mortars L67 (1:2:9), L50 (1:1:6), and Ref (1:0:5). Specific results have been discussed below:

1. Compressive strength: It was found that the presence of lime in the binder, contributed to greater vertical deformation capacity at peak load and contributed to lower strength and stiffness of masonry. Compressive strength of masonry with three different mortars L67, L50, and Ref was found to be in the range of 6.0 to 7.2 MPa, while E-modulus was found to range from 3.8 to 4.5 GPa. The ratio of E-modulus to compressive strength was found to be similar for all mortars, and between 600-650. The estimation of masonry strength by Eurocode 6 based on the strength of its components, brick, and mortar, resulted in values significantly higher than experimental results, by a margin of 50% to 70%.
2. Flexural strength (parallel and perpendicular): As expected, the flexural strength of masonry with all mortars (L50, L67, and Ref) was found to be higher in the perpendicular direction (0.8 – 1.2 MPa) compared to the parallel direction (0.1 – 0.23 MPa). The strength of the mortar influenced the flexural strength of masonry in both directions. The mix L67 with the lowest strength at the mortar level, also resulted in the lowest flexural strength in masonry, in both parallel and perpendicular directions. Similarly, the two mixes L50 and Ref that have similar strength at the mortar level, appear to result in similar values of flexural strength in masonry as well. All experimental values were found to be greater than the recommendations of Eurocode 6, except for L67 in the parallel direction, the characteristic value of which was less than 0.1 MPa.
3. Shear bond strength: The shear strength of masonry triplets with different mortars was tested for three different levels of vertical pre-compression – 0.2, 0.6, and 1 MPa. As expected, it was found that maximum shear stress increases with increasing values of vertical pre-compression. Concerning cohesion (0.29 – 0.41 MPa) and coefficient of friction (0.58 – 0.87) of masonry, the values seemed to be influenced by the strength of the mortar used, but a clear trend, as a function of mortar strength was not observed. All experimentally obtained values of cohesion were found to be greater than the recommended values of Eurocode 6.
4. In-plane cyclic shear loading: Horizontal lateral displacements were imposed on masonry specimens subjected to a vertical pre-compression of 0.78 MPa. The maximum lateral capacity was found to be the highest for L50 (0.55 MPa), followed by Ref (0.50 MPa) and L67 (0.46 MPa), respectively. The range of values of lateral forces was between 40 and 50 kN. Interestingly, the secant stiffness at maximum load was found to be the lowest for L50 (19 kN/mm), followed by L67(22 kN/mm), and Ref (25 kN/mm). Drift at cracking was the highest for L50 (0.08%) followed by L67 (0.06%) and Ref (0.05%). Similarly drift at peak capacity followed the same order of L50, L67, and Ref, with values of 0.31%, 0.22%, and 0.20% respectively. The ratio of $\frac{H_{cr}}{H_{max}}$ which indicates at what percentage of

its maximum capacity does masonry begin to first crack, was the highest for L50, followed by L67 and Ref, with values of 0.60, 0.55, and 0.51 respectively. Finally, the ratio of $\frac{H_u}{H_{max}}$ was found to be approximately 0.91 for all specimens. Energy dissipation and stiffness degradation were found to be similar for all specimens. Eurocode 6 tends to overestimate the lateral capacity of masonry with different mortars, while the analytical expression by Magenes et al. [310] provides a good estimation of the in-plane shear capacity of masonry, with a difference of less than 15% between analytic and experimental values.

6.3 Recommendations for future research

Through this research, an attempt has been made at better understanding the influence of different lime-cement ratios on the mechanical behavior of mortars. However, there are still mechanisms and behaviors of masonry that are not well understood, regarding the influence of the type of mortar used. More investigations would be of help for the modern construction industry and possibly historic constructions. Keeping this in mind, the following suggestions have been made:

1. At the mortar level, further research is required to quantify the influence of lime-cement mortars on fracture energy, E-modulus, and Poisson's ratio, up to 365 days of age, accounting for different B/Ag ratios and more lime-cement ratios. Such information would be useful in forming factorial plans and in feeding numerical models.

   Triaxial compression of lime-cement mortars is another interesting property that could help advance knowledge on the behavior of masonry, concerning different failure mechanisms.
2. At the masonry level, it would be useful to perform the tests performed in this research, with the same mortar compositions but with different types of units such as low suction extruded clay bricks and concrete blocks, to understand how the compatibility between lime-cement mortars and corresponding unit impacts the behavior of masonry. This knowledge is imperative to understand if and how the information currently possessed can be generalized.
3. Validated micro-models that involve the unit, mortar, and the interface would prove useful since experiments are expensive, time-consuming, and resource-intensive. While experiments are required for numerical simulations to be accurate, the goal would eventually be to have a reliable model that can accurately predict the mechanical behavior of masonry accounting for the type of mortars used. Multi-physics numerical simulations could also help vastly if long-term effects of carbonation are

considered. Of course, for this last part, more experiments would be required to record the rate of carbonation in different lime-cement mortars.

4. For future experiments, it is suggested to involve another reference cement mortar, with a possible B/Ag ratio of 1:6. More importantly, this mortar must have lower strength than the three mortars that were researched at the masonry level – Ref (1:5), L50 (1:1:6), and L67 (1:2:9). The reason is that if the mortars are to be analyzed only from the point of view of understanding the influence of lime, the factor of mechanical strength of mortar must be removed, as a possible cause of the difference in behavior.

   It would also be beneficial to study a cement mortar with an air-entraining agent, as is often used on construction and to compare its performance with lime-cement mortars.

5. Aspects of restrained shrinkage of mortar in masonry, vapor permeability, and freeze-thaw resistance merit investigation, regarding the influence of lime-cement ratios in the mortar. It may also be interesting to study the effects of workmanship and aspects of execution in the construction of masonry on its mechanical behavior since all tests performed in this research were made in a controlled environment.

References

[1] Graymont, History of lime in mortars. https://www.graymont.com/en/markets/building-construction/mortar/history-lime-mortar. (Accessed 29 September 2020).
[2] Ö. Cizer, Competition between carbonation and hydration on the hardening of calcium hydroxide and calcium silicate binders, FACULTEIT INGENIEURSWETENSCHAPPEN, KATHOLIEKE UNIVERSITEIT LEUVEN, 2009.
[3] Jonathon, History of lime mortar, 2019. https://brickandlime.com/blog/2019/04/10/history-of-lime-mortar/. (Accessed 29 September 2020).
[4] E. Aggelakopoulou, A. Bakolas, A. Moropoulou, Lime putty versus hydrated lime powder: Physicochemical and mechanical characteristics of lime based mortars, Construction and Building Materials 225 (2019) 633-641.
[5] A. Bentur, Cementitious Materials—Nine Millennia and A New Century: Past, Present, and Future, Journal of Materials in Civil Engineering 14(1) (2002) 2-22.
[6] J.-L. Galvez-Martos, H. Schoenberger, An analysis of the use of life cycle assessment for waste co-incineration in cement kilns, Resources, Conservation and Recycling 86 (2014) 118-131.
[7] B.A. Silva, A.P. Ferreira Pinto, A. Gomes, Natural hydraulic lime versus cement for blended lime mortars for restoration works, Construction and Building Materials 94 (2015) 346-360.
[8] A. Smith, F. Verlhelst, C. Denayer, R. Givens, Quantifying the benefits of lime additions in cement based mortars

9th International Masonry Conference, Guimaraes, Portugal, 2014, pp. 1-10.
[9] R. Hendrickx, The Adequate measurement of the workability of masonry mortar, Leuven : Katholieke Universiteit Leuven, Faculty of Engineering, KU Leuven, 2009.
[10] L. EULA, Lime in mortars (Hydrated lime - Benefits of use in mortars).
[11] V.G. Haach, G. Vasconcelos, P.B. Lourenço, Assessment of Compressive Behavior of Concrete Masonry Prisms Partially Filled by General Mortar, Journal of Materials in Civil Engineering 26(10) (2014).
[12] A. Costigan, S. Pavía, O. Kinnane, An experimental evaluation of prediction models for the mechanical behavior of unreinforced, lime-mortar masonry under compression, Journal of Building Engineering 4 (2015) 283-294.
[13] H.B. Kaushik, D.C. Rai, S.K. Jain, Stress-Strain Characteristics of Clay Brick Masonry under Uniaxial Compression, Journal of Materials in Civil Engineering 19(9) (2007) 728-739.
[14] K. Venu Madhava Rao, B.V. Venkatarama Reddy, K.S. Jagadish, Flexural bond strength of masonry using various blocks and mortars, Materials and Structures 29(2) (1996) 119-124.
[15] G.R. Kingsley, Masonry, Encyclopedia of Physical Science and Technology2003, pp. 133-143.
[16] CEN, EN 1015-11:1999 Methods of Test for Mortar for Masonry - Part 11: Determination of Flexural and Compressive Strength of Hardened Mortar, 2007.
[17] CEN, EN 1052-1:1999 Methods of test for masonry - Part 1: Determination of compressive strength, 1999.
[18] CEN, EN 1996-1-1 Eurocode 6 - Design of masonry structures - Part 1-1: General rules for reinforced and unreinforced masonry structures, 2005.
[19] J.J. Thomas, The Science of Concrete 2009. http://iti.northwestern.edu/publications/utc/tea-21/FR-5-Jennings-Thomas.pdf. 2019).
[20] H.F.W. Taylor, Portland cement and its major constituent phases, Cement chemistry1997, pp. 1-28.
[21] CEN, EN 197-1:2000 Cement. Composition, specifications and conformity criteria for common cements, 2000.
[22] P.P.C. Association, How cement is made. https://www.cement.org/cement-concrete-applications/how-cement-is-

made#:~:text=Cement%20is%20manufactured%20through%20a,silica%20sand%2C%20and%20iron%20ore. (Accessed 23 September 2020).
[23] M. Michaux, E.B. Nelson, B. Vidick, 2 Chemistry and Characterization of Portland Cement, Well Cementing1990, pp. 2-1-2-17.
[24] I.G. Richardson, The calcium silicate hydrates, Cement and Concrete Research 38(2) (2008) 137-158.
[25] H.-M. Ludwig, W. Zhang, Research review of cement clinker chemistry, Cement and Concrete Research 78 (2015) 24-37.
[26] M. Courtial, M.N. de Noirfontaine, F. Dunstetter, G. Gasecki, M. Signes-Frehel, Polymorphism of tricalcium silicate in Portland cement: A fast visual identification of structure and superstructure, Powder Diffraction 18(1) (2012) 7-15.
[27] F. Dunstetter, M.N. de Noirfontaine, M. Courtial, Polymorphism of tricalcium silicate, the major compound of Portland cement clinker, Cement and Concrete Research 36(1) (2006) 39-53.
[28] M.N. de Noirfontaine, F. Dunstetter, M. Courtial, G. Gasecki, M. Signes-Frehel, Polymorphism of tricalcium silicate, the major compound of Portland cement clinker, Cement and Concrete Research 36(1) (2006) 54-64.
[29] I. Maki, K. Goto, Factors influencing the phase constitution of alite in portland cement clinker, Cement and Concrete Research 12(3) (1982) 301-308.
[30] T.L. Ávalos-Rendón, E.A.P. Chelala, C.J. Mendoza Escobedo, I.A. Figueroa, V.H. Lara, L.M. Palacios-Romero, Synthesis of belite cements at low temperature from silica fume and natural commercial zeolite, Materials Science and Engineering: B 229 (2018) 79-85.
[31] K.L. Scrivener, P. Juilland, P.J.M. Monteiro, Advances in understanding hydration of Portland cement, Cement and Concrete Research 78 (2015) 38-56.
[32] A.K. Chatterjee, High belite cements—Present status and future technological options: Part I, Cement and Concrete Research 26(8) (1996) 1213-1225.
[33] P.C. Association, N.R.M.C. Association, M. CSHub., Improving Concrete Sustainability Through Alite and Belite Reactivity MIT Concrete Sustainability Hub, 2013.
[34] K.L. Scrivener, A. Nonat, Hydration of cementitious materials, present and future, Cement and Concrete Research 41(7) (2011) 651-665.
[35] A. Kumar, S. Bishnoi, K.L. Scrivener, Modelling early age hydration kinetics of alite, Cement and Concrete Research 42(7) (2012) 903-918.
[36] S. Bishnoi, K.L. Scrivener, Studying nucleation and growth kinetics of alite hydration using μic, Cement and Concrete Research 39(10) (2009) 849-860.
[37] H.F.W. Taylor, Hydration of Portland cement, Cement chemistry1997, pp. 187-225.
[38] P. Feng, C. Miao, J.W. Bullard, R. Riman, Factors Influencing the Stability ofAFm andAFt in the Ca–Al–S–O–H System at 25°C, Journal of the American Ceramic Society 99(3) (2015) 1031-1041.
[39] I. Odler, S. Abdul-Maula, Possibilities of quantitative determination of the AFt-(ettringite) and AFm-(monosulphate) phases in hydrated cement pastes, Cement and Concrete Research 14(1) (1984) 133-141.
[40] N. Winter, Cement hydration. https://www.understanding-cement.com/hydration.html. (Accessed 23 September 2020).
[41] M. Lawrence, A study of carbonation in non-hydraulic lime mortars

Department of Architecture & Civil Engineering, University of Bath 2006.
[42] M.A.N. Oliveira, A Multi–Physics Approach Applied to Masonry Structures with Non–Hydraulic Lime Mortars, University of Minho, 2015.
[43] CEN, EN 459-1:2010 Building lime-Part 1: Definitions, specifications and conformity criteria, 2010.
[44] C. Rodriguez-Navarro, E. Hansen, W.S. Ginell, Calcium Hydroxide Crystal Evolution upon Aging of Lime Putty, Journal of the American Ceramic Society 81(11) (2005) 3032-3034.

[45] M. Arandigoyen, B. Bicer-Simsir, J.I. Alvarez, D.A. Lange, Variation of microstructure with carbonation in lime and blended pastes, Applied Surface Science 252(20) (2006) 7562-7571.
[46] V.A. Juvekar, M.M. Sharma, Absorption of CO2 in a suspension of lime, Chemical Engineering Science 28(3) (1973) 825-837.
[47] K. Van Balen, Carbonation reaction of lime, kinetics at ambient temperature, Cement and Concrete Research 35(4) (2004) 647-657.
[48] Ö. Cizer, K.V. Balen, D.V. Gemert, J. Elsen, Blended lime–cement mortars for conservation purposes: microstructure and strength development, 6th International Conference - Structural Analysis of Historic Construction, 2008, pp. 965-972.
[49] J.R. Welty, C.E. Wicks, R.E. Wilson, G.L. Rorrer, Fundamentals of Momentum, Heat, and Mass Transfer, 5 ed.2000.
[50] Y.S. Han, G. Hadiko, M. Fuji, M. Takahashi, Effect of flow rate and CO2 content on the phase and morphology of CaCO3 prepared by bubbling method, Journal of Crystal Growth 276(3-4) (2005) 541-548.
[51] S. Martinez-Ramirez, S. Sanchez-Cortes, J.V. Garcia-Ramos, C. Domingo, C. Fortes, M.T. Blanco-Varela, Micro-Raman spectroscopy applied to depth profiles of carbonates formed in lime mortar, Cement and Concrete Research 33(12) (2003) 2063-2068.
[52] G. Nehrke, P. Van Cappellen, Framboidal vaterite aggregates and their transformation into calcite: A morphological study, Journal of Crystal Growth 287(2) (2006) 528-530.
[53] M. Tate, The most important property of cement-lime mortar in masonry construction is, International building lime symposium, 2005.
[54] R.T.-R.m. J. Hughes, The role of mortar in masonry: an introduction to requirements for the design of repair mortars, in: J. Válek, C. Groot, J.J. Hughes (Eds.) 2nd Conference on Historic Mortars - HMC 2010 and RILEM TC 203-RHM final workshop, 2010.
[55] Y. Wang, H. He, F. He, Effect of slaked lime and aluminum sulfate on the properties of dry-mixed masonry mortar, Construction and Building Materials 180 (2018) 117-123.
[56] M.J. Mosquera, B. Silva, B. Prieto, E. Ruiz-Herrera, Addition of cement to lime-based mortars: Effect on pore structure and vapor transport, Cement and Concrete Research 36(9) (2006) 1635-1642.
[57] M. Kržan, S. Gostič, S. Cattari, V. Bosiljkov, Acquiring reference parameters of masonry for the structural performance analysis of historical buildings, Bulletin of Earthquake Engineering 13(1) (2014) 203-236.
[58] J. Lanas, J.I. Alvarez-Galindo, Masonry repair lime-based mortars: factors affecting the mechanical behavior, Cement and Concrete Research 33(11) (2003) 1867-1876.
[59] M. Arandigoyen, J.I. Alvarez, Pore structure and mechanical properties of cement–lime mortars, Cement and Concrete Research 37(5) (2007) 767-775.
[60] R. Jaafri, A. Aboulayt, S.-Y. Alam, Influence of lime on the properties of cement-based materials, 10th ACI/RILEM International Conference on Cementitious Materials and Alternative Binders for Sustainable Concrete, Montreal, Canada, 2017.
[61] ASTM, Standard Specification for Mortar for Unit Masonry (Revision 19A), 2019.
[62] J.S. Pozo-Antonio, Evolution of mechanical properties and drying shrinkage in lime-based and lime cement-based mortars with pure limestone aggregate, Construction and Building Materials 77 (2015) 472-478.
[63] A. Moropoulou, A. Bakolas, P. Moundoulas, E. Aggelakopoulou, S. Anagnostopoulou, Strength development and lime reaction in mortars for repairing historic masonries, Cement and Concrete Composites 27(2) (2005) 289-294.
[64] L. Gulbe, I. Vitina, J. Setina, The Influence of Cement on Properties of Lime Mortars, Procedia Engineering 172 (2017) 325-332.

[65] V.G. Haach, R. Carrazedo, L.M.F. Oliveira, Resonant acoustic evaluation of mechanical properties of masonry mortars, Construction and Building Materials 152 (2017) 494-505.
[66] M. Arandigoyen, J.L.P. Bernal, M.A.B. López, J.I. Alvarez, Lime-pastes with different kneading water: Pore structure and capillary porosity, Applied Surface Science 252(5) (2005) 1449-1459.
[67] M. Arandigoyen, J.I. Alvarez, Blended pastes of cement and lime: Pore structure and capillary porosity, Applied Surface Science 252(23) (2006) 8077-8085.
[68] V.S. Ramachandran, R.M. Paroli, J.J. Beaudoin, A.H. Delgado, Handbook of Thermal Analysis of Construction Materials, 2002.
[69] M. Collepardi, G. Baldini, M. Pauri, M. Corradi, Tricalcium aluminate hydration in the presence of lime, gypsum or sodium sulfate, Cement and Concrete Research 8(5) (1978) 571-580.
[70] A. Morandeau, M. Thiéry, P. Dangla, Investigation of the carbonation mechanism of CH and C-S-H in terms of kinetics, microstructure changes and moisture properties, Cement and Concrete Research 56 (2014) 153-170.
[71] J.J. Chen, J.J. Thomas, H.M. Jennings, Decalcification shrinkage of cement paste, Cement and Concrete Research 36(5) (2006) 801-809.
[72] J.J. Chen, J.J. Thomas, H.F.W. Taylor, H.M. Jennings, Solubility and structure of calcium silicate hydrate, Cement and Concrete Research 34(9) (2004) 1499-1519.
[73] ASTM, ASTM C270 - 19ae1 Standard Specification for Mortar for Unit Masonry, 2019.
[74] R. Hendrickx, M. J, K.V. Balen, D.V. Gemert, Workability of mortars with building lime: Assessment by a panel of masons versus lab testing, 14th International Brick and Block Masonry Conference, Sydney, Australia, 2008.
[75] CEN, EN 1015-3:1999 Methods of test for mortar for masonry - Part 3: Determination of consistence of fresh mortar (by flow table), 2007.
[76] CEN, EN 1015-4 Methods of test for mortar for masonry - Part 4: Determination of consistence of fresh mortar (by plunger penetration), 1999.
[77] K. Elert, C. Rodriguez-Navarro, E.S. Pardo, E. Hansen, O. Cazalla, Lime Mortars for the Conservation of Historic Buildings, Studies in Conservation 47(1) (2002).
[78] W.E. Emley, Measurement of plasticity of mortars and plasters Technologic papers of the bureau of standards (1920).
[79] BLA, Lime in mortars and renders (British Lime Association). https://britishlime.org/technical/lime_in_mortars.php. (Accessed 30 September 2020).
[80] M.L. Thomson, Why is type S hydrated lime so special, International Building Lime Symposium, Orlando, Florida, 2005.
[81] C. Ince, M.A. Carter, M.A. Wilson, The water retaining characteristics of lime mortar, Materials and Structures 48(4) (2013) 1177-1185.
[82] R. Hanley, S. Pavía, A study of the workability of natural hydraulic lime mortars and its influence on strength, Materials and Structures 41(2) (2007) 373-381.
[83] M. Tate, The most important property of cement-lime mortar in masonry construction is .... International Building Lime Symposium Orlando, Florida, 2005.
[84] C. Ince, M.A. Carter, M.A. Wilson, N.C. Collier, A. El-Turki, R.J. Ball, G.C. Allen, Factors affecting the water retaining characteristics of lime and cement mortars in the freshly-mixed state, Materials and Structures 44(2) (2010) 509-516.
[85] R. Hendrickx, S. Roels, K. Van Balen, Measuring the water capacity and transfer properties of fresh mortar, Cement and Concrete Research 40(12) (2010) 1650-1655.
[86] K.M. Green, M.A. Carter, W.D. Hoff, M.A. Wilson, The effects of lime and admixtures on the water-retaining properties of cement mortars, Cement and Concrete Research 29(11) (1999) 1743-1747.
[87] R.J. S., B.R. L., Investigation of Commercial Masonry Cements, Journal of Research of the National Bureau of Standards 13 (1934).

[88] P.L. A., P.D. A., A study of the properties of mortars and bricks and their relation to bond, Bureau of Standards Journal of Research 12 (1934).
[89] X. Chen, S. Wu, J. Zhou, Influence of porosity on compressive and tensile strength of cement mortar, Construction and Building Materials 40 (2013) 869-874.
[90] G. Xiaoyu, F. Yingfang, L. Haiyang, The compressive behavior of cement mortar with the addition of nano metakaolin, Nanomaterials and Nanotechnology 8 (2018).
[91] V.G. Haach, L.M. Juliani, M.R.D. Roz, Ultrasonic evaluation of mechanical properties of concretes produced with high early strength cement, Construction and Building Materials 96 (2015) 1-10.
[92] A. Drougkas, P. Roca, C. Molins, Compressive strength and elasticity of pure lime mortar masonry, Materials and Structures 49(3) (2015) 983-999.
[93] CEN, EN 1992-1-1 Eurocode 2 - Design of concrete structures - Part 1-1 : General rules and rules for buildings, 2004.
[94] L. Garijo, X. Zhang, G. Ruiz, J.J. Ortega, R.C. Yu, Advanced mechanical characterization of NHL mortars and cohesive simulation of their failure behavior, Construction and Building Materials 153 (2017) 569-577.
[95] S.M. Macharia, Creep mechanisms in cement and lime mortared masonry Department of architecture and civil engineering University of Bath Somerset, United Kingdom, 2015, p. 338.
[96] V.G. Haach, G. Vasconcelos, P.B. Lourenço, Influence of aggregates grading and water/cement ratio in workability and hardened properties of mortars, Construction and Building Materials 25(6) (2011) 2980-2987.
[97] M.M.T. Lakshani, T.K.G.A. Jayathilaka, J.A. Thamboo, Experimental investigation of the unconfined compressive strength characteristics of masonry mortars, Journal of Building Engineering 32 (2020).
[98] M. Stefanidou, I. Papayianni, The role of aggregates on the structure and properties of lime mortars, Cement and Concrete Composites 27(9-10) (2005) 914-919.
[99] B.V. Venkatarama Reddy, A. Gupta, Influence of sand grading on the characteristics of mortars and soil–cement block masonry, Construction and Building Materials 22(8) (2008) 1614-1623.
[100] R.M. Ferreira, S. Jalali, NDT measurements for the prediction of 28-day compressive strength, NDT & E International 43(2) (2010) 55-61.
[101] M. Gomez-Heras, D. Benavente, C. Pla, J. Martinez-Martinez, R. Fort, V. Brotons, Ultrasonic pulse velocity as a way of improving uniaxial compressive strength estimations from Leeb hardness measurements, Construction and Building Materials 261 (2020).
[102] T. Voigt, Z. Sun, S.P. Shah, Comparison of ultrasonic wave reflection method and maturity method in evaluating early-age compressive strength of mortar, Cement and Concrete Composites 28(4) (2006) 307-316.
[103] M.T. Liang, J. Wu, Theoretical elucidation on the empirical formulae for the ultrasonic testing method for concrete structures, Cement and Concrete Research 32(11) (2002) 1763-1769.
[104] G. Vasconcelos, Experimental investigations on the mechanics of stone masonry: Characterization of granites and behavior of ancient masonry shear walls, School of Engineering, Universidade do Minho, Guimaraes, Portugal 2005.
[105] G. Mavko, Basic Geophysical Concepts. https://pt.slideshare.net/oncel/rock-physics-basic-concepts. (Accessed 23-07 2020).
[106] J. Valek, M.D.R. Veiga, Characterisation of mechanical properties of historic mortars - Testing of irregular samples, WIT Transactions on the Built Environment 20 (2005) 365-374.
[107] R. Veiga, Air lime mortars: What else do we need to know to apply them in conservation and rehabilitation interventions? A review, Construction and Building Materials 157 (2017) 132-140.
[108] P. Cikrle, J. Adámek, M. Stehlik, Ultrasonic testing of properties of mortars, 5th SAHC conference - Structural Analysis of Historical Constructions 2005, pp. 407-412.

[109] G.N. Özerkan, Ö.Đ. Yaman, Evaluation of cement mortars by ultrasound 4th Middle East NDT Conference and Exhibition, Kingdom of Bahrain, 2007.
[110] I. Palomar, G. Barluenga, Assessment of lime-cement mortar microstructure and properties by P- and S- ultrasonic waves, Construction and Building Materials 139 (2017) 334-341.
[111] V. Rosário, S. Maria, B. Kristin, I.A. José, N. Cristiana, T. Magdalini, F. Paulina, P. Ioanna, v.H. Rob, Durability of lime based renders: A review of some degredation mechanisms and assessment test methods, RILEM Spring Convention & International Conference on Sustainable Materials, Systems and Structures, RILEM Publications SARL, Rovinj, Croatia 2019.
[112] L. Berto, Failure mechanism of masonry prism loaded in axial compression: computational aspects, Materials and Structures 38(276) (2005) 249-256.
[113] H.H. K, Investigation into the failure mechanism of brick masonry loaded in axial compression, Proceedings of International Conference on Masonry Structural Systems, Gulf Publishing Co, Houston, Texas, 1969.
[114] V.G. Haach, R. Carrazedo, L.M.F. Oliveira, M.R.S. Corrêa, Application of acoustic tests to mechanical characterization of masonry mortars, NDT & E International 59 (2013) 18-24.
[115] J. Granja, Continuous characterization of stiffness of cement - based materials: experimental analysis and micro-mechanics modelling, Universidade do Minho, Portugal 2016.
[116] A.I. Marques, J. Morais, P. Morais, M.d.R. Veiga, C. Santos, P. Candeias, J.G. Ferreira, Modulus of elasticity of mortars: Static and dynamic analyses, Construction and Building Materials 232 (2020).
[117] CEN, EN 12390-13:2013 Testing hardened concrete. Determination of secant modulus of elasticity in compression, 2013.
[118] G. Mohamad, F.S. Fonseca, H.R. Roman, A. Vermeltfoort, E. Rizzatti, Behavior of mortar under multiaxial stress, 12th North American Masonry Conference, Denver, Colorado, 2015.
[119] P. Walker, S. Kioy, A. Jowsey, An experimental comparison of hydrated lime and an admixture for masonry mortars, 9th International Masonry Conference 2014.
[120] P. Mira, V.G. Papadakis, S. Tsimas, Effect of lime putty addition on structural and durability properties of concrete, Cement and Concrete Research 32(5) (2002) 683-689.
[121] J.R. Rosell, I.R. Cantalapiedra, Método simple para determinar el módulo de Young dinámico a partir de una excitación por impacto, aplicado a morteros de cal y cemento, Materiales de Construcción 61(301) (2010) 39-48.
[122] T. Kanstad, T.A. Hammer, Ø. Bjøntegaard, E.J. Sellevold, Mechanical properties of young concrete: Part I: Experimental results related to test methods and temperature effects, Materials and Structures 36(4) (2003) 218-225.
[123] T. Kanstad, T.A. Hammer, Ø. Bjøntegaard, E.J. Sellevold, Mechanical properties of young concrete: Part II: Determination of model parameters and test program proposals, Materials and Structures 36(4) (2003) 226-230.
[124] J.L.D. Granja, M. Azenha, C.F. Sousa, C. Ferreira, Comparison between different experimental techniques for stiffness monitoring of cement pastes, Journal of Advanced Concrete Technology (2014).
[125] B. Delsaute, C. Boulay, J. Granja, J. Carette, M. Azenha, C. Dumoulin, G. Karaiskos, A. Deraemaeker, S. Staquet, Testing Concrete E-modulus at Very Early Ages Through Several Techniques: An Inter-laboratory Comparison, Strain 52(2) (2016) 91-109.
[126] B. Delsaute, S. Staquet, Testing Concrete Since Setting Time Under Free and Restrained Conditions, Advanced Techniques for Testing of Cement-Based Materials2020, pp. 177-209.
[127] M. Azenha, J. Silva, J. Granja, A. Gomes-Correia, A Retrospective View of EMM-ARM: Application to Quality Control in Soil-improvement and Complementary Developments, Procedia Engineering 143 (2016) 339-346.
[128] J. Silva, Continuous monitoring of deformability of stabilized soils based on modalidentification, Universdade do Minho 2017.

[129] J. Granja, M. Azenha, Towards a robust and versatile method for monitoring E-modulus of concrete since casting: Enhancements and extensions of EMM-ARM, Strain 53(4) (2017).
[130] D. Rosato, D. Rosato, Design Parameter, Plastics Engineered Product Design2003, pp. 161-197.
[131] M. Dhanasekar, P.W. Kleeman, A.W. Page, Biaxial Stress-strain Relations for Brick Masonry, Journal of Structural Engineering 111(5) (1985) 1085-1100.
[132] J.J. Brooks, Elasticity of Masonry, Concrete and Masonry Movements2015, pp. 95-136.
[133] G. Mohamad, P.B. Lourenço, H. Roman, Poisson behaviour of bedding mortar under multiaxial stress state, 2006.
[134] A.T. Vermeltfoort, Brick-mortar interaction in masonry under compression, Technische Universiteit Eindhoven, 2005.
[135] L. Berto, A. Saetta, R. Scotta, R. Vitaliani, Failure mechanism of masonry prism loaded in axial compression: computational aspects, Materials and Structures 38(2) (2005) 249-256.
[136] R.H. Atkinson, J.L. Noland, D.P. Abrams, S. McNary, Deformation Failure Theory For Stack-Bond Brick Masonry Prisms In Compression, Third North American Masonry Conference, Arlington, Texas, 1985.
[137] G. Mohamad, F.S. Fonseca, A.T. Vermeltfoort, A. Lubeck, Stiffness plasticity degradation of masonry mortar under compression: preliminar results, Revista IBRACON de Estruturas e Materiais 11(2) (2018) 279-295.
[138] R. Hayen, K.V. Balen, D. Gemert, The mechanical behaviour of mortars in triaxial compression, 2003.
[139] M. Kohees, J. Sanjayan, P. Rajeev, Stress-strain relationship of cement mortar under triaxial compression, Construction and Building Materials 220 (2019) 456-463.
[140] N.S. Ottosen, Constitutive Model for Short-Time Loading of Concrete, 1979.
[141] C.V. Uday Vyas, B.V. Venkatarama Reddy, Prediction of solid block masonry prism compressive strength using FE model, Materials and Structures 43(5) (2009) 719-735.
[142] S.Y. Wang, S.W. Sloan, A.J. Abbo, M.J. Masia, C.A. Tang, Numerical simulation of the failure process of unreinforced masonry walls due to concentrated static and dynamic loading, International Journal of Solids and Structures 49(2) (2012) 377-394.
[143] A. Zucchini, P.B. Lourenço, Mechanics of masonry in compression: Results from a homogenisation approach, Computers & Structures 85(3-4) (2007) 193-204.
[144] W. Yao, K. Xia, H.-W. Liu, Influence of heating on the dynamic tensile strength of two mortars: Experiments and models, International Journal of Impact Engineering 122 (2018) 407-418.
[145] A. Gudmarsson, N. Ryden, H. Di Benedetto, C. Sauzéat, Complex modulus and complex Poisson's ratio from cyclic and dynamic modal testing of asphalt concrete, Construction and Building Materials 88 (2015) 20-31.
[146] J. Carrillo, J. Ramirez, J. Lizarazo-Marriaga, Modulus of elasticity and Poisson's ratio of fiber-reinforced concrete in Colombia from ultrasonic pulse velocities, Journal of Building Engineering 23 (2019) 18-26.
[147] J.J. Brooks, Elasticity of Concrete, Concrete and Masonry Movements2015, pp. 61-93.
[148] A. Zucchini, P.B. Lourenço, A micro-mechanical model for the homogenisation of masonry, International Journal of Solids and Structures 39(12) (2002) 3233-3255.
[149] A. Brencich, C. Corradi, L. Gambarotta, G. Mantegazza, E. Sterpi, Compressive Strength Of Solid Clay Brick Masonry Under Eccentric Loading, 6th International Masonry Conference, London, UK, 2002.
[150] A.J. Francis, H.C. B, J.L. E, The effect of joint thickness and other factors on the compressive strength of brickwork, Second International Brick Masonry Conference, Stoke-on-Trent, 1971, pp. 31-37.
[151] N. Batista, M.F.P. Pereira, J.L.B.d. Aguiar, Mechanical characterization for mortar for masonry Fifth International Conference on Construction in the 21st Century (CITC-V) "Collaboration and Integration in Engineering, Management and Technology", Istanbul, Turkey, 2009.

[152] A.T. Zehnder, Griffith Theory of Fracture, Encyclopedia of Tribology2013, pp. 1570-1573.
[153] F. Wittmann, Z. Sun, T. Zhao, Strength and fracture energy of concrete in seawater, 2007.
[154] G.A. Arnold, The phenomena of rupture and flow in solids, Philosophical Transactions of the Royal Society of London. Series A, Containing Papers of a Mathematical or Physical Character 221(582-593) (1921) 163-198.
[155] R. David, Introduction to fracture mechanics Department of Materials Science and Engineering, Massachusetts Institute of Technology, 2001.
[156] T.H. Courtney, Mechanical Behavior of Materials, McGraw-Hill, New York, 1990.
[157] A. Hillerborg, M. Modéer, P.E. Petersson, Analysis of crack formation and crack growth in concrete by means of fracture mechanics and finite elements, Cement and Concrete Research 6(6) (1976) 773-781.
[158] RILEM, 50-FMC, Determination of the fracture energy of mortar and concrete by means of three-point bend tests on notched beams, Materials and Structures 18(484) (1985) 287-290.
[159] N.P. Uday, Experimental Determination of Fracture Energy by RILEM Method, The International Journal of Engineering and Science 06(03) (2017) 106-115.
[160] G.V. Guinea, J. Planas, M. Elices, Measurement of the fracture energy using three-point bend tests: Part 1—Influence of experimental procedures, Materials and Structures 25(4) (1992) 212-218.
[161] J. Planas, M. Elices, G.V. Guinea, Measurement of the fracture energy using three-point bend tests: Part 2—Influence of bulk energy dissipation, Materials and Structures 25(5) (1992) 305-312.
[162] M. Elices, G.V. Guinea, J. Planas, Measurement of the fracture energy using three-point bend tests: Part 3—influence of cutting theP-δ tail, Materials and Structures 25(6) (1992) 327-334.
[163] L. Garijo, X. Zhang, G. Ruiz, J.J. Ortega, Age effect on the mechanical properties of natural hydraulic and aerial lime mortars, Construction and Building Materials 236 (2020).
[164] J. García-Cuadrado, A. Rodríguez, I.I. Cuesta, V. Calderón, S. Gutiérrez-González, Study and analysis by means of surface response to fracture behavior in lime-cement mortars fabricated with steelmaking slags, Construction and Building Materials 138 (2017) 204-213.
[165] Z. Zhao, S.H. Kwon, S.P. Shah, Effect of specimen size on fracture energy and softening curve of concrete: Part I. Experiments and fracture energy, Cement and Concrete Research 38(8-9) (2008) 1049-1060.
[166] S. Khalilpour, E. BaniAsad, M. Dehestani, A review on concrete fracture energy and effective parameters, Cement and Concrete Research 120 (2019) 294-321.
[167] M.R.M. Aliha, A. Razmi, A. Mansourian, The influence of natural and synthetic fibers on low temperature mixed mode I + II fracture behavior of warm mix asphalt (WMA) materials, Engineering Fracture Mechanics 182 (2017) 322-336.
[168] F. Kesikidou, M. Stefanidou, Natural fiber-reinforced mortars, Journal of Building Engineering 25 (2019).
[169] V. Nežerka, J. Zeman, J. Němeček, Micromechanics-based simulations of compressive and tensile testing on lime-based mortars, Mechanics of Materials 105 (2017) 49-60.
[170] Y. Zhu, S.L. Xu, Fracture properties of cement paste and mortar : an experimental investigation, 2007.
[171] M. Naftaly, I. Tikhomirov, P. Hou, D. Markl, Measuring Open Porosity of Porous Materials Using THz-TDS and an Index-Matching Medium, Sensors 20(11) (2020).
[172] S. Maria, Methods for porosity measurement in lime-based mortars, Construction and Building Materials 24(12) (2010) 2572-2578.
[173] H. Paiva, A. Velosa, R. Veiga, V.M. Ferreira, Effect of maturation time on the fresh and hardened properties of an air lime mortar, Cement and Concrete Research 40(3) (2010) 447-451.
[174] R.F. Feldman, P.J. Sereda, A model for hydrated Portland cement paste as deduced from sorption-length change and mechanical properties, Matériaux et Constructions 1(6) (1968) 509-520.

[175] J. Lanas, R. Sirera, J.I. Alvarez, Study of the mechanical behavior of masonry repair lime-based mortars cured and exposed under different conditions, Cement and Concrete Research 36(5) (2006) 961-970.
[176] RILEM, TC 25-PEM, Recommended tests to measure the deterioration of stone and to assess the effectiveness of treatment methods, Materials and Structures 13(75) (1980) 175-253.
[177] A. Anna, C. Giuseppe, The water transfer properties and drying shrinkage of aerial lime-based mortars: an assessment of their quality as repair rendering materials, Environmental Earth Sciences 71(4) (2013) 1699-1710.
[178] ASTM, ASTM C595-01 Standard Test Method for Drying Shrinkage of Mortar Containing Hydraulic Cement, 2001.
[179] W. Mateusz, D.B. Carmelo, L. Pietro, Prediction of Drying Shrinkage of Cement-based Mortars with Poroelastic Approaches – A Critical Review, 6th Biot Conference on Poromechanics, Paris, France, 2017.
[180] Z.P. Bažant, J.-K. Kim, Consequences of diffusion theory for shrinkage of concrete, Materials and Structures 24(5) (1991) 323-326.
[181] T. Shimomura, K. Maekawa, Analysis of the drying shrinkage behaviour of concrete using a micromechanical model based on the micropore structure of concrete, Magazine of Concrete Research 49(181) (1997) 303-322.
[182] V. Baroghel-Bouny, M. Mainguy, T. Lassabatere, O. Coussy, Characterization and identification of equilibrium and transfer moisture properties for ordinary and high-performance cementitious materials, Cement and Concrete Research 29(8) (1999) 1225-1238.
[183] J. Hogancamp, Z. Grasley, The use of microfine cement to enhance the efficacy of carbon nanofibers with respect to drying shrinkage crack resistance of portland cement mortars, Cement and Concrete Composites 83 (2017) 405-414.
[184] O.Z. Cebeci, S.I. Al-Noury, W.H. Mirza, Strength and drying shrinkage of masonary mortars in various temperature-humidity environments, Cement and Concrete Research 19(1) (1989) 53-62.
[185] M. Lenart, Assessment of Mortar Shrinkage in Aspect of Organic and Inorganic Modifiers Use, Procedia Engineering 108 (2015) 309-315.
[186] H. Beushausen, P. Arito, The influence of mix composition, w/b ratio and curing on restrained shrinkage cracking of cementitious mortars, Construction and Building Materials 174 (2018) 38-46.
[187] A.S. Smith, R. Givens, A review of research and experimental findings on the effects of hydrated (air) lime addition to cement-based masonry mortars on the properties of the mortars and associated masonry, Brick and Block Masonry2016, pp. 1897-1904.
[188] W. Zhang, Y. Hama, S.H. Na, Drying shrinkage and microstructure characteristics of mortar incorporating ground granulated blast furnace slag and shrinkage reducing admixture, Construction and Building Materials 93 (2015) 267-277.
[189] C. Li, Q. Wang, J. Chen, S. Jia, L. Jiang, J. He, Effect of polyether-type SRA on the drying shrinkage, pore structure and properties of blended mortar incorporating limestone powder, Construction and Building Materials 264 (2020).
[190] M. Wu, Y. Zhang, Y. Jia, W. She, G. Liu, Study on the role of activators to the autogenous and drying shrinkage of lime-based low carbon cementitious materials, Journal of Cleaner Production 257 (2020).
[191] P. Ioanna, Creep Deformation of Lime-based Repair Mortars. The Effect of Aggregate Size, 13th International Brick and Block Masonry Conference Amsterdam, Netherlands, 2004.
[192] B. Raudhah, Shrinkage in lime stucco: Does “banking” mortar help mitigate shrinkage? , Graduate School of Architecture, Planning and Preservation Columbia University 2016.
[193] A.W. Hendry, Masonry Materials in Compression, in: A.W. Hendry (Ed.), Structural Masonry, Macmillan Education UK, London, 1998, pp. 16-55.
[194] C.R. Willis, Design of unreinforced masonry walls for out-of-plane loading, School of civil and environmental engineering University of Adelaide 2004.

[195] S.B. Singh, P. Munjal, Bond strength and compressive stress-strain characteristics of brick masonry, Journal of Building Engineering 9 (2017) 10-16.
[196] A. Rahman, T. Ueda, Experimental Investigation and Numerical Modeling of Peak Shear Stress of Brick Masonry Mortar Joint under Compression, Journal of Materials in Civil Engineering 26(9) (2014).
[197] F. Verhelst, E. Kjaer, W. Jaeger, B. Middendorf, K.V. Balen, P. Walker, Sustainable masonry: The importance of mortar quality, 15th International Brick and Block Masonry Conference Florianópolis, Brazil 2012.
[198] J.A. Thamboo, M. Dhanasekar, Correlation between the performance of solid masonry prisms and wallettes under compression, Journal of Building Engineering 22 (2019) 429-438.
[199] K. Cheng-lim, A failure criterion for brickwork in axial compression, Department of Civil Engineering & Building Science University of Edinburgh, Edinburgh, Scotland, 1972.
[200] G. Sarangapani, B.V. Venkatarama Reddy, K.S. Jagadish, Brick-Mortar Bond and Masonry Compressive Strength, Journal of Materials in Civil Engineering 17(2) (2005) 229-237.
[201] N.N. Thaickavil, J. Thomas, Behaviour and strength assessment of masonry prisms, Case Studies in Construction Materials 8 (2018) 23-38.
[202] M.B. Ravula, K.V.L. Subramaniam, Experimental investigation of compressive failure in masonry brick assemblages made with soft brick, Materials and Structures 50(1) (2016).
[203] S.R. Balasubramanian, D. Maheswari, A. Cynthia, K. Balaji Rao, R. Goswami, P. Sivakumar, Experimental Determination of Statistical Parameters Associated with Uniaxial Compression Behaviour of Brick Masonry, Current Science 109(11) (2015).
[204] D.C. Rai, S.C. Goel, Seismic Strengthening of Unreinforced Masonry Piers with Steel Elements, Earthquake Spectra 12(4) (2019) 845-862.
[205] G. Sarangapani, V.B.V. Reddy, K.S. Jagadish, Structural characteristics of bricks, mortar and masonry, Journal of Structural Engineering 29 (2002).
[206] M. Tomaževič, Earthquake-Resistant Design of Masonry Buildings, Imperial College Press1999.
[207] P. Murthi, M. Bhavani, M.S. Musthaq, M.O. Jauhar, V. Rama Devi, Development of relationship between compressive strength of brick masonry and brick strength, Materials Today: Proceedings (2020).
[208] P.B. Lourenço, L.F. Ramos, Characterization of Cyclic Behavior of Dry Masonry Joints, Journal of Structural Engineering 130(5) (2004) 779-786.
[209] J. Liu, The effect of height-to-thickness ratio on the compressive strength of concrete masonry, 2012.
[210] H.E. Wong, R.G. Drysdale, Compression Characteristics of Concrete Block Masonry Prisms, Masonry: Research, Application, and Problems1985, pp. 167-167-11.
[211] F.M. Khalaf, Factors influencing compressive strength of concrete masonry prisms, Magazine of Concrete Research 48(175) (1996) 95-101.
[212] B. Zengin, B. Toydemir, S. Ulukaya, D. Oktay, N. Yuzer, A. Kocak, The effect of mortar type and joint thickness on mechanical properties of conventional masonry walls, Structural Engineering and Mechanics 67(6) (2018) 579-585.
[213] B.V.V. Reddy, R. Lal, K.S.N. Rao, Influence of Joint Thickness and Mortar-Block Elastic Properties on the Strength and Stresses Developed in Soil-Cement Block Masonry, Journal of Materials in Civil Engineering 21(10) (2009) 535-542.
[214] S.M. Monteagudo, M.J. Casati, J.C. Gálvez, Influence of the bed joint thickness on the bearing capacity of the brick masonry under compression loading: an ultrasound assessment, Revista de la construcción 14(1) (2015) 9-15.
[215] N.G. Shrive, Compressive strength and strength testing of masonry 7th International Brick and Block Masonry Conference, Melbourne, Australia, 1985.

[216] K.S. Gumaste, K.S. Nanjunda Rao, B.V. Venkatarama Reddy, K.S. Jagadish, Strength and elasticity of brick masonry prisms and wallettes under compression, Materials and Structures 40(2) (2006) 241-253.
[217] P.G. Asteris, I. Argyropoulos, L. Cavaleri, H. Rodrigues, H. Varum, J. Thomas, P.B. Lourenço, Masonry Compressive Strength Prediction Using Artificial Neural Networks, in: A. Moropoulou, M. Korres, A. Georgopoulos, C. Spyrakos, C. Mouzakis (Eds.) Transdisciplinary Multispectral Modeling and Cooperation for the Preservation of Cultural Heritage, Springer International Publishing, Cham, 2019, pp. 200-224.
[218] L. Binda, A. Fontana, G. Frigerio, Mechanical behavior of brick masonries derived from unit and mortar characteristics, 8th International Brick and Block Masonry Conference, Dublin, Ireland, 1988.
[219] M.J.N. Priestley, D.M. Elder, Stress-Strain Curves for Unconfined and Confined Concrete Masonry, ACI Journal Proceedings 80(3) (1983).
[220] J. Garzón-Roca, C.O. Marco, J.M. Adam, Compressive strength of masonry made of clay bricks and cement mortar: Estimation based on Neural Networks and Fuzzy Logic, Engineering Structures 48 (2013) 21-27.
[221] K. Chaimoon, M.M. Attard, Modeling of unreinforced masonry walls under shear and compression, Engineering Structures 29(9) (2007) 2056-2068.
[222] P.B. Lourenço, G. Milani, A. Tralli, A. Zucchini, Analysis of masonry structures: review of and recent trends in homogenization techniques, Canadian Journal of Civil Engineering 34(11) (2007) 1443-1457.
[223] M. Mishra, A.S. Bhatia, D. Maity, Predicting the compressive strength of unreinforced brick masonry using machine learning techniques validated on a case study of a museum through nondestructive testing, Journal of Civil Structural Health Monitoring 10(3) (2020) 389-403.
[224] C. Dymiotis, B.M. Gutlederer, Allowing for uncertainties in the modelling of masonry compressive strength, Construction and Building Materials 16(8) (2002) 443-452.
[225] F.B. Lima, A.N. Lima, W.S. Assis, Study of the influence of compressive strength and thickness of capping-mortar and compressive strength of prisms of structural clay blocks 15th International Brick and Block Masonry Conference, Brazil, 2012.
[226] A.W.H. Fouad M. Khalaf, R.F. Daniel, Study of the Compressive Strength of Blockwork Masonry, ACI Structural Journal 91(4).
[227] P. Dayaratnam, Brick and reinforced brick structures, Oxford and IBH, New Delhi, India, 1987.
[228] W. Mann, Statistical evaluation of tests on masonry by potential functions, 6th International Brick Masonry Conference, Rome, Italy 1982.
[229] K. Sajanthan, B. Balagasan, N. Sathiparan, Prediction of Compressive Strength of Stabilized Earth Block Masonry, Advances in Civil Engineering 2019 (2019) 1-13.
[230] R.M. Bennett, K.A. Boyd, R.D. Flanagan, Compressive Properties of Structural Clay Tile Prisms, Journal of Structural Engineering 123(7) (1997) 920-926.
[231] F.C. Christy, D. Tensing, M.R. Shanthi, Experimental study on axial compressive strength and elastic modulus of the clay and fly ash brick masonry, Journal of Civil Engineering and Construction Technology (2013).
[232] H.R. Kumavat, An Experimental Investigation of Mechanical Properties in Clay Brick Masonry by Partial Replacement of Fine Aggregate with Clay Brick Waste, Journal of The Institution of Engineers (India): Series A 97(3) (2016) 199-204.
[233] A.W. Hendry, M.H. Malek, Characteristic compressive strength of brickwork walls from collected test results, 7th International Masonry Conference 1986.
[234] S.R. Sarhat, E.G. Sherwood, The prediction of compressive strength of ungrouted hollow concrete block masonry, Construction and Building Materials 58 (2014) 111-121.

[235] R. Lumantarna, D.T. Biggs, J.M. Ingham, Uniaxial Compressive Strength and Stiffness of Field-Extracted and Laboratory-Constructed Masonry Prisms, Journal of Materials in Civil Engineering 26(4) (2014) 567-575.
[236] M. Rostampour, Aspects of the design of the multistorey buildings in light-weight concrete blockwork, Department of Civil. Engineering and Building Science University of Edinburgh, Edinburgh, Scotland, 1973.
[237] J. Thomas, E.M. Ansar, Parametric study of the strength of brickwork prisms, First CUSAT National Conference on Recent Advances in Civil Engineering, Kochi, India, 2004.
[238] A.A. Hamid, B.E. Abboud, H.G. Harris, Direct Modeling of Concrete Block Masonry Under Axial Compression, Masonry: Research, Application, and Problems1985, pp. 151-151-16.
[239] G. Mohamad, P.B. Lourenço, H.R. Roman, Mechanics of hollow concrete block masonry prisms under compression: Review and prospects, Cement and Concrete Composites 29(3) (2007) 181-192.
[240] A. Costigan, S. Pavía, Compressive, flexural and bond strength of brick/lime mortar masonry, PROHITEC Taylor and Francis Group, London, 2009, pp. 1609-1615.
[241] R. de C.S.S. Alvarenga, G.H. Nalon, L.A.F. Fioresi, M.C. Pinto, L.G. Pedroti, J.C.L. Ribeiro, Experimental Evaluation of the Influence of Mortar's Mechanical Properties on the Behavior of Clay Masonry, Characterization of Minerals, Metals, and Materials 20172017, pp. 671-679.
[242] A. Zucchini, P.B. Lourenço, A coupled homogenisation–damage model for masonry cracking, Computers & Structures 82(11-12) (2004) 917-929.
[243] V.G. Haach, G. Vasconcelos, P.B. Lourenço, G. Mohamad, Influence of the mortar on the compressive behavior of concerete masonry prisms Experimental Mechanics (Portuguese Association for Experimental Stress Analysis) 18 (2010).
[244] X. Wang, C.C. Lam, V.P. Iu, Characterization of mechanical behaviour of grey clay brick masonry in China, Construction and Building Materials 262 (2020).
[245] S.M. Moayedian, M. Hejazi, Stress-strain relationships for scaled gypsum mortar and cement mortar brick masonry, Journal of Building Engineering 33 (2021).
[246] N. Krishna, S. Sachidan, Model for Cyclic Compressive Behavior of Brick Masonry, ACI Structural Journal 88(5) (1991).
[247] J. Thamboo, M. Dhanasekar, Assessment of the characteristics of lime mortar bonded brickwork wallettes under monotonic and cyclic compression, Construction and Building Materials 261 (2020).
[248] I.C. Council, International Building Code, 2003.
[249] R.G. Drysdale, A.A. Hamid, L.R. Baker, Masonry structures : behavior and design, Englewood Cliffs, New Jersey 1994.
[250] K.-H. Yang, Y. Lee, Y.-H. Hwang, A Stress-Strain Model for Brick Prism under Uniaxial Compression, Advances in Civil Engineering 2019 (2019) 1-10.
[251] T. Paulay, M.J.N. Priestly, Seismic Design of Reinforced Concrete and Masonry Buildings, 1992.
[252] D.C. Kent, R. Park, Flexural Members with Confined Concrete, 1971.
[253] D. Manicka, G.S. Nigel, Strength and Deformation of Confined and Unconfined Grouted Concrete Masonry, ACI Structural Journal 99(6) (2002).
[254] H.H. Knutson, The stress-strain relationship for Masonry, Journal of the British Masonry Society (Masonry International) (1993).
[255] G. Mohamad, P.B. Lourenço, H.R. Roman, C.d.S. Barbosa, E. Rizzatti, Stress-strain behavior of concrete block masonry prisms under compression, 15th International Brick and Block Masonry Conference Brazil, 2012.
[256] F. Sawko, M.A. Rouf, Technical Note. On the Stiffness Properties of Masonry, Proceedings of the Institution of Civil Engineers 77(1) (1984) 1-12.
[257] Q. Zhou, F. Wang, F. Zhu, X. Yang, Stress–strain model for hollow concrete block masonry under uniaxial compression, Materials and Structures 50(2) (2016).

[258] M. Valente, G. Milani, Advanced numerical insights into failure analysis and strengthening of monumental masonry churches under seismic actions, Engineering Failure Analysis 103 (2019) 410-430.
[259] A. Penna, P. Morandi, M. Rota, C.F. Manzini, F. da Porto, G. Magenes, Performance of masonry buildings during the Emilia 2012 earthquake, Bulletin of Earthquake Engineering 12(5) (2013) 2255-2273.
[260] S. Lagomarsino, Damage assessment of churches after L'Aquila earthquake (2009), Bulletin of Earthquake Engineering 10(1) (2011) 73-92.
[261] P.K.V.R. Padalu, Y. Singh, S. Das, Analytical modelling of out-of-plane flexural response of unreinforced and strengthened masonry walls, Engineering Structures 218 (2020).
[262] S. Banerjee, S. Nayak, S. Das, Shear and flexural behaviour of unreinforced masonry wallets with steel wire mesh, Journal of Building Engineering 30 (2020).
[263] L. La Mendola, M. Papia, G. Zingone, Stability of Masonry Walls Subjected to Seismic Transverse Forces, Journal of Structural Engineering 121(11) (1995) 1581-1587.
[264] N. Giordano, P. Crespi, A. Franchi, Flexural strength-ductility assessment of unreinforced masonry cross-sections: analytical expressions, Engineering Structures 148 (2017) 399-409.
[265] P.B. Lourenço, N. Mendes, R. Marques, Earthquake Design and Assessment of Masonry Structures: Review and Applications, Trends in Civil and Structural Engineering Computing2009, pp. 77-101.
[266] J.J. Roberts, O. Brooker, How to design masonry structures using Eurocode 6 - Part 3: Lateral resistance, How to design masonry structures using Eurocode 6, MPA The Concrete Centre, 38-44 Gillingham Street, London.
[267] R.G. Drysdale, A.S. Essawy, Out-of-Plane Bending of Concrete Block Walls, Journal of Structural Engineering 114(1) (1988) 121-133.
[268] R.B. Duarte, B.P. Sinha, Lateral Strength of Brickwork Panels with Openings, Proceedings of the Institution of Civil Engineers - Structures and Buildings 94(4) (1992) 397-402.
[269] B.P. Sinha, C.L. Ng, R.F. Pedreschi, Failure Criterion and Behavior of Brickwork in Biaxial Bending, Journal of Materials in Civil Engineering 9(2) (1997) 70-75.
[270] CEN, EN 1052-2:1999 Methods of test for masonry - Part 2: Determination of flexural strength, 1999.
[271] V. Singhal, D.C. Rai, Suitability of Half-Scale Burnt Clay Bricks for Shake Table Tests on Masonry Walls, Journal of Materials in Civil Engineering 26(4) (2014) 644-657.
[272] G. Melis, Displacement-based seismic analysis for out of plane bending of unreinforced masonry walls, Rose School, University of Pavia, Italy, 2002.
[273] L. Sorrentino, D. D'Ayala, G. de Felice, M.C. Griffith, S. Lagomarsino, G. Magenes, Review of Out-of-Plane Seismic Assessment Techniques Applied To Existing Masonry Buildings, International Journal of Architectural Heritage (2016) 1-20.
[274] D.D. Ayala, E. Speranza, An integrated procedure for the assessment of seismic vulnerability of historic buildings, 2002.
[275] R.V.D. Pluijm, Out-of-plane bending of masonry : behaviour and strength, Technische Universiteit Eindhoven, 1999.
[276] K. Gourav, B.V. Venkatarama Reddy, Out-of-plane flexure behaviour of fly ash-lime-gypsum brick masonry walls, Engineering Structures 173 (2018) 241-250.
[277] C. Jayasinghe, R.S. Mallawaarachchi, Flexural strength of compressed stabilized earth masonry materials, Materials & Design 30(9) (2009) 3859-3868.
[278] F. Graziotti, U. Tomassetti, A. Penna, G. Magenes, Out-of-plane shaking table tests on URM single leaf and cavity walls, Engineering Structures 125 (2016) 455-470.
[279] S.B. Singh, R. Patil, P. Munjal, Study of flexural response of engineered cementitious composite faced masonry structures, Engineering Structures 150 (2017) 786-802.

[280] T.C. Triantafillou, Strengthening of Masonry Structures Using Epoxy-Bonded FRP Laminates, Journal of Composites for Construction 2(2) (1998) 96-104.
[281] CEN, EN 1052-5:2005 Methods of test for masonry - Part 5: Determination of bond strength by the bond wrench method, 2005.
[282] M.J. Masia, G. Simundic, A.W. Page, Assessment of the AS3700 relationship between shear bond strength and flexural tensile bond strength in unreinforced masonry 15th International Brick and Block Masonry Conference, Florianópolis, Brazil, 2012.
[283] S. Jafari, J.G. Rots, R. Esposito, F. Messali, Characterizing the Material Properties of Dutch Unreinforced Masonry, Procedia Engineering 193 (2017) 250-257.
[284] F. Mosteller, R.E. Rourke, Sturdy statistics (non-parametrics and order statistics), Addison-Wesley Pub Co1973.
[285] P.B. Lourenco, J.A.O. Barros, Size effect of masonry subjected to out of plane loading 12th International Brick/Block Masonry Conference, Madrid, Spain, 2000.
[286] V.G. Haach, G. Vasconcelos, P.B. Lourenço, Characterization of the tensile and shear bond strength of concrete block masonry 8º Congresso Nacional de Mecânica Experimental, Guimaraes, Portugal 2010.
[287] L. Abdou, R.A. Saada, F. Meftah, A. Mebarki, Experimental investigations of the joint-mortar behaviour, Mechanics Research Communications 33(3) (2006) 370-384.
[288] J.A. Thamboo, M. Dhanasekar, C. Yan, Flexural and shear bond characteristics of thin layer polymer cement mortared concrete masonry, Construction and Building Materials 46 (2013) 104-113.
[289] G. Bei, I. Papayianni, Experimental study of shear bond strength of traditional masonry 13th International Brick and Brick Masonry Conference, Amsterdam, Netherlands, 2004.
[290] CEN, EN 1052-3:2002 Methods of test for masonry - Part 3: Determination of initial shear strength

2007.
[291] P.B. Lourenço, J.O. Barros, J.T. Oliveira, Shear testing of stack bonded masonry, Construction and Building Materials 18(2) (2004) 125-132.
[292] G.P.A.G. van Zijl, Modeling Masonry Shear-Compression: Role of Dilatancy Highlighted, Journal of Engineering Mechanics 130(11) (2004) 1289-1296.
[293] G. Henrique Nalon, C.F.R. Santos, L.G. Pedroti, J.C.L. Ribeiro, G.d.S. Veríssimo, F.A. Ferreira, Strength and failure mechanisms of masonry prisms under compression, flexure and shear: Components' mechanical properties as design constraints, Journal of Building Engineering 28 (2020).
[294] R. Lumantarna, D.T. Biggs, J.M. Ingham, Compressive, Flexural Bond, and Shear Bond Strengths of In Situ New Zealand Unreinforced Clay Brick Masonry Constructed Using Lime Mortar between the 1880s and 1940s, Journal of Materials in Civil Engineering 26(4) (2014) 559-566.
[295] S.A.B.-M. Structures), AS 3700:2018 - Masonry Structures 2018.
[296] M. Tomaževič, Shear resistance of masonry walls and Eurocode 6: shear versus tensile strength of masonry, Materials and Structures 42(7) (2008) 889-907.
[297] G.M. Calvi, G.R. Kingsley, G. Magenes, Testing of Masonry Structures for Seismic Assessment, Earthquake Spectra 12(1) (1996) 145-162.
[298] P.B. Shing, J.L. Noland, E. Klamerus, H. Spaeh, Inelastic Behavior of Concrete Masonry Shear Walls, Journal of Structural Engineering 115(9) (1989) 2204-2225.
[299] M. Tomaževič, M. Gams, S. Lu, Modelling of shear failure mechanism of masonry walls, 11th Canadian Masonry Symposium, Toronto, Ontario, 2009.
[300] O.J. Sandoval, C. Takeuchi, J. Carrillo, B. Barahona, Performance of unreinforced masonry panels strengthened with mortar overlays reinforced with welded wire mesh and transverse connectors, Construction and Building Materials (2020).
[301] M. Tomaževič, M. Lutman, L. Petković, Seismic Behavior of Masonry Walls: Experimental Simulation, Journal of Structural Engineering 122(9) (1996) 1040-1047.

[302] U. Andreaus, Failure Criteria for Masonry Panels under In-Plane Loading, Journal of Structural Engineering 122(1) (1996) 37-46.
[303] A. Salmanpour, N. Mojsilovic, J. Schwartz, Deformation capacity of unreinforced masonry walls subjected to in-plane loading: a state-of-the-art review, International Journal of Advanced Structural Engineering 5(1) (2013).
[304] S.R. Balasubramanian, C.V. Vaidyanathan, N. Lakshmanan, M.B. Anoop, K.B. Rao, In-plane Shear Behaviour of Unreinforced Brick Masonry – A Literature Review in: P.B. Lourenço, P.R.C. Modena, S. Agrawal (Eds.) Structural Analysis of Historical Constructions, New Delhi 2006.
[305] M. Javed, Seismic Risk Assessment of Unreinforced Brick Masonry Buildings System of Northern Pakistan, Department of Civil Engineering, N-W.F.P. University of Engineering and Technology, Peshawar, Pakistan, 2009.
[306] F. Parisi, I. Iovinella, A. Balsamo, N. Augenti, A. Prota, In-plane behaviour of tuff masonry strengthened with inorganic matrix–grid composites, Composites Part B: Engineering 45(1) (2013) 1657-1666.
[307] A. Tomar, D.K. Paul, P. Agarwal, Compression and Cyclic Shear Behavior of Lime Mortar Brick Masonry, Journal of Earthquake and Tsunami 11(05) (2017).
[308] L. Mercedes, E. Bernat-Maso, L. Gil, In-plane cyclic loading of masonry walls strengthened by vegetal-fabric-reinforced cementitious matrix (FRCM) composites, Engineering Structures 221 (2020).
[309] V. Turnsek, F. Cacovic, Some experimental results on the strength of brick masonry walls, 2nd International Brick-Masonry Conference, British Ceramic Society, Stoke-on-Trent, 1971, pp. 149-156.
[310] G. Magenes, G.M. Calvi, In-plane seismic response of brick masonry walls, Earthquake Engineering & Structural Dynamics 26(11) (1997) 1091-1112.
[311] W. Mann, H. Mueller, Failure of shear-stressed masonry Ð An enlarged theory, tests and application to shear walls, Proceedings of the British Ceramic Society, 1982.
[312] T. Stratford, G. Pascale, O. Manfroni, B. Bonfiglioli, Shear Strengthening Masonry Panels with Sheet Glass-Fiber Reinforced Polymer, Journal of Composites for Construction 8(5) (2004) 434-443.
[313] G. Marcari, G. Manfredi, A. Prota, M. Pecce, In-plane shear performance of masonry panels strengthened with FRP, Composites Part B: Engineering 38(7-8) (2007) 887-901.
[314] M. Deng, W. Zhang, N. Li, In-plane cyclic loading tests of concrete hollow block masonry walls retrofitted with high ductile fiber-reinforced concrete, Construction and Building Materials 238 (2020).
[315] G. Vasconcelos, P.B. Lourenço, In-Plane Experimental Behavior of Stone Masonry Walls under Cyclic Loading, Journal of Structural Engineering 135(10) (2009) 1269-1277.
[316] A.H. Salmanpour, Displacement capacity of structural masonry ETH Zurich 2017.
[317] CEN, EN 459-2:2010 Building lime - Part 2: Test methods, 2010.
[318] S. Boualleg, M. Bencheikh, L. Belagraa, A. Daoudi, M.A. Chikouche, The Combined Effect of the Initial Cure and the Type of Cement on the Natural Carbonation, the Portlandite Content, and Nonevaporable Water in Blended Cement, Advances in Materials Science and Engineering 2017 (2017) 1-17.
[319] S.M. Monteagudo, A. Moragues, J.C. Gálvez, M.J. Casati, E. Reyes, The degree of hydration assessment of blended cement pastes by differential thermal and thermogravimetric analysis. Morphological evolution of the solid phases, Thermochimica Acta 592 (2014) 37-51.
[320] P. Mounanga, A. Khelidj, A. Loukili, V. Baroghel-Bouny, Predicting Ca(OH)2 content and chemical shrinkage of hydrating cement pastes using analytical approach, Cement and Concrete Research 34(2) (2004) 255-265.
[321] K. Scrivener, R. Snellings, B. Lothenbach, A Practical Guide to Microstructural Analysis of Cementitious Materials, 2018.
[322] J.I. Bhatty, Hydration versus strength in a portland cement developed from domestic mineral wastes — a comparative study, Thermochimica Acta 106 (1986) 93-103.

[323] Societe Nouvelle Du Littoral (S.N.L) https://www.standard-sand.com/en/. (Accessed 11 November 2020).
[324] CEN, EN 13139:2013 Aggregates for mortars, 2013.
[325] CEN, EN 1097-3 Tests for mechanical and physical properties of aggregates - Part 3: Determination of loose bulk density and voids, 1998.
[326] CEN, EN 1097-6: 2013 Tests for mechanical and physical properties of aggregates - Part 6: Determination of particle density and water absorption, 2013.
[327] P.B. Lourenço, F.M. Fernandes, F. Castro, Handmade Clay Bricks: Chemical, Physical and Mechanical Properties, International Journal of Architectural Heritage 4(1) (2009) 38-58.
[328] K.A. Hooker, Mortar, Brick and IRA, 1994. https://www.concreteconstruction.net/how-to/construction/mortar-brick-and-ira_o. (Accessed 10 October 2020).
[329] B.D. Association, The UK clay brickmaking process, 2017.
[330] E. Thomaz, H. Sousa, H. Roman, J. Morton, J.M. Silva, M. Corrêa, O. Pfeffermann, P.B. Lourenço, R.S. Vicente, R. Sousa, Defects in Masonry Walls. Guidance on Cracking: Identification, Prevention and Repair, International Council for Research and Innovation in Building and Construction 2014.
[331] H. Sousa, Portuguese masonry building enclosures practices and problems, University of Porto 2002.
[332] J.G. Rots, Structural Masonry: An Experimental/ Numerical Basis for Practical Design Rules (CUR Report 171), CRC Press1997.
[333] Construction & Civil Engineering. https://www.eula.eu/lime-applications/construction-civil-engineering/. (Accessed 20 October 20 2020).
[334] M. Lavagna, C. Baldassarri, A. Campioli, S. Giorgi, A. Dalla Valle, V. Castellani, S. Sala, Benchmarks for environmental impact of housing in Europe: Definition of archetypes and LCA of the residential building stock, Building and Environment 145 (2018) 260-275.
[335] R.S. Vicente, H. Rodrigues, H. Varum, A. Costa, J.A.R. Mendes da Silva, Performance of masonry enclosure walls: lessons learned from recent earthquakes, Earthquake Engineering and Engineering Vibration 11(1) (2012) 23-34.
[336] CEN, EN 771-1:2011 2011 Specification for masonry units - Part 1: Clay masonry units, 2011.
[337] CEN, BS EN 772-21:2011 Methods of test for masonry units - Part 21: Determination of water absorption of clay and calcium silicate masonry units by cold water absorption, 2011.
[338] CEN, BS EN 772-11:2011 Methods of test for masonry units - Part 11: Determination of water absorption of aggregate concrete, autoclaved aerated concrete, manufactured stone and natural stone masonry units due to capillary action and the initial rate of water absorption of clay masonry units, 2011.
[339] Matest, E090 KIT Hand operated flow table, EN. https://www.matest.com/en/product/e090-kit-hand-operated-flow-table-en. (Accessed 12 November 2020).
[340] Matest, E093 Automatic mortar mixer. https://www.matest.com/en/product/e093-automatic-mortar-mixer. (Accessed 12 November 2020).
[341] Matest, E105 Three gang mould, hardness 55 HRB. https://www.matest.com/en/product/e105-three-gang-mould-hardness-55-hrb. (Accessed 12 November 2020).
[342] Matest, E130 Jolting Apparatus. https://www.matest.com/en/product/e130-jolting-apparatus. (Accessed 12 November 2020).
[343] T. 1404, Extended Round Robin Testing Programme. https://www.tu1404.eu/rrt/testing-methods-and-techniques. (Accessed 22 October 2020).
[344] CEN, EN 196-1:2005 Methods of testing cement – Part 1: Determination of strength, 2005.
[345] E. International, Vibrating Table (34-6250/01). https://www.ele.com/Product/vibrating-table-600-x-400mm-table-top-220-240v-50hz-1ph-supplied-with-clamping-assm-. (Accessed 12 November 2020).
[346] CEN, EN 12390-2:2019 Testing hardened concrete - Part 2: Making and curing specimens for strength tests, 2019.

[347] Building Mortar, Building Materials in Civil Engineering2011, pp. 150-423.
[348] C. 115, NP EN 1996-1-1: 2015 Portuguese National Annex to Eurocode 6 - Design of masonry structures Part 1-1: General rules for reinforced and unreinforced masonry structures, 2015.
[349] BSI, NA to EN 1996-1-1:2005+A1:2012 UK National Annex to Eurocode 6: Design of masonry structures – Part 1-1: General rules for reinforced and unreinforced masonry structures, 2013.
[350] NBN, NBN EN 1996-1-1 ANB - Belgian National Annex to Eurocode 6: Design of masonry structures – Part 1-1: General rules for reinforced and unreinforced masonry structures, 2010.
[351] UNI, UNI EN 1996-1-1: 2013 Italian National Annex to Eurocode 6: Design of masonry structures – Part 1-1: General rules for reinforced and unreinforced masonry structures, 2013.
[352] DIN, DIN EN 1996-1-1/NA/A1 German National Annex to Eurocode 6: Design of masonry structures – Part 1-1: General rules for reinforced and unreinforced masonry structures (Nationally determined parameters), 2014.
[353] HRN, HRN EN 1996-1-1:2012/NA Croatian National Annex to Eurocode 6: Design of masonry structures – Part 1-1: General rules for reinforced and unreinforced masonry structures, 2012.
[354] IST, ÍST EN 1996-1-1:2005 Icelandic National Annex to Eurocode 6: Design of masonry structures – Part 1-1: General rules for reinforced and unreinforced masonry structures, 2005.
[355] NF, NF EN 1996-1-1/NA French National Annex to Eurocode 6: Design of masonry structures – Part 1-1: General rules for reinforced and unreinforced masonry structures, 2009.
[356] CEN, 1015-3:1999 Methods of Test for Mortar for Masonry, Part 3: Determination of consistence of fresh mortar (by flow table), 2007.
[357] CEN, EN 1015-10:1999 Methods of test for mortar for masonry - Part 10: Determination of dry bulk density of hardened mortar, 2007.
[358] CEN, EN 12617-4:2002 Products and systems for the protection and repair of concrete structures - Test methods - Part 4: Determination of shrinkage and expansion, 2002.
[359] J. Granja, EMM-ARM User's Guide. Version 2.0.1. Appendix-A. PhD Thesis. Continuous characterization of stiffness of cement - based materials: experimental analysis and micro-mechanics modelling, School of engineering, University of Minho, 2016.
[360] M. Ramesh, M. Azenha, P.B. Lourenço, Quantification of impact of lime on mechanical behaviour of lime cement blended mortars for bedding joints in masonry systems, Construction and Building Materials 229 (2019).
[361] S.B. Singh, P. Munjal, N. Thammishetti, Role of water/cement ratio on strength development of cement mortar, Journal of Building Engineering 4 (2015) 94-100.
[362] A. ElNemr, Generating water/binder ratio -to- strength curves for cement mortar used in Masnory walls, Construction and Building Materials 233 (2020).
[363] Applications and benefits of cement mortars in construction http://www.constructionnews.co.in/applications-and-benefits-of-cement-mortars-in-construction.html. (Accessed 18 August 2020.
[364] BDA, Mortar for brickwork, 2018. https://www.brick.org.uk/admin/resources/mortar-for-brickwork.pdf. (Accessed 28 July 2020.
[365] Ž. Radovanović, R.S. Grebović, S. Dimovska, N. Serdar, N. Vatin, V. Murgul, The Mechanical Properties of Masonry Walls - Analysis of the Test Results, Procedia Engineering 117 (2015) 865-873.
[366] A.T. Vermeltfoort, D.R.W. Martens, G.P.A.G. Van Zijl, Brick–mortar interface effects on masonry under compression Canadian Journal of Civil Engineering 34(11) (2007) 1475-1485.
[367] R. TC, LUM B1 Compressive strength of small walls and prisms, 1991, in: RILEM (Ed.), RILEM Recommendations for the Testing and Use of Constructions Materials1994, pp. 474-477.
[368] LIDL, PARKSIDE® paint and mortar stirrer PFMR 1400 B1. https://www.lidl.de/de/parkside-farb-und-moertelruehrer-pfmr-1400-b1/p173507. (Accessed 26 October 2020).

[369] A.T.C.A.-b. ATC-58c), FEMA 461 - Interim Testing Protocols for Determining the Seismic Performance Characteristics of Structural and Nonstructural Components 2007.
[370] OriginLab, Origin and Origin Pro. https://www.originlab.com/index.aspx?go=Products/Origin. (Accessed 25 November 2020).
[371] Introduction to Colab and Python. https://colab.research.google.com/github/tensorflow/examples/blob/master/courses/udacity_intro_to_tensorflow_for_deep_learning/l01c01_introduction_to_colab_and_python.ipynb. (Accessed 25 November 2020).
[372] S. Glen, F Statistic / F Value: Simple Definition and Interpretation, 2020. https://www.statisticshowto.com/probability-and-statistics/f-statistic-value-test/.
[373] G. James, D. Witten, T. Hastie, R. Tibshirani, An Introduction to Statistical Learning, Springer-Verlag New York2013.
[374] M.S. Thiese, B. Ronna, U. Ott, P value interpretations and considerations, Journal of Thoracic Disease 8(9) (2016) E928-E931.
[375] OriginLab, Interpreting Regression Results. https://www.originlab.com/doc/Origin-Help/Interpret-Regression-Result#:~:text=F%20Value%20is%20a%20ratio,the%20mean%20square%20of%20error. (Accessed 25 November 2020).
[376] CEN, EN 998-2:2010 Specification for mortar for masonry - Part 2: Masonry mortar, 2010.
[377] PN, PN EN 1996-1-1 - Polish National Annex to Eurocode 6: Design of masonry structures – Part 1-1: General rules for reinforced and unreinforced masonry structures, 2010.
[378] Proceq, Pundit Lab / Pundit Lab+ Ultrasonic Instrument, 2017. https://www.proceq.com/uploads/tx_proceqproductcms/import_data/files/Pundit%20Lab_Operating%20Instructions_English_high.pdf. (Accessed 24 November 2020).
[379] K. Jurowski, S. Grzeszczyk, The Influence of Concrete Composition on Young's Modulus, Procedia Engineering 108 (2015) 584-591.
[380] G. Trtnik, F. Kavčič, G. Turk, Prediction of concrete strength using ultrasonic pulse velocity and artificial neural networks, Ultrasonics 49(1) (2009) 53-60.
[381] T. RILEM, Determination of the fracture energy of mortar and concrete by means of three-point bend tests on notched beams, Materials and Structures 18(106) (1985) 285-290.
[382] H. Fallahnejad, M.R. Davoodi, I.M. Nikbin, The influence of aging on the fracture characteristics of recycled aggregate concrete through three methods, Structural Concrete (2020).
[383] P.E. Peterson, Fracture energy of concrete: Method of determination, Cement and Concrete Research 10(1) (1980) 79-89.
[384] F.H. Wittmann, P.E. Roelfstra, H. Mihashi, Y.-Y. Huang, X.-H. Zhang, N. Nomura, Influence of age of loading, water-cement ratio and rate of loading on fracture energy of concrete, Materials and Structures 20(2) (1987) 103-110.
[385] P. Nath, P.K. Sarker, Fracture properties of GGBFS-blended fly ash geopolymer concrete cured in ambient temperature, Materials and Structures 50(1) (2016).
[386] f.-f.i.d. beton, Model Code 2010 - First complete draft, Volume 1, 2010.
[387] R. TC 25-PEM, Essais recommandés pour mesurer l'altération des pierres et évaluer l'efficacité des méthodes de traitement / Recommended tests to measure the deterioration of stone and to assess the effectiveness of treatment methods, Materials and Structures 13(75) (1980) 175-253.
[388] U.d.B. Interior, Porosity test Laboratórios de Construção (Cimentos e Durabilidade de Betões).
[389] M.J. Mosquera, D. Benítez, S.H. Perry, Pore structure in mortars applied on restoration, Cement and Concrete Research 32(12) (2002) 1883-1888.
[390] F. Collins, J.G. Sanjayan, Effect of pore size distribution on drying shrinking of alkali-activated slag concrete, Cement and Concrete Research 30(9) (2000) 1401-1406.

[391] M. Azenha, Numerical simulation of the structural behaviour of concrete since its early ages, Faculdade de Eengenharia Universidade do Porto Porto, Portugal 2009.
[392] M. Azenha, R. Faria, F. Magalhães, L. Ramos, Á. Cunha, Measurement of the E-modulus of cement pastes and mortars since casting, using a vibration based technique, Materials and Structures 45(1-2) (2011) 81-92.
[393] M. Fourmentin, P. Faure, S. Gauffinet, U. Peter, D. Lesueur, D. Daviller, G. Ovarlez, P. Coussot, Porous structure and mechanical strength of cement-lime pastes during setting, Cement and Concrete Research 77 (2015) 1-8.
[394] M. Bouasker, P. Mounanga, P. Turcry, A. Loukili, A. Khelidj, Chemical shrinkage of cement pastes and mortars at very early age: Effect of limestone filler and granular inclusions, Cement and Concrete Composites 30(1) (2008) 13-22.
[395] L. Trifone, A study of the correlation between static and dynamic modulus of elasticity on different concrete mixes West Virginia University 2017.
[396] RDP, D5 & D6 LVDT Displacement Transducer. https://www.rdpe.com/ex/d5-d6.htm. (Accessed 15 December 2020).
[397] T. Sotinco, Betume Poliester http://www.sotinco.pt/produtos/betume-poliester. (Accessed 15 December 2020).
[398] S. Direct, Hot-Melt Adhesive https://www.sciencedirect.com/topics/engineering/hot-melt-adhesive. (Accessed 15 December 2020).
[399] CEN, BS EN 772-1:2011 Methods of tests for masonry units - Part I: Determination of compressive strength, 2011.
[400] B.D. Ewing, M.J. Kowalsky, Compressive Behavior of Unconfined and Confined Clay Brick Masonry, Journal of Structural Engineering 130(4) (2004) 650-661.
[401] A. Penna, S. Lagomarsino, A. Galasco, A nonlinear macroelement model for the seismic analysis of masonry buildings, Earthquake Engineering & Structural Dynamics 43(2) (2014) 159-179.
[402] Instron, Glossary of Materials Testing Terms (S) - Secant Modulus of Elasticity. https://www.instron.us/our-company/library/glossary/s/secant-modulus-of-elasticity. (Accessed 28 August 2020).
[403] B.V. Wilding, K. Beyer, Effective stiffness of unreinforced brick masonry walls, in: C. Modena, F.d. Porto, M.R. Valluzzi (Eds.) Brick and Block Masonry – Trends, Innovations and Challenges, Taylor & Francis Group, London 2016.
[404] M.J.N. Priestley, Ductility of unconfined masonry shear walls Bulletin of New Zealand National Society for Earthquake Engineering 14 (1981).
[405] P.K.V.R. Padalu, Y. Singh, S. Das, Experimental investigation of out-of-plane behaviour of URM wallettes strengthened using welded wire mesh, Construction and Building Materials 190 (2018) 1133-1153.
[406] Z. Jiao, Y. Wang, W. Zheng, W. Huang, Y. Zhao, Bond properties of alkali-activated slag concrete hollow block masonry with different mortar strength grades, Construction and Building Materials 216 (2019) 149-165.
[407] S. P, Tensile and flexural strengths of masonry - Influences, test methods and test results, 10th International Brick and Block Masonry Conference, Calgary, Canada 1994.
[408] Mapei, Lampocem (Cimento Rapido). https://www.jon.pt/public/files/a16a6049c07ae9232605158a46bb5a5a.pdf. (Accessed 15 December 2020).
[409] B. Silva, M. Dalla Benetta, F. da Porto, C. Modena, Experimental assessment of in-plane behaviour of three-leaf stone masonry walls, Construction and Building Materials 53 (2014) 149-161.

[410] N. Mojsilović, A.H. Salmanpour, Masonry walls subjected to in-plane cyclic loading: application of digital image correlation for deformation field measurement, International Journal of Masonry Research and Innovation 1(2) (2016).
[411] A.E. Schultz, Seismic performance of partially grouted masonry-shear walls, Eleventh world conference on earthquake engineering Acapulco, Mexico, 1996.
[412] N. Mojsilović, G. Simundic, A. Page, Static-cyclic Shear Tests on Masonry Wallettes with a Damp-proof Course Membrane, 2009.
[413] J. Milosevic, M. Lopes, A.S. Gago, R. Bento, In-plane seismic response of rubble stone masonry specimens by means of static cyclic tests, Construction and Building Materials 82 (2015) 9-19.
[414] D.P. Abrams, Performance-based engineering concepts for unreinforced masonry building structures, Progress in Structural Engineering and Materials 3(1) (2001) 48-56.
[415] D.P. Abrams, Seismic assessment and rehabilitation of unreinforced masonry buildings in the USA, SÍSMICA 2004 - 6° Congresso Nacional de Sismologia e Engenharia Sísmica, Guimarães, Portugal, 2004.

Annexes

Annex-Table 1: Values of compressive strength predicted by Equation 13 and values of coefficients a and b for each mix

Mortars	R^2	a	b	fc-7 (MPa)	fc-14 (MPa)	fc-28 (MPa)	fc-90 (MPa)	fc-180 (MPa)	fc-365 (MPa)
9C1L30S (10%)	0.66	14.53	-1.24	9.10	10.44	11.50	12.75	13.25	13.62
3C1L12S (25%)	0.56	11.47	-0.90	8.15	9.01	9.67	10.43	10.72	10.94
2C1L9S (33%)	0.93	9.43	-1.02	6.42	7.18	7.78	8.47	8.74	8.94
1C1L6S (50%)	0.83	7.22	-1.49	4.12	4.85	5.45	6.18	6.47	6.68
1C2L9S (67%)	0.94	3.01	-1.70	1.58	1.91	2.18	2.51	2.65	2.75
1C3L12S (75%)	0.89	1.88	-2.21	0.82	1.04	1.24	1.49	1.60	1.68
1C9L30S (90%)	0.97	0.55	-3.38	0.15	0.22	0.29	0.39	0.43	0.46
3C1L16S (25%)	0.88	8.45	-1.44	4.89	5.74	6.43	7.25	7.58	7.83
2C1L12S (33%)	0.69	6.43	-1.37	3.83	4.46	4.96	5.56	5.80	5.98
1C1L8S (50%)	0.72	3.68	-1.00	2.52	2.82	3.05	3.32	3.42	3.50
1C2L12S (67%)	0.59	1.65	-1.40	0.97	1.13	1.27	1.42	1.49	1.53
2C1L15S (33%)	0.82	3.88	-1.53	2.17	2.58	2.90	3.30	3.46	3.58
1C1L10S (50%)	0.77	2.11	-1.12	1.38	1.56	1.71	1.87	1.94	1.99
1C2L15S (67%)	0.74	1.05	-1.52	0.59	0.70	0.79	0.89	0.93	0.97
1C1L12S (50%)	0.55	1.58	-1.19	1.01	1.15	1.26	1.39	1.44	1.48

Annex-Table 2: Difference between values of compressive strength predicted by equation 13 (Annex-Table 1) and actual values, also expressed in % (Table 14, Chapter 4)

	Absolute difference (MPa)						Difference in %					
Mortars	7 (MPa)	14 (MPa)	28 (MPa)	90 (MPa)	180 (MPa)	365 (MPa)	7 (%)	14 (%)	28 (%)	90 (%)	180 (%)	365 (%)
9C1L30S (10%)	0.2	-0.2	-0.6	0.5	2.0	-1.8	1.8	-1.9	-5.0	4.4	17.4	-11.9
3C1L12S (25%)	0.5	-0.9	-0.3	1.1	0.8	-1.3	6.4	-9.1	-2.8	12.4	8.1	-10.3
2C1L9S (33%)	0.3	-0.2	-0.3	-0.1	0.0	0.3	5.4	-2.4	-4.3	-1.2	0.1	3.4
1C1L6S (50%)	0.0	-0.6	0.8	-0.1	0.2	-0.3	0.0	-10.3	16.5	-0.9	2.5	-4.7
1C2L9S (67%)	0.1	0.0	-0.2	0.1	0.0	0.1	6.9	0.5	-8.7	2.6	-1.5	3.0
1C3L12S (75%)	0.2	-0.1	-0.1	0.0	0.0	0.1	29.6	-10.1	-9.5	-2.5	3.0	4.2
1C9L30S (90%)	0.0	0.0	0.0	0.0	0.0	0.0	10.3	2.0	-2.5	-5.4	-4.3	7.9
3C1L16S (25%)	0.3	-0.7	0.4	0.2	-0.3	0.1	6.6	-11.1	7.0	2.9	-3.4	0.8
2C1L12S (33%)	0.6	-0.6	-0.1	-0.2	-0.5	0.8	18.7	-11.4	-2.5	-2.9	-8.5	15.9
1C1L8S (50%)	0.2	-0.3	0.0	-0.2	0.3	-0.1	9.2	-9.6	1.6	-6.1	10.3	-1.8
1C2L12S (67%)	0.2	-0.2	-0.1	0.2	0.0	-0.1	26.1	-17.2	-10.2	19.6	2.5	-5.3
2C1L15S (33%)	0.3	-0.3	-0.2	0.0	-0.2	0.3	16.8	-9.0	-5.7	1.2	-6.2	9.8
1C1L10S (50%)	0.1	-0.2	0.1	0.1	-0.1	-0.1	5.4	-11.7	7.3	7.7	-2.5	-3.0

1C2L15S (67%)	0.1	-0.1	-0.1	0.0	0.0	0.0	28.0	-16.0	-7.6	3.7	3.9	0.7
1C1L12S (50%)	0.2	-0.2	-0.1	0.2	0.1	-0.1	18.5	-14.3	-9.3	16.9	7.7	-8.5

Annex-Table 3: Values of flexural strength predicted by Equation 13 and values of coefficients a and b for each mix

Mortars	R^2	a	b	fc-7 (MPa)	fc-14 (MPa)	fc-28 (MPa)	fc-90 (MPa)	fc-180 (MPa)	fc-365 (MPa)
9C1L30S (10%)	0.54	4.70	-1.53	2.64	3.13	3.52	4.00	4.20	4.34
3C1L12S (25%)	0.88	4.65	-2.46	1.84	2.41	2.92	3.59	3.87	4.09
2C1L9S (33%)	0.88	3.38	-1.78	1.73	2.10	2.42	2.80	2.96	3.08
1C1L6S (50%)	0.97	2.74	-1.98	1.30	1.62	1.89	2.23	2.37	2.47
1C2L9S (67%)	0.93	1.13	-2.37	0.46	0.60	0.72	0.88	0.95	1.00
1C3L12S (75%)	0.82	0.65	-1.79	0.33	0.40	0.47	0.54	0.57	0.59
1C9L30S (90%)	0.74	0.34	-4.49	0.06	0.10	0.15	0.21	0.25	0.27
3C1L16S (25%)	0.95	3.26	-2.47	1.28	1.68	2.04	2.51	2.71	2.86
2C1L12S (33%)	0.83	2.50	-1.79	1.27	1.55	1.78	2.07	2.19	2.28
1C1L8S (50%)	0.91	1.36	-1.52	0.77	0.91	1.03	1.16	1.22	1.26
1C2L12S (67%)	0.59	0.61	-1.25	0.38	0.44	0.48	0.54	0.56	0.57
2C1L15S (33%)	0.92	1.51	-1.80	0.76	0.93	1.07	1.24	1.32	1.37
1C1L10S (50%)	0.91	0.85	-1.81	0.43	0.52	0.60	0.70	0.74	0.77
1C2L15S (67%)	0.48	0.39	-1.06	0.26	0.29	0.32	0.35	0.36	0.37
1C1L12S (50%)	0.83	0.62	-1.73	0.32	0.39	0.45	0.52	0.55	0.57

Annex-Table 4: Difference between values of flexural strength predicted by equation 13 (Annex-Table 3) and actual values, also expressed in % (Table 15, Chapter 4)

	Absolute difference (MPa)						Difference in %					
Mortars	7 (MPa)	14 (MPa)	28 (MPa)	90 (MPa)	180 (MPa)	365 (MPa)	7 (%)	14 (%)	28 (%)	90 (%)	180 (%)	365 (%)
9C1L30S (10%)	0.03	0.02	0.36	-0.85	-0.44	0.88	1.3	0.8	9.4	-27.0	-11.8	16.8
3C1L12S (25%)	0.11	0.17	-0.17	-0.37	-0.24	0.51	5.8	6.7	-6.0	-11.5	-6.5	11.2
2C1L9S (33%)	-0.21	0.21	0.18	-0.28	0.06	0.03	-13.9	9.3	6.9	-11.2	2.1	0.8
1C1L6S (50%)	-0.07	0.07	0.07	-0.08	-0.06	0.07	-5.8	4.2	3.7	-4.0	-2.5	2.7
1C2L9S (67%)	-0.06	0.10	-0.04	-0.02	0.04	-0.02	-13.7	13.8	-5.7	-2.6	4.3	-2.5
1C3L12S (75%)	-0.05	0.03	0.02	0.04	0.04	-0.08	-17.3	7.2	3.2	6.5	6.2	-14.8
1C9L30S (90%)	-0.02	-0.06	0.05	0.06	0.01	-0.06	-48.6	-132.3	24.5	22.7	4.5	-27.5
3C1L16S (25%)	-0.05	0.04	0.06	-0.16	0.24	-0.12	-4.3	2.2	2.7	-6.9	8.0	-4.4
2C1L12S (33%)	-0.15	-0.05	0.30	0.01	0.07	-0.20	-13.2	-3.5	14.6	0.7	3.2	-9.6
1C1L8S (50%)	-0.07	0.04	0.06	0.04	0.02	-0.09	-10.6	3.9	5.4	3.2	1.8	-7.3
1C2L12S (67%)	-0.08	0.09	0.04	-0.03	-0.05	0.03	-26.1	17.6	7.4	-6.9	-9.6	4.7

2C1L15S (33%)	-0.10	0.06	0.09	0.01	-0.02	-0.05	-15.2	5.8	7.8	1.0	-1.5	-3.5
1C1L10S (50%)	-0.06	0.06	0.04	-0.04	0.00	0.00	-16.2	9.7	6.3	-5.7	0.4	-0.6
1C2L15S (67%)	-0.05	0.05	0.03	0.00	0.03	-0.06	-26.4	13.3	9.6	1.4	7.4	-19.1
1C1L12S (50%)	-0.04	0.03	0.05	-0.04	-0.04	0.04	-13.3	6.4	10.9	-8.7	-7.7	5.8

Annex-Table 5: Relation between compressive strength at day 365 and day 7 based on experimentally obtained values from (Table 14, Chapter 4)

	Experimentally obtained values as specified in Table 14, Chapter 4			Ratio of compressive strength at different ages	
Mortars	7 (MPa)	28 (MPa)	365 (MPa)	$\frac{\text{fc } 365}{\text{fc } 7}$	$\frac{\text{fc } 365}{\text{fc } 28}$
9C1L30S (10%)	8.94	12.11	15.46	1.7	1.3
3C1L12S (25%)	7.66	9.95	12.19	1.6	1.2
2C1L9S (33%)	6.09	8.13	8.65	1.4	1.1
1C1L6S (50%)	4.12	4.68	7.01	1.7	1.5
1C2L9S (67%)	1.48	2.39	2.67	1.8	1.1
1C3L12S (75%)	0.63	1.37	1.61	2.6	1.2
1C9L30S (90%)	0.14	0.3	0.43	3.1	1.4
3C1L16S (25%)	4.59	6.01	7.77	1.7	1.3
2C1L12S (33%)	3.23	5.09	5.16	1.6	1.0
1C1L8S (50%)	2.31	3	3.56	1.5	1.2
1C2L12S (67%)	0.77	1.41	1.62	2.1	1.1
2C1L15S (33%)	1.86	3.08	3.26	1.8	1.1
1C1L10S (50%)	1.31	1.59	2.05	1.6	1.3
1C2L15S (67%)	0.46	0.85	0.96	2.1	1.1
1C1L12S (50%)	0.85	1.39	1.62	1.9	1.2

Annex-Table 6: Relation between flexural strength at day 365 and day 7 based on experimentally obtained values from (Table 15, Chapter 4)

	Experimentally obtained values as specified in Table 15, Chapter 4			Ratio of flexural strength at different ages	
Mortars	7 (MPa)	28 (MPa)	365 (MPa)	$\frac{\text{f}_\text{f}\ 365}{\text{f}_\text{f}\ 7}$	$\frac{\text{f}_\text{f}\ 365}{\text{f}_\text{f}\ 28}$
9C1L30S (10%)	2.67	3.89	5.22	2.0	1.3
3C1L12S (25%)	1.95	2.76	4.60	2.4	1.7
2C1L9S (33%)	1.52	2.60	3.11	2.1	1.2
1C1L6S (50%)	1.23	1.96	2.54	2.1	1.3
1C2L9S (67%)	0.41	0.69	0.98	2.4	1.4
1C3L12S (75%)	0.28	0.48	0.52	1.8	1.1
1C9L30S (90%)	0.04	0.19	0.21	5.0	1.1

3C1L16S (25%)	1.23	2.10	2.74	2.2	1.3
2C1L12S (33%)	1.12	2.09	2.08	1.9	1.0
1C1L8S (50%)	0.70	1.08	1.17	1.7	1.1
1C2L12S (67%)	0.30	0.52	0.60	2.0	1.2
2C1L15S (33%)	0.66	1.16	1.32	2.0	1.1
1C1L10S (50%)	0.37	0.64	0.77	2.1	1.2
1C2L15S (67%)	0.21	0.35	0.31	1.5	0.9
1C1L12S (50%)	0.29	0.50	0.60	2.1	1.2

Annex-Table 7: Difference between values of compressive strength estimated from Equation 14 and experimentally obtained values from Table 14, Chapter 4

	Absolute difference (MPa)						Difference in %				
Mortars	7 (MPa)	14 (MPa)	28 (MPa)	90 (MPa)	180 (MPa)	365 (MPa)	14 (%)	28 (%)	90 (%)	180 (%)	365 (%)
9C1L30S (10%)	9.73	11.16	12.30	13.64	14.17	14.57	4.9	1.6	11.6	25.6	-5.8
3C1L12S (25%)	8.33	9.56	10.54	11.69	12.15	12.48	-3.5	5.9	26.0	22.4	2.4
2C1L9S (33%)	6.63	7.60	8.38	9.29	9.66	9.93	3.3	3.0	8.4	10.6	14.7
1C1L6S (50%)	4.48	5.14	5.67	6.29	6.53	6.71	-4.9	21.1	0.9	3.5	-4.2
1C2L9S (67%)	1.81	2.20	2.51	2.91	3.07	3.19	15.6	5.2	18.6	14.0	19.4
1C3L12S (75%)	0.77	0.93	1.07	1.24	1.31	1.36	-19.4	-21.9	-19.1	-15.8	-15.7
3C1L16S (25%)	4.99	5.73	6.31	7.00	7.28	7.48	-11.3	5.1	-0.7	-7.3	-3.7
2C1L12S (33%)	3.51	4.03	4.44	4.93	5.12	5.26	-19.8	-12.7	-14.0	-19.2	2.0
1C1L8S (50%)	2.51	2.88	3.18	3.52	3.66	3.76	-7.6	5.9	-0.1	18.1	5.8
1C2L12S (67%)	0.94	1.14	1.31	1.51	1.60	1.66	-16.6	-7.2	27.1	10.0	2.4
2C1L15S (33%)	2.02	2.32	2.56	2.84	2.95	3.03	-18.0	-16.9	-12.9	-20.1	-7.0
1C1L10S (50%)	1.43	1.64	1.80	2.00	2.08	2.14	-7.6	13.3	14.9	4.4	4.1
1C2L15S (67%)	0.56	0.68	0.78	0.90	0.95	0.99	-17.8	-8.0	5.1	5.9	3.2
1C1L12S (50%)	0.92	1.06	1.17	1.30	1.35	1.39	-20.8	-15.9	9.0	0.6	-14.5

Annex-Table 8: Difference between values of flexural strength estimated from Equation 14 and experimentally obtained values from Table 15, Chapter 4

	Absolute difference (MPa)						Difference in %				
Mortars	7 (MPa)	14 (MPa)	28 (MPa)	90 (MPa)	180 (MPa)	365 (MPa)	14 (%)	28 (%)	90 (%)	180 (%)	365 (%)
9C1L30S (10%)	3.00	3.66	4.22	4.91	5.19	5.41	16.3	8.6	55.8	38.3	3.5
3C1L12S (25%)	2.19	2.67	3.08	3.58	3.79	3.94	3.4	11.6	11.1	4.1	-14.4
2C1L9S (33%)	1.70	2.08	2.39	2.78	2.94	3.06	-10.4	-7.9	10.3	-2.8	-1.4
1C1L6S (50%)	1.38	1.68	1.94	2.25	2.38	2.48	-0.3	-1.2	5.2	3.2	-2.4
1C2L9S (67%)	0.46	0.56	0.64	0.75	0.79	0.82	-20.1	-6.1	-13.0	-20.3	-15.7

1C3L12S (75%)	0.32	0.39	0.45	0.52	0.55	0.57	-11.2	-7.2	-10.2	-10.0	10.3
3C1L16S (25%)	1.38	1.68	1.94	2.26	2.39	2.48	-2.3	-7.7	-3.9	-19.0	-9.4
2C1L12S (33%)	1.26	1.54	1.77	2.06	2.18	2.27	2.7	-15.1	-1.1	-3.5	9.3
1C1L8S (50%)	0.78	0.95	1.10	1.28	1.35	1.41	0.7	1.4	6.4	9.0	19.9
1C2L12S (67%)	0.34	0.42	0.48	0.56	0.59	0.61	-22.1	-8.6	10.6	15.4	1.6
2C1L15S (33%)	0.74	0.91	1.04	1.21	1.28	1.34	-8.3	-10.2	-3.5	-1.0	0.9
1C1L10S (50%)	0.41	0.50	0.58	0.67	0.71	0.74	-12.9	-9.6	2.0	-3.9	-2.9
1C2L15S (67%)	0.23	0.28	0.33	0.38	0.40	0.42	-16.4	-7.6	7.4	3.2	35.0
1C1L12S (50%)	0.32	0.39	0.45	0.52	0.55	0.58	-6.5	-10.5	9.9	9.2	-4.3

Annex-Table 9: Compressive strength estimated using Table 17 and difference between estimated and experimental values shown in Table 14

	Estimated strength (MPa)						Difference (%) between estimated and actual values					
Mortars	7 (MPa)	14 (MPa)	28 (MPa)	90 (MPa)	180 (MPa)	365 (MPa)	7 (%)	14 (%)	28 (%)	90 (%)	180 (%)	365 (%)
B/Ag ratio 1:3												
9C1L30S (10%)	Not applicable since experimental value was used for regression - benchmark mix for B/Ag ratio 1:3											
3C1L12S (25%)	7.02	8.43	9.57	9.76	9.08	12.20	-8.3	-14.9	-3.8	5.2	-8.4	0.1
2C1L9S (33%)	5.96	7.21	8.15	8.40	7.86	10.39	-2.2	-2.1	0.3	-2.0	-9.9	20.1
1C1L6S (50%)	3.83	4.76	5.33	5.67	5.42	6.77	-7.1	-12.1	14.0	-8.9	-14.2	-3.4
1C2L9S (67%)	1.57	2.16	2.33	2.78	2.82	2.93	6.4	13.9	-2.6	13.5	5.0	9.8
1C3L12S (75%)	0.64	1.08	1.09	1.58	1.75	1.34	1.8	-6.6	-20.3	2.9	12.3	-16.5
B/Ag ratio 1:4												
3C1L16S (25%)	4.31	6.22	5.95	6.96	7.59	7.06	-6.0	-3.8	-0.9	-1.3	-3.3	-9.1
2C1L12S (33%)	3.61	5.25	5.04	5.83	6.32	5.95	11.9	4.2	-0.9	1.7	-0.4	15.3
1C1L8S (50%)	2.22	3.29	3.22	3.56	3.77	3.72	-4.0	5.6	7.3	1.0	21.7	4.5
1C2L12S (67%)	0.74	1.22	1.29	1.16	1.06	1.37	-3.3	-10.6	-8.7	-2.9	-27.0	-15.5
B/Ag ratio 1:5												
2C1L15S (33%)	1.91	2.80	2.94	3.14	3.57	3.22	2.3	-1.0	-4.6	-3.7	-3.2	-1.0
1C1L10S (50%)	1.22	1.83	1.86	1.98	2.22	2.11	-6.8	3.3	16.9	13.6	11.4	3.1
1C2L15S (67%)	0.50	0.81	0.72	0.75	0.78	0.93	8.6	-3.2	-15.7	-13.1	-12.8	-3.1

Annex-Table 10: Flexural strength estimated using Table 18 and difference between estimated and experimental values shown in Table 15

	Estimated strength (MPa)						Difference (%) between estimated and actual values					
Mortars	7 (MPa)	14 (MPa)	28 (MPa)	90 (MPa)	180 (MPa)	365 (MPa)	7 (%)	14 (%)	28 (%)	90 (%)	180 (%)	365 (%)
B/Ag ratio 1:3												
9C1L30S (10%)	Not applicable since experimental value was used for regression - benchmark mix for B/Ag ratio 1:3											

3C1L12S (25%)	2.11	2.53	3.10	2.57	3.04	4.13	8.1	-2.1	12.3	-20.1	-16.3	-10.3
2C1L9S (33%)	1.79	2.18	2.66	2.25	2.65	3.53	18.4	-5.7	2.4	-10.8	-12.4	13.4
1C1L6S (50%)	1.16	1.49	1.78	1.61	1.86	2.31	-5.1	-11.4	-9.2	-25.1	-19.3	-8.9
1C2L9S (67%)	0.50	0.76	0.85	0.92	1.03	1.03	22.1	9.2	23.9	7.2	3.6	5.4
1C3L12S (75%)	0.22	0.46	0.46	0.64	0.68	0.50	-21.8	5.2	-3.9	10.4	11.7	-4.1
B/Ag ratio 1:4												
3C1L16S (25%)	1.26	1.71	2.22	2.38	2.81	2.59	2.8	-0.4	5.6	1.4	-4.5	-5.5
2C1L12S (33%)	1.08	1.48	1.88	2.01	2.34	2.18	-4.2	-1.4	-9.9	-3.7	3.5	4.8
1C1L8S (50%)	0.70	1.00	1.21	1.27	1.40	1.36	0.9	6.0	11.4	5.4	12.7	15.4
1C2L12S (67%)	0.31	0.50	0.49	0.48	0.40	0.48	1.3	-5.7	-5.6	-4.9	-22.0	-20.1
B/Ag ratio 1:5												
2C1L15S (33%)	0.63	0.95	1.12	1.20	1.26	1.30	-4.0	-3.3	-3.7	-4.3	-3.0	-1.8
1C1L10S (50%)	0.41	0.64	0.73	0.77	0.82	0.81	12.6	10.9	13.4	15.8	10.4	5.6
1C2L15S (67%)	0.18	0.31	0.31	0.30	0.35	0.29	-13.0	-9.3	-11.5	-14.5	-9.2	-7.8

Annex-Table 11: Compressive strength estimated using Table 19 and difference between estimated and experimental values shown in Table 14

	Estimated strength (MPa)						Difference (%) between estimated and actual values					
Mortars	7 (MPa)	14 (MPa)	28 (MPa)	90 (MPa)	180 (MPa)	365 (MPa)	7 (%)	14 (%)	28 (%)	90 (%)	180 (%)	365 (%)
Lime content 33%												
2C1L9S – 1:3	Not applicable since experimental value was used for regression - benchmark mix for Lime 33%											
2C1L12S – 1:4	3.40	4.63	5.00	5.34	5.72	5.26	5.3	-8.1	-1.8	-6.7	-9.8	1.9
2C1L15S – 1:5	1.79	2.99	3.11	3.41	3.92	3.22	-4.0	5.5	1.1	4.5	6.1	-1.2
Lime content 50%												
1C1L6S – 1:3	Not applicable since experimental value was used for regression - benchmark mix for Lime 50%											
1C1L8S – 1:4	2.44	3.28	2.94	3.60	3.70	4.13	5.4	5.1	-2.1	2.2	19.7	15.9
1C1L10S – 1:5	1.42	2.00	1.89	2.03	2.14	2.40	8.4	12.8	18.8	16.2	7.5	17.1
1C1L12S – 1:6	0.75	1.15	1.20	0.98	1.10	1.25	-12.2	-14.1	-13.7	-18.1	-18.2	-22.9
Lime content 67%												
1C2L9S – 1:3	Not applicable since experimental value was used for regression - benchmark mix for Lime 67%											
1C2L12S – 1:4	0.83	1.26	1.43	1.40	1.54	1.61	7.8	-8.2	1.3	17.7	6.1	-0.5
1C2L15S – 1:5	0.43	0.87	0.85	0.78	0.86	0.97	-5.7	4.8	-1.0	-10.2	-4.2	0.3

Annex-Table 12: Flexural strength estimated using Table 20 and difference between estimated and experimental values shown in Table 15

	Estimated strength (MPa)						Difference (%) between estimated and actual values					
Mortars	7 (MPa)	14 (MPa)	28 (MPa)	90 (MPa)	180 (MPa)	365 (MPa)	7 (%)	14 (%)	28 (%)	90 (%)	180 (%)	365 (%)

Lime content 33%												
2C1L9S – 1:3	Not applicable since experimental value was used for regression - benchmark mix for Lime 33%											
2C1L12S – 1:4	1.01	1.49	1.77	1.79	2.00	2.01	-10.4	-0.7	-15.3	-14.1	-11.4	-3.4
2C1L15S – 1:5	0.70	0.99	1.27	1.36	1.39	1.35	6.3	0.4	9.6	7.8	7.2	2.0
Lime content 50%												
1C1L6S – 1:3	Not applicable since experimental value was used for regression - benchmark mix for Lime 50%											
1C1L8S – 1:4	0.73	1.03	1.19	1.27	1.37	1.50	4.8	8.4	9.9	5.8	10.5	27.6
1C1L10S – 1:5	0.43	0.63	0.73	0.75	0.81	0.87	17.5	9.1	13.7	13.3	8.9	14.1
1C1L12S – 1:6	0.23	0.37	0.42	0.40	0.43	0.46	-18.3	-12.4	-16.2	-15.8	-14.6	-24.4
Lime content 67%												
1C2L9S – 1:3	Not applicable since experimental value was used for regression - benchmark mix for Lime 67%											
1C2L12S – 1:4	0.29	0.48	0.49	0.54	0.59	0.57	-5.6	-9.0	-7.1	6.6	16.6	-5.6
1C2L15S – 1:5	0.21	0.36	0.37	0.34	0.36	0.32	2.7	4.9	3.5	-3.6	-8.8	4.5

Annex-Table 13: Values of mechanical strength (compression, flexure) as predicted by equation 15, Chapter 4

Mortar mix	x – lime (% by volume)	y – B/Ag (% by volume)	t – time (days)	f_c (MPa) - exp	f_c (MPa) - pred	f_c (MPa) - diff	f_f (MPa) - exp	f_f (MPa) - pred	f_f (MPa) - diff
9C1L30S	10	33.33	7	8.94	10.77	-1.83	2.67	3.23	-0.55
	10	33.33	14	10.64	10.91	-0.27	3.15	3.30	-0.15
	10	33.33	28	12.11	11.11	1.00	3.89	3.41	0.48
	10	33.33	90	12.22	11.65	0.57	3.15	3.69	-0.54
	10	33.33	180	11.29	12.16	-0.87	3.75	3.96	-0.20
	10	33.33	365	15.46	12.89	2.57	5.22	4.34	0.88
3C1L12S	25	33.33	7	7.66	8.64	-0.98	1.95	2.59	-0.64
	25	33.33	14	9.91	8.78	1.13	2.58	2.66	-0.08
	25	33.33	28	9.95	8.98	0.97	2.76	2.77	-0.01
	25	33.33	90	9.28	9.52	-0.24	3.22	3.05	0.17
	25	33.33	180	9.92	10.03	-0.11	3.64	3.32	0.32
	25	33.33	365	12.19	10.76	1.43	4.60	3.70	0.90
2C1L9S	33.33	33.33	7	6.09	7.46	-1.37	1.52	2.23	-0.72
	33.33	33.33	14	7.36	7.60	-0.24	2.32	2.31	0.01
	33.33	33.33	28	8.13	7.80	0.33	2.60	2.41	0.19
	33.33	33.33	90	8.57	8.34	0.23	2.52	2.69	-0.17
	33.33	33.33	180	8.73	8.85	-0.12	3.03	2.96	0.07
	33.33	33.33	365	8.65	9.58	-0.93	3.11	3.34	-0.24
1C1L6S	50	33.33	7	4.12	5.09	-0.97	1.23	1.52	-0.29
	50	33.33	14	5.41	5.24	0.17	1.69	1.59	0.09
	50	33.33	28	4.68	5.44	-0.76	1.96	1.70	0.26

	50	33.33	90	6.23	5.98	0.25	2.14	1.98	0.16
	50	33.33	180	6.31	6.48	-0.17	2.31	2.25	0.06
	50	33.33	365	7.01	7.22	-0.21	2.54	2.63	-0.09
1C2L9S	66.67	33.33	7	1.48	1.69	-0.21	0.41	0.57	-0.17
	66.67	33.33	14	1.90	1.93	-0.03	0.70	0.67	0.03
	66.67	33.33	28	2.39	2.09	0.30	0.69	0.73	-0.05
	66.67	33.33	90	2.45	2.27	0.18	0.86	0.80	0.06
	66.67	33.33	180	2.69	2.34	0.35	0.99	0.83	0.16
	66.67	33.33	365	2.67	2.39	0.28	0.98	0.85	0.13
1C3L12S	75	33.33	7	0.63	1.06	-0.43	0.28	0.38	-0.09
	75	33.33	14	1.16	1.29	-0.13	0.44	0.47	-0.03
	75	33.33	28	1.37	1.46	-0.09	0.48	0.54	-0.05
	75	33.33	90	1.53	1.64	-0.11	0.58	0.61	-0.03
	75	33.33	180	1.55	1.71	-0.16	0.61	0.63	-0.02
	75	33.33	365	1.61	1.75	-0.14	0.52	0.65	-0.13
1C9L30S	90	33.33	7	0.14	-0.18	0.32	0.04	-0.01	0.05
	90	33.33	14	0.22	0.06	0.16	0.04	0.08	-0.04
	90	33.33	28	0.30	0.23	0.07	0.19	0.15	0.04
	90	33.33	90	0.41	0.41	0.00	0.28	0.22	0.06
	90	33.33	180	0.45	0.47	-0.02	0.26	0.25	0.01
	90	33.33	365	0.43	0.52	-0.09	0.21	0.27	-0.05
3C1L16S	25	25	7	4.59	5.68	-1.09	1.23	1.72	-0.49
	25	25	14	6.46	5.82	0.64	1.72	1.79	-0.07
	25	25	28	6.01	6.02	-0.01	2.10	1.90	0.20
	25	25	90	7.05	6.56	0.49	2.35	2.18	0.17
	25	25	180	7.85	7.07	0.78	2.95	2.45	0.50
	25	25	365	7.77	7.80	-0.03	2.74	2.83	-0.09
2C1L12S	33.33	25	7	3.23	4.50	-1.27	1.12	1.36	-0.24
	33.33	25	14	5.03	4.64	0.39	1.50	1.44	0.06
	33.33	25	28	5.09	4.84	0.25	2.09	1.54	0.55
	33.33	25	90	5.73	5.38	0.35	2.09	1.83	0.26
	33.33	25	180	6.34	5.89	0.45	2.26	2.09	0.17
	33.33	25	365	5.16	6.62	-1.46	2.08	2.48	-0.40
1C1L18S	50	25	7	2.31	2.13	0.18	0.70	0.65	0.05
	50	25	14	3.12	2.27	0.85	0.95	0.73	0.22
	50	25	28	3.00	2.47	0.53	1.08	0.83	0.25
	50	25	90	3.53	3.02	0.51	1.20	1.11	0.09
	50	25	180	3.10	3.52	-0.42	1.24	1.38	-0.14

	50	25	365	3.56	4.26	-0.70	1.17	1.76	-0.59
1C2L12S	66.67	25	7	0.77	0.91	-0.14	0.30	0.32	-0.01
	66.67	25	14	1.37	1.15	0.22	0.53	0.41	0.12
	66.67	25	28	1.41	1.32	0.09	0.52	0.48	0.05
	66.67	25	90	1.19	1.50	-0.31	0.50	0.55	-0.04
	66.67	25	180	1.45	1.57	-0.12	0.51	0.57	-0.06
	66.67	25	365	1.62	1.61	0.01	0.60	0.59	0.01
2C1L15S	33.33	20	7	1.86	2.72	-0.86	0.66	0.84	-0.18
	33.33	20	14	2.83	2.86	-0.03	0.99	0.92	0.07
	33.33	20	28	3.08	3.06	0.02	1.16	1.02	0.14
	33.33	20	90	3.26	3.60	-0.34	1.26	1.30	-0.05
	33.33	20	180	3.69	4.11	-0.42	1.30	1.57	-0.27
	33.33	20	365	3.26	4.84	-1.58	1.32	1.95	-0.63
1C1L10S	50	20	7	1.31	0.36	0.95	0.37	0.13	0.24
	50	20	14	1.77	0.50	1.27	0.58	0.20	0.37
	50	20	28	1.59	0.70	0.89	0.64	0.31	0.33
	50	20	90	1.74	1.24	0.50	0.66	0.59	0.07
	50	20	180	1.99	1.74	0.25	0.74	0.86	-0.12
	50	20	365	2.05	2.48	-0.43	0.77	1.24	-0.48
1C2L15S	66.67	20	7	0.46	0.39	0.07	0.21	0.14	0.07
	66.67	20	14	0.83	0.62	0.21	0.34	0.23	0.11
	66.67	20	28	0.85	0.79	0.06	0.35	0.30	0.05
	66.67	20	90	0.86	0.97	-0.11	0.36	0.37	-0.02
	66.67	20	180	0.90	1.04	-0.14	0.39	0.40	-0.01
	66.67	20	365	0.96	1.08	-0.12	0.31	0.42	-0.11

Annex-Table 14: Values of UPV and hardened density for lime-cement blended mixes at different curing ages

Mortar mix	x – lime (%	y – B/Ag	t – time	UPV (m/s)			Bulk density (kg/m³)		
	volume)	(% volume)	(days)	Control	Batch tested	Diff %	Control	Batch tested	Diff %
9C1L30S	10	33.33	7	3290.2	3199.3	2.8	2105.3	2002.3	-4.9
	10	33.33	14	3321.1	3231.6	2.7	2077.0	1983.3	-4.5
	10	33.33	28	3253.6	3234.5	0.6	2067.1	2047.4	-1.0
	10	33.33	90	3183.2	3127.3	1.8	2072.6	1988.0	-4.1
	10	33.33	180	3221.5	3166.4	1.7	2081.1	1985.6	-4.6
	10	33.33	365	3362.3	3362.3	0.0	2093.3	2093.3	0.0
3C1L12S	25	33.33	7	3054.2	3074.3	-0.7	2068.5	2048.8	-1.0
	25	33.33	14	3052.4	3066.8	-0.5	2021.1	2011.6	-0.5
	25	33.33	28	3005.0	3026.5	-0.7	2012.4	2024.3	0.6

	25	33.33	90	3000.0	2941.3	2.0	2019.2	1944.5	-3.7
	25	33.33	180	3053.5	3011.3	1.4	2028.6	1960.9	-3.3
	25	33.33	365	3131.9	3131.9	0.0	2035.2	2035.2	0.0
2C1L9S	33.33	33.33	7	2810.9	2862.4	-1.8	1998.4	2028.9	1.5
	33.33	33.33	14	2878.6	2866.2	0.4	1964.9	1998.8	1.7
	33.33	33.33	28	2710.3	2768.2	-2.1	1958.4	1990.5	1.6
	33.33	33.33	90	2848.7	2517.1	11.6	1964.5	2001.8	1.9
	33.33	33.33	180	2876.2	2848.7	1.0	1976.9	1953.9	-1.2
	33.33	33.33	365	2915.1	2915.1	0.0	1979.1	1979.1	0.0
1C1L6S	50	33.33	7	2542.0	2521.5	0.8	2005.5	1998.3	-0.4
	50	33.33	14	2589.2	2608.3	-0.7	1964.7	1977.7	0.7
	50	33.33	28	2463.4	2507.8	-1.8	1952.0	1904.8	-2.4
	50	33.33	90	2579.4	2564.1	0.6	1969.9	1951.9	-0.9
	50	33.33	180	2644.6	2670.2	-1.0	1972.5	1918.9	-2.7
	50	33.33	365	2659.4	2659.4	0.0	1979.8	1979.8	0.0
1C2L9S	66.67	33.33	7	1821.6	1790.7	1.7	1904.8	1907.9	0.2
	66.67	33.33	14	1887.3	1864.4	1.2	1860.0	1892.2	1.7
	66.67	33.33	28	1794.9	1778.9	0.9	1859.3	1890.0	1.7
	66.67	33.33	90	1979.5	1990.4	-0.6	1872.3	1961.0	4.7
	66.67	33.33	180	1970.5	1969.1	0.1	1874.9	1944.5	3.7
	66.67	33.33	365	1972.1	1972.1	0.0	1884.4	1884.4	0.0
1C3L12S	75	33.33	7	1433.7	1395.9	2.6	1941.1	1964.3	1.2
	75	33.33	14	1540.8	1630.8	-5.8	1868.2	1949.7	4.4
	75	33.33	28	1525.1	1523.9	0.1	1871.4	1911.1	2.1
	75	33.33	90	1649.5	1655.2	-0.3	1883.0	1915.6	1.7
	75	33.33	180	1620.3	1683.1	-3.9	1885.0	1952.8	3.6
	75	33.33	365	1634.2	1634.2	0.0	1885.7	1885.7	0.0
3C1L16S	25	25	7	2865.7	2820.3	1.6	2050.7	2010.2	2.1
	25	25	14	2819.4	2873.7	-1.9	1997.2	2054.2	-2.8
	25	25	28	2824.0	2707.4	4.1	1986.2	1951.4	1.8
	25	25	90	2782.2	2818.7	-1.3	1991.3	2030.3	-1.9
	25	25	180	2810.5	2809.0	0.1	1997.4	2000.2	-0.1
	25	25	365	2806.1	2806.1	0.0	1997.9	1997.9	0.0
2C1L12S	33.33	25	7	2493.9	2499.6	-0.2	1981.1	1965.6	0.8
	33.33	25	14	2543.7	2603.1	-2.3	1919.2	1931.7	-0.7
	33.33	25	28	2614.7	2806.0	-7.3	1910.8	1911.5	0.0
	33.33	25	90	2485.9	2550.6	-2.6	1918.1	1942.5	-1.3
	33.33	25	180	2480.7	2568.2	-3.5	1921.1	1963.5	-2.2

	33.33	25	365	2512.7	2512.7	0.0	1921.6	1921.6	0.0
1C1L18S	50	25	7	2168.7	2263.8	-4.4	1988.3	2021.1	-1.7
	50	25	14	2126.3	2185.1	-2.8	1938.7	1963.2	-1.3
	50	25	28	2197.8	2257.8	-2.7	1937.0	1965.5	-1.5
	50	25	90	2229.5	2336.9	-4.8	1944.8	1981.8	-1.9
	50	25	180	2175.2	2294.7	-5.5	1946.2	1938.8	-0.4
	50	25	365	2214.5	2214.5	0.0	1945.7	1945.7	0.0
1C2L12S	66.67	25	7	1617.0	1672.8	-3.5	2081.9	2066.5	0.7
	66.67	25	14	1753.7	1801.1	-2.7	1975.4	1961.3	0.7
	66.67	25	28	1748.1	1744.9	0.2	1975.7	1966.1	0.5
	66.67	25	90	1794.4	1582.8	11.8	1978.2	1857.6	6.1
	66.67	25	180	1782.4	1621.7	9.0	1978.8	1873.8	5.3
	66.67	25	365	1787.5	1787.5	0.0	1977.6	1977.6	0.0
2C1L15S	33.33	20	7	2252.8	2234.7	0.8	2006.2	2003.0	0.2
	33.33	20	14	2346.0	2303.4	1.8	1935.6	1912.8	1.2
	33.33	20	28	2324.1	2282.1	1.8	1926.1	1899.3	1.4
	33.33	20	90	2325.2	2442.5	-5.0	1929.1	2013.3	-4.4
	33.33	20	180	2281.0	2375.2	-4.1	1930.2	1974.0	-2.3
	33.33	20	365	2296.3	2296.3	0.0	1929.0	1929.0	0.0
1C1L10S	50	20	7	1932.9	1941.0	-0.4	1988.5	1981.9	0.3
	50	20	14	1996.3	2027.5	-1.6	1929.0	1927.9	0.1
	50	20	28	2029.4	1880.2	7.4	1930.8	1878.2	2.7
	50	20	90	2002.5	1849.1	7.7	1920.2	1876.0	2.3
	50	20	180	1935.1	1963.2	-1.5	1931.7	1936.5	-0.2
	50	20	365	1951.0	1951.0	0.0	1935.0	1935.0	0.0
1C2L15S	66.67	20	7	1236.1	1373.0	-11.1	2042.6	1974.9	3.3
	66.67	20	14	1504.5	1454.6	3.3	1924.2	1891.2	1.7
	66.67	20	28	1503.9	1466.0	2.5	1924.4	1923.8	0.0
	66.67	20	90	1535.5	1469.0	4.3	1930.8	1886.2	2.3
	66.67	20	180	1531.1	1524.4	0.4	1930.7	1942.8	0.6
	66.67	20	365	1512.8	1512.8	0.0	1929.2	1929.2	0.0

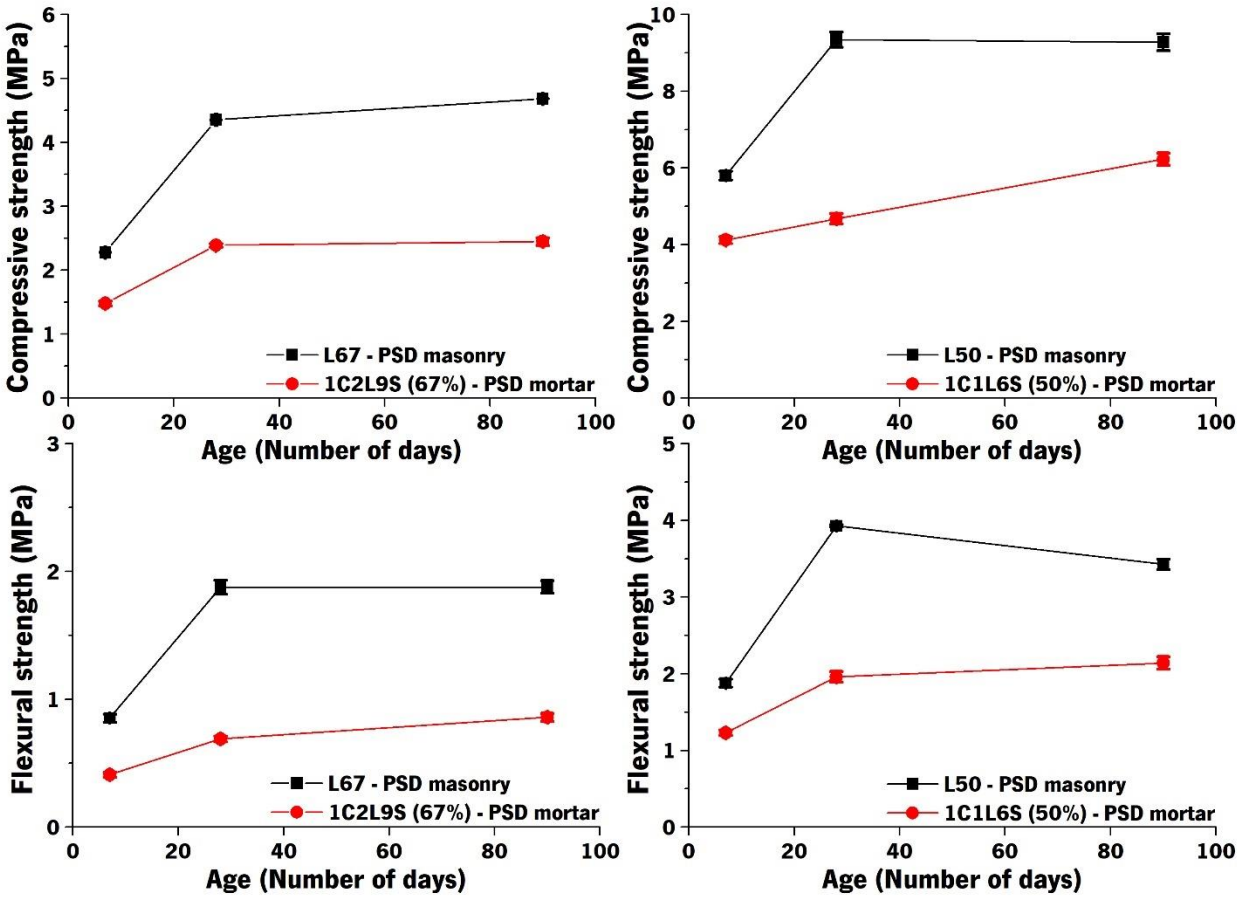

Annex-Figure 1: Comparison of mechanical strength of mortars with original vs modified PSD of aggregates (Figure 18)

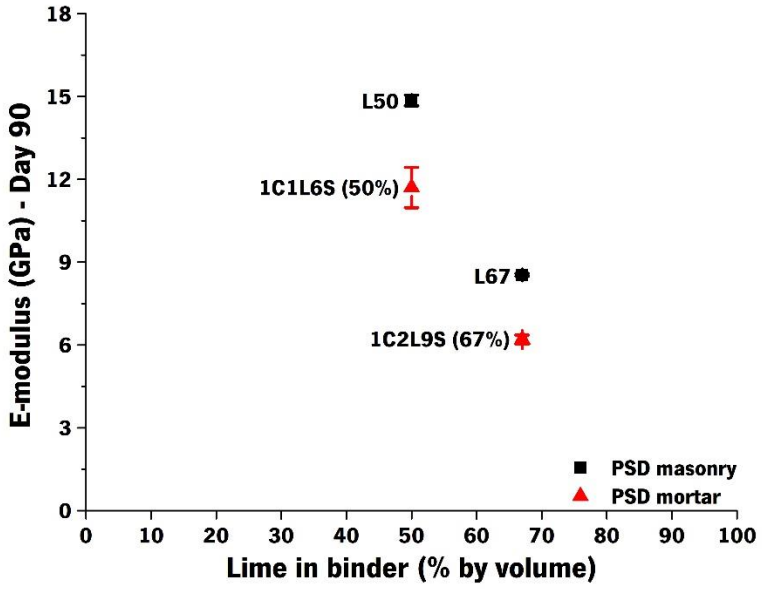

Annex-Figure 2: Comparison of E-modulus of mortars with original vs modified PSD of aggregates (Figure 18)